AWARD NUMBER:
W81XWH-14-1-0500

TITLE: Toward a Molecular Understanding of Noise-Induced Hearing Loss

PRINCIPAL INVESTIGATOR: Ronna Hertzano, MD PhD

CONTRACTING ORGANIZATION: University of Maryland School of Medicine

REPORT DATE: Dec 2019

TYPE OF REPORT: Final Technical Report

PREPARED FOR: U.S. Army Medical Research and Materiel Command
Fort Detrick, Maryland 21702-5012

REPORT DOCUMENTATION PAGE

Form Approved
OMB No. 0704-0188

1. REPORT DATE	**2. REPORT TYPE**	**3. DATES COVERED**
December 2019	Final Report	**09/30/2014 - 09/29/2019**

4. TITLE AND SUBTITLE

Toward a Molecular Understanding of Noise-Induced Hearing Loss

5a. CONTRACT NUMBER

5b. GRANT NUMBER
W81XWH-14-1-0500

5c. PROGRAM ELEMENT NUMBER

6. AUTHOR(S)

Ronna Hertzano, MD, PhD

E-Mail: rhertzano@smail.umaryland.edu

5d. PROJECT NUMBER

5e. TASK NUMBER

5f. WORK UNIT NUMBER

7. PERFORMING ORGANIZATION NAME(S) AND ADDRESS(ES)
University of Maryland School of Medicine

8. PERFORMING ORGANIZATION REPORT NUMBER

9. SPONSORING / MONITORING AGENCY NAME(S) AND ADDRESS(ES)

U.S. Army Medical Research and Materiel Command
Fort Detrick, Maryland 21702-5012

10. SPONSOR/MONITOR'S ACRONYM(S)

11. SPONSOR/MONITOR'S REPORT NUMBER(S)

12. DISTRIBUTION / AVAILABILITY STATEMENT

Approved for Public Release; Distribution Unlimited

13. SUPPLEMENTARY NOTES

14. ABSTRACT

The purpose of this project is to generate the cell type-specific molecular blueprint of changes in gene expression following different types of noise exposure and their treatments, in the inner ear. To this end, we have (a) Established the hair cell (HC) and supporting (SC) cell-specific translatomes of adult mouse inner ears and identified key regulators of OHC maturation and function; (b) Established the molecular changes induced by permanent and temporary threshold shift resulting noise exposure in HC, SC and whole inner ears, 6 and 24 hours after noise exposure; (c) We identified critical differences in the response of male and female mice to noise, and obtained approval to modify Specific Aim 3 to repeat the baseline as well as temporary and permanent threshold shift analysis using male and female mice separately.

15. SUBJECT TERMS

Permanent threshold shift, Temporary threshold shift, Noise induced hearing loss, Ribotag, RNA-seq, hair cell, supporting cell, SAHA, Heat shock, sex differences

16. SECURITY CLASSIFICATION OF:			**17. LIMITATION OF ABSTRACT**	**18. NUMBER OF PAGES**	**19a. NAME OF RESPONSIBLE PERSON**
a. REPORT	**b. ABSTRACT**	**c. THIS PAGE**			USAMRMC
Unclassified	Unclassified	Unclassified	Unclassified		**19b. TELEPHONE NUMBER** *(include area code)*

TABLE OF CONTENTS

	Page
1. Introduction	3
2. Keywords	3
3. Accomplishments	3
4. Impact	14
5. Changes/Problems	15
6. Products	17
7. Participants & Other Collaborating Organizations	19
8. Special Reporting Requirements	23
9. Appendices	23

1. INTRODUCTION

Noise induced hearing loss (NIHL) is a major health concern for the Department of Defense. Noise exposure often is inevitable and may results in a permanent loss of hearing. Unfortunately, there are no treatments to prevent or reverse NIHL. As a first step towards designing targeted therapeutics, we suggested to generate mouse models which allow cell type-specific translatome analysis in the ear. These, in turn, will be used to analyze the genes expressed in the hair cells (HC) and supporting cells (SC) of adult mice before and after different types of noise exposure as well as pre-conditioning treatments, which in mice, can ameliorate NIHL. Here we report our progress over the five years of the project, in which we (a) followed the plan obtained in the in-person review to extend the cell type-specific blueprint following noise to be sex-specific and (b) consolidated our findings from the first three years of the project and published three peer reviewed manuscripts with additional manuscripts in preparation.

2. KEYWORDS:

Permanent threshold shift, Temporary threshold shift, Noise induced hearing loss, Ribotag, RNA-seq, Hair cell, Supporting cell, SAHA, Heat shock, Sex differences, Estrogen

3. ACCOMPLISHMENTS:

What were the major goals of the project?

Specific Aim 1: To determine the OHC- and SC-specific transcriptional and signaling cascades activated in vivo in response to PTS-inducing noise exposure

a. Major Task 1: To establish the OHC- and SC-specific translatome of adult mouse inner ears. Progress by subtasks:
   i. Obtain ACURO approval following UMSOM IACUC approval – complete.
   ii. Mouse crosses and tissue harvesting – complete.
   iii. Tissue processing – complete, polysome IP – complete, submission of samples for RiboTag-seq – complete; RiboTag-seq – complete**.**

   Major task 1 is 100% complete.

b. Major Task 2: To determine the OHC- and SC-specific transcriptional and signaling cascades activated in response to PTS-inducing noise injury. Progress by subtasks:
   i. Mouse crosses, noise exposure, tissue harvesting, histological analysis, ABR and DPOAE measurements. Complete.
   ii. Tissue processing – complete.
   iii. Data analysis – largely reported last year.
   iv. Validation experiments – polysome IP to be used for RT-qPCR – complete. Tissue harvesting for immunohistochemistry and in situ hybridization - complete.

   Major task 2 is 100% complete.

Specific Aim 2: To determine the OHC- and SC-specific signaling cascades activated in vivo in response to otoprotective interventions.

This Aim was designed to define the cell type-specific molecular blueprint of interventions that may ameliorate NIHL. In previous annual reports, we discussed the rationale for maintaining the TTS and Heat Shock. The heat shock goal was transferred to a modified Specific Aim 3 that is also sex-specific.

Major Task: TTS-inducing noise exposure male and female mice combined.

Major task is 100% complete.

Specific Aim 3: Following the in-person review of the award in the summer 2017, specific aim 3 was redesigned to allow us to both study the response to Heat Shock with and without noise exposure as originally planned as well as obtain all tissue separately from male and female mice.

a. Major Task 1: male and female tissue collected separately for baseline, PTS and TTS
   i. New baseline - Tissue collection, tissue processing, library preparation for sequencing: 100% complete
   ii. PTS (105dB) – Tissue collection, tissue processing, library preparation for sequencing of OHC: 100% complete. Tissue collection, tissue processing for SC: 100% complete. Library preparation for sequencing for SC: 42% complete
   iii. TTS (94db) – Tissue collection, tissue processing, library preparation for sequencing of OHC: 100% complete. Library preparation for sequencing for SC: 25% complete

b. Major Task 2: male and female tissue collected separately for heat shock with/without noise
   i. Heat shock only - Tissue collection for OHC: 100% complete. Tissue processing for OHC: 89% complete. Library preparation for sequencing of OHC: 11% complete. Tissue collection, tissue processing, library preparation for sequencing of SC: discontinued.
   ii. Heat shock and noise – discontinued.

What was accomplished under these goals?

Accomplishments

Year 1

- We validated the use of the PrestinCreER^{T2};RiboTag and Sox2-CreER^{T2};RiboTag mouse models to obtain RNA enriched in transcripts from outer hair cells (OHC) and supporting cells (SC) respectively (**Figure 1A**). Additionally, using a reporter mouse, we determined that PrestinCreER^{T2} induces recombination specifically in OHC (**Figure 1B**), while Sox2CreER^{T2} induces recombination in supporting cells as well as in glial cells of the spiral ganglion (**Figure 1C,D**).

A

Cell type	Gene	PrestinCre;Ribotag		Sox2Cre;Ribotag	
		Input	IP	Input	IP
Hair cells	Ocm	68.2	530.9	65.5	41.5
	Gfi1	4.4	17.3	4.4	1.6
	Slc26a5	10.0	47.6	13.0	4.6
	Myo7a	13.6	36.5	11.4	19.1
Supporting cells	Sox2	28.8	16.3	17.1	95.5
	Fgfr3	42.0	69.1	56.9	283.7
	Jag1	36.3	37.0	26.7	87.1

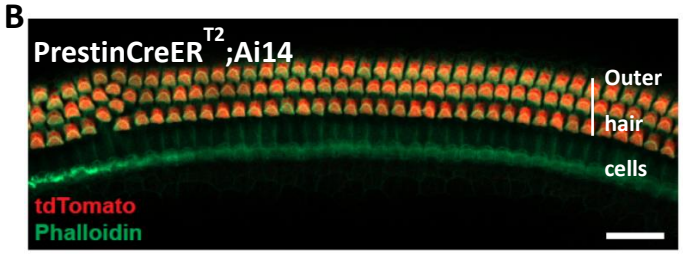

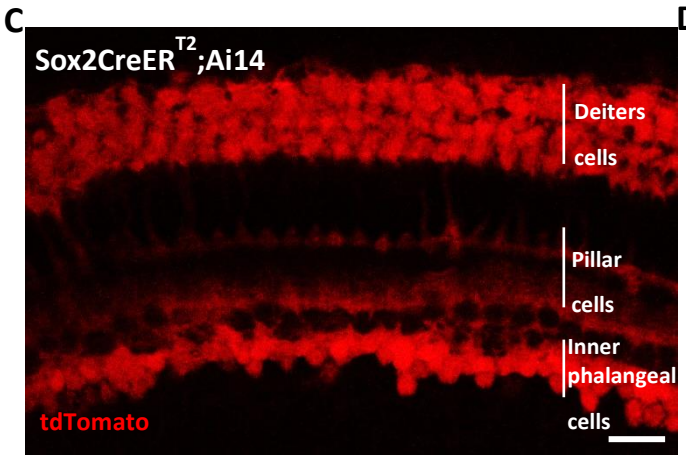

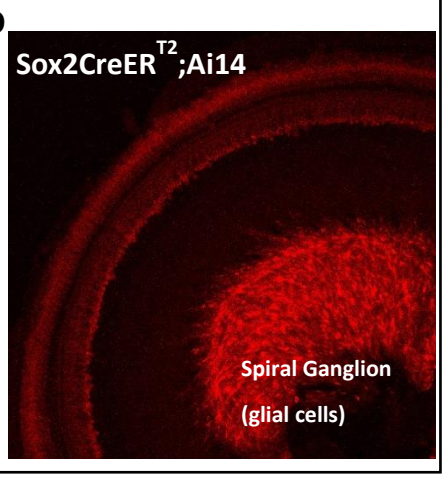

Figure 1. Specificity of the Cre recombinase models. A) Significant enrichment of transcripts from OHC and supporting cells in the IP samples of the corresponding Cre. **B)** tdTomato used as a reporter indicate the specificity of PrestinCreER^{T2} for OHC. **C-D)** tdTomato expression indicates Cre recombination from the Sox2CreER^{T2} in SC (C) and glial cells of the spiral ganglion (D). Scale bar = 20μm.

- We determined and validated two noise paradigms to obtain a Permanent Threshold Shift (PTS) and a Temporary Threshold Shift (TTS).
  PTS: 105dB for 2h, octave band 8-16kHz (**Figure 2A**)
  TTS: 94dB for 2h, octave band 8-16kHz (**Figure 2B**)

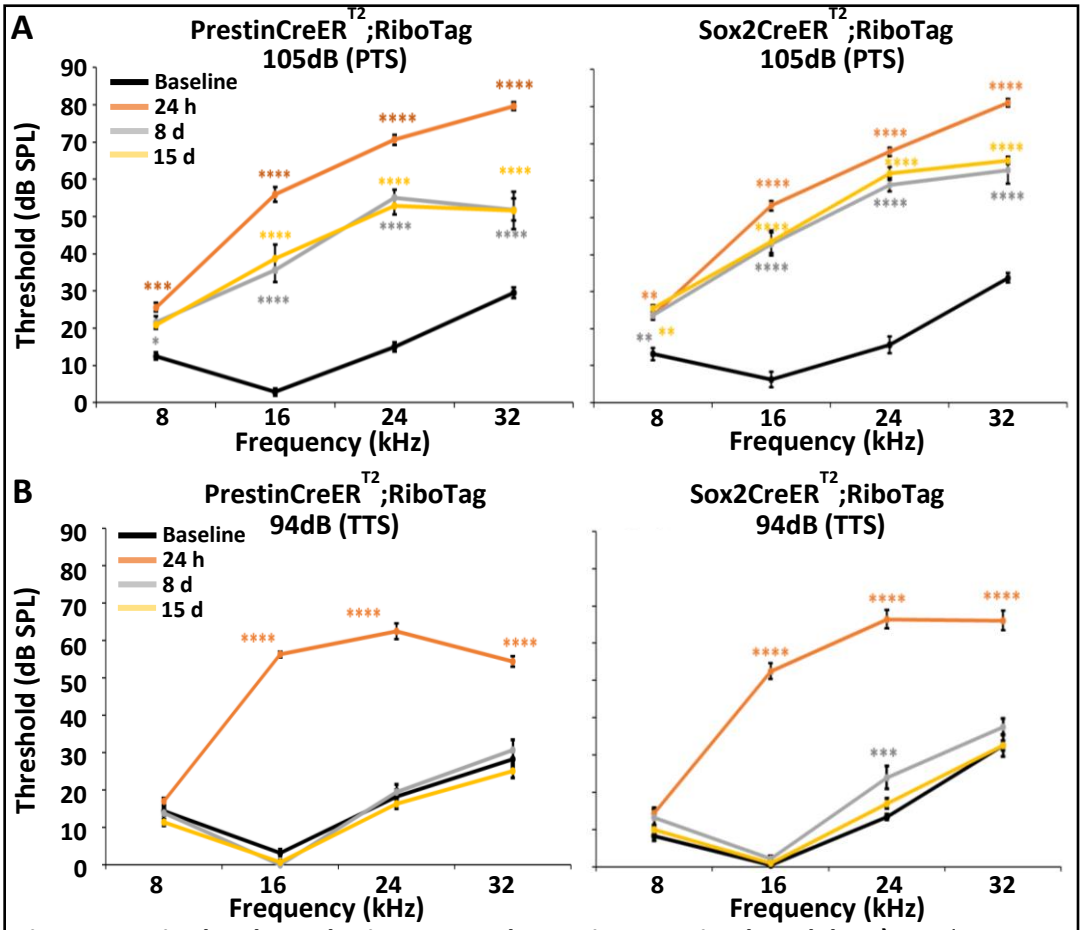

Figure 2. Noise levels to obtain a PTS and a TTS in our animal models. A) 105dB octave band 8-16kHz for 2 hours induces a PTS in both PrestinCreER^{T2};RiboTag and Sox2CreER^{T2};RiboTag. **B)** 94dB octave band 8-16kHz for 2 hours induces a TTS in both PrestinCreER^{T2};RiboTag and Sox2CreER^{T2};RiboTag. Error bars = SEM. * p<0.05; **p<0.01; ***p<0.001; ****p<0.0001.

Year 2

- We identified the adult OHC and SC-specific translatome. This will allow for the identification of new deafness-causing genes and additional cell type-specific markers in the adult mouse inner ear. We defined a transcript as enriched in a cell-type if the log2 enrichment between IP and input is >1.5 and if the transcript is enriched at least 2-fold in the specific dataset when compared to the other dataset. Using this criterion, we identified 436 genes for OHC and 248 genes for SC. Gene ontology analysis of each gene list found functional enrichment in hearing, and in membrane and synapses for the OHC and SC gene list respectfully (**Figure 3**). Interestingly, 92 of the OHC genes and 58 of the SC genes have human orthologs located in unresolved loci for deafness-related diseases. Additionally, we identified IKZF2 as an important transcription factor for OHC development and maintenance in adult tissue (**Chessum L, Matern M, et al., 2018 – appendix 1**).

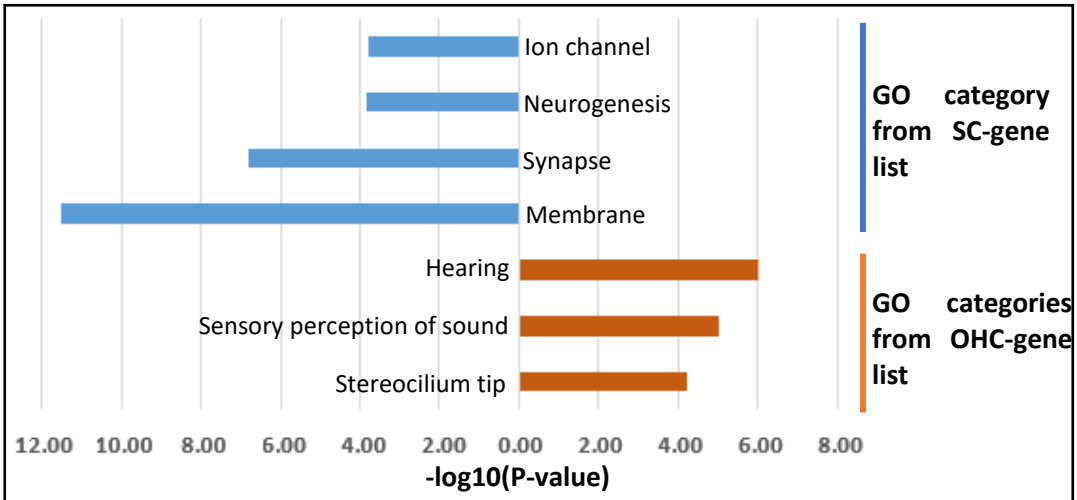

Figure 3. Gene ontology categories over-represented in the OHC-enriched gene list and in the SC-enriched gene list. SC-enriched gene list (blue-top) is functionally related to membrane, synapse and neurogenesis. OHC-enriched gene list (orange-bottom) is functionally related to hearing, perception of sound and stereocilium tip.

- We identified critical differences in the response to noise between male and female mice (**Figure 4**). This resulted in a change in experiment design both for us but likely for other researchers funded to study NIHL.

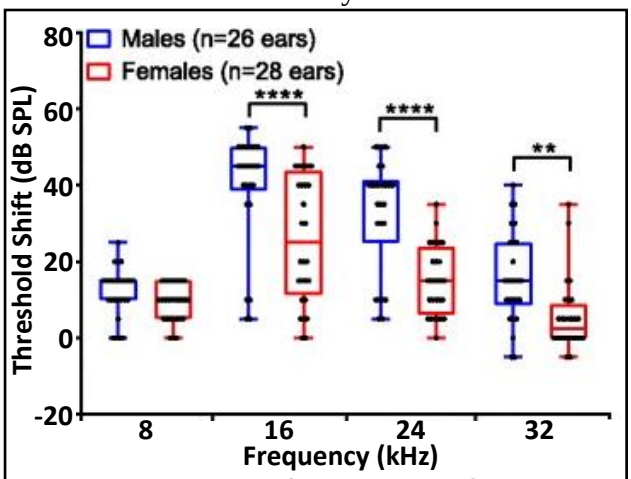

Figure 4. Threshold shifts in male and female mice following noise exposure. Female mice have lower threshold shifts following a PTS- inducing noise-exposure. **p<0.01; ****p<0.0001 (**Milon et al., 2018 – appendix 2**).

- We developed new protocols for sequencing low input translatomes. A comprehensive analysis of different sequencing kits led us to identify the TaKaRa SMART-Seq v4 Ultra Low Input RNA Kit as efficient for sequencing from very small amount of RNA, allowing us to reduce the number of animals used per replicate (**Song et al., 2018 – appendix 3**).

Year 3

- Molecular description of the response to PTS in OHC, SC and whole inner ear.

  We applied an unbiased cluster analysis to divide genes with a change in expression following noise into different clusters according to their response pattern at 6h and 24h post noise exposure. The entire cochlea data (input samples) were compared to the OHC- and SC-enriched samples in order to detect common and specific responses. The analysis revealed 3 and 4 patterns of up-regulated expression for the OHC (**Figure 5A**) and SC (**Figure 5C**) datasets respectively. Additionally, 5 and 3 patterns of down-regulated expression were detected for the OHC (**Figure 5B**) and SC (**Figure 5D**) datasets respectively.

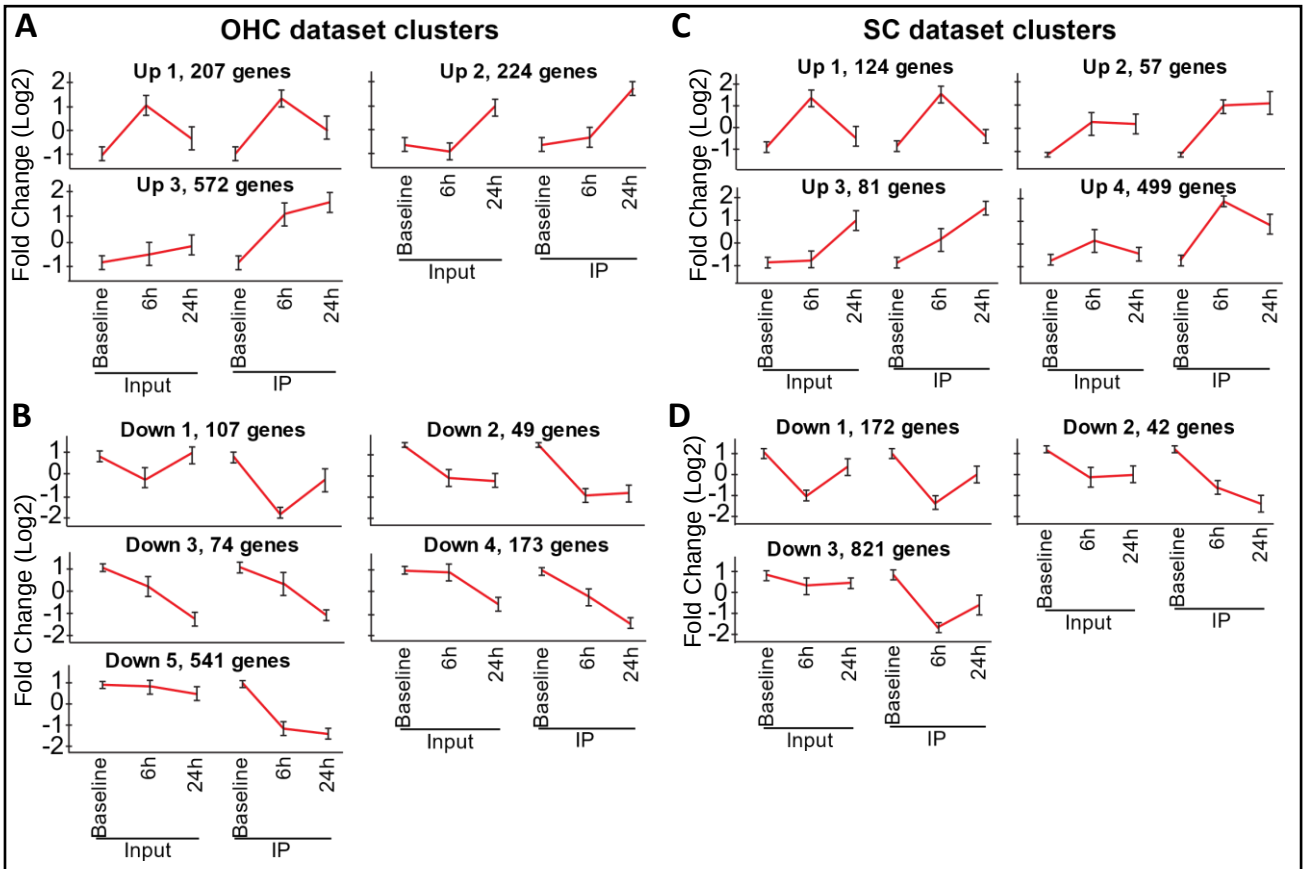

Figure 5 Expression clusters for the OHC and SC datasets A-B) Expression patterns in the OHC dataset for genes up-regulated (A) and down-regulated (B) following noise exposure. **C-D)** Expression patterns in the SC dataset for genes up-regulated (C) and down-regulated (D) following noise exposure.

We then subjected each cluster to a gene ontology (GO) enrichment analysis. The results of the GO analysis revealed that up-regulated genes from both datasets share common functional enrichment such as apoptosis 6h post noise exposure and immune response 24h post noise (**Table 1**). However, the clusters with down-regulated genes are more specific to cell-types and we decided to focus on those for validation. For example, the results suggest that OHC repress genes involved in RNA metabolism/splicing, while SC down-regulate genes involved in neuronal transmission (**Table 1**).

Dataset	Cluster	Enriched GO categories	# of genes (*p*-value)
OHC	UP1	Regulation of apoptotic process - GO:0042981	39 (2.6E-10)
	UP2	Innate immune response - GO:0045087	19 (4.1E-13)
SC	UP1	Regulation of apoptotic process - GO:0042981	21 (1.7E-6)
	UP3	Innate immune response - GO:0045087	15 (3.7E-15)
OHC	DOWN5	mRNA metabolic process - GO:0016071 Regulation of RNA splicing - GO:0043484	36 (5.4E-12) 11 (4.1E-7)
SC	DOWN3	Transmission of nerve impulse - GO:0019226 Regulation of neurogenesis - GO:0050767	48 (1.9E-10) 41 (8.0E-7)

Table 1. Gene Ontology Enrichment Analysis of the Clusters.

- We identified key differences between the response to a TTS-inducing noise and a PTS-inducing noise. **Figure 6** shows 4 of the gene clusters based on expression pattern that are uniquely changed after either PTS- or TTS-inducing noise exposures. Cluster 4 (**Figure 6A**) and cluster 2 (**Figure 6B**) represent genes that are induced only after a PTS noise while they are mostly unchanged following a TTS. Cluster 1 represents genes repressed after a TTS noise, suggesting genes which expression is deleterious following noise exposure (**Figure 6C**). A particularly interesting cluster is cluster 3 which consists of genes uniquely upregulated only following TTS noise exposure (**Figure 6D**). Within this cluster, a striking novel example is DFNA5 which absence in mice and human lead to genetic hearing loss. Here our data suggest that overexpression of this gene may have a role in otoprotection.

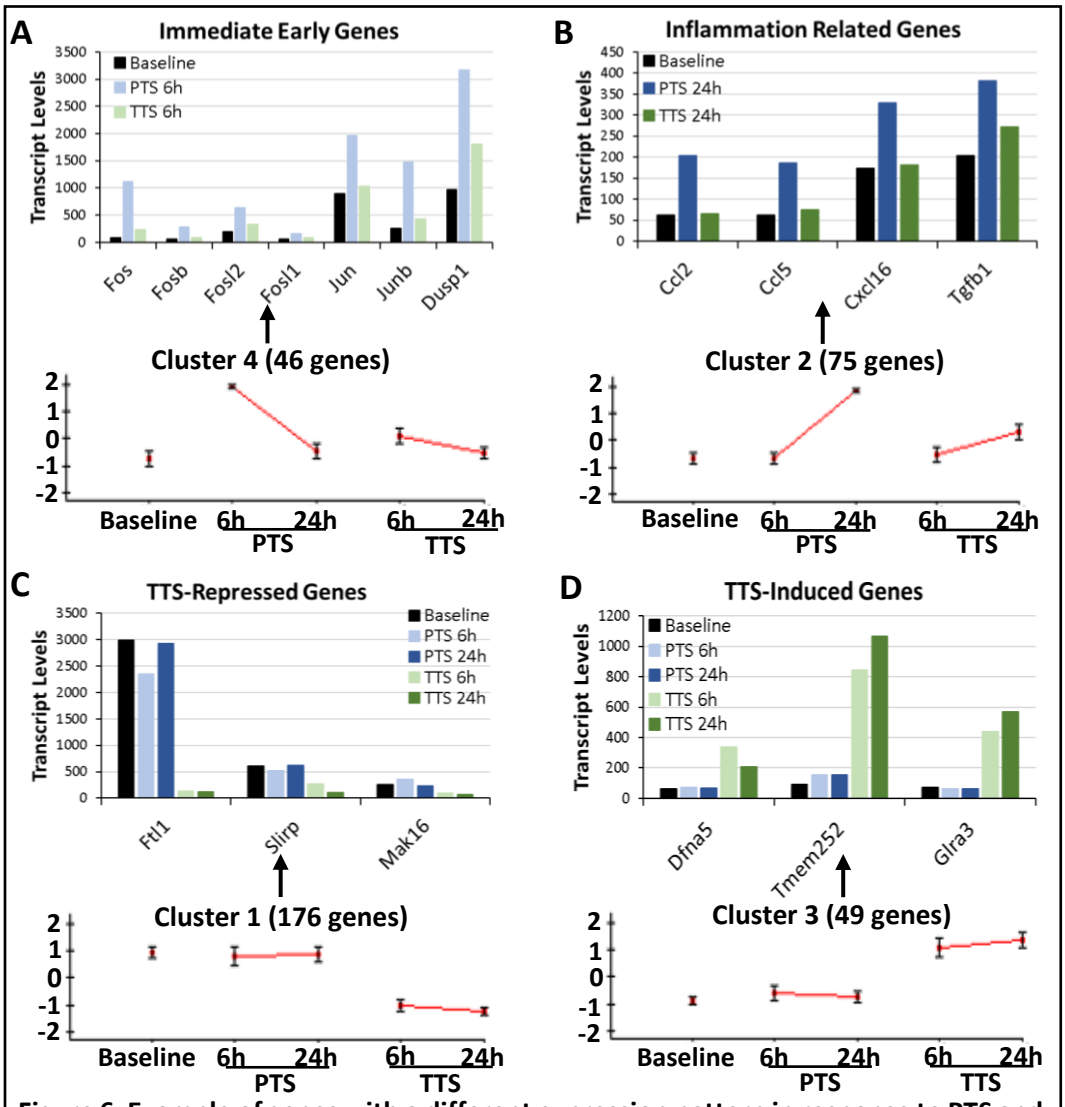

Figure 6. Example of genes with a different expression pattern in response to PTS and TTS. A) Induction of early immediate gene expression is lower or absent in TTS compared to PTS. **B)** Genes involved in inflammatory response are not induced after a TTS-inducing noise. **C)** Example of genes found to be repressed after a TTS noise when compare to baseline and PTS noise. **D)** Example of genes found to be induced after a TTS noise when compare to baseline and PTS noise.

Year 4 (no cost extension)

- During year 4, we published three peer-reviewed manuscripts describing key findings from the project:
    - Our findings about the differences in response to noise exposure between male and female mice were published in Biology of Sex Differences (**Milon et al., 2018 – appendix 2**).
    - Our results from the comparison of different sequencing kits for low input RNA from RiboTag samples were published in BMC Genomics (**Song et al., 2018 – appendix 3**).
    - The identification of IKZF2 as a main regulator of outer hair cell development was published in Nature (**Chessum, Matern et al., 2018 – appendix 1**).

Year 5 (no cost extension)

- Cluster DOWN 5 from the OHC dataset showed an enrichment for gene ontologies related to RNA metabolism and more specifically to the regulation of RNA splicing (**Table 1**). In this last reporting period, we re-analyzed the RNA-seq dataset for alternative splicing events that would differ when comparing before and after noise exposure. Through this analysis, we found a 2-fold increase in exon-skipping pattern following noise exposure when comparing the entire cochlea (input samples) to the samples enriched for OHC transcripts (IP samples).
- Following the completion of RNA sequencing from male and female mice separately for the OHC model, we started the analysis to identify molecular differences between male and female after noise exposure. Shown in **Figure 7** are example of genes which expression

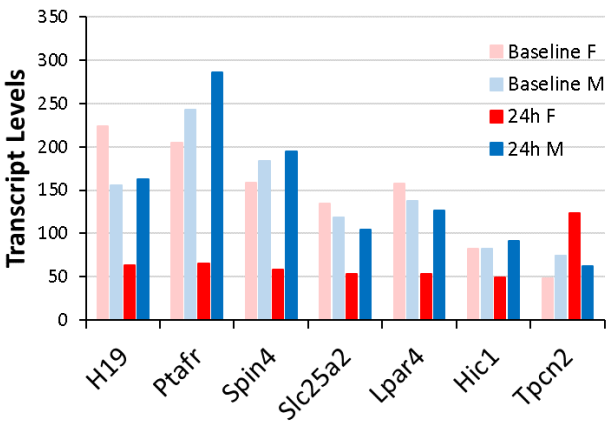

Figure 7. Gene expression in male and female mice following a PTS-noise exposure. Data from the OHC-enriched samples identify genes with a sex-specific expression pattern after a PTS-noise exposure.

differs in male and female mice following noise exposure. These preliminary results confirm the validity of our model to study sex-specific differences to noise.

- We validated selected genes that were dysregulated following noise exposure using nanoString technologies (**Figure 8**).

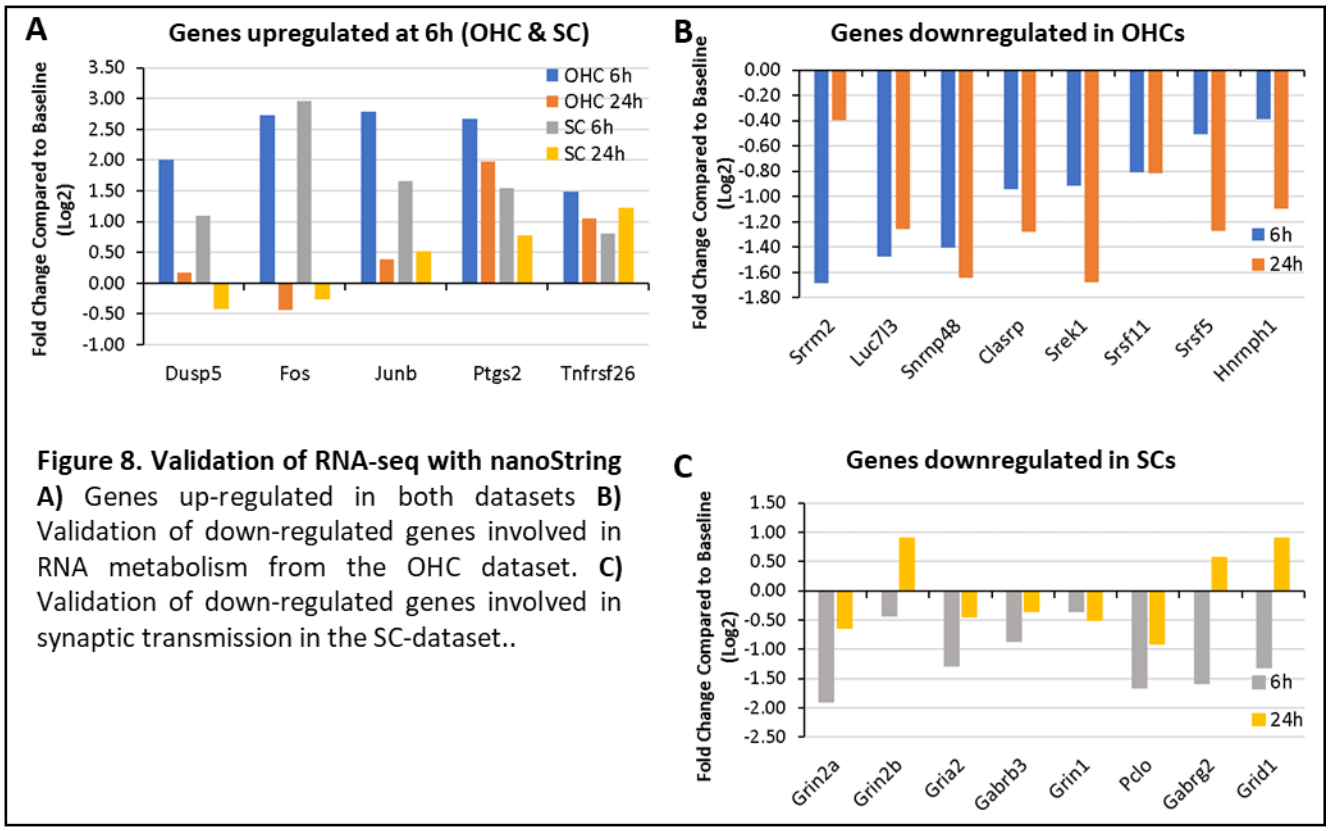

Figure 8. Validation of RNA-seq with nanoString **A)** Genes up-regulated in both datasets **B)** Validation of down-regulated genes involved in RNA metabolism from the OHC dataset. **C)** Validation of down-regulated genes involved in synaptic transmission in the SC-dataset..

- We published two reviews related to the project:
    - Review of literature about the relation between hearing and estrogen was published in The Journal of the Acoustical Society of America (**appendix 4**).
    - Review of literature about genetic susceptibility to noise-induced hearing loss and tinnitus was published in The Journal of the Acoustical Society of America and genome paper (**appendix 5**).

In conclusion, this body of work, generously funded by the DoD has resulted in several novel and important findings to the field, which are likely to initiate new drug development to treat NIHL as well as support the work of other laboratories in the field. Specifically, (a) it resulted in the first blueprint of the cell type specific molecular changes in response to noise between male and female mice and PTS and TTS in two time points (6 and 24h); (b) it identified key molecular signaling pathways for focused intervention to prevent/reverse NIHL; (c) it identified critical physiologic differences in the response to noise between sexes with *immediate* impact on study design in the field; finally, it identified IKZF2 as a critical regulator of OHC maturation and function, a finding which was published in the journal *Nature*.

What opportunities for training and professional development has the project provided?

Training

1. The PI, Ronna Hertzano, participated in an RNA-seq course performed at the NIH. This led to the identification of new analysis platforms and specifically, familiarity with the Cytoscape environment now used in the laboratory (Year 1). Detailed engagement in leading a study on physiology of hearing and the response to noise exposure that led to developing 5 years of experience and expertise in the field. Engagement in conversation and scientific exchange with numerous investigators in the field and organization of a symposium focused on acquired hearing loss at the University of Maryland School of Medicine (2017).
2. Zachary Margulies, a technician hired for the project was mentored by the Co-I Didier Depireux. Zachary learned over the first year of the project how to perform and analyze ABR and DPOAE and became proficient at performing these tasks routinely (Years 1-2).
3. Yoko Ogawa, PhD, a developmental biologist originally trained in the field of zebrafish, was hired for the project and was trained by Beatrice Milon, PhD to perform inner ear dissections, cytocochleograms and immunohistochemistry (Years 1-2).
4. Sunayana Mitra, PhD was mentored by the Co-I Didier Depireux on how perform and analyze ABR and DPOAE and became proficient at performing these tasks routinely (Years 2-3). Sunayana participated in a pre-conditioning conference (Preconditioning in Biology and Medicine Mechanisms and Translational Research, April 19-20, 2016) and was carrying out the pre-conditioning experiments for the project (Years 2-3). Sunayana participated in the Association for Research in Otolaryngology meeting where she was selected for an oral presentation, as well as in the EARssentials course at the NIH (Year 3).
5. Beatrice Milon, PhD – learned to perform cytocochleograms, and synapse counts and has been training the other members of the team to perform these techniques (Years 1-5). Beatrice participated in the Association for Research in Otolaryngology meetings (Years 3-4-5) as well as in the Gordon Research Conference where she expanded her knowledge both on hidden hearing loss as well as central pathways in auditory processing (Year 4).
6. Ryan Casserly, MD, worked in the Hertzano laboratory in a 5-month full time research rotation to characterize the differential response to noise between male and female mice (Year 3). Ryan learned how to perform and analyze ABR, and presented his findings in the Association for Research in Otolaryngology (Year 4).
7. Benjamin Shuster, BS, learned how to perform and analyze ABR. Benjamin participated in the Association for Research in Otolaryngology (Years 4-5) as well as in the Gordon Research Conference where he presented data on sex differences in hearing and the response to noise (Year 4).
8. Laboratory meetings - since obtaining funding from the DoD the entire Hertzano laboratory engages in in-depth study of current literature and techniques to study NIHL and has been increasing their knowledge and experience through laboratory meetings and journal clubs. The team has also trained two additional laboratories in the department (laboratories of Drs. Ahmed and Riazuddin) who now focus some of their work on NIHL.

Professional Development

The group formed an RNA-seq consultation team which includes Yang Song, an informatics specialist at the Institute for Genome Sciences (IGS), who was attending all laboratory meetings. Through routine weekly meetings, the group was challenged and solved difficulties regarding sequencing of very small amounts of starting material, precipitated from RiboTag mice, and continues to actively learn and review all literature in the field (Years 1-5). In addition, we developed a new series of laboratory meetings named H&H (Hearing and Hormones) attended by Dr. Jessica A. Mong (a neuroendocrinologist with a focus on sex differences in the brain) and our group (Years 3-5). Finally, the PI organized a translational auditory and vestibular research day focused on NIHL in the fall of 2017. This day was a tremendous success with over 100 participants from universities in the region was used to educate and disseminate knowledge on NIHL (**agenda attached in appendix 6**).

How were the results disseminated to communities of interest?

The results were disseminated through multiple abstracts resulting in oral presentations and posters at conferences including the MidWinter Meeting of the Association for Research in Otolaryngology in years 3, 4 and 5, as well as the Gordon Research Conference, Auditory System in year 4.

The results were also disseminated through a translational auditory and vestibular research day organized by the PI at the University of Maryland Baltimore in year 3.

During the 5 years of the project, we published three manuscripts describing our results and two reviews.

What do you plan to do during the next reporting period to accomplish the goals?

Nothing to report

4. IMPACT:

What was the impact on the development of the principal discipline(s) of the project?

The results of the project were impactful in several ways:

First, by studying the translatome of adult outer hair cells, we made a major breakthrough, discovering a regulatory gene with a key role in outer hair cell development and function. The significance of this discovery is mirrored by its publication as a manuscript in the journal *Nature*. Second, our studies were the first to both discover and perform an in-depth report of sex-differences in the susceptibility to noise induced hearing loss. While this led to a series of mechanistic studies in our laboratory, its first immediate contribution was in elevating the awareness to this sex-dependent dimorphism in hearing and the response to noise. Based on our presentations and publication (already cited 14 times since published in 2018), this finding has had a widespread impact on the field on changing the standard requirements of experimental design – now mandating separating the analysis for males and females in many studies. Third, our transcriptome analyses of the cell type-specific outcomes from permanent and temporary threshold

shift noise exposures are being prepared for publication and will serve as the molecular blueprint for NIHL. The data are going to be disseminated via the gEAR portal we developed (umgear.org) which allows researchers easy and meaningful access to genomic data without the requirement for knowledge of programming. In addition, we expect these data to form the foundation for hypothesis generation and drug development to prevent and treat NIHL. Last, our published studies will shed light on the molecular differences in the response of male and female mice to noise exposure. Importantly, the scope of the proposed work in the grant was purely descriptive and the funding did not include any support for downstream mechanistic analyses.

What was the impact on other disciplines?

As part of our study we had to develop new and improved approaches to analyze gene expression from minute amounts of genetic starting material. Our approach was described in a published manuscript (Song et al. 2018) that while new, was already cited 5 times since published in 2018.

What was the impact on technology transfer?

This research has led to a change in the standard protocols used to study NIHL. Based on our published findings and follow up articles (e.g., Sex differences in hearing: Probing the role of estrogen signaling. Shuster BZ, Depireux DA, Mong JA and Hertzano R. J Acoust Soc Am. 2019 Jun;145(6):3656. PMID: 31255106) many researchers in the field now both include females in their studies and separate the analyses for males in females. Furthermore, the study of both males and females, separately, is more strongly enforced by study sections, and a number of laboratories have taken studying sex differences in hearing as a primary interest. In addition, several pharma companies including, for example, *Decibel Therapeutics*, have expressed interest in the data generated by the project. While we have not established contracts to share the data with them pre-publication, we anticipate them using the data post-publication for drug development.

What was the impact on society beyond science and technology?

We believe that our study results will change the way female animals are included in studies for noise induced hearing loss. Several publications have addressed the lack of inclusion of female subjects in research of NIHL (e.g., Sex bias in basic and preclinical noise-induced hearing loss research. Lauer AM, Schrode KM. Noise Health. 2017 Sep-Oct;19(90):207-212. PMID: 28937014), however, until our studies were published no studies provided a strong rationale for including females in such studies.

5. CHANGES/PROBLEMS: Changes in approach and reasons for change

Years 1-2: We compared the efficacy of pre-conditioning treatments and reported that some of the canonical pre-conditioning treatments may have limited efficacy such as restraint stress or steroids. As our goal was to focus on the molecular mechanism of robust pre-conditioning interventions, we decided to focus on TTS-inducing noise and heat-shock. Additionally, a new publication at that time reported SAHA as a treatment for NIHL so we decided to test its efficacy in our model.

Year 2: Our calibration experiments for SAHA led us to find that there are profound differences in the response to noise exposure between male and female mice. Therefore, we changed the approach to analyze male and female mice separately.

Year 2: Change in sequencing approach – the original project called for sequencing using the NuGEN kit. Detailed analysis identified multiple deficiencies when taking this approach. We therefore performed a comprehensive analysis and decided to use the NEB kit instead. This analysis resulted in a manuscript.

Years 3-4: The approach was changed to study male and female mice separately with the approval of the awarding agency grants official. The comprehensive analysis of different sequencing kits led us to identify TaKaRa SMART-Seq v4 Ultra Low Input RNA Kit as a kit efficient for sequencing from very small amount of RNA, allowing us to reduce the number of animals per replicate.

Year 5: The work continued as planned. While we budgeted for the additional animals in the revised plan approved by the DoD (for including both males and females in repeating much of the work of years 1-3), we did not budget for the labor. We used discretionary funds to continue the labor. Delays in obtaining mice from our specialized crosses extended the project far beyond the planned timeline. We therefore completed the sequencing and analysis of the TTS and PTS separated by sex and will complete part of the heat shock experiments as time and animals allow – as the latter, extended far above the allotted funds for the project.

Actual or anticipated problems or delays and actions or plans to resolve them

Year 1: An initial delay occurred due to late ACURO approval. As animal experiments started later than originally planned, we hired the post doc for the project only in January of 2015 and planned to continue working on the project 3-9 months following its official completion.

Years 1-2: As a result of the variability in the efficacy of pre-conditioning treatments, we added a calibration and cross-comparison step. However, the delay caused by these calibrations was outweighed by the quality and significance of the results.

Years 3-4: We had a delay in the breeding efficiency and therefore the baseline heat shock experiments were done on C57BL/6 and not the mixed background. However, with improvements to the sequencing protocol, we were able to catch up over the year thanks to requiring less mice per biological replicate.

Year 5: In year 5 we continued working on the project supporting the labor and animal costs primarily from discretionary funds.

Changes that had a significant impact on expenditures

Years 1-2: New research published indicated an important role for additional inner ear cell types following noise exposure. To maximize the use of the tissue obtained from our noise exposed animals, we decided to sequence both the entire cochlea as well as the immuno-precipitated cell type-enriched RNA. While this results in a much better understanding of the molecular changes and their origin in the sequenced samples, it did increase the cost. However, the cost of sequencing was offset by molecularly investigating only the top 1-2 most efficacious pre-conditioning treatments instead of all three as stated in the original plan.

Year 2: The calibration experiments and identification of significant differences in the response to noise between male and female mice originally resulted in an increase in animal costs and reagents for histology, confocal analysis and personnel time. The findings, however, are of great significance, both to our project as well as to the ear research community that is focused on studying NIHL.

Years 3-4: All changes in structure and expenditures had been reported in the in-person review (within the presentation) and were within the limits of the budget of the project.

Year 5: We realized that while we budgeted for the increase in sequencing costs and animals, we did not for the labor. This led to using discretionary funds to support much of the labor. The PI also did not withdraw salary from the grant starting from year 4 to offset the cost. We carried the project as far as possible to support it without additional funding.

Significant changes in use or care of human subjects, vertebrate animals, biohazards, and/or select agents

Significant changes in use or care of human subjects

Nothing to report

Significant changes in use or care of vertebrate animals

Years 1-2: Amendments were submitted to include Dexamethasone and SAHA as pre-conditioning treatments. Both amendments were approved by the IACUC and ACURO.

Year 3: An amendment to request additional mice to focus on the immune system response after noise exposure was approved by the IACUC and the ACURO. An amendment to change the breeding scheme for heat shock experiment was approved.

Year 4: Our IACUC animal protocol #0915006 linked to this project expired on September 16th, 2018. A new animal protocol to complete the experiments was submitted and approved by the IACUC.

Year 5: Nothing to report.

Significant changes in use of biohazards and/or select agents

Years 1-2: Amendments were submitted to include Dexamethasone and SAHA as pre-conditioning treatments. Both amendments were approved by the IACUC and ACURO.

Year 3-5: Nothing to report

6. PRODUCTS:

- **Publications, conference papers, and presentations**

  Journal publications

Udagawa T, Milon B, Atkinson PJ, Song Y, Huarcaya Najarro E, Scheibinger M, Hertzano R, Cheng AG. *Robust mitotic regeneration by hidden progenitors after ablation of Lgr5+ cochlear cells*. In revision for Developmental Cell

Clifford RE, Hertzano R, Ohlemiller KK. *Untangling the genomics of noise-induced hearing loss and tinnitus: Contributions of Mus musculus and Homo sapiens*. J Acoust Soc Am. 2019;146(5):4007. doi:10.1121/1.5132552. Federal support: yes

Shuster BZ, Depireux DA, Mong JA, Hertzano R. *Sex differences in hearing: Probing the role of estrogen signaling*. J Acoust Soc Am. 2019;145(6):3656. Federal support: yes

Chessum L, Matern MS, Kelly MC, Johnson SL, Ogawa Y, Milon B, McMurray M, Driver EC, Parker A, Song Y, Codner G, Esapa CT, Prescott J, Trent G, Wells S, Dragich AK, Frolenkov GI, Kelley MW, Marcotti W, Brown SDM, Elkon R, Bowl MR, Hertzano R. *Helios is a key transcriptional regulator of outer hair cell maturation*. Nature. 2018 Nov;563(7733):696-700. Federal support: yes

Song Y, Milon B, Ott S, Zhao X, Sadzewicz L, Shetty A, Boger E.T, Tallon LJ, Morell RJ, Mahurkar A, Hertzano R. *A Comparative Analysis of Library Prep Approaches for Sequencing Low Input Translatome Samples*. BMC Genomics 2018. Federal support: yes

Milon B, Mitra S, Song Y, Margulies Z, Casserly R, Drake V, Mong JA, Depireux DA, Hertzano R. *The impact of biological sex on the response to noise and otoprotective therapies against acoustic injury in mice*. Biol Sex Differ. 2018 Mar 12;9(1):12. Federal support: yes

Books or other non-periodical, one-time publications.

Nothing to report.

Other publications, conference papers and presentations.

*Mitra S, Drake V, Margulies Z, Milon B, Song Y, Depireux D and Hertzano R (2017) *The impact of sex on the response to noise and otoprotective therapies against acoustic injury in mice*. Association for Research in Otolaryngology, Baltimore, MD, USA.

*Song Y, Milon B, Ott S, Zhao X, Sadzewicz L, Mahurkar A and Hertzano R (2017) *RiboTag-Seq: a comparative analysis of library prep approaches for sequencing low input translatome samples*. Association for Research in Otolaryngology, Baltimore, MD, USA.

May L, Ryals M, Milon B, Boger E, Hertzano R, Morell R, Cunningham L (2017). *Cell-type Specific Transcriptional and Translational Responses to Heat Shock in Mouse Utricle*. Association for Research in Otolaryngology, Baltimore, MD, USA

Hertzano H, Milon B, Mitra S, Ogawa Y, Shetty A, Zhang X, Depireux D, Elkon R (2018) *A cell-type specific blueprint of the molecular changes following noise exposure*. Association for Research in Otolaryngology, San Diego, CA, USA.

Casserly R, Mitra S, Viechweg S, Shuster B, Myers A, Song Y, Milon B, Depireux D, Mong J, Hertzano H (2018) *Estrogenic protection from noise-induced hearing loss in*

females but not in males. Association for Research in Otolaryngology, San Diego, CA, USA.

Milon B, Ogawa Y, Song Y, Elkon R, Hertzano R (2018) *Translatome Analysis of Outer Hair Cells and Supporting Cells from Adult Mouse Inner Ears*. Association for Research in Otolaryngology, San Diego, CA, USA.

*Shuster B, Casserly R, Viechweg S, Myers A, Milon B, Depireux D, Mong J, Hertzano H (2018) *Probing the Role of Estrogen in Hearing*. Gordon Research Conference, Auditory System, Smithfield, RI, USA.

Milon B, Mitra S, Ogawa Y, Shuster B, Song Y, Depireux D, Elkon R, Hertzano R (2019) *The Cell-Type Specific Response to Noise in Adult Mouse Inner Ears*. Association for Research in Otolaryngology, Baltimore, MD, USA

* Shuster B, Milon B, Casserly R, McMurray M, Viechweg S, Davidson K, Depireux D, Mong J, Hertzano R (2019) *Probing Estrogen's Role in Hearing Physiology: Implications for Noise-Induced Hearing Loss*. Association for Research in Otolaryngology, Baltimore, MD, USA

Sadler E, Ryals M, May L A, Milon B, Boger E T, Morell R J, Hertzano R, Cunningham L (2019). *Cell-Specific Transcriptional Responses to Heat Shock in the Mouse Utricle Using RiboTag.* Association for Research in Otolaryngology, 42TH Annual MidWinter Meeting, Baltimore, MD, USA

- **Website(s) or other Internet site(s)**

  umgear.org – is a portal for multi-omic data visualization, sharing and analysis, pioneered, developed and maintained by the PI of this proposal. All of the molecular data generated by this proposal will be shared via this portal at the time of publication. The portal is the #1 go-to site in the ear field for mining genomic data with over 600 researchers with active accounts.

- **Technologies or techniques**

  Improved approaches for sequencing translatome data as described in Song et al. 2018 (**appendix 3**).

- **Inventions, patent applications, and/or licenses**

  Nothing to report.

- **Other Products**

  Models: We have generated and validated the following mouse models crossed for experiments of cell type-specific translatome analysis:

  - PrestinCreER^{T2};RiboTag for outer hair cell translatome analysis.

- Sox2CreER^{T2};RiboTag for supporting cell and glial cells of the spiral ganglion translatome analysis.

Equipment: We developed a noise exposure chamber for mice that we described in Milon et al. This chamber allows exposing 8 mice simultaneously to sound in a sound proof box. The model has since been replicated by the laboratory of Saima Riazuddin, PhD, following blueprints obtained by our laboratory.

Data: We have developed a molecular blueprint for the inner ear cell type-specific outcomes of both temporary and permanent noise induced hearing loss, which will serve as a foundation for drug development and biomarker analysis of noise and treatment outcomes in the field.

7. PARTICIPANTS & OTHER COLLABORATING ORGANIZATIONS

What individuals have worked on the project?

Name	Ronna Hertzano
Project Role	PI
Researcher identifier	
Nearest person month worked:	2 (Y1); 2 (Y2); 2 (Y3); 2 (Y4); 2 (Y5)
Contribution to the project	Overall responsibility for the proposal and all aspects of the research program including: hiring and training personnel, ensuring quality of data, interpretation of data, oversight of methods, administrative responsibility and reporting to the DoD.
Funding support	NIH R01, DC013817; Action on Hearing Loss. G65_Bowl; NIH R01, DC003544, Hearing Health Foundation – HRP support for gEAR. MPower The State Grant – Center for Excellence in Cochlear Implants (Co-PI); R01 DC016595 (Co-I); NIMH, R24MH114815 (PI)

Name	Didier Depireux
Project Role	Co-I
Researcher identifier	
Nearest person month worked:	1.2 (Y1); 1.2 (Y2); 1.2 (Y3); 1.2 (Y4); 1.2 (Y5)

Contribution to the project	Set up the noise exposure system, ordered the noise exposure box, trained Zachary Margulies, oversees the noise exposure protocols, ABR and DPOAE setup and measurements.
Funding support	MII, Translational Research in Hearing Foundation, Capita foundation, NIH/NIDCR

Name	Ran Elkon
Project Role	Co-I
Researcher identifier	
Nearest person month worked:	1.2 (Y1); 1.2 (Y2); 1.2 (Y3); 1.2 (Y4); 1.2 (Y5)
Contribution to the project	Data analysis and study design
Funding support	

Name	Beatrice Milon
Project Role	Research Specialist and Supervisor
Researcher identifier	
Nearest person month worked:	6 (Y1); 6 (Y2); 6 (Y3); 6 (Y4); 6 (Y5)
Contribution to the project	Study design, tissue collection, schedule oversight, training of Yoko Ogawa, RiboTag IP and RNA analysis
Funding support	NIH R01, DC013817

Name	Yoko Ogawa
Project Role	Post-Doctoral Fellow
Researcher identifier	
Nearest person month worked:	9 (Y1); 5 (Y2); 5 (Y3)
Contribution to the project	Tissue collection, cytocochleograms, validation, animal care
Funding support	

Name	Zachary Margulies
Project Role	Research Assistant
Researcher identifier	
Nearest person month worked:	12 (Y1); 7 (Y2)
Contribution to the project	Performs all noise exposures, hearing measurements, pre-conditioning, assists with writing animal protocols
Funding support	

Name	Sunayana Mitra
Project Role	Post-Doctoral Fellow
Researcher identifier	
Nearest person month worked:	5 (Y2); 12 (Y3)
Contribution to the project	Performs all noise exposures, hearing measurements, pre-conditioning, tissue collection, animal care, assists with writing animal protocols
Funding support	

Name	Yang Song
Project Role	Informatics Analyst
Researcher identifier	
Nearest person month worked:	1.2 (Y3); 1.2 (Y4); 1.2 (Y5)
Contribution to the project	Data analysis
Funding support	

Name	Ryan Casserly
Project Role	Resident
Researcher identifier	
Nearest person month worked:	5 (Y3)

Contribution to the project	Characterized the sex differences in hearing
Funding support	

Name	Benjamin Shuster
Project Role	Research Assistant
Researcher identifier	
Nearest person month worked:	12 (Y4); 12 (Y5)
Contribution to the project	Tissue collection, noise exposures, male/female analysis, preparation of review on sex differences in hearing
Funding support	

Has there been a change in the active other support of the PD/PI(s) or senior/key personnel since the last reporting period?

Year 1: The PI and Beatrice Milon, PhD are now supported also by a NIH grant (NIH R01, DC013817). This does not conflict with the current project. The PI changed effort from 20% to 15%.

Year 1: Ran Elkon (Co-I) changed position from a research fellow in the Netherlands Cancer Institute to a Principal Investigator at the Sackler School of Medicine, Tel Aviv University.

Year 2: Yang Song, PhD, has been working on the project 20% effort (informatics support) but the PI has not been asked to pay for her salary (supported by the Institute of Genome Sciences).

Year 3: The PI has been partially supported by the HRP grant to use the gEAR portal to support the HRP.

Year 4, 5 – Starting from year 4, the PI has stopped to draw support from the grant, as it was a 3-year grant, and with the change in work plan to accommodate for critical sex-specific changes in the response to noise between males and females, the project was extended and also more expensive. During this time, the PI has obtained support from philanthropy (which also supported some of the work for the project by others), grant support from the NIH/NIDCD as a co-investigator on a grant looking at the downstream signaling cascade from Pou3f4, from the NIH/NIMH to support the BRAIN initiative neuroscience multi-omic archive (NeMO Archive) with a visualization and analysis environment, and from the BSF to study molecular pathways in inner ear development.

What other organizations were involved as partners?

Tel Aviv University – Ran Elkon, PhD – bioinformatic analysis.

8. SPECIAL REPORTING REQUIREMENTS

COLLABORATIVE AWARDS: N/A

QUAD CHARTS: submitted – W81XWH Hertzano FINAL.

9. APPENDICES:

Appendix 1: Copy of the manuscript published in Nature describing Ikzf2/Helios as a major transcription factor regulating maturation of outer hair cells.

Appendix 2: Copy of the manuscript published in Biology of Sex Differences describing the different response to noise exposure between male and female mice.

Appendix 3: Copy of the manuscript published in BMC Genomics describing the comparison of several kits for library preparation from low amount of RNA.

Appendix 4: Copy of the manuscript published in The Journal of the Acoustical Society of America reviewing the literature about the relation between estrogen and hearing.

Appendix 5: Copy of the manuscript published in The Journal of the Acoustical Society of America reviewing the literature about the genetic susceptibility to noise-induced hearing loss and tinnitus.

Appendix 6: Copy of the program of the Translational Auditory and Vestibular Research Day focused on noise-induced hearing loss organized by Dr Hertzano.

LETTER

https://doi.org/10.1038/s41586-018-0728-4

Helios is a key transcriptional regulator of outer hair cell maturation

Lauren Chessum[1,11], Maggie S. Matern[2,11], Michael C. Kelly[3], Stuart L. Johnson[4], Yoko Ogawa[2], Beatrice Milon[2], Mark McMurray[2], Elizabeth C. Driver[3], Andrew Parker[1], Yang Song[5], Gemma Codner[6], Christopher T. Esapa[1], Jack Prescott[1], Graham Trent[2], Sara Wells[6], Abigail K. Dragich[7], Gregory I. Frolenkov[7], Matthew W. Kelley[3], Walter Marcotti[4], Steve D. M. Brown[1], Ran Elkon[8,9], Michael R. Bowl[1,12]* & Ronna Hertzano[2,5,10,12]*

The sensory cells that are responsible for hearing include the cochlear inner hair cells (IHCs) and outer hair cells (OHCs), with the OHCs being necessary for sound sensitivity and tuning[1]. Both cell types are thought to arise from common progenitors; however, our understanding of the factors that control the fate of IHCs and OHCs remains limited. Here we identify *Ikzf2* (which encodes Helios) as an essential transcription factor in mice that is required for OHC functional maturation and hearing. Helios is expressed in postnatal mouse OHCs, and in the *cello* mouse model a point mutation in *Ikzf2* causes early-onset sensorineural hearing loss. *Ikzf2*$^{cello/cello}$ OHCs have greatly reduced prestin-dependent electromotile activity, a hallmark of OHC functional maturation, and show reduced levels of crucial OHC-expressed genes such as *Slc26a5* (which encodes prestin) and *Ocm*. Moreover, we show that ectopic expression of *Ikzf2* in IHCs: induces the expression of OHC-specific genes; reduces the expression of canonical IHC genes; and confers electromotility to IHCs, demonstrating that *Ikzf2* can partially shift the IHC transcriptome towards an OHC-like identity.

The mature mammalian cochlea contains two distinct types of sensory cells, IHCs and OHCs, each of which are highly specialized and, in humans, do not regenerate once they are damaged or lost[2]. Progressive loss of these cells, particularly the OHCs, underlies much of the aetiology of age-related hearing loss—a worldwide epidemic[3,4]. Although these two cell types were first described by Retzius in the 1800s, the mechanisms that underlie the specification of their common progenitor cells to functional inner versus outer hair cells remain poorly understood. In addition, attempts to direct stem cells towards hair cell fates have, so far, resulted only in the formation of immature cells that lack many of the markers of mature IHCs or OHCs[5]. Given the vulnerability of the OHCs, identifying factors that specify OHC fate is crucial, not only for understanding the biology of this unique cell type, but also for ultimately working towards regenerative therapies for hearing loss.

To define a set of high-confidence OHC-expressed genes for downstream gene regulation analyses, we crossed the knock-in prestin-CreER^{T2} mouse, which can be induced to express Cre recombinase specifically in OHCs, with a transgenic RiboTag mouse, to enable OHC-specific ribosome immunoprecipitation[6,7]. Cochlear ducts from the resulting *RiboTag*$^{HA/+}$;*prestin*$^{creERT2/+}$ mice were collected at five postnatal time points (postnatal day (P) 8, 14 and 28, and 6 and 10 weeks), and actively translated OHC transcripts were enriched for by ribosome immunoprecipitation, followed by RNA sequencing (RNA-seq) of all immunoprecipitated and paired input RNA (Extended Data Fig. 1a, b, Supplementary Table 1). We calculated an OHC enrichment factor based on the immunoprecipitated/input RNA $\log_2$ fold change for each gene at each time point (Supplementary Table 2). Reassuringly, known postnatal hair cell-enriched and OHC-expressed genes such as *Pou4f3*, *Gfi1*, *Strc*, *Ocm* and *Slc26a5* generally had high enrichment factor values across all time points (enrichment factor (EF) > 1), whereas prominent IHC marker genes such as *Otof*, *Atp2a3* and *Slc17a8* were generally depleted from the immunoprecipitated samples (EF < -1). In addition, marker genes for supporting cells, neurons and otic mesenchyme were also depleted (Extended Data Fig. 1c). Further informatics analyses of our RiboTag OHC dataset demonstrated a systematic enrichment of OHC markers and a depletion of IHC markers previously identified in an adult mouse OHC and IHC transcriptomic dataset[8], and classified the OHC-enriched transcripts into three clusters (Extended Data Fig. 1d–f, Supplementary Table 3). Intersecting genes with transcripts that were enriched in OHCs in our most mature RiboTag OHC data point (10 weeks, EF > 0.5) compared with the published dataset[8] resulted in a list of 100 highly confident postnatal OHC markers that are significantly and consistently enriched in postnatal OHCs (Fig. 1a, Supplementary Table 4). We and others have previously shown that relevant transcriptional regulators can be discovered by analysing the promoters of cell-type-specific genes to identify statistically over-represented transcription factor-binding motifs[9,10]. A transcription factor-binding motif prediction analysis of the 100 OHC marker genes identified several enriched motifs in the 20-kb regions that centred around the transcription start site, the top five of which correspond to the transcription factors HNF4A, MZF1, POU3F2, Helios and RFX3[11]. Of these, only *Ikzf2* (which encodes Helios) was included in the list of 100 OHC marker genes, and was found to be markedly enriched in OHCs at all time points (Fig. 1b, c), with an approximately fourfold enrichment in OHCs compared to IHCs in the previously published dataset[8] (Supplementary Table 4). Further characterization of Helios protein expression in the inner ear confirmed that it is restricted to the OHC nuclei starting from P4, and persists in functionally mature OHCs (Fig. 1d–f, Extended Data Fig. 2a). Together, these data suggest an important role for Helios in regulating the OHC transcriptome from early postnatal to adult stages.

A recent phenotype-driven *N*-ethyl-*N*-nitrosourea (ENU) mutagenesis screen, undertaken at the MRC Harwell Institute, identified a C-to-A transversion at nucleotide 1551 of *Ikzf2* in the *cello* mouse mutant, causing a non-synonymous histidine-to-glutamine substitution (p.H517Q) in the encoded Helios transcription factor[12] (Fig. 1g, Extended Data Fig. 2b–d). A combination of in silico mutation analyses, structural 3D modelling, immunolabelling of Helios in the *cello* mutant mice, and in vitro assays predicted and validated a deleterious effect of the *cello* mutation on the ability of Helios to dimerize, without impairing its cellular localization (Fig. 1g, Extended Data Figs. 2e and 3). We further investigated the functional role of Helios in hearing by

[1]Mammalian Genetics Unit, MRC Harwell Institute, Oxfordshire, UK. [2]Department of Otorhinolaryngology Head and Neck Surgery, University of Maryland School of Medicine, Baltimore, MD, USA. [3]National Institute on Deafness and Other Communication Disorders, National Institutes of Health, Bethesda, MD, USA. [4]Department of Biomedical Science, University of Sheffield, Sheffield, UK. [5]Institute for Genome Sciences, University of Maryland School of Medicine, Baltimore, MD, USA. [6]Mary Lyon Centre, MRC Harwell Institute, Oxfordshire, UK. [7]Department of Physiology, College of Medicine, University of Kentucky, Lexington, KY, USA. [8]Department of Human Molecular Genetics and Biochemistry, Sackler School of Medicine, Tel Aviv University, Tel Aviv, Israel. [9]Sagol School of Neuroscience, Tel Aviv University, Tel Aviv, Israel. [10]Department of Anatomy and Neurobiology, University of Maryland School of Medicine, Baltimore, MD, USA. [11]These authors contributed equally: Lauren Chessum, Maggie S. Matern. [12]These authors jointly supervised this work: Michael R. Bowl, Ronna Hertzano. *e-mail: m.bowl@har.mrc.ac.uk; rhertzano@som.umaryland.edu

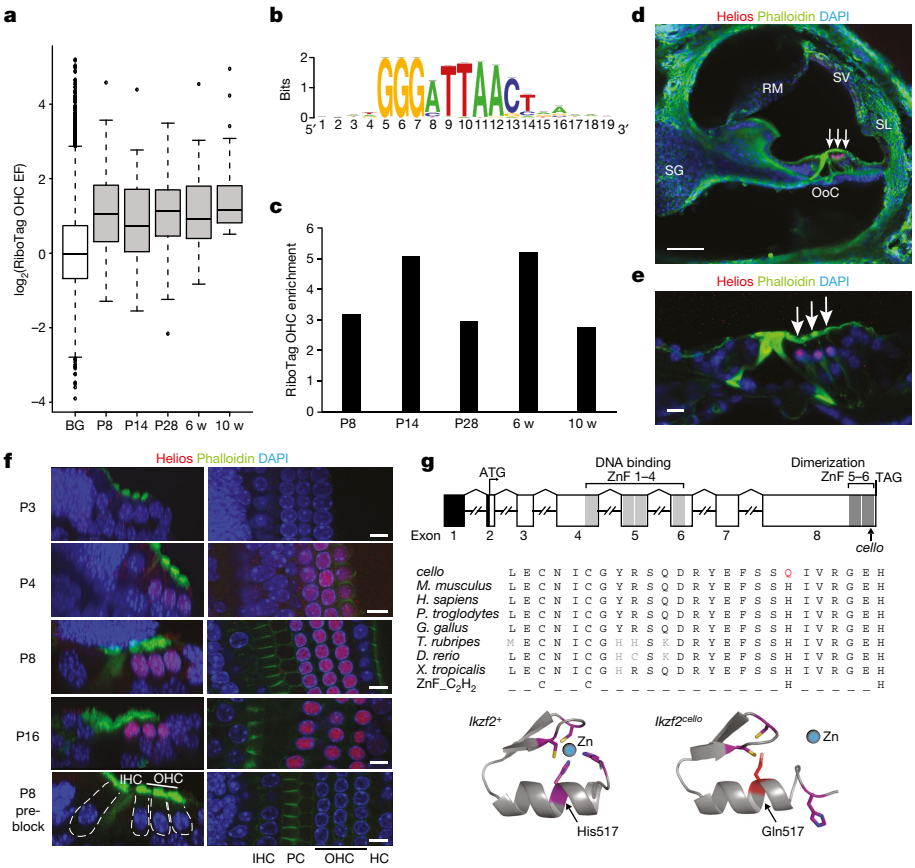

Fig. 1 | Helios is a candidate regulator of OHC genes. a, The 100 OHC marker genes ($n = 100$) are enriched in OHCs at all RiboTag OHC dataset time points compared to the expression of all other genes detected (background, BG) ($n = 13{,}044$). *P* values: P8 $= 1.73 \times 10^{-17}$, P14 $= 6.55 \times 10^{-12}$, P28 $= 1.60 \times 10^{-18}$, 6 weeks (w) $= 7.79 \times 10^{-18}$, 10 weeks $= 1.43 \times 10^{-33}$ (two-sided Wilcoxon's test). Centre line represents median enrichment factor (EF; $\log_2$ fold change), box demarcates first and third quartiles, whiskers demarcate first and third quartile $\pm 1.5 \times$ interquartile range (IQR) values, dots denote single outliers. **b**, Transcription factor-binding motif analysis using the 100 highly confident OHC marker genes identifies the binding signature for Helios as significantly overrepresented. Normalized enrichment score (NES) $= 3.85$; NES ≥ 3.0 corresponds to a false discovery rate (FDR) of 3–9%; see ref. [11]. **c**, *Ikzf2* transcript enrichment in OHCs as measured by RiboTag OHC RNA-seq. **d**, Specific expression of Helios in the nuclei of wild-type P8 OHCs (white arrows). $n = 3$ biologically independent samples. Scale bar, 50 μm. OoC, organ of Corti; RM, Reissner's membrane; SG, spiral ganglion; SL, spiral ligament; SV, stria vascularis. **e**, Helios expression is maintained in wild-type OHCs at 1 month (white arrows). $n = 3$ biologically independent samples. Scale bar, 10 μm. **f**, Helios is detected in wild-type OHCs from P4 and is maintained in mature P16 OHCs. $n = 2$ (P3) and $n = 4$ (P4, P8 and P16) biologically independent samples. Specificity is confirmed by the loss of labelling when the anti-Helios antibody is 'pre-blocked' with its immunizing peptide. $n = 5$ biologically independent samples. Scale bars, 10 μm. HC, Hensen's cells; PC, pillar cells. **g**, Top, the genomic and domain structure of *Ikzf2*. Black, 5′ untranslated region; light grey, N-terminal DNA-binding domain; dark grey, C-terminal dimerization domain. The *Ikzf2*^{cello} mutation lies in ZnF6. Bottom, further alignment of the Helios ZnF6 sequence with its paralogues and the classical Cys_2His_2 ZnF motif shows that the H517Q *cello* mutation causes substitution of a highly conserved zinc-coordinating histidine residue. 3D modelling of wild-type *Ikzf2*$^{+}$ ZnF6 and mutant *Ikzf2*^{cello} ZnF6 illustrates the requirement of residue His517 for zinc coordination, which is not possible when residue Gln517 is substituted.

assessing auditory brainstem response (ABR) thresholds in wild-type and *cello* mice across several time points. Results show that *Ikzf2*$^{cello/cello}$ mice have progressive deterioration of hearing function that starts as early as P16 (>60 dB sound pressure level (SPL)), with a threshold of ≥85 dB SPL by 9 months (Fig. 2a, b, Extended Data Fig. 4a–c). Using scanning electron microscopy, we show that the ultrastructure of the cochlear sensory epithelia and hair cell stereocilia bundles in the *cello* mice appear normal up to 1 month of age, after which the OHC bundles, and later the IHC bundles, begin to degenerate (Extended Data Figs. 4d, 5a–d, Supplementary Tables 5, 6). These data indicate that the hearing impairment in *cello* mice precedes the loss of hair cell bundles, and suggest that the Helios mutation instead leads to a functional deficit in OHCs. Furthermore, by using a second *Ikzf2* mutant allele (*Ikzf2*^{del890}), which leads to an in-frame deletion of the third coding exon, we confirm *Ikzf2* as the causative gene that underlies the auditory dysfunction in the *cello* mutants. At 1 month of age, *Ikzf2*$^{cello/del890}$ compound heterozygotes display increased ABR thresholds (up to 40 dB SPL) compared to heterozygotes and wild-type mice (Extended Data Fig. 5e, f), confirming *Ikzf2*^{cello} as the causative allele in the *cello* mutant.

To explore the effect of the *cello* mutation on OHC physiology, we investigated the basolateral properties of OHCs. We found that the mechanoelectrical transducer (MET) current (Extended Data Fig. 6a–c) and the adult-like potassium (K^+) current $I_{K,n}$ (Extended Data Fig. 6d–h) have normal biophysical characteristics in *Ikzf2*$^{cello/cello}$ OHCs. The resting membrane potential (V_m) of OHCs is also similar between genotypes (*Ikzf2*$^{cello/+}$: -68 ± 2 mV (mean ± s.e.m.); *Ikzf2*$^{cello/cello}$: -70 ± 1 mV). We then investigated whether Helios regulates OHC electromotile activity. We found that stepping the membrane potential from −64 mV to +56 mV causes the OHCs from both genotypes to shorten (Fig. 2c, d), as previously described[13–15]. However, *Ikzf2*$^{cello/cello}$ OHCs show significantly reduced movement compared to *Ikzf2*$^{cello/+}$ control OHCs (Fig. 2e), even when the values are normalized to their reduced surface area (Fig. 2f). We also found that young adult *Ikzf2*$^{cello/cello}$ mice have significantly reduced distortion product oto-acoustic emission (DPOAE) responses (≤−15 dB SPL) compared to littermate controls (Fig. 2g), further demonstrating impaired OHC function.

To identify genes regulated by Helios in OHCs, we compared gene expression from the cochleae of P8 *Ikzf2*$^{cello/cello}$ and their wild-type

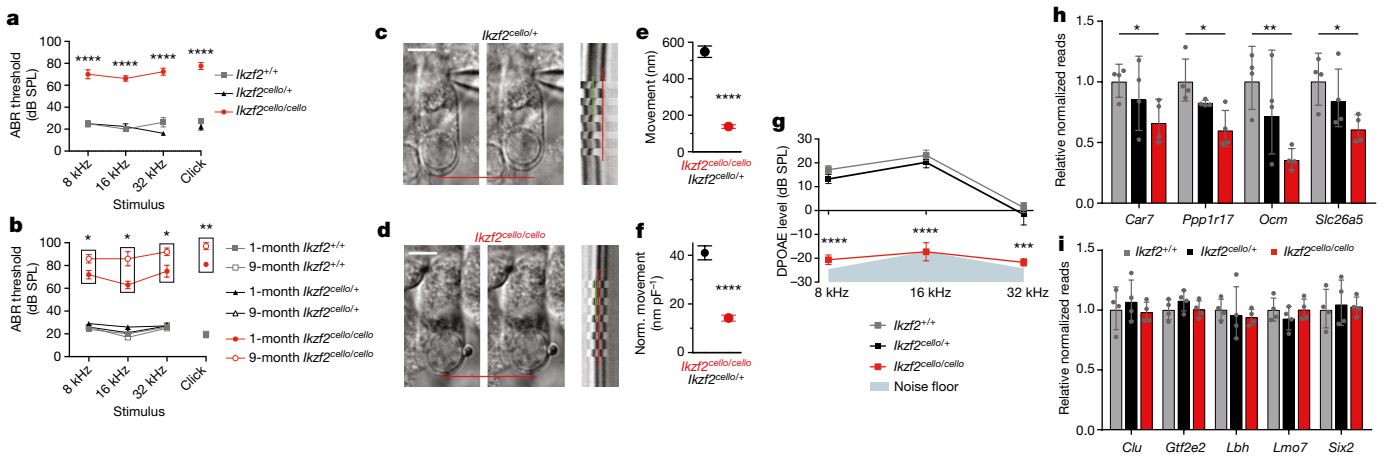

Fig. 2 | Helios is required for hearing and OHC electromotility. **a**, **b**, Averaged ABR thresholds for *cello* mice at P16 (**a**) and 1 and 9 months of age (**b**). Age-matched $Ikzf2^{+/+}$ and $Ikzf2^{cello/+}$ controls display thresholds within the expected range (15–30 dB SPL) at all time points tested. $n = 4$ (**a**) and $n = 5$ (**b**) biologically independent animals per genotype at each time period. Data are mean ± s.e.m. $^{****}P < 0.0001$ (P16 $Ikzf2^{cello/cello}$ vs $Ikzf2^{+/+}$ and vs $Ikzf2^{cello/+}$ at 8 kHz, 16 kHz, 32 kHz, and click stimulus); $^{*}P = 0.0284$ (1- vs 9-month $Ikzf2^{cello/cello}$ at 8 kHz); $^{*}P = 0.0166$ (1- vs 9-month $Ikzf2^{cello/cello}$ at 16 kHz); $^{*}P = 0.0303$ (1- vs 9-month $Ikzf2^{cello/cello}$ at 32 kHz); $^{**}P = 0.0042$ (1- vs 9-month $Ikzf2^{cello/cello}$ click stimulus) (one-way ANOVA with Tukey post hoc test (**a**) or two-sided Welch's *t*-test (**b**)). See also Extended Data Fig. 4. **c**, **d**, Left, images show a patch pipette attached to an OHC from control $Ikzf2^{cello/+}$ (**c**) and mutant $Ikzf2^{cello/cello}$ (**d**) cochleae at P16–P18. Red lines indicate the position of the OHC basal membrane before (left) and during (right) a depolarizing voltage step from −64 mV to +56 mV, highlighting the shorting of the cells. Scale bars, 5 μm. Right, time-based *z*-stack projections, in which red lines indicate the resting position of the basal membrane and the green lines indicate the movement. $n = 10$ ($Ikzf2^{cello/+}$) and $n = 21$ ($Ikzf2^{cello/cello}$) *z*-stack projections (one set per OHC) from 5 biologically independent animals per genotype. **e**, **f**, Average movement was significantly reduced in $Ikzf2^{cello/cello}$ OHCs compared to $Ikzf2^{cello/+}$ at P16–P18 (**e**), even after normalization to respective membrane capacitance (**f**) (for this set of recordings, $Ikzf2^{cello/+}$: 13.6 ± 0.4 pF; $Ikzf2^{cello/cello}$: 10.0 ± 0.3 pF). Data are mean ± s.e.m. $n = 10$ ($Ikzf2^{cello/+}$) and $n = 21$ ($Ikzf2^{cello/cello}$) OHCs from 5 biologically independent animals per genotype. $^{****}P < 0.0001$ (two-sided Welch's *t*-test). **g**, Average DPOAE responses for *cello* mice at 1 month of age ($n = 5$ biologically independent animals per genotype). Data are mean ± s.e.m. $^{****}P < 0.0001$ ($Ikzf2^{cello/cello}$ vs $Ikzf2^{+/+}$ and vs $Ikzf2^{cello/+}$ at 8 kHz, 16 kHz); $^{***}P = 0.0004$ ($Ikzf2^{cello/cello}$ vs $Ikzf2^{+/+}$ at 32 kHz); $^{***}P = 0.0012$ ($Ikzf2^{cello/cello}$ vs $Ikzf2^{cello/+}$ at 32 kHz) (one-way ANOVA with Tukey post hoc test). **h**, **i**, NanoString validations of genes downregulated in $Ikzf2^{cello/cello}$ cochleae at P8 (**h**) and results showing no change in expression of other OHC transcription factors (**i**). Data are normalized to wild-type ($Ikzf2^{+/+}$) and shown as mean ± s.d. ($n = 4$ biologically independent samples per genotype). $^{*}P = 0.028$ (*Car7*; $Ikzf2^{cello/cello}$ vs $Ikzf2^{+/+}$); $^{*}P = 0.017$ (*Ppp17r1*); $^{**}P = 0.006$ (*Ocm*); $^{*}P = 0.017$ (*Slc26a5*) (two-sided Welch's *t*-test).

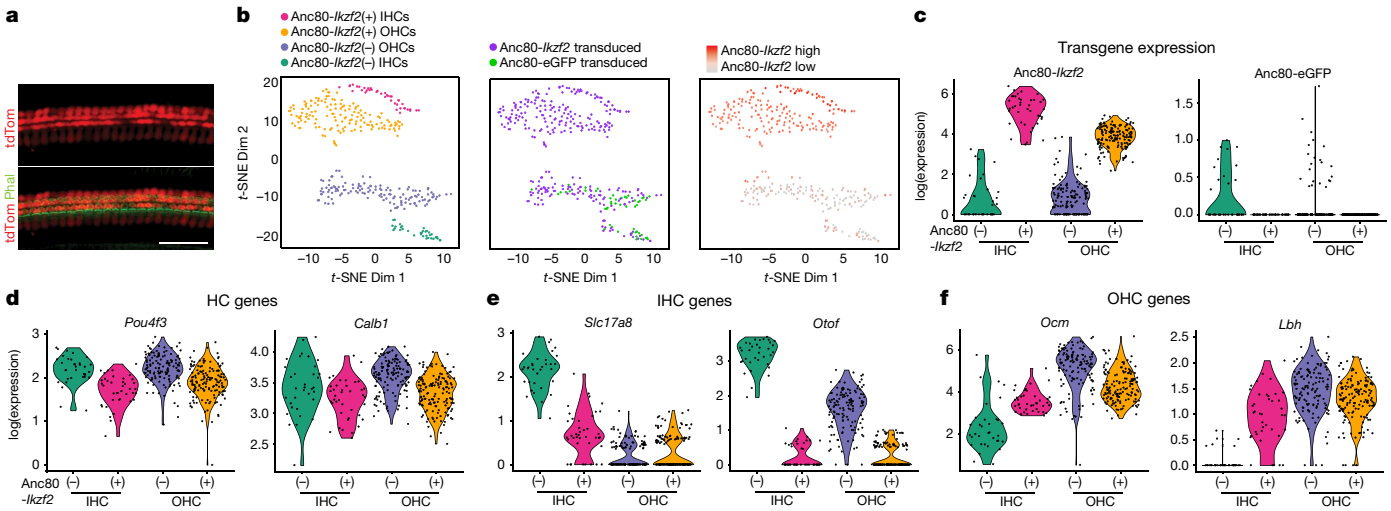

Fig. 3 | Partial transcriptional conversion of Anc80-*Ikzf2* transduced IHCs identified by scRNA-seq. **a**, Representative $Myo15^{cre/+}$;$ROSA26^{CAG\text{-}tdTomato}$ cochlear whole-mount staining. $Myo15^{cre}$-driven tdTomato expression is hair cell specific at P6 ($n = 3$ biologically independent samples with similar results). Scale bar, 50 μm. **b**, *t*-distributed stochastic neighbour embedding (*t*-SNE) plots of all cochlear hair cells profiled by scRNA-seq, including the cluster to which each cell was assigned, the experimental origin of each cell (cochlea injected with Anc80-*Ikzf2* or Anc80-eGFP), and the relative transcript abundance of Anc80-*Ikzf2* measured in each cell. **c**, Anc80-*Ikzf2* is highly expressed in the Anc80-*Ikzf2*(+) IHCs and OHCs, whereas Anc80-eGFP expression is only seen in the cells assigned to the Anc80-*Ikzf2*(−) IHC and OHC clusters. Dots represent the expression values of individual cells, with width of violins summarizing overall relative distribution of expression. **d**, Canonical hair cell (HC) markers are highly expressed in all clusters, and not notably changed as a result of Anc80-*Ikzf2* expression. **e**, IHC-enriched genes that are highly expressed in control IHCs vs control OHCs, but are significantly reduced in Anc80-*Ikzf2*(+) IHCs. Anc80-*Ikzf2*(−) IHC ($n = 34$) vs Anc80-*Ikzf2*(+) IHC ($n = 40$) FDR: $Slc17a8 = 2.25 \times 10^{-12}$, $Otof = 6.76 \times 10^{-14}$ (Kruskal–Wallis test followed by post hoc pairwise Wilcoxon ranked sum test adjusted for multiple comparisons). **f**, OHC-enriched genes that are induced in Anc80-*Ikzf2*(+) IHCs. Anc80-*Ikzf2*(−) IHC ($n = 34$) vs Anc80-*Ikzf2*(+) IHC ($n = 40$) FDR: $Ocm = 3.65 \times 10^{-8}$, $Lbh = 1.81 \times 10^{-10}$ (Kruskal–Wallis test followed by post hoc pairwise Wilcoxon ranked sum test adjusted for multiple comparisons). See also Extended Data Figs. 8 and 9.

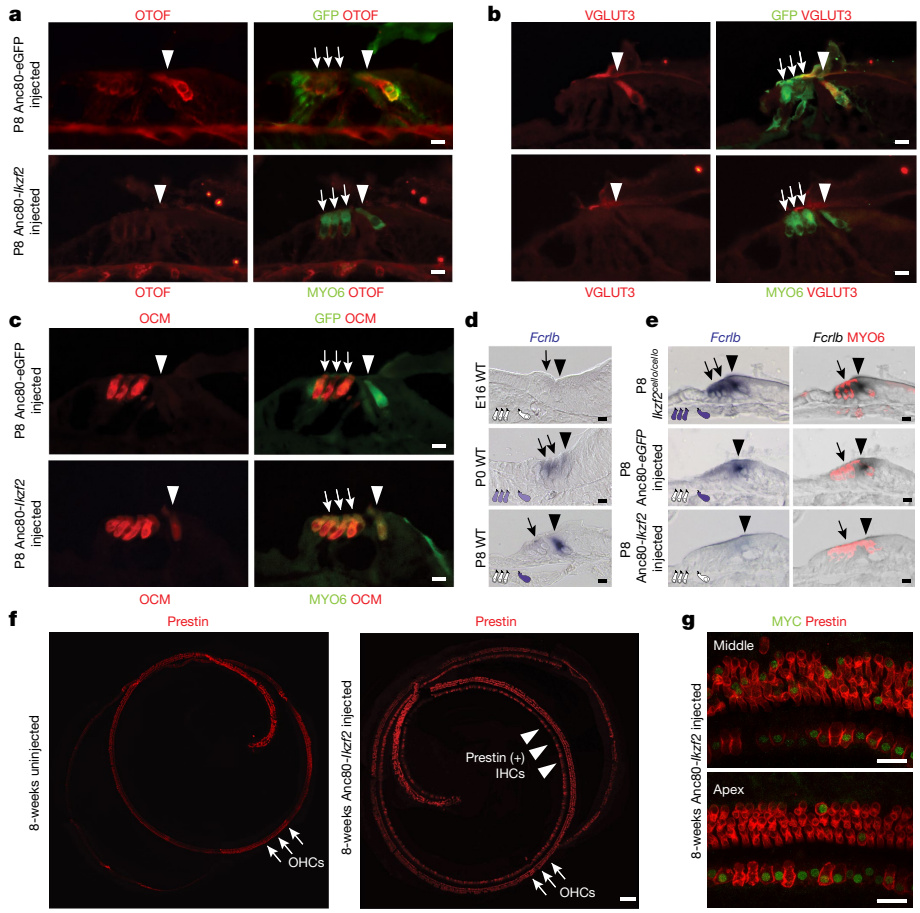

Fig. 4 | Helios overexpression modulates expression of hair cell markers. a, **b**, The IHC markers OTOF and VGLUT3 are downregulated in Anc80-*Ikzf2*-transduced IHCs ($n = 3$ biologically independent samples). **c**, The OHC marker OCM is expressed in Anc80-*Ikzf2*-transduced IHCs ($n = 3$ biologically independent samples per condition). **d**, *Fcrlb* expression during wild-type (WT) mouse inner ear development as detected by in situ hybridization. At embryonic day (E) 16, *Fcrlb* expression is not detected in the inner ear, but by P0 it is detected in both IHCs and OHCs, and is largely restricted to the IHCs by P8 ($n = 3$ biologically independent samples per time point). **e**, In the absence of functional Helios (*Ikzf2*$^{cello/cello}$ mouse), *Fcrlb* is robustly expressed in IHCs and OHCs at P8. IHC expression of *Fcrlb* is not affected by Anc80-eGFP transduction, whereas *Fcrlb* expression is lost in Anc80-*Ikzf2*-transduced hair cells ($n = 3$ biologically independent samples per condition). **f**, **g**, Prestin expression can be seen in Anc80-*Ikzf2*-transduced IHCs up to 8 weeks of age ($n = 3$ biologically independent samples at 6–8 weeks) (**f**), and overlaps with MYC staining (**g**). Scale bars, 10 μm (**a**–**e**), 100 μm (**f**) and 20 μm (**g**). Arrows denote OHCs, arrowheads denote IHCs. See also Extended Data Fig. 10.

littermate controls by RNA-seq. We identified 105 upregulated and 36 downregulated genes in *Ikzf2*$^{cello/cello}$ cochleae (Supplementary Table 7), including downregulation of the canonical OHC markers *Slc26a5* and *Ocm*, which was confirmed by NanoString validation (Fig. 2h). Furthermore, we did not observe modulation of other OHC-expressed transcription factors selected from a previously published dataset[16] (Fig. 2i), suggesting that the observed dysregulation in OHC genes results from disruption of a specific transcriptional cascade. Notably, by P16, the transcript levels of *Car7*, *Ocm* and *Slc26a5*, but not *Ppp1r17*, in *Ikzf2*$^{cello/cello}$ cochleae are similar to the levels of wild-type littermate controls, suggesting that other factors may be compensating for the functional loss of Helios by this time point (Extended Data Fig. 6i).

To characterize the transcriptional cascade downstream of Helios, we performed in vivo Anc80L65 adeno-associated virus (AAV) gene delivery of a Myc-tagged *Ikzf2* or enhanced green fluorescent protein (eGFP) (hereafter termed Anc80-*Ikzf2* or Anc80-eGFP, respectively) to neonatal inner ears of *Myo15*$^{cre/+}$;*ROSA26*$^{CAG\text{-}tdTomato}$ mice, sorted the cochlear hair cells at P8, and measured resultant changes in gene expression using single-cell RNA sequencing (scRNA-seq)[17,18] (Fig. 3a, Extended Data Fig. 7). The hair cells from inner ears injected with Anc80-*Ikzf2* separated into two distinct sets of clusters, containing both IHCs and OHCs. One set of IHCs and OHCs completely overlapped with the hair cells from the control ears injected with Anc80-eGFP (Fig. 3b, bottom clusters), whereas the other set clustered separately (Fig. 3b, top clusters). Separation of the two sets of clusters showed a clear correlation with expression of the Anc80-*Ikzf2* transgene (Fig. 3b), in which hair cells in the bottom clusters had lower expression of Anc80-*Ikzf2*, and the hair cells in the top clusters had higher expression of Anc80-*Ikzf2* (hereafter defined as Anc80-*Ikzf2* low (−) and high (+), respectively). Because the hair cells defined as Anc80-*Ikzf2*(−) clustered together with the hair cells transduced with Anc80-eGFP, these two groups of hair cells were merged and named Anc80-*Ikzf2*(−) IHCs and OHCs for all downstream analyses (Fig. 3b, c).

Although the overexpression of *Ikzf2* in IHCs and OHCs did not change the expression of hair cell markers such as *Pou4f3* and *Calb1* (Fig. 3d), it led to a significant downregulation of many genes whose transcripts were identified as IHC-enriched in the control hair cell populations, including *Slc17a8*, *Otof*, *Rprm*, *Atp2a3* and *Fgf8* (Fig. 3e, Extended Data Fig. 8, Supplementary Tables 8–10). Notably, some of the genes that are downregulated in both Anc80-*Ikzf2*(+) IHCs and OHCs are genes that are normally expressed in both cell types in early postnatal development, and that later become IHC-specific[19,20] (for example, *Pvalb* and *Otof*; Supplementary Table 10). This suggests that the overexpression of *Ikzf2* in OHCs results in an accelerated downregulation of these genes. Furthermore, *Ikzf2* overexpression in IHCs results in the upregulation of genes that are normally enriched in OHCs, such as *Ocm*, *Pde6d*, *Ldhb* and *Lbh* (Fig. 3f, Extended Data Fig. 8). Overall, these data suggest that during normal OHC development, Helios

functions to decrease the expression of early pan-hair-cell markers, such as *Otof*, in the maturating OHCs, as well as to upregulate OHC marker genes. A correlation analysis further validates the role of Helios in regulating OHC-related gene expression (Extended Data Figs. 8, 9, Supplementary Table 11). The effect of *Ikzf2* transduction on IHC gene expression was also validated by immunolabelling for OTOF, VGLUT3, OCM or prestin and by in situ hybridization for *Fcrlb* (Fig. 4, Extended Data Fig. 10a, b). Analysis of the surface characteristics of the transduced IHCs does not show a change from an IHC-like to an OHC-like stereociliary bundle, consistent with a partial role for Helios in regulating OHC-fate (Extended Data Fig. 10c). However, *Ikzf2* transduction resulted in the appearance of prominent voltage-dependent (nonlinear) capacitance in IHCs (Extended Data Fig. 10d, e), which is an electrical 'signature' of prestin-dependent OHC electromotility[21,22]. These data indicate that Anc80-*Ikzf2*-transduced IHCs start to acquire the major function of normal OHCs.

In conclusion, our study demonstrates that Helios is necessary for hearing and is a crucial regulator of gene expression in the maturing postnatal OHC. In particular, our results suggest that Helios functions to suppress IHC and early pan-hair-cell gene expression in OHCs, as well as to upregulate canonical OHC marker genes. It further shows that Helios is sufficient to induce the essential functional characteristic of electromotility and many of the molecular characteristics of OHCs when expressed in early postnatal IHCs, albeit not all of them, supporting the notion that additional OHC-expressed transcription factors are involved in postnatal OHC development. To our knowledge, this is the first study to demonstrate functional shifts in postnatal hair-cell molecular identities via viral gene delivery, and it suggests that the delivery of combinations of transcription factors may lead to successful regeneration of functional OHCs in the deafened cochlea.

Online content

Any methods, additional references, Nature Research reporting summaries, source data, statements of data availability and associated accession codes are available at https://doi.org/10.1038/s41586-018-0728-4.

Received: 15 August 2018; Accepted: 25 October 2018;
Published online 21 November 2018.

1. Dallos, P. et al. Prestin-based outer hair cell motility is necessary for mammalian cochlear amplification. *Neuron* **58**, 333–339 (2016).
2. Ehret, G. Development of absolute auditory thresholds in the house mouse (*Mus musculus*). *J. Am. Audiol. Soc.* **1**, 179–184 (1976).
3. Bielefeld, E. C., Tanaka, C., Chen, G. D. & Henderson, D. Age-related hearing loss: is it a preventable condition? *Hear. Res.* **264**, 98–107 (2010).
4. World Health Organization. *Deafness and Hearing Loss*; available at: http://www.who.int/mediacentre/factsheets/fs300/en/ (2018).
5. Mittal, R. et al. Recent advancements in the regeneration of auditory hair cells and hearing restoration. *Front. Mol. Neurosci.* **10**, 236 (2017).
6. Fang, J. et al. Outer hair cell-specific prestin-CreER^{T2} knockin mouse lines. *Genesis* **50**, 124–131 (2012).
7. Sanz, E. et al. Cell-type-specific isolation of ribosome-associated mRNA from complex tissues. *Proc. Natl Acad. Sci. USA* **106**, 13939–13944 (2009).
8. Liu, H. et al. Characterization of transcriptomes of cochlear inner and outer hair cells. *J. Neurosci.* **34**, 11085–11095 (2014).
9. Elkon, R. et al. RFX transcription factors are essential for hearing in mice. *Nat. Commun.* **6**, 8549 (2015).
10. Hertzano, R. et al. Cell type-specific transcriptome analysis reveals a major role for Zeb1 and miR-200b in mouse inner ear morphogenesis. *PLoS Genet.* **7**, e1002309 (2011).
11. Janky, R. et al. iRegulon: from a gene list to a gene regulatory network using large motif and track collections. *PLOS Comput. Biol.* **10**, e1003731 (2014).
12. Potter, P. K. et al. Novel gene function revealed by mouse mutagenesis screens for models of age-related disease. *Nat. Commun.* **7**, 12444 (2016).
13. Ashmore, J. F. A fast motile response in guinea-pig outer hair cells: the cellular basis of the cochlear amplifier. *J. Physiol. (Lond.)* **388**, 323–347 (1987).
14. Brownell, W. E., Bader, C. R., Bertrand, D. & de Ribaupierre, Y. Evoked mechanical responses of isolated cochlear outer hair cells. *Science* **227**, 194–196 (1985).
15. Marcotti, W. & Kros, C. J. Developmental expression of the potassium current $I_{K,n}$ contributes to maturation of mouse outer hair cells. *J. Physiol. (Lond.)* **520**, 653–660 (1999).
16. Li, Y. et al. Transcription factors expressed in mouse cochlear inner and outer hair cells. *PLoS One* **11**, e0151291 (2016).
17. Zinn, E. et al. In silico reconstruction of the viral evolutionary lineage yields a potent gene therapy vector. *Cell Reports* **12**, 1056–1068 (2015).
18. Landegger, L. D. et al. A synthetic AAV vector enables safe and efficient gene transfer to the mammalian inner ear. *Nat. Biotechnol.* **35**, 280–284 (2017).
19. Roux, I. et al. Otoferlin, defective in a human deafness form, is essential for exocytosis at the auditory ribbon synapse. *Cell* **127**, 277–289 (2006).
20. Simmons, D. D., Tong, B., Schrader, A. D. & Hornak, A. J. Oncomodulin identifies different hair cell types in the mammalian inner ear. *J. Comp. Neurol.* **518**, 3785–3802 (2010).
21. Santos-Sacchi, J. Reversible inhibition of voltage-dependent outer hair cell motility and capacitance. *J. Neurosci.* **11**, 3096–3110 (1991).
22. Zheng, J. et al. Prestin is the motor protein of cochlear outer hair cells. *Nature* **405**, 149–155 (2000).

Acknowledgements We thank L. Vizor, J. Sanderson and W. Chien for technical help and Z. Ahmed for comments on the manuscript. This work was supported by Action on Hearing Loss (G65 to M.R.B., R.H., W.M. and S.D.M.B.), Medical Research Council (MC_U142684175 to S.D.M.B.), Wellcome Trust (102892 to W.M.), NIDCD/NIH R01DC013817 and R01DC03544 (R.H.), DOD CDMRP MR130240 (R.H.), NIDCD/NIH T32DC00046 and F31DC016218 (M.S.M.), the Intramural Program at NIDCD DC000059 (M.W.K.), and NIDCD/NIH R01DC014658 (G.I.F.). S.L.J. is a Royal Society University Research Fellow. R.E. is a Faculty Fellow of the Edmond J. Safra Center for Bioinformatics at Tel Aviv University.

Reviewer information *Nature* thanks M. Montcouquiol, B. Walters and the anonymous reviewer(s) for their contribution to the peer review of this work.

Author contributions L.C., M.S.M., M.C.K., Y.O., B.M., M.M., G.C., C.T.E., G.I.F., M.W.K., W.M., S.D.M.B., M.R.B. and R.H. designed and interpreted the experiments. L.C., M.S.M., M.C.K., S.L.J., Y.O., B.M., M.M., A.P., J.P., R.H., E.C.D., G.T., A.K.D., G.I.F. and W.M. performed the experiments. Y.S. and R.E. analysed the gene expression data. S.W. aided in the management of the *cello* colony. M.R.B. and R.H. conceived and coordinated the study. L.C., M.S.M., M.C.K., W.M., S.D.M.B., R.E., M.R.B. and R.H. wrote the manuscript.

Competing interests The authors declare no competing interests.

Additional information
Extended data is available for this paper at https://doi.org/10.1038/s41586-018-0728-4.
Supplementary information is available for this paper at https://doi.org/10.1038/s41586-018-0728-4.
Reprints and permissions information is available at http://www.nature.com/reprints.
Correspondence and requests for materials should be addressed to M.R.B. or R.H.
Publisher's note: Springer Nature remains neutral with regard to jurisdictional claims in published maps and institutional affiliations.

METHODS

No statistical methods were used to predetermine sample size. The experiments were not randomized, and investigators were not blinded to allocation during experiments and outcome assessment unless stated otherwise.

Animal procedures. Animal procedures performed at the University of Maryland School of Medicine were carried out in accordance with the National Institutes of Health Guide for the Care and Use of Laboratory Animals and have been approved by the Institutional Animal Care and Use Committee at the University of Maryland, Baltimore (protocol numbers 1112005 and 1015003). The RiboTag (maintained on a C57BL/6N background), *prestin*^{creERT2} and *Myo15*^{cre} mouse models (maintained on a C57BL/6J background) have been described previously[6,7,23], and were provided by M. K. Lobo (RiboTag), J. Zuo (*prestin*^{creERT2}), and C. Petit and T. Friedman (*Myo15*^{cre}). CBA/CaJ mice (stock 000654) and B6.Cg-*Gt(ROSA)26Sor*$^{tm14(CAG-tdTomato)Hze}$/J mice (stock 007914, referred to as *ROSA26*$^{CAG-tdTomato}$) were procured from the Jackson Laboratory. The specificity of *prestin*^{creERT2} was determined by crossing *prestin*$^{creERT2/creERT2}$ mice to *ROSA26*$^{CAG-tdTomato}$ mice, and the resulting offspring were dissected at P21 for whole-mount immunohistochemistry. To generate animals for the RiboTag OHC RNA-seq dataset, *RiboTag*$^{HA/HA}$ mice were crossed to *prestin*$^{creERT2/creERT2}$ mice to produce *RiboTag*$^{HA/+}$;*prestin*$^{creERT2/+}$ mice. These mice were further intercrossed to obtain double homozygous *RiboTag*$^{HA/HA}$;*prestin*$^{creERT2/creERT2}$ animals, which were then crossed to CBA/CaJ mice to generate F_1 *RiboTag*$^{HA/+}$;*prestin*$^{creERT2/+}$ offspring on a mixed CBA/C57BL/6 background, avoiding the recessively inherited age-related hearing loss phenotype inherent to C57BL/6 mice[24]. Recombination was induced by tamoxifen injection (3 mg per 40 g body weight in mice younger than 21 days, 9 mg per 40 g body weight in mice 21 days or older), and cochlear tissues were collected at the following ages: P8, P14, P28, 6 weeks and 10 weeks. For the *cello* RNA-seq and NanoString experiments, cochlear ducts from *Ikzf2*$^{+/+}$, *Ikzf2*$^{cello/+}$ and *Ikzf2*$^{cello/cello}$ mice were dissected at P8 and P16. CD-1 or C57BL/6 pregnant females were procured from Charles River or the University of Maryland School of Medicine Veterinary Resources. Resulting neonates were injected with Anc80L65 virus between P1 and P3, and dissected for later analyses between P8 and 8 weeks. For the Anc80L65-transduced IHC scRNA-seq experiment, *Myo15*$^{cre/cre}$ mice were crossed to *ROSA26*$^{CAG-tdTomato}$ mice, and resulting offspring were injected with Anc80L65 virus between P1 and P3, and the cochlear epithelium was collected at P8. Additionally, several litters with Anc80-*Ikzf2*-injected pups and their control littermates (aged P7–P8), together with a mother, were sent to the University of Kentucky for the measurements of nonlinear (voltage-dependent) capacitance, an electrical 'signature' of electromotility. All animal procedures for these experiments were approved by the Institutional Animal Care and Use Committee at the University of Kentucky (protocol 00903M2005). Both male and female animals were used for all experiments.

Animal procedures performed at the MRC Harwell Institute were licensed by the Home Office under the Animals (Scientific Procedures) Act 1986, UK and additionally approved by the relevant Institutional Ethical Review Committees. The *cello* mutant mouse was originally identified from the MRC Harwell Institute phenotype-driven *N*-ethyl-*N*-nitrosourea (ENU) Ageing Screen[12]. In this screen, ENU-mutagenized C57BL/6J males were mated with wild-type 'sighted C3H' (C3H.Pde6b+) females[25]. The resulting G_1 males were crossed with C3H.Pde6b+ females to produce G_2 females, all of which were screened for the *Cdh23*^{ahl} allele[24]. *Cdh23*$^{+/+}$ G_2 females were then backcrossed to their G_1 fathers to generate recessive G_3 pedigrees, which entered a longitudinal phenotyping pipeline. Auditory phenotyping comprised clickbox testing at 3, 6, 9 and 12 months of age and ABR at 9 months of age. The *Ikzf2*^{del890} mutant line was generated by the Molecular and Cellular Biology group at the MRC Harwell Institute using a CRISPR–Cas9-mediated deletion approach. Both male and female mice were used for experiments.

RiboTag immunoprecipitations. RiboTag immunoprecipitations were performed as described previously[7]. In brief, for one biological sample, 10 cochlear ducts from 5 mice were pooled and homogenized in 1 ml of supplemented homogenization buffer (50 mM Tris-HCl, pH 7, 100 mM KCl, 12 mM $MgCl_2$, 1% Nonidet P-40, 1 mM 1,4-dithiothreitol, 1× protease inhibitor cocktail, 200 U ml^{-1} RNaseOUT, 100 μg ml^{-1} cycloheximide, 1 mg ml^{-1} heparin). Homogenates were spun down (9,400*g* for 10 min at 4 °C) to remove particulates. Then, 40 μl of homogenate was reserved for total RNA isolation (input control), and the remaining homogenate was incubated with 5 μg haemagglutinin (HA) antibody (BioLegend) at 4 °C under gentle rotation for 4–6 h. The supernatant was then added to 300 μl of rinsed Invitrogen Dynabeads Protein G magnetic beads (Thermo Fisher), and incubated overnight at 4 °C under gentle rotation. The next day, bound beads were rinsed three times with 800 μl high-salt buffer (50 mM Tris-HCl, pH 7, 300 mM KCl, 12 mM $MgCl_2$, 1% Nonidet P-40, 1 mM 1,4-dithiothreitol, 100 μg ml^{-1} cycloheximide) at 4 °C for 10 min, rotating. Buffer RLT (350 μl) from the RNeasy Plus Micro kit (Qiagen) was then added to the beads or reserved input sample, and vortexed for 30 s to release bound ribosomes and RNA. RNA was extracted according to the manufacturer's instructions for the RNeasy Plus Micro kit (Qiagen), using 16 μl of nuclease free water for elution as described previously[10]. This method yielded an average of 10.9 ng of immunoprecipitated RNA (average concentration = 0.68 ng μl^{-1}) and 185.6 ng of input RNA (average concentration = 10.9 ng μl^{-1}) for downstream analyses. All RNA samples used for RNA-seq had a minimum RNA integrity number (RIN) of 8.

***cello* cochlear RNA extractions.** For the *cello* RNA-seq, cochlear ducts from P8 *Ikzf2*$^{+/+}$ and *Ikzf2*$^{cello/cello}$ mice were dissected and pooled (6 cochlear ducts per sample) to generate two biological replicates per genotype. For the NanoString validations, cochlear ducts from P8 *Ikzf2*$^{cello/cello}$, *Ikzf2*$^{cello/+}$ and *Ikzf2*$^{+/+}$ mice were dissected and pooled (2–4 cochlear ducts per sample) to generate four biological replicates per genotype. RNA was extracted using the Direct-zol RNA MiniPrep kit (Zymo Research) following the manufacturer's instructions. RNA quality and concentration were assessed using the Agilent RNA Pico kit (Agilent Technologies). All RNA samples used for RNA-seq had a minimum RNA integrity number (RIN) of 8.

RNA-seq and normalization. RiboTag OHC RNA-seq libraries were prepared using the NEBNext Ultra Directional RNA Library Prep Kit for Illumina (New England Biolabs), and samples were sequenced in at least biological duplicates on a HiSeq 4000 system (Illumina) using a 75-bp paired end read configuration. P8 *Ikzf2*$^{+/+}$ and *Ikzf2*$^{cello/cello}$ RNA libraries were prepared using the TruSeq RNA Sample Prep kit (Illumina), and samples were sequenced in biological duplicates on a HiSeq 2000 system (Illumina) and a 125-bp paired-end read configuration. Reads were aligned to the *Mus musculus* reference genome (assembly GRCm38.87 (RiboTag) or GRCm38.84 (P8 *cello*)) using TopHat v.2.0.8[26], and HTSeq was used to quantify the number of reads aligning to predicted coding regions[27]. See Supplementary Table 12 for alignment statistics. Expression levels were normalized using quantile normalization. In downstream analyses, only genes covered by at least 20 reads in a minimum of two samples from the same biological condition were considered as expressed. Significant differential gene expression between samples was assessed using DEseq[28]. In addition to statistical significance between samples (FDR ≤ 0.05), we also required a complete separation of expression levels between compared conditions for a gene to be called as differentially expressed. That is, for a gene to be called downregulated in condition A compared to condition B, we required that all normalized expression levels measured in the samples of condition A to be lower than all normalized expression levels measured in the samples of condition B. To avoid inflation of fold change estimates for lowly expressed genes, a floor level equal to the tenth percentile of the distribution of the expression levels was applied (that is, all expression values below the tenth percentile were set to the tenth percentile value). The OHC enrichment factors were calculated for each gene and time point by comparing the RiboTag immunoprecipitated samples to matched input samples, and are defined as the $\log_2$ ratio of expression levels between the immunoprecipitated and input samples. Inspection of these enrichment factors revealed a systematic association to transcripts length (Supplementary Fig. 2a). Therefore, we used a locally weighted regression, implemented by the R lowess function, to remove this systematic effect (Supplementary Fig. 2b).

Gene expression analyses. Genes with a changed level of expression in OHC immunoprecipitated samples at any time point relative to P8 were subjected to a clustering analysis using the CLICK algorithm, implemented in the EXPANDER package[29,30]. Gene Ontology (GO) enrichment analysis was carried out using the EXPANDER implemented tool TANGO[29]. The adult mouse IHC and OHC transcriptomic dataset used for comparisons was generated previously[8] and can be accessed through the GEO database (accession number GSE111348)[8]. The expanded motif prediction analysis was performed using iRegulon[11] through the Cytoscape visualization tool[31]. The analysis was performed on the putative regulatory region of 20 kb centred around the transcription start site using default settings.

Immunohistochemistry. For cochlear sections, mice were euthanized by cervical dislocation and inner ears fixed in 4% paraformaldehyde (PFA) overnight at 4 °C then decalcified in 4% EDTA in PBS. Ears were positioned in 4% low melting temperature agarose (Sigma-Aldrich) in upturned BEEM capsules (Agar Scientific) at a 45° diagonal angle, with the apex of the cochlea facing down and the vestibular system uppermost. Once set, the agarose block was removed from the BEEM capsule and 200 μm sections were cut through the mid-modiolar plane of the cochlea using a Leica VT1000S Vibratome. Sections were simultaneously permeabilized and blocked with 10% donkey serum (Sigma) in 0.3% Triton-X for 30 min at room temperature then labelled with primary antibodies for 3 h at room temperature. To enable detection, samples were incubated with fluorophore-coupled secondary antibodies for 2 h at room temperature then stained with 4′,6-diamidino-2-phenylindole dihydrochloride (DAPI; 1:2,500, Thermo Fisher) for 5 min. Sections were transferred to WillCo glass bottom dishes (Intracel) and visualized free-floating in PBS using a Zeiss 700 inverted confocal microscope (10–40× magnification). Primary antibodies: goat anti-Helios M-20 (1:400, Santa Cruz Biotechnology) and mouse anti-β-actin (1:500, Abcam). Secondary antibodies: Alexa Fluor 568 donkey

anti-goat (Invitrogen, 1:200) and Alexa Fluor 488 donkey anti-mouse (Invitrogen, 1:200).

For cochlear whole-mounts, mice were euthanized by cervical dislocation and inner ears fixed in 2% PFA for 30 min at 4 °C. After fixation, ears were fine dissected to expose the sensory epithelium then immediately permeabilized in 0.2% Triton-X for 10 min and blocked with 10% donkey serum (Sigma) for 1 h at room temperature. Cochleae were immunolabelled with goat anti-Helios M-20 (1:400, Santa Cruz Biotechnology) overnight at 4 °C then incubated with Alexa Fluor 568 donkey anti-goat secondary (1:200, Invitrogen) and the F-actin marker Alexa Fluor 488 Phalloidin (1:200, Invitrogen) for 1 h at room temperature. Samples were washed with DAPI (1:2,500, Thermo Fisher) for 60 s to stain nuclei then mounted onto slides with SlowFade Gold (Life Technologies) and visualized using a Zeiss LSM 710 fluorescence confocal microscope and 63× oil magnification.

Identification of the *cello* mutation. DNA was extracted from ear biopsies of affected G_3 mice using the DNeasy Blood and Tissue Kit (Qiagen) and used for an initial genome-wide linkage study, using SNP markers polymorphic between the parental strains C57BL/6J and C3H.Pde6b+ (Tepnel Life Sciences). Following linkage to a 21.57 Mb region on chromosome 1, additional SNP markers were identified and genotyped using standard PCR and restriction endonuclease protocols to delineate an 8.4 Mb critical interval between SNPs rs31869113 and rs13475914. Subsequently, high-quality DNA was extracted from the tail of an affected G_3 mouse using the Illustra Nucleon BACC2 Genomic DNA Extraction Kit (GE Healthcare) and sequenced by the Oxford Genomics Centre (Wellcome Trust Centre for Human Genetics) using the HiSeq system (Illumina). Sequencing reads were aligned to the mouse reference genome (assembly GRCm38) and known C57BL/6J and C3H.Pde6b+ SNPs were filtered out, leaving variants that were then given a quality score based on their sequencing read depth. Variants within the 8.4 Mb critical region which were deemed heterozygous, low-confidence (quality score < 200), non-coding or synonymous were discounted. The putative *Ikzf2* lesion was amplified by standard PCR (see Supplementary Table 13 for genotyping primers) and validated by Sanger sequencing, using DNA from an affected G_3 animal, as well an unaffected G_3 (control). Sequence gaps that spanned coding regions were amplified by PCR using DNA from an affected G_3 mouse and analysed by Sanger sequencing. In all cases, sequence data were assessed for variation using DNASTAR Lasergene software (version 12.0.0).

In silico analyses. Three independent online tools were used to predict the functional effect of the *cello* mutation in silico: Sorting Intolerant From Tolerant (SIFT); Polymorphism Phenotyping version 2 (PolyPhen-2); and Protein Variation Effect Analyser (PROVEAN)[32–34]. Structural 3D representations of wild-type and H517Q helios ZnF6 were predicted with RaptorX[35], using peptide sequences as input, and visualized using pyMOL software (version 1.7).

In vitro analyses. A full-length *Ikzf2*$^{+}$ Helios construct was prepared using the pGEM-T Vector System II Kit (Promega) and used as a template for the generation of an *Ikzf2*^{cello} Helios construct with the QuikChange Lightning Site-Directed Mutagenesis Kit (Agilent Technologies). Plasmid DNA was prepared using the Wizard Plus SV Miniprep Purification System (Promega) and validated by Sanger sequencing. Sequence-verified *Ikzf2*$^{+}$ and *Ikzf2*^{cello} constructs were subcloned in-frame into pCMV-Myc and pEGFP-C3 mammalian expression vectors (provided by C. Esapa), to yield N-terminally tagged *Ikzf2*$^{+}$ and *Ikzf2*^{cello} Helios. See Supplementary Table 13 for cloning and mutagenesis oligonucleotide sequences.

Constructs were subsequently used for subcellular localization studies using male *Cercopithecus aethiops* SV40 transformed kidney cells (Cos-7) cells that had been seeded onto 22 × 22 mm glass coverslips in six-well plates, at a volume of 1×10^5 cells per well. After 24 h (or when 50–60% confluent), cells were transiently transfected with 1 μg DNA of the *Ikzf2*$^{+}$-Myc or *Ikzf2*^{cello}-Myc Helios construct using JetPEI DNA Transfection Reagent (Polyplus Transfection). At 24 h after transfection, cells were fixed in 4% PFA for 10 min and permeabilized with 1% Triton-X for 15 min at room temperature. After blocking in 10% donkey serum (Sigma) for 1 h at room temperature, cells were immunolabelled with goat anti-Helios M-20 primary antibody (1:600, Santa Cruz Biotechnology) overnight at 4 °C, then incubated with Alexa Fluor 488 donkey anti-goat secondary antibody (1:200, Invitrogen) and F-actin marker Texas Red-X Phalloidin (1:200, Invitrogen) for 1 h at room temperature. Cells were washed with DAPI (1:2,500, Thermo Fisher) for 60 s. Coverslips were mounted onto slides with SlowFade Gold (Life Technologies) and cells were visualized using a Zeiss LSM 710 multiphoton fluorescence confocal microscope and 63× oil magnification.

Constructs were also used for co-immunoprecipitation studies using human embryonic kidney (HEK293T) cells that had been seeded directly onto six-well plates at a volume of 5×10^5 cells per well. Cells were transiently co-transfected 24 h later with a total of 2 μg plasmid DNA to mimic the wild-type (1 μg *Ikzf2*$^{+}$-Myc Helios + 1 μg *Ikzf2*$^{+}$-GFP Helios), heterozygous (1 μg *Ikzf2*$^{+}$-Myc Helios + 1 μg *Ikzf2*^{cello}-GFP Helios; 1 μg *Ikzf2*^{cello}-Myc Helios + 1 μg *Ikzf2*$^{+}$-GFP Helios) or homozygous (1 μg *Ikzf2*^{cello}-Myc Helios + 1 μg *Ikzf2*^{cello}-GFP Helios) states using JetPEI DNA Transfection Reagent (Polyplus Transfection). Single transfections with either 1 μg *Ikzf2*$^{+}$-GFP Helios or 1 μg *Ikzf2*$^{+}$-Myc Helios were also carried out for negative controls. Cells were lysed in 250 μl of 1× RIPA buffer (150 mM NaCl, 1% NP-40, 0.5% deoxycholate, 0.1% SDS, 50 mM Tris, pH 7.5, in milliQ water) 48 h after transfection, then incubated with Protein G Sepharose Beads (Sigma) for 2 h at 4 °C. The beads were pelleted by centrifugation and the supernatant incubated with either 1 μg of mouse anti-cMyc 9E10 antibody (Developmental Studies Hybridoma Bank) or 1–2 μg of custom-made rabbit anti-GFP antibody overnight at 4 °C. The immunoprecipitation complexes were captured using Protein G beads, washed with RIPA buffer and released by incubation with NuPAGE Reducing Agent (Novex). Immunoprecipitation reactions and their corresponding reduced cell lysate were analysed by western blotting. Samples were electrophoresed on NuPage 4–12% Bis-Tris gels (Invitrogen) and transferred onto nitrocellulose membranes using the iBlot system (Invitrogen). Membranes were incubated with mouse anti-cMyc 9E10 antibody (1:5,000, Developmental Studies Hybridoma Bank) and custom-made rabbit anti-GFP (1:1,000, CUK-1819 MGU-GFP-FL) primary antibodies. Mouse 12G10 anti-α-tubulin (1:10,000, Developmental Studies Hybridoma Bank) was also used as a loading control. For detection, membranes were incubated with goat anti-mouse IRDye 680RD (1:15,000, LI-COR) and goat anti-rabbit IRDye 800CW secondary antibodies (1:15,000, LI-COR) and imaged using the Odyssey CLx Infrared Imaging System (LI-COR). For quantification, band intensities were determined using the Image Studio Lite Ver 5.2 software and used to calculate the relative ratio of the co-immunoprecipitation to immunoprecipitation signal. Cos-7 and HEK293T cell lines used in this study were provided by C. Esapa, were not authenticated, but were tested and confirmed to be free of mycoplasma contamination. Cells were grown at 37 °C under 5% CO_2 conditions in DMEM (Invitrogen) containing 10% heat-inactivated fetal bovine serum (FBS) (Invitrogen) and 1× penicillin/streptomycin (Invitrogen).

ABR. ABR tests were performed using a click stimulus in addition to frequency-specific tone-burst stimuli to screen mice for auditory phenotypes and investigate auditory function[36]. Mice were anaesthetized by intraperitoneal injection of ketamine (100 mg ml^{-1} at 10% v/v) and xylazine (20 mg ml^{-1} at 5% v/v) administered at the rate of 0.1 ml per 10 g body mass. Animals were placed on a heated mat inside a sound-attenuated chamber (ETS Lindgren) and electrodes were placed subdermally over the vertex (active), right mastoid (reference) and left mastoid (ground). ABR responses were collected, amplified and averaged using TDT System 3 (Tucker Davies Technology) in conjunction with either BioSig RP (version 4.4.11) or BioSig RZ (v5.7.1) software. The TDT system click ABR stimuli comprised clicks of 0.1 ms broadband noise spanning approximately 2–48 kHz, presented at a rate of 21.1 s^{-1} with alternating polarity. Tone-burst stimuli were of 7 ms duration, inclusive of 1 ms rise/fall gating using a Cos2 filter, presented at a rate of 42.5 s^{-1} and were measured at 8, 16 and 32 kHz. All stimuli were presented free-field to the right ear of the mouse, starting at 90 dB SPL and decreasing in 5 dB increments. Auditory thresholds were defined as the lowest dB SPL that produced a reproducible ABR trace pattern and were determined manually. All ABR waveform traces were viewed and re-scored by a second operator blinded to genotype. Animals were recovered using 0.1 ml of anaesthetic reversal agent atipamezole (Antisedan, 5 mg ml^{-1} at 1% v/v), unless aged P16, when the procedure was performed terminally.

Generation of *Ikzf2*^{del890} mice. The *Ikzf2*^{del890} mutant line was generated by the Molecular and Cellular Biology group at the Mary Lyon Centre, MRC Harwell Institute using CRISPR–Cas9 gene editing, as described previously[37] (see Supplementary Table 13 for single-guide RNA (sgRNA) sequences, donor oligonucleotide sequences and genotyping primers). For construction of each sgRNA plasmid, a pair of single-stranded donor oligonucleotides (IDT) was hybridized and cloned using Gibson Assembly Master Mix (NEB) into linearized p_1.1 plasmid digested with StuI and AflII to express sgRNAs under the T7 promoter.

The p_1.1_sgRNA plasmids were linearized with XbaI, purified with phenol–chloroform, and the products were used as templates from which sgRNAs were in vitro transcribed. sgRNAs were synthesized using MEGAshortscript T7 Transcription Kit (Ambion). RNAs were purified using MEGAclear Transcription Clean-Up Kit (Ambion). RNA quality was assessed using a NanoDrop (Thermo Scientific) and by electrophoresis on 2% agarose gel containing Ethidium Bromide (Fisher Scientific).

As this exon deletion mutant was generated as part of an experiment to generate a floxed mutant, a *Ikzf2* flox long single-stranded DNA (lssDNA) donor was also synthesized as described previously for inclusion in the microinjection mix[38].

For microinjections, the pronucleus of one-cell stage C57BL/6NTac embryos were injected with a mix containing *Cas9* mRNA (5meC,Ψ, Tebu-Bio/TriLink Biotechnologies) at 100 ng μl^{-1}, the four *Ikzf2* sgRNAs, each at 50 ng μl^{-1} and the *Ikzf2* flox lssDNA donor at 50 ng μl^{-1} prepared in microinjection buffer. Injected embryos were re-implanted in pseudo-pregnant CD-1 females, which were allowed to litter and rear F_0 progeny.

For genotyping, genomic DNA was extracted from ear biopsies of F_0 and F_1 mice using DNA Extract All Reagents Kit (Applied Biosystems) and amplified by PCR using high fidelity Expand Long Range dNTPack (Roche) and specific genotyping

primers (see Supplementary Table 13). PCR products were further purified using QIAquick Gel Extraction Kit (Qiagen) and analysed by Sanger sequencing. Copy counting experiments by droplet digital PCR (ddPCR) against a known two copy reference (*Dot1l*) were also carried out to confirm the exon deletion and that there were no additional integrations of the lssDNA donor. Mice carrying the *del890* deletion allele were subsequently mated with mice carrying the *cello* mutation to generate *Ikzf2*$^{cello/del890}$ compound heterozygotes for complementation testing.

Scanning electron microscopy. Mice were euthanized by cervical dislocation and inner ears were removed and fixed in 2.5% glutaraldehyde (TAAB Laboratories Equipment Ltd) in 0.1 M phosphate buffer for 4 h at 4 °C. After decalcification in 4.3% EDTA, cochleae were dissected to expose the organ of Corti, and subjected to 'OTO' processing (1 h incubation in 1% osmium tetroxide (TAAB Laboratories Equipment), 30 min incubation in 1% thiocarbohydrazide (Sigma), 1 h incubation in 1% osmium tetroxide), before dehydration in increasing concentrations of ethanol (25%, 40%, 60%, 80%, 95%, 2 × 100%) at 4 °C. Samples were critical point dried with liquid CO_2 using an Emitech K850 (EM Technologies), then mounted on stubs using silver paint (Agar Scientific) and sputter coated with platinum using a Quorum Q150R S sputter coater (Quorum Technologies). Samples were examined using a JEOL JSM-6010LV Scanning Electron Microscope. Hair cell bundle counts were performed by counting the number of OHC and IHC bundles adjacent to ten pillar cells in the apical (<180° from apex), mid (180–450° from apex) and basal (>450° from apex) regions of the cochlea. At least three ears (one ear per mouse) were analysed for each genotype at each time point.

Electrophysiological analyses. Electrophysiological recordings were made from OHCs of *cello* mice aged P9–P18. Cochleae were dissected in normal extracellular solution (in mM): 135 NaCl, 5.8 KCl, 1.3 $CaCl_2$, 0.9 $MgCl_2$, 0.7 NaH_2PO_4, 5.6 D-glucose, 10 HEPES-NaOH. Sodium pyruvate (2 mM), MEM amino acids solution (50×, without L-glutamine) and MEM vitamins solution (100×) were added from concentrates (Fisher Scientific). The pH was adjusted to 7.5 (osmolality approximately 308 mmol kg^{-1}). The dissected cochleae were transferred to a microscope chamber, immobilized as previously described[39] and continuously perfused with a peristaltic pump using the above extracellular solution. The organs of Corti were viewed using an upright microscope (Nikon FN1) with Nomarski optics (60× objective).

MET currents were elicited by stimulating the hair bundles of P9 OHCs in the excitatory and inhibitory direction using a fluid jet from a pipette (tip diameter 8–10 μm) driven by a piezoelectric disc[39]. The pipette tip of the fluid jet was positioned near to the bundles to elicit a maximal MET current. Mechanical stimuli were applied as 50 Hz sinusoids (filtered at 0.25 kHz, 8-pole Bessel) with driving voltages of ±40 V. MET currents were recorded with a patch pipette solution containing (in mM): 106 Cs-glutamate, 20 CsCl, 3 $MgCl_2$, 1 EGTA-CsOH, 5 Na_2ATP, 0.3 Na_2GTP, 5 HEPES-CsOH, 10 sodium phosphocreatine (pH 7.3). Membrane potentials were corrected for the liquid junction potential (–11 mV).

Patch clamp recordings were performed using an Optopatch (Cairn Research) amplifier. Patch pipettes were made from soda glass capillaries (Harvard Apparatus) and had a typical resistance in extracellular solution of 2–3 MΩ. To reduce the electrode capacitance, patch electrodes were coated with surf wax (Mr. Zog's SexWax). Potassium current recordings were performed at room temperature (22–24 °C) and the intracellular solution contained (in mM): 131 KCl, 3 $MgCl_2$, 1 EGTA-KOH, 5 Na_2ATP, 5 HEPES-KOH, 10 Na_2-phosphocreatine (pH 7.3; osmolality approximately 296 mmol kg^{-1}). Data acquisition was controlled by pClamp software (version 10) using Digidata 1440A boards (Molecular Devices). Recordings were low-pass filtered at 2.5 kHz (8-pole Bessel), sampled at 5 kHz and stored on computer for off-line analysis (Origin, OriginLab). Membrane potentials in voltage clamp were corrected for the voltage drop across the uncompensated residual series resistance and for a liquid junction potential (−4 mV).

The presence of electromotile activity in P16–P18 OHCs was estimated by applying a depolarizing voltage step from the holding potential of −64 mV to +56 mV. Changes in cell length were viewed and recorded with a Nikon FN1 microscope (75× magnification) with a Flash 4.0 SCCD camera (Hamamatsu). Cell body movement was tracked using Fiji software. Lines were drawn across the basal membrane of patched OHCs, perpendicular to the direction of cell motion, and a projected time-based *z*-stack of the pixels under the line was made. Cell movement was measured with Photoshop as a pixel shift and then converted to nanometres (290 pixels = 10 μm).

Nonlinear (voltage-dependent) capacitance of IHCs in Anc80-*Ikzf2*-injected mice and their non-injected littermates was studied at P12–P16 using conventional whole-cell patch clamp recordings. Apical turn of the organ of Corti was carefully dissected in Leibovitz's L-15 cell culture medium (21083027, Gibco/ThermoFisher) containing the following inorganic salts (in mM): 137 NaCl, 5.4 KCl, 1.26 $CaCl_2$, 1.0 $MgCl_2$, 1.0 Na_2HPO_4, 0.44 KH_2PO_4 and 0.81 $MgSO_4$ and placed into a custom-made recording chamber, where it was held by two strands of dental floss. The organ of Corti explants were viewed with an upright microscope (BX51WIF, Olympus), equipped with a high numerical aperture (NA) objective (100×, 1.0 NA). To block voltage-gated ion channels in IHCs, the bath solution was made of L-15 medium supplemented with 10 mM tetraethylammonium-Cl, 2 mM $CoCl_2$, 10 mM CsCl and 0.1 mM nifedipine (all from Sigma), while the intrapipette solution contained (in mM): 140 CsCl, 2.5 $MgCl_2$, 2.5 Na_2ATP, 1.0 EGTA and 5 HEPES. During recordings, the organs of Corti were continuously perfused with the above extracellular bath solution. Whole-cell current responses were recorded with MultiClamp 700B patch clamp amplifier (Molecular Devices), controlled by jClamp software (SciSoft). Membrane capacitance was measured during the voltage ramp with a dual sinusoidal, FFT-based method[40]. The recorded capacitance was fitted to the first derivative of a two-state Boltzmann function that is typically used to fit nonlinear capacitance of OHCs plus a small correction for the membrane area changes between expanded and contracted states of prestin[41], as follows:

$C_m = C_v + C_{lin}$, in which C_m is the total membrane capacitance, C_v is a voltage-dependent (nonlinear) component, and C_{lin} is a voltage-independent (linear) component.

$$C_V = Q_{max}\frac{ze}{kT}\frac{b}{(1+b)^2} + \frac{\Delta C_{sa}}{(1+b^{-1})}; b = \exp\left(\frac{-ze(V-V_{pk})}{kT}\right)$$

in which Q_{max} is the maximum nonlinear charge moved, V_{pk} is a voltage at peak capacitance, V is membrane potential, z is valence, e is electron charge, k is Boltzmann's constant, T is absolute temperature, and ΔC_{sa} is the maximum increase in capacitance that occurs when all prestin molecules change from compact to expanded state. To account for some variability in sizes of IHCs, statistical data are shown as the maximum of voltage-dependent component of capacitance (C_v) normalized to the linear capacitance of the cell (C_v/C_{lin}).

DPOAEs. DPOAE tests were performed using frequency-specific tone-burst stimuli at 8, 16 and 32 kHz with the TDT RZ6 System 3 hardware and BioSig RZ (version 5.7.1) software (Tucker Davis Technology). An ER10B+ low noise probe microphone (Etymotic Research) was used to measure the DPOAE near the tympanic membrane. Tone stimuli were presented via separate MF1 (Tucker Davis Technology) speakers, with f_1 and f_2 at a ratio of $f_2/f_1 = 1.2$ (L1 = 65 dB SPL, L2 = 55 dB SPL), centred around the frequencies of 8, 16 and 32 kHz. Surgical anaesthesia was achieved by intraperitoneal injection of ketamine (100 mg ml^{-1} at 10% v/v), xylazine (20 mg ml^{-1} at 5% v/v) and acepromazine (2 mg ml^{-1} at 8% v/v) administered at a rate of 0.1 ml per 10 g body mass. Once the required depth of anaesthesia was confirmed by the lack of the pedal reflex, a section of pinna was removed to allow unobstructed access to the external auditory meatus. Mice were then placed on a heated mat inside a sound-attenuated chamber (ETS-Lindgren) and the DPOAE probe assembly was inserted into the ear canal using a pipette tip to aid correct placement. In-ear calibration was performed before each test. The f_1 and f_2 tones were presented continuously and a fast-Fourier transform was performed on the averaged response of 356 epochs (each approximately 21 ms). The level of the $2f_1 - f_2$ DPOAE response was recorded and the noise floor calculated by averaging the four frequency bins either side of the $2f_1 - f_2$ frequency.

NanoString validation. Cochlear RNA extracted from biological triplicates of *Ikzf2*$^{cello/cello}$, *Ikzf2*$^{cello/+}$ and *Ikzf2*$^{+/+}$ animals at P8 were processed for NanoString validation at the UMSOM Institute for Genome Sciences using the nCounter Master Kit per manufacturer's instructions, and quantified using the NanoString nCounter platform. See Supplementary Table 13 for NanoString probe sequences. Data were analysed using nSolver 4.0 software (NanoString).

Anc80L65 AAV vector construction. The Anc80L65-Myc-*Ikzf2*$^{+}$ (Anc80-*Ikzf2*) expression vector was designed to drive expression of a Myc-tagged *Ikzf2* construct followed by a bovine Growth Hormone poly-adenylation (BGH pA) site under control of the cytomegalovirus (CMV) promoter. The Anc80L65-eGFP (Anc80-eGFP) expression construct also contained a Woodchuck Hepatatis Virus Posttranscriptional Regulatory Element (WPRE) preceding the BGH pA site. Anc80L65 AAV vectors[17,18] were produced by the Gene Transfer Vector Core, Grousbeck Gene Therapy Center at the Massachusetts Eye and Ear Infirmary (http://vector.meei.harvard.edu/).

Inner ear gene delivery. For in vivo hair cell transductions, mice were injected with Anc80L65 AAVs between P1 and P3 via the posterior semicircular canal using the injection method described previously[42]. In brief, animals were anesthetized on ice before a post-auricular incision was made on either the left or right side. Tissues were further dissected to reveal the posterior semicircular canal, and a Nanolitre 2010 microinjection system (World Precision Instruments) equipped with a loaded glass needle was used to inject 700 nl of 1.13×10^{13} genome copies (GC) per ml Anc80-*Ikzf2* or 500 nl of 4.85×10^{12} GC per ml Anc80-eGFP. Injections into the inner ear were performed in 50 nl increments over the course of 2 min. The needle was then removed, the incision sutured, and animals were placed on a 37 °C heating pad to recover before being returned to their cage.

FACS. For the scRNA-seq analysis of Anc80-*Ikzf2* transduced hair cells, inner ears of neonatal *Myo15*$^{cre/+}$;*ROSA26*$^{CAG\text{-}tdTomato}$ mice were injected with Anc80-*Ikzf2* (4 mice) or control Anc80-eGFP (2 mice) via the posterior semicircular canal.

Cochlear tissues from both injected and uninjected ears were obtained at P8 and further dissected to reveal the sensory epithelium. Inclusion of the uninjected ear in the single cell analysis allowed for the study of changes in gene expression that occur in response to a gradient of transgene expression. This is because, in mice, inner ear gene delivery often results in transduction in the contralateral ear, albeit at a lower intensity[18]. Cochlear tissues were then dissociated for fluorescence activated cell sorting (FACS) using the method described previously[9]. In brief, the sensory epithelia from Anc80-eGFP- and Anc80-*Ikzf2*-injected mice were pooled separately into two wells of a 48-well plate containing 0.5 mg ml^{-1} thermolysin (Sigma). Tissues were incubated at 37 °C for 20 min, after which the thermolysin was removed and replaced with accutase enzyme (MilliporeSigma). After a 3-min incubation at 37 °C, tissues were mechanically disrupted using a 23G blunt ended needle connected to a 1 ml syringe. This step was performed twice. After confirming tissue dissociation by direct visualization, the dissociation reaction was stopped by adding an equal volume of IMDM supplemented with 10% heat-inactivated FBS to the Accutase enzyme solution. Cells were passed through a 40 mm cell strainer (BD) to remove cell clumps. tdTomato-expressing hair cells were sorted into ice-cold tubes containing IMDM with 10% FBS on a BD FACSAria II (BD Biosciences) and processed for scRNA-seq. Flow cytometry analyses were performed with assistance from X. Fan at the University of Maryland Marlene and Stewart Greenebaum Comprehensive Cancer Center Flow Cytometry Shared Service.

scRNA-seq. tdTomato-positive sorted hair cells were pelleted once (300*g* at 4 °C) and resuspended in a minimal remaining volume (around 30 μl). Hair cell-enriched single-cell suspensions were then used as input on the 10× Genomics Chromium platform with 3′ Single Cell v2 chemistry (10× Genomics). After capture and library preparation, scRNA-seq libraries were sequenced on a NextSeq 500 (Illumina) in collaboration with the NIDCD Genomics and Computational Biology Core. Samples were sequenced to an average depth of over 300,000 reads per cell, which resulted in detection of a median of >3,000 genes (Anc80-eGFP) and >4,000 genes (Anc80-*Ikzf2*) per cell, ensuring maximal transcriptional complexity and detection of low-abundance transcripts (see Extended Data Fig. 9b, c). Reads were aligned to a modified mm10 mouse reference containing the sequences for the Ai14 locus, as well as Anc80-eGFP and Anc80-*Ikzf2* viral sequences (Extended Data Fig. 9a) using the 10× Genomics Cell Ranger (version 2.0.2) package to generate the read counts matrix files. Read counts from viral and Ai14 loci were removed from the expression matrix before dimensionality reduction so as to not influence data clustering. Cells from these hair cell clusters were determined to be Anc80-*Ikzf2*(+) versus Anc80-*Ikzf2*(−), and IHCs versus OHCs, based on their expression of Anc80-*Ikzf2* and *Slc17a8*, respectively (Fig. 3, Extended Data Figs. 8 and 9, Supplementary Table 9). *Slc26a5* was not well detected in the scRNA-seq dataset and was therefore not used as an OHC marker. After clustering, four hair cells were excluded based on co-expression of a contaminating cell type. Secondary analyses, including shared nearest neighbour (SNN) clustering, *t*-SNE embedding, and differential expression testing (using either Wilcoxon ranked sum for marker gene identification or MAST for pairwise comparison between control IHCs and OHCs) were performed in R with Seurat (version 2.1.0)[43,44]. Non-parametric analysis of variance between the four classified groups of HCs (IHCs and OHCs with either high or low Anc80-*Ikzf2* expression) using a Kruskal–Wallis test was performed to help qualify genes that had statistical difference across these cell populations. This was followed by post hoc pairwise Wilcoxon ranked sum comparisons to assess multiple-comparison-adjusted *P* values. Additional plots were generated by NMF (version 0.20.6) and ggplot2 (version 2.2.1)[45,46]. These analyses used the computational resources of the NIH HPC Biowulf cluster (http://hpc.nih.gov).

Immunohistochemistry of AAV-injected cochleae. Mouse inner ears injected with either Anc80-*Ikzf2* or Anc80-eGFP were between P8 and 8 weeks, fixed in 4% PFA in PBS overnight at 4 °C, and decalcified in a solution of 5% EDTA in RNAlater (Invitrogen). Decalcified ears were processed by sucrose gradient and embedded in OCT compound (Tissue-Tek) for cryosectioning, or fine dissected for whole-mount immunohistochemistry. Cryosections (10 μm) on positively charged glass slides were used for in situ hybridization (ISH) and section immunohistochemistry. For whole-mount immunolabelling at 6–8 weeks, hair cell loss was observed in the injected ear and therefore the contralateral ear, expressing a lower level of the Anc80-*Ikzf2* virus, was used. Primary antibodies: goat anti-prestin N-20 (1:200, Santa Cruz Biotechnology); goat anti-oncomodulin N-19 (1:100, Santa Cruz Biotechnology); rabbit anti-myosinVI (1:1,000, Proteus BioSciences); rabbit anti-GFP (1:100, Life Technologies); mouse anti-cMyc 9E10 (1:100, Santa Cruz Biotechnology) and mouse anti-otoferlin (1:100, Abcam). The guinea pig anti-VGLUT3 antibody (1:5,000) used in this study was donated by R. Seal. Corresponding Alexa Fluor 488 and 546 (1:800, Invitrogen) were used for secondary detection, Alexa Fluor 488 Phalloidin (1:1,000, Invitrogen) was used to mark F-actin, and DAPI (1:20,000, Thermo Fisher) was used to mark cell nuclei. Images were acquired using a Nikon Eclipse E600 microscope (Nikon) equipped with a Lumenera Infinity 3 camera. Whole-mount images were acquired using a Zeiss LSM DUO confocal microscope, located at the UMSOM Confocal Microscopy Core, at 63× oil magnification. Images were processed using Infinity Capture and Infinity Analyze software (Lumenera), and ImageJ software.

RNA in situ hybridization. In situ hybridization was performed as described previously[47]. In brief, slides were re-fixed in 4% PFA, and then treated with 2 μg ml^{-1} Proteinase-K for 10 min. Proteinase K reaction was stopped by soaking slides again in 4% PFA, followed by acetylation and permeabilization. Hybridization for the digoxigenin labelled *Fcrlb* probe was performed overnight at 65 °C (see Supplementary Table 13 for *Fcrlb* probe primers). After a series of washes in saline sodium citrate, slides were incubated with sheep-anti-digoxigenin antibody conjugated to alkaline phosphatase (Sigma-Aldrich, 1:100) overnight at 4 °C. Slides were then incubated in BM purple AP substrate precipitating solution (Roche) to localize bound anti-digoxigenin antibody.

Reporting summary. Further information on research design is available in the Nature Research Reporting Summary linked to this paper.

Data availability

The RiboTag OHC RNA-seq, P8 cello cochlea RNA-seq, and P8 Anc80-*Ikzf2* and Anc80-eGFP injected cochlea scRNA-seq data have been submitted to the Gene Expression Omnibus (GEO) database under accessions GSE116703, GSE116702 and GSE120462, and are also available for viewing through the gEAR portal (https://umgear.org/).

23. Caberlotto, E. et al. Usher type 1G protein sans is a critical component of the tip-link complex, a structure controlling actin polymerization in stereocilia. *Proc. Natl Acad. Sci. USA* **108**, 5825–5830 (2011).
24. Johnson, K. R., Zheng, Q. Y. & Noben-Trauth, K. Strain background effects and genetic modifiers of hearing in mice. *Brain Res.* **1091**, 79–88 (2006).
25. Hoelter, S. M. et al. "Sighted C3H" mice—a tool for analysing the influence of vision on mouse behaviour? *Front. Biosci.* **13**, 5810–5823 (2008).
26. Kim, D. et al. TopHat2: accurate alignment of transcriptomes in the presence of insertions, deletions and gene fusions. *Genome Biol.* **14**, R36 (2013).
27. Anders, S., Pyl, P. T. & Huber, W. HTSeq—a Python framework to work with high-throughput sequencing data. *Bioinformatics* **31**, 166–169 (2015).
28. Anders, S. & Huber, W. Differential expression analysis for sequence count data. *Genome Biol.* **11**, R106 (2010).
29. Ulitsky, I. et al. Expander: from expression microarrays to networks and functions. *Nat. Protocols* **5**, 303–322 (2010).
30. Sharan, R., Maron-Katz, A. & Shamir, R. CLICK and EXPANDER: a system for clustering and visualizing gene expression data. *Bioinformatics* **19**, 1787–1799 (2003).
31. Shannon, P. et al. Cytoscape: a software environment for integrated models of biomolecular interaction networks. *Genome Res.* **13**, 2498–2504 (2003).
32. Adzhubei, I. A. et al. A method and server for predicting damaging missense mutations. *Nat. Methods* **7**, 248–249 (2010).
33. Choi, Y., Sims, G. E., Murphy, S., Miller, J. R. & Chan, A. P. Predicting the functional effect of amino acid substitutions and indels. *PLoS One* **7**, e46688 (2012).
34. Kumar, P., Henikoff, S. & Ng, P. C. Predicting the effects of coding non-synonymous variants on protein function using the SIFT algorithm. *Nat. Protocols* **4**, 1073–1081 (2009).
35. Källberg, M. et al. Template-based protein structure modeling using the RaptorX web server. *Nat. Protocols* **7**, 1511–1522 (2012).
36. Hardisty-Hughes, R. E., Parker, A. & Brown, S. D. M. A hearing and vestibular phenotyping pipeline to identify mouse mutants with hearing impairment. *Nat. Protocols* **5**, 177–190 (2010).
37. Mianné, J. et al. Correction of the auditory phenotype in C57BL/6N mice via CRISPR/Cas9-mediated homology directed repair. *Genome Med.* **8**, 16 (2016).
38. Codner, G. F. et al. Application of long single-stranded DNA donors in genome editing: generation and validation of mouse mutants. *BMC Biol.* **16**, 70 (2018).
39. Corns, L. F., Johnson, S. L., Kros, C. J. & Marcotti, W. Calcium entry into stereocilia drives adaptation of the mechanoelectrical transducer current of mammalian cochlear hair cells. *Proc. Natl Acad. Sci. USA* **111**, 14918–14923 (2014).
40. Santos-Sacchi, J. Determination of cell capacitance using the exact empirical solution of partial $\delta Y/\delta C_m$ and its phase angle. *Biophys. J.* **87**, 714–727 (2004).
41. Santos-Sacchi, J. & Navarrete, E. Voltage-dependent changes in specific membrane capacitance caused by prestin, the outer hair cell lateral membrane motor. *Pflugers Arch.* **444**, 99–106 (2002).
42. Isgrig, K. et al. Gene therapy restores balance and auditory functions in a mouse model of usher syndrome. *Mol. Ther.* **25**, 780–791 (2017).
43. Finak, G. et al. MAST: a flexible statistical framework for assessing transcriptional changes and characterizing heterogeneity in single-cell RNA sequencing data. *Genome Biol.* **16**, 278 (2015).
44. Satija, R., Farrell, J. A., Gennert, D., Schier, A. F. & Regev, A. Spatial reconstruction of single-cell gene expression data. *Nat. Biotechnol.* **33**, 495–502 (2015).
45. Wickham, H. *ggplot2: Elegant Graphics for Data Analysis* (Springer, New York, 2009).
46. Gaujoux, R. & Seoighe, C. A flexible R package for nonnegative matrix factorization. *BMC Bioinformatics* **11**, 367 (2010).
47. Geng, R. et al. Comprehensive expression of Wnt signaling pathway genes during development and maturation of the mouse cochlea. *PLoS One* **11**, e0148339 (2016).

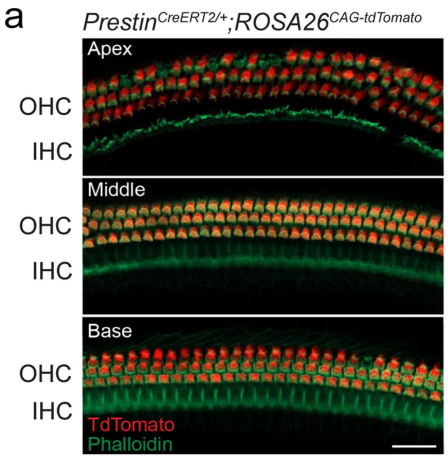

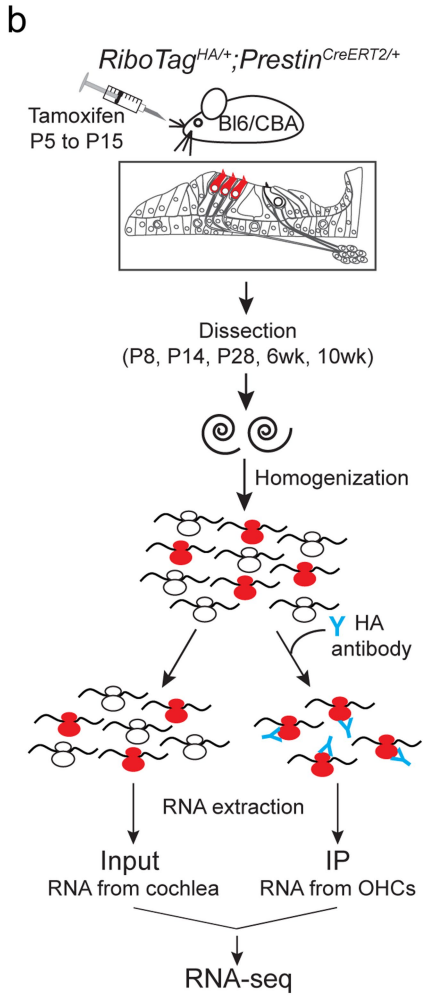

c

Cell type	Gene	Prestin^{CreERT2}; RiboTag IP				
		Log_2EF P8	Log_2EF P14	Log_2EF P28	Log_2EF 6wk	Log_2EF 10wk
Outer hair cells	*Ocm*	3.42	2.75	3.2	2.69	4.95
	Slc26a5	2.68	0.57	-0.06	0.47	2.91
	Strc	3.04	1.08	2.69	1.17	2.74
All hair cells	*Gfi1*	2.25	1.32	0.21	1.04	2.33
	Pou4f3	3.83	0.91	0.5	1.09	2.58
Inner hair cells	*Atp2a3*	-0.65	-2.01	-1.31	-1.72	-2.02
	Otof	0.46	-1.16	-1.03	-1.12	-0.25
	Slc17a8	-0.27	-0.68	-0.86	-1.77	-1.35
Supporting cells	*Sox2*	0.28	-0.03	0.71	0.29	-0.48
	Jag1	-0.6	-1.11	-1.00	-1.11	-0.24
Neurons	*Tubb3*	-1.91	-1.2	-0.02	-0.59	-1.13
Mesenchyme	*Pou3f4*	-0.08	-0.61	-1.17	-0.82	-1.11

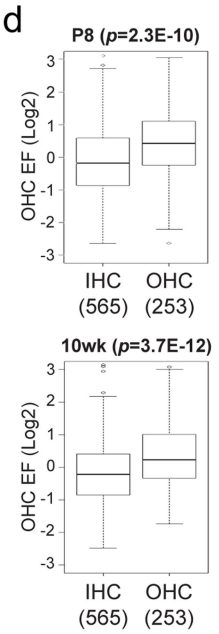

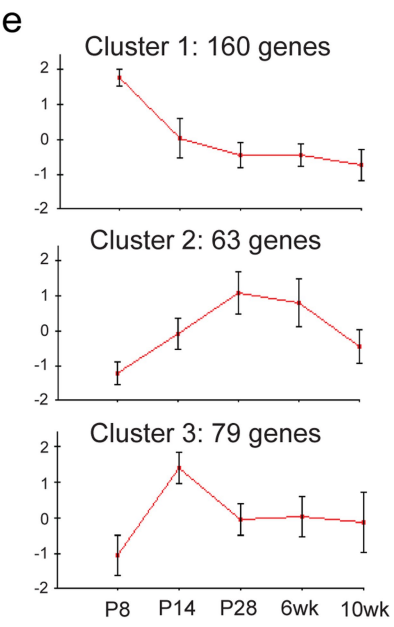

f

Cluster	GO category	*p*-value	Empirical *p*-value
Cluster 1	anatomical structure morphogenesis - GO:0009653	3.51E-08	0.001
	skeletal system morphogenesis - GO:0048705	2.17E-06	0.003
	locomotion - GO:0040011	3.98E-06	0.006
	extracellular matrix structural constituent - GO:0005201	8.34E-06	0.018
	cell motility - GO:0048870	3.53E-05	0.047
Cluster 2	cell development - GO:0048468	3.52E-11	0.001
	voltage-gated cation channel activity - GO:0022843	3.08E-06	0.005
	transmission of nerve impulse - GO:0019226	1.07E-05	0.02

Extended Data Fig. 1 | RiboTag immunoprecipitation enriches for known OHC-expressed transcripts. a, Representative *prestin*$^{creERT2/+}$;*ROSA26*$^{CAG\text{-}tdTomato}$ cochlear whole-mount. The *prestin*^{creERT2}-driven tdTomato expression is OHC-specific at P21 ($n = 1$). Scale bar, 20 μm. **b**, Schematic of the RiboTag immunoprecipitation protocol. Red OHCs represent Cre/HA-tagged ribosome expression. **c**, RiboTag RNA-seq log_2 enrichment and depletion of transcripts for known inner ear cell type markers (EF = log_2(IP/input)). **d**, Genes at least two-fold enriched in IHCs ($n = 565$ genes) or OHCs ($n = 253$ genes) in the published dataset[8] are significantly depleted or enriched, respectively, by the RiboTag OHC immunoprecipitation at all time points examined (two-sided Wilcoxon's test). Black line represents median EF, box demarcates first and third quartiles, whiskers demarcate first and third quartiles ± 1.5 × IQR values, dots represent single outliers. **e**, Clustering of genes differentially expressed across OHC postnatal development. Error bars denote s.d. Before clustering, expression levels were standardized to mean = 0 and s.d. = 1. **f**, Enriched Gene Ontology (GO) functional categories identified for the gene clusters in **e** (cluster 1 $n = 160$ genes, cluster 2 $n = 63$ genes). No significantly enriched GO categories were found for cluster 3 ($n = 79$ genes). Enrichment and statistical analyses were performed using the EXPANDER implemented tool TANGO.

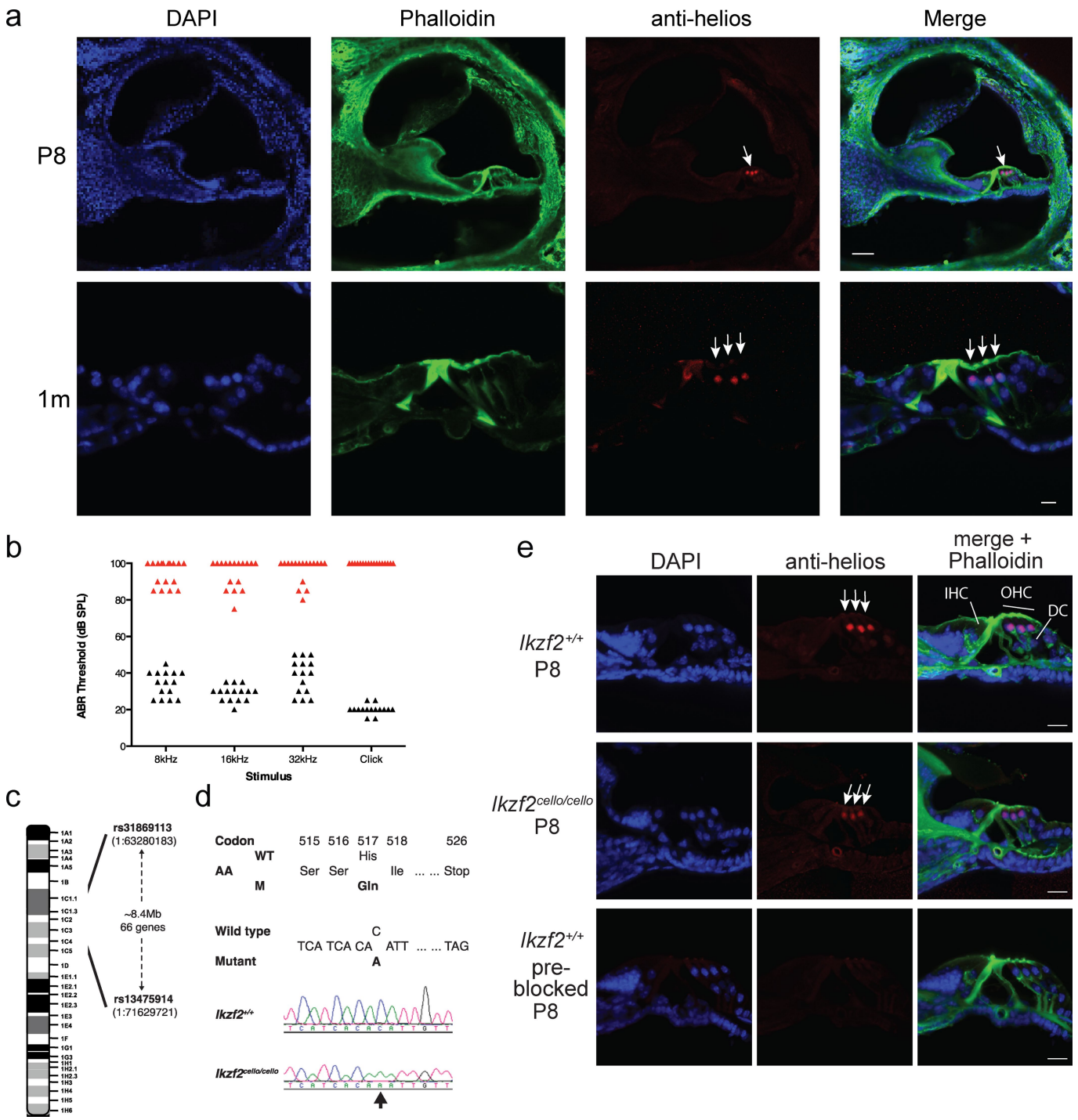

Extended Data Fig. 2 | Auditory phenotyping, SNP mapping and whole-genome sequencing of mouse pedigree MPC173, subsequently named *cello*. **a**, Specific expression of Helios can be seen in the nuclei of wild-type P8 OHCs (white arrow), and is maintained in wild-type OHCs at 1 month (white arrows). Scale bars, 50 μm (P8) and 10 μm (1 month). $n = 3$ biologically independent samples for each time point. **b**, Auditory brainstem response phenotyping of pedigree MPC173 at 9 months of age identified 17 biologically independent animals with increased hearing thresholds (red triangles) compared to their normal hearing colony mates (black triangles). $n = 15$ biologically independent animals. **c**, The mutation mapped to an 8.4-Mb region on chromosome 1 between single nucleotide polymorphism (SNP) rs31869113 and rs13475914 (chr1: 63280183–71629721), containing 66 genes. **d**, Detection of a non-synonymous mutation in *cello*. DNA sequencing identified a nucleotide transversion (c.1551C>A) in the *Ikzf2* gene at codon 517, thus altering the wild-type sequence CAC, encoding histidine, to the mutant (M) sequence CAA, encoding glutamine. Electropherograms derived from a *cello* mutant mouse ($Ikzf2^{cello/cello}$) and a wild-type colony mate ($Ikzf2^{+/+}$) control showing the sequence surrounding *Ikzf2* nucleotide 1551 (indicated by an arrow). e, Helios is expressed in the OHC nuclei of both $Ikzf2^{+/+}$ and $Ikzf2^{cello/cello}$ mice at P8. $n = 3$ biologically independent samples per genotype. Loss of labelling when the anti-Helios antibody is 'pre-blocked' confirms specificity. $n = 1$ biologically independent sample. Scale bars, 20 μm. DC, Deiters' cells.

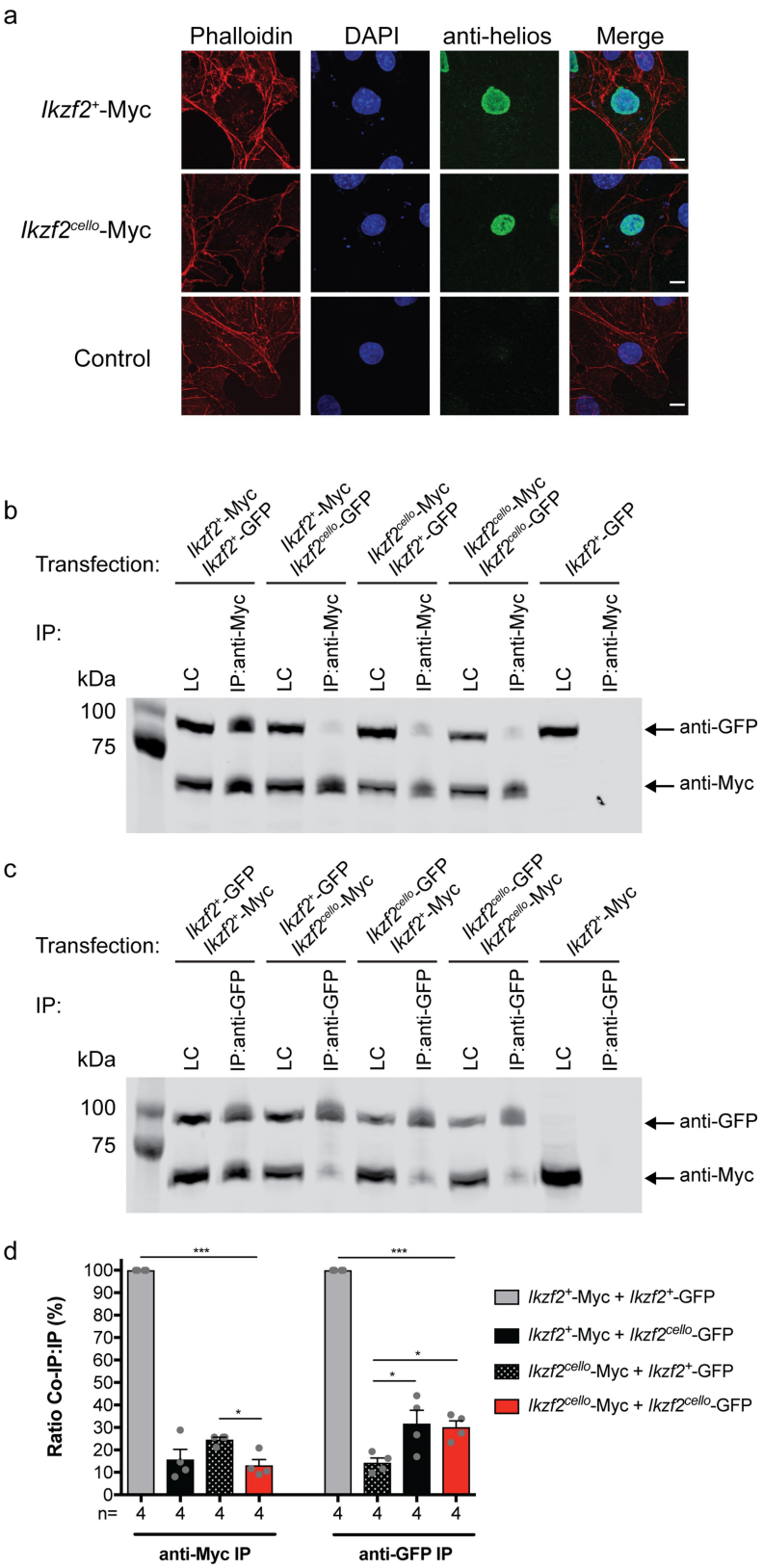

Extended Data Fig. 3 | See next page for caption.

Extended Data Fig. 3 | The *Ikzf2*^{cello} mutation disrupts homodimerization of Helios. a, Cos-7 cells transfected with *Ikzf2*$^{+}$- or *Ikzf2*^{cello}-Myc. Nuclear localization is unaffected by the *Ikzf2*^{cello} mutation. $n = 2$ biologically independent experiments. Scale bars, 10 μm. **b**, Co-immunoprecipitation (IP) of Myc-tagged (62 kDa) and GFP-tagged (88 kDa) *Ikzf2*$^{+}$ and *Ikzf2*^{cello} constructs. Transfected cell lysates were immunoprecipitated using an anti-Myc antibody and analysed by western blotting with both anti-Myc and anti-GFP antibodies. Results show that wild-type *Ikzf2*$^{+}$ Helios can dimerize, but that dimerization is impaired by the *cello* mutation. LC, cell lysate loading control. **c**, Reciprocal immunoprecipitation reactions using an anti-GFP antibody confirm dimerization of wild-type *Ikzf2*$^{+}$ Helios and reduced dimerization of mutant *Ikzf2*^{cello} Helios. **d**, Quantification of co-immunoprecipitation western blots. Band intensities were determined and used to calculate the relative ratio of the co-immunoprecipitation to immunoprecipitation signal. $n = 4$ biologically independent experiments. Data are mean ± s.e.m. Anti-Myc IP: ***$P < 0.0001$ (*Ikzf2*$^{+}$-Myc + *Ikzf2*$^{+}$-GFP vs *Ikzf2*$^{+}$-Myc + *Ikzf2*^{cello}-GFP, vs *Ikzf2*^{cello}-Myc + *Ikzf2*$^{+}$-GFP and vs *Ikzf2*^{cello}-Myc + *Ikzf2*^{cello}-GFP). *$P = 0.0476$ (*Ikzf2*^{cello}-Myc + *Ikzf2*$^{+}$-GFP vs *Ikzf2*^{cello}-Myc + *Ikzf2*^{cello}-GFP). $P = 0.1488$ (*Ikzf2*$^{+}$-Myc + *Ikzf2*^{cello}-GFP vs *Ikzf2*^{cello}-Myc + *Ikzf2*$^{+}$-GFP). $P = 0.9020$ (*Ikzf2*$^{+}$-Myc + *Ikzf2*^{cello}-GFP vs *Ikzf2*^{cello}-Myc + *Ikzf2*^{cello}-GFP). Anti-GFP IP: ***$P < 0.0001$ (*Ikzf2*$^{+}$-Myc + *Ikzf2*$^{+}$-GFP vs *Ikzf2*^{cello}-Myc + *Ikzf2*$^{+}$-GFP, vs *Ikzf2*$^{+}$-Myc + *Ikzf2*^{cello}-GFP and vs *Ikzf2*^{cello}-Myc + *Ikzf2*^{cello}-GFP). *$P = 0.0202$ (*Ikzf2*^{cello}-Myc + *Ikzf2*$^{+}$-GFP vs *Ikzf2*$^{+}$-Myc + *Ikzf2*^{cello}-GFP) *$P = 0.0346$ (*Ikzf2*^{cello}-Myc + *Ikzf2*$^{+}$-GFP vs *Ikzf2*^{cello}-Myc + *Ikzf2*^{cello}-GFP). $P = 0.9894$ (*Ikzf2*$^{+}$-Myc + *Ikzf2*^{cello}-GFP vs + *Ikzf2*^{cello}-Myc + *Ikzf2*^{cello}-GFP) (one-way ANOVA with Tukey post hoc test). See Supplementary Fig. 1 for source images.

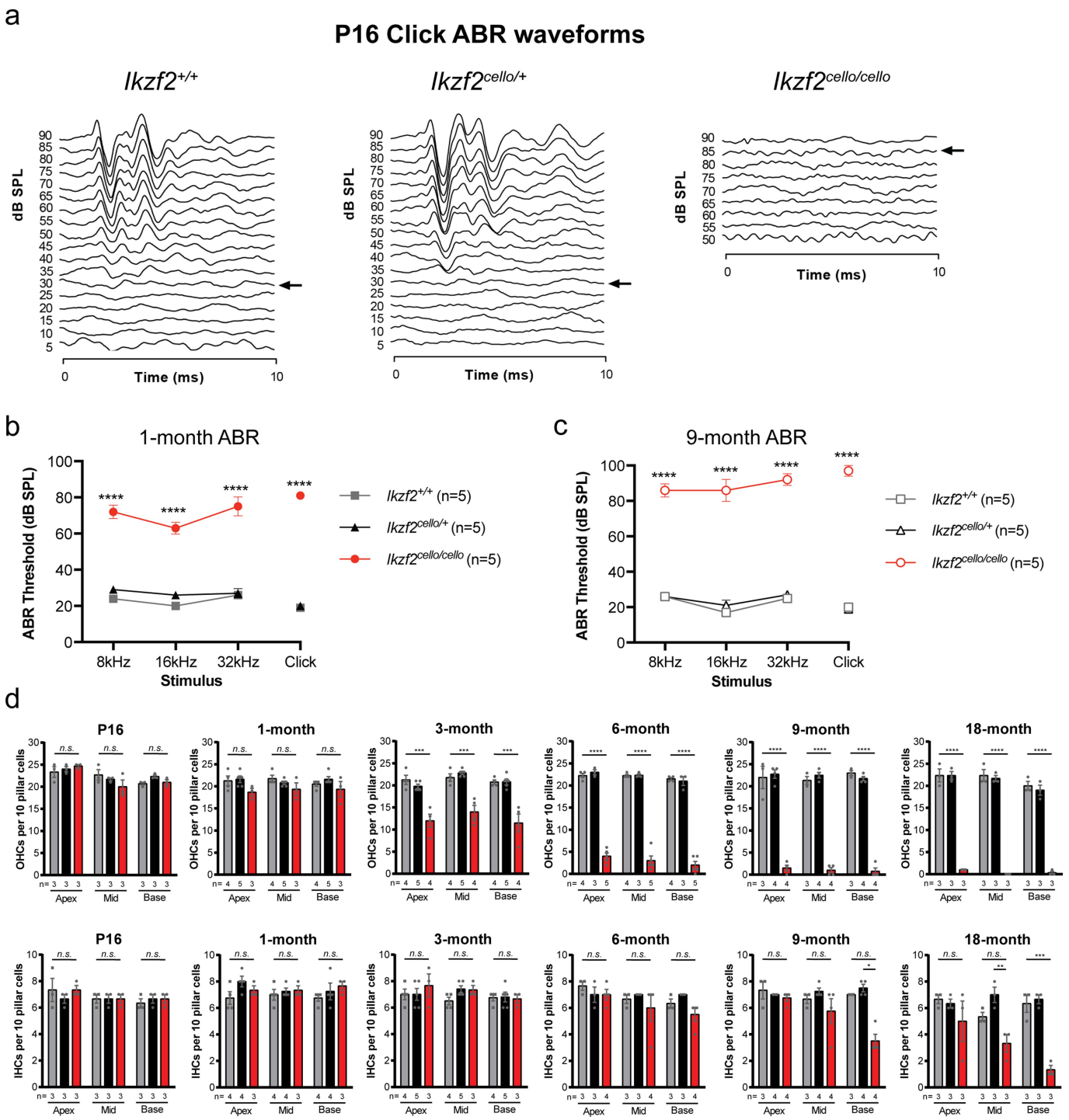

Extended Data Fig. 4 | Auditory function and HC bundle survival in *cello* mice. a, Representative click ABR waveforms for *Ikzf2*$^{+/+}$, *Ikzf2*$^{cello/+}$ and *Ikzf2*$^{cello/cello}$ littermates at P16. $n = 4$ biologically independent animals per genotype. **b**, **c**, Averaged ABR thresholds for *cello* mice at 1-month of age (**b**) and 9 months of age (**c**). Age-matched *Ikzf2*$^{+/+}$ and *Ikzf2*$^{cello/+}$ controls display thresholds within the expected range (15–30 dB SPL) at all time points tested. $n = 5$ biologically independent animals per genotype. Data are mean thresholds ± s.e.m. 1-month *Ikzf2*$^{cello/cello}$ vs *Ikzf2*$^{+/+}$: $^{****}P < 0.0001$ (8 kHz, 16 kHz, 32 kHz, click). 1-month *Ikzf2*$^{cello/cello}$ vs 1 *Ikzf2*$^{cello/+}$: $^{****}P < 0.0001$ (8 kHz, 16 kHz, 32 kHz, click). 9-month *Ikzf2*$^{cello/cello}$ vs *Ikzf2*$^{+/+}$: $^{****}P < 0.0001$ (8 kHz, 16 kHz, 32 kHz, click). 9-month *Ikzf2*$^{cello/cello}$ vs *Ikzf2*$^{cello/+}$: $^{****}P < 0.0001$ (8 kHz, 16 kHz, 32 kHz, click) (one-way ANOVA with Tukey post hoc test). **d**, OHC and IHC bundle counts for *cello* mice from P16 to 18 months of age. Grey, *Ikzf2*$^{+/+}$; black, *Ikzf2*$^{cello/+}$; red, *Ikzf2*$^{cello/cello}$. Data are mean ± s.e.m. *n.s.*, non-significant. $^{*}P < 0.05$, $^{**}P < 0.01$, $^{***}P < 0.001$, $^{****}P < 0.0001$ (one-way ANOVA with Tukey post hoc test). Number of biologically independent samples for OHC and IHC bundle counts are shown. See also Supplementary Table 5 and 6.

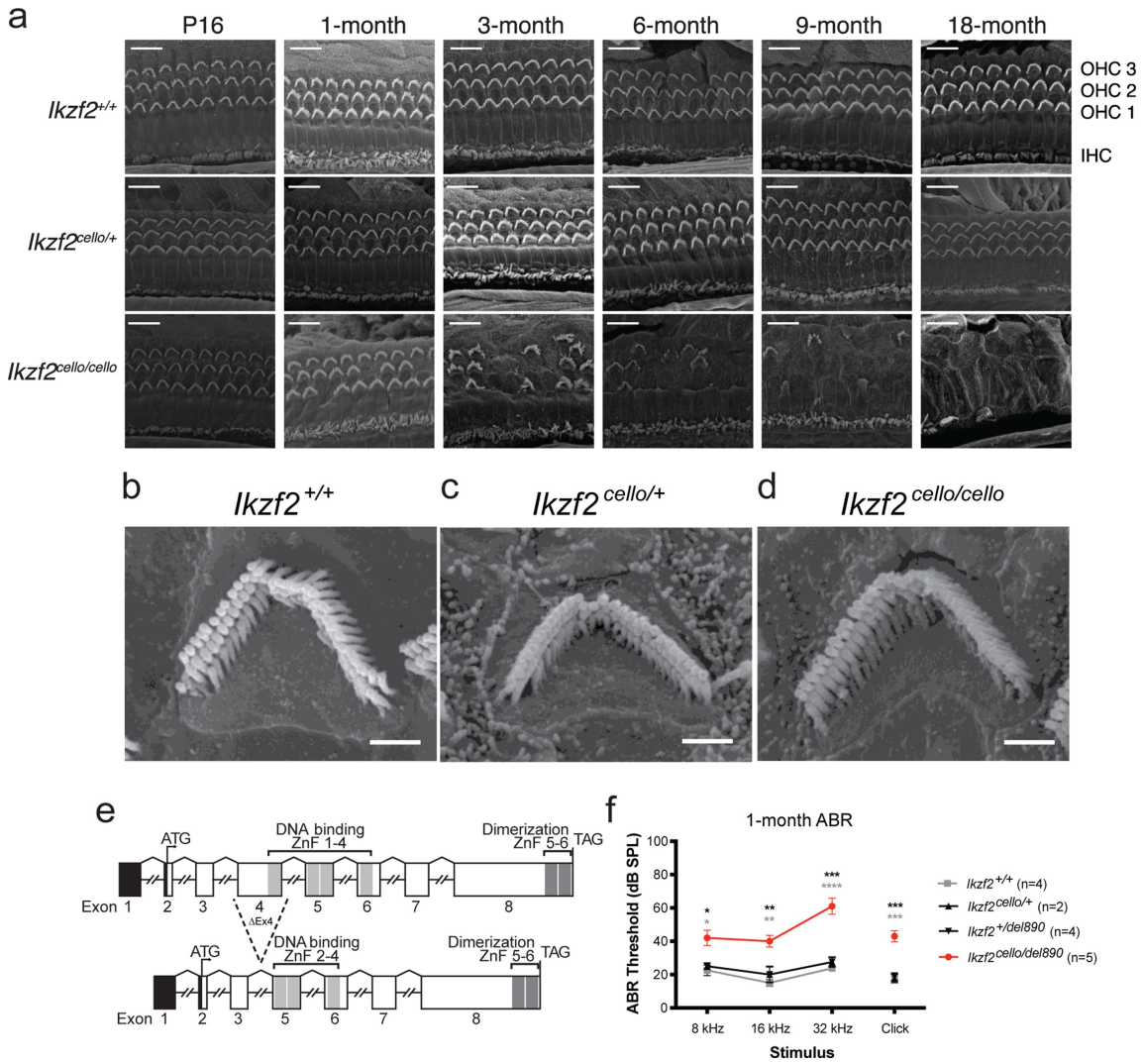

Extended Data Fig. 5 | Scanning electron microscopy of *cello* mice and auditory function of *Ikzf2*$^{cello/del890}$ compound heterozygotes. **a**, Scanning electron micrographs of the organ of Corti of *cello* mice from P16 to 18 months of age. Representative images from the mid-region of the cochlear spiral are shown. Scale bars, 10 μm. $n = 3$ (P16 *Ikzf2*$^{cello/+}$, P16 *Ikzf2*$^{cello/cello}$, 1-m *Ikzf2*$^{cello/cello}$, 9-m *Ikzf2*$^{+/+}$, 18-m *Ikzf2*$^{+/+}$, 18-m *Ikzf2*$^{cello/+}$, 18-m *Ikzf2*$^{cello/cello}$), $n = 4$ (P16 *Ikzf2*$^{+/+}$, 1-m *Ikzf2*$^{+/+}$, 3-m *Ikzf2*$^{+/+}$, 3-m *Ikzf2*$^{cello/cello}$, 6-m *Ikzf2*$^{+/+}$, 6-m *Ikzf2*$^{cello/cello}$, 9-m *Ikzf2*$^{cello/+}$, 9-m *Ikzf2*$^{cello/cello}$) and $n = 5$ (1-m *Ikzf2*$^{cello/+}$, 3-m *Ikzf2*$^{cello/+}$, 6-m *Ikzf2*$^{cello/+}$) biologically independent samples. **b**–**d**, Scanning electron micrographs of OHC stereocilia bundles of *cello* mice at P16, showing that wild-type *Ikzf2*$^{+/+}$ (**b**), *Ikzf2*$^{cello+}$ (**c**) and mutant *Ikzf2*$^{cello/cello}$ (**d**) mice display overall expected bundle patterning. Images are from the mid-region of the cochlear spiral. Scale bars, 1 μm. $n = 3$ biologically independent samples for each genotype. **e**, The genomic and domain structure of *Ikzf2*^{del890}. Black, 5′ untranslated region; light grey, N-terminal DNA-binding domain; dark grey, C-terminal dimerization domain. The *Ikzf2*^{cello} mutation lies in ZnF6. The *del890* mutation deletes exon 4 and the surrounding intronic sequence. **f**, Averaged ABR thresholds for *Ikzf2*$^{cello/del890}$ compound heterozygotes at 1 month of age, showing increased thresholds (≥40 dB SPL) at all frequencies tested compared to *Ikzf2*$^{+/+}$, *Ikzf2*$^{cello/+}$ and *Ikzf2*$^{del890/+}$ control colony mates. Data are mean ± s.e.m. $n = 4$ (*Ikzf2*$^{+/+}$, *Ikzf2*$^{+/del890}$), $n = 2$ (*Ikzf2*$^{cello/+}$) and $n = 5$ (*Ikzf2*$^{cello/del890}$) biologically independent samples. *Ikzf2*$^{cello/del890}$ vs *Ikzf2*$^{+/+}$: $^{*}P = 0.011$ (8 kHz), $^{**}P = 0.002$ (16 kHz), $^{****}P < 0.0001$ (32 kHz), $^{***}P = 0.0001$ (click); *Ikzf2*$^{cello/del890}$ vs *Ikzf2*$^{cello/+}$: $P = 0.078$ (8 kHz), $^{*}P = 0.034$ (16 kHz), $^{**}P = 0.001$ (32 kHz), $^{**}P = 0.001$ (click); *Ikzf2*$^{cello/del890}$ vs *Ikzf2*$^{+/del890}$: $^{*}P = 0.025$ (8 kHz), $^{**}P = 0.009$ (16 kHz), $^{***}P = 0.0002$ (32 kHz), $^{***}P = 0.0002$ (click) (one-way ANOVA with Tukey post hoc test).

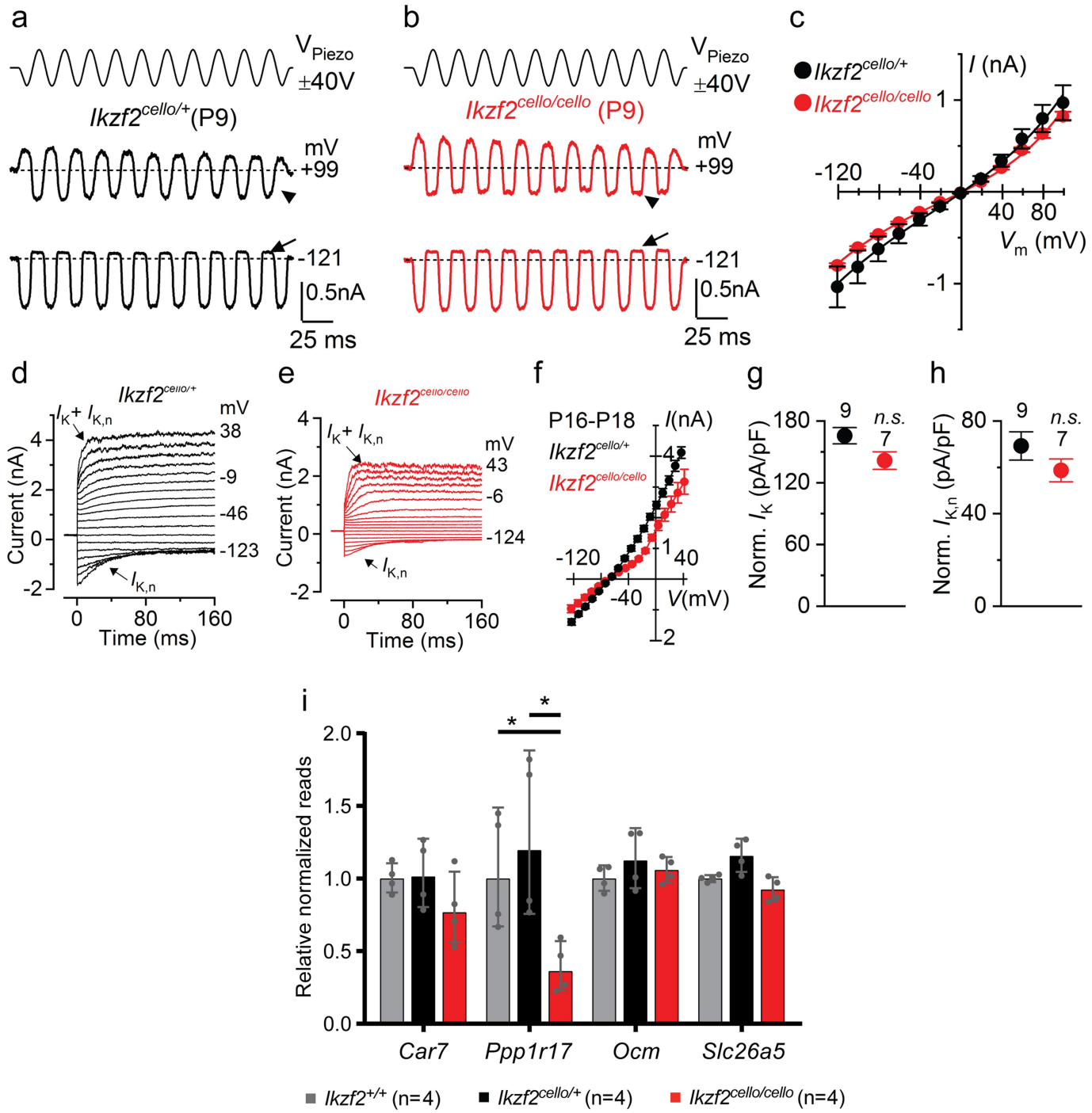

Extended Data Fig. 6 | See next page for caption.

Extended Data Fig. 6 | The MET and adult-like potassium currents are normal in *Ikzf2*^{cello} mice. a, **b**, MET currents were recorded from OHCs of P9 *Ikzf2*$^{cello/cello}$ and *Ikzf2*$^{cello/+}$ (control) littermates. During voltage steps, hair bundles were displaced by applying a 50-Hz sinusoidal force stimuli (the driver voltage to the fluid jet is shown above the traces)[39]. At hyperpolarized membrane potentials (−121 mV), saturating excitatory bundle stimulation (that is, towards the taller stereocilia) elicited a large inward MET current from both *Ikzf2*$^{cello/+}$ and *Ikzf2*$^{cello/cello}$ OHCs, whereas inhibitory bundle stimulation (that is, away from the taller stereocilia) closed the MET channels and reduced the resting current. Because the MET current reverses near 0 mV, it became outward when excitatory bundle stimulation was applied during voltage steps positive to its reversal potential. At positive membrane potentials (+99 mV), excitatory bundle stimulation now elicited similar outward MET currents with larger resting amplitudes. Arrows indicate closure of the MET channels (that is, disappearance of the resting current) during inhibitory bundle displacements, arrowheads indicate the larger resting MET current at +99 mV compared to −121 mV. **c**, Peak-to-peak current–voltage curves obtained from *Ikzf2*$^{cello/+}$ ($n = 10$ biologically independent samples) and *Ikzf2*$^{cello/cello}$ ($n = 8$ biologically independent samples) OHCs at P9. The maximal MET current and the resting open probability of the MET channel were found to be similar between the two genotypes. Data are mean ± s.e.m. **d**, **e**, Total K^+ currents recorded from P18 *Ikzf2*$^{cello/+}$ control (**d**) and *Ikzf2*$^{cello/cello}$ mutant (**e**) OHCs. The size of the K^+ current, which is mainly due to the negatively activated $I_{K,n}$ (in addition to a small delayed rectifier I_K[15]), was smaller in *Ikzf2*$^{cello/cello}$ OHCs. **f**, Average peak current–voltage relationship for the total K^+ current recorded from the OHCs of *Ikzf2*$^{cello/+}$ ($n = 9$ OHCs from 6 biologically independent animals) and *Ikzf2*$^{cello/cello}$ ($n = 7$ OHCs from 5 biologically independent animals) mice at P16–P18. Data are mean ± s.e.m. **g**, **h**, After normalization to the significantly reduced surface area of *Ikzf2*$^{cello/cello}$ OHCs (for this set of experiments: *Ikzf2*$^{cello/+}$: 14.2 ± 0.4 pF; *Ikzf2*$^{cello/cello}$: 11.2 ± 0.5 pF; $P < 0.0005$), both the total I_K (**g**) and isolated $I_{K,n}$ (**h**) were not significantly different between the two genotypes at P16–P18 (two-sided Welch's *t*-test). Data are mean ± s.e.m. **i**, NanoString validations of genes downregulated in P8 *Ikzf2*$^{cello/cello}$ cochleae at P16, normalized to wild-type reads. Data are mean ± s.d. ($n = 4$ biologically independent samples per genotype). *$P = 0.038$ (*Ppp17r1* in *Ikzf2*$^{cello/cello}$ vs *Ikzf2*$^{+/+}$), *$P = 0.037$ (*Ppp17r1* in *Ikzf2*$^{cello/cello}$ vs *Ikzf2*$^{cello/+}$) (two-sided Welch's *t*-test).

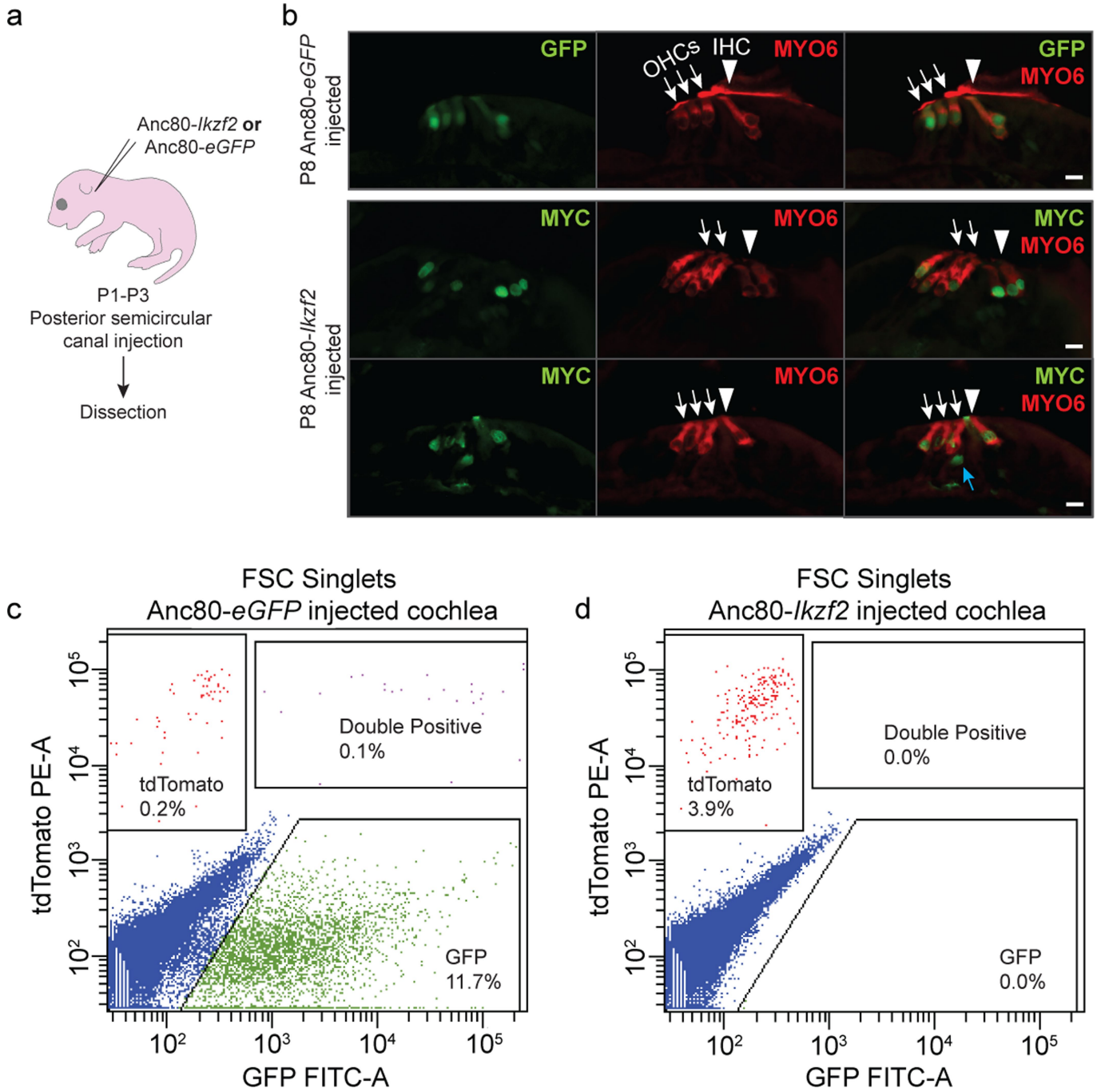

Extended Data Fig. 7 | Transduction of cochlear hair cells using Anc80L65 and hair cell enrichment by flow cytometry. a, Schematic representation of inner ear viral gene delivery via the posterior semicircular canal of CD-1 mice for hair cell marker immunolabelling. **b**, Immunolabelling for GFP in the Anc80-eGFP injected, and MYC in the Anc80-*Ikzf2* injected ears, showing mainly hair cell transduction, although some MYC staining could also be observed in supporting cells (blue arrow). $n = 3$ biologically independent samples per condition. Nuclear MYC staining suggests proper trafficking of the MYC-tagged Helios protein in transduced cells. White arrows indicate OHCs, white arrowheads indicate IHCs. Scale bars, 10 μm. **c**, **d**, Flow cytometry of dissociated cochlear GFP-positive and tdTomato-positive cells from P8 *Myo15*$^{cre/+}$;*ROSA26*$^{CAG\text{-}tdTomato}$ mice injected with either Anc80-eGFP (**c**, 2 mice) or Anc80-*Ikzf2* (**d**, 4 mice). Cells were first gated by forward and side scatter to exclude doublets. For the Anc80-eGFP-transduced cochlear sample, transduced cells were identified based on GFP expression, and hair cells were further identified by tdTomato expression. tdTomato single-positive, GFP single-positive and tdTomato and GFP double-positive cells were collected. For the Anc80-*Ikzf2*-transduced cochlear sample, hair cells were gated based on tdTomato single-positive expression and collected.

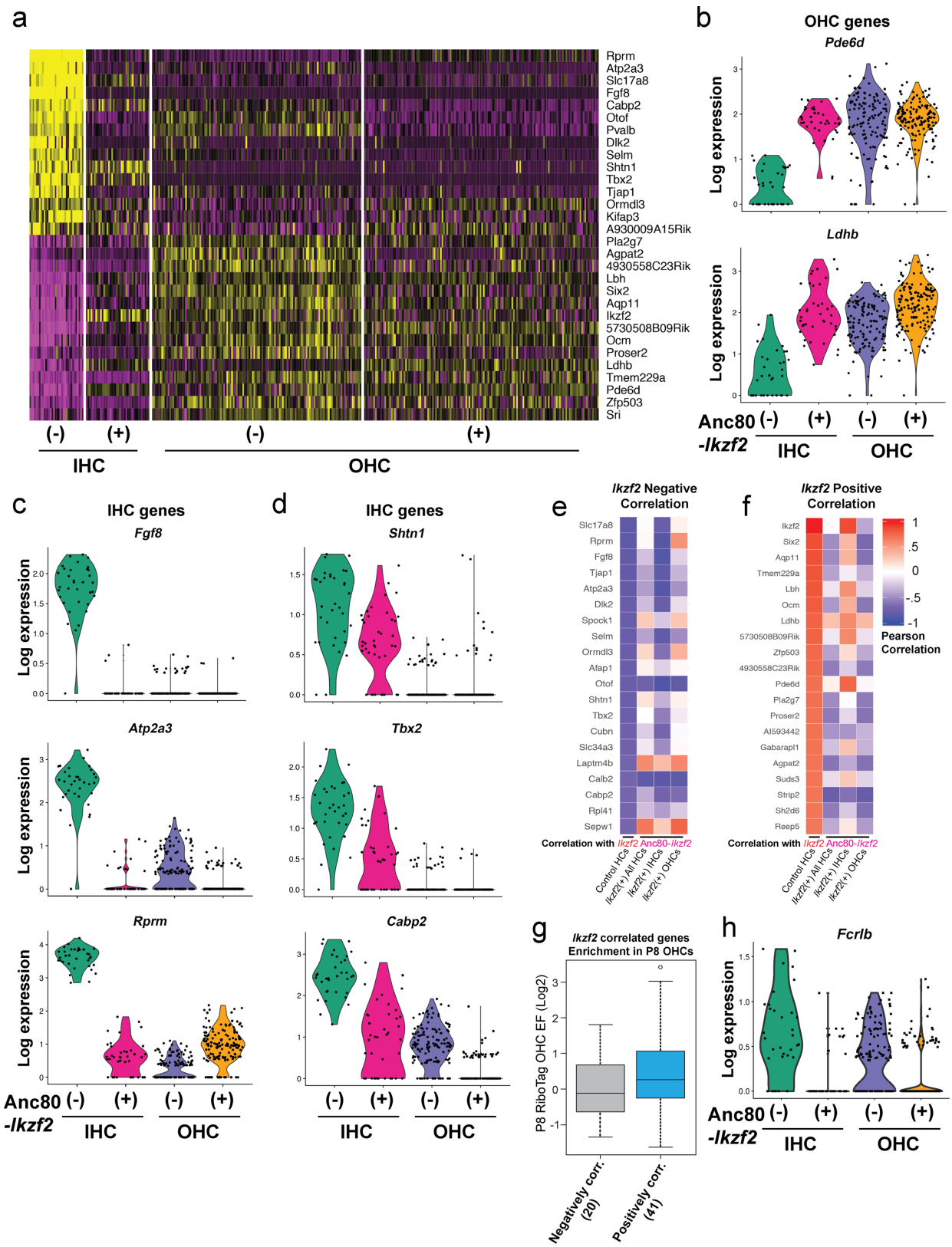

Extended Data Fig. 8 | See next page for caption.

Extended Data Fig. 8 | Transcriptional conversion of Anc80-*Ikzf2*-transduced IHCs. a, Heat map for the top 30 differently expressed genes between all hair cells profiled. Scaled expression values shown as *z*-scores, with yellow indicating higher and purple indicating lower expression than the mean. **b**, OHC enriched genes that are induced in Anc80-*Ikzf2*(+) IHCs. Anc80-*Ikzf2*(−) IHC ($n = 34$) vs Anc80-*Ikzf2*(+) IHC ($n = 40$) FDR: *Pde6d* $= 2.03 \times 10^{-12}$, *Ldhb* $= 3.74 \times 10^{-11}$. Dots represent the expression values of individual cells, with width of violins summarizing overall relative distribution of expression. **c**, IHC enriched genes that are highly expressed in control IHCs vs control OHCs, but are significantly reduced in Anc80-*Ikzf2*(+) IHCs. Anc80-*Ikzf2*(−) IHC ($n = 34$) vs Anc80-*Ikzf2*(+) IHC ($n = 40$) FDR: *Fgf8* $= 3.30 \times 10^{-14}$, *Atp2a3* $= 2.46 \times 10^{-13}$, *Rprm* $= 2.27 \times 10^{-13}$ (Kruskal–Wallis test followed by post hoc pairwise Wilcoxon ranked sum test adjusted for multiple comparisons). **d**, IHC-enriched genes that show only moderately reduced expression in Anc80-*Ikzf2*(+) IHCs. Anc80-*Ikzf2*(−) IHC ($n = 34$) vs Anc80-*Ikzf2*(+) IHC ($n = 40$) FDR: *Shtn1* $= 8.59 \times 10^{-5}$, *Tbx2* $= 3.88 \times 10^{-8}$, *Cabp2* $= 1.40 \times 10^{-10}$ (Kruskal–Wallis test followed by post hoc pairwise Wilcoxon ranked sum adjusted for multiple comparisons). **e**, **f**, Top 20 genes negatively (**e**) or positively (**f**) correlated with *Ikzf2* expression in control hair cells, shown alongside corresponding correlations of gene expression within all Anc80-*Ikzf2*-transduced hair cells, Anc80-*Ikzf2*-transduced IHCs, or Anc80-*Ikzf2* transduced-OHCs. See also Extended Data Fig. 9. **g**, Genes that are negatively correlated with *Ikzf2* ($n = 20$, Pearson correlation < -0.6) are not enriched in OHCs at P8 compared to all other genes detected in the RiboTag OHC dataset (background genes, $n = 13{,}124$). Genes that are positively correlated with *Ikzf2* ($n = 41$, Pearson correlation > 0.6) are significantly enriched in OHCs at P8 compared to background genes ($n = 13{,}103$) ($P = 0.025$, two-sided Wilcoxon's test). Black line represents median enrichment factor ($\log_2$ fold change), box demarcates first and third quartiles, whiskers demarcate first and third quartile $\pm 1.5 \times$ IQR values, dots represent single outliers. **h**, One of the most differentially expressed genes observed in our scRNA-seq experiment was *Fcrlb*, a gene which encodes an Fc receptor like protein, and the expression of which has not been previously described in the ear. *Fcrlb* is significantly downregulated in Anc80-*Ikzf2*(+) hair cells. Anc80-*Ikzf2*(−) IHC ($n = 34$) vs Anc80-*Ikzf2*(+) IHC ($n = 40$) FDR $= 4.89 \times 10^{-6}$. Anc80-*Ikzf2*(−) OHC ($n = 132$) vs Anc80-*Ikzf2*(+) OHC ($n = 148$) FDR $= 6.88 \times 10-^{8}$ (Kruskal–Wallis test followed by post hoc pairwise Wilcoxon ranked sum test adjusted for multiple comparisons). See also Supplementary Tables 8–11.

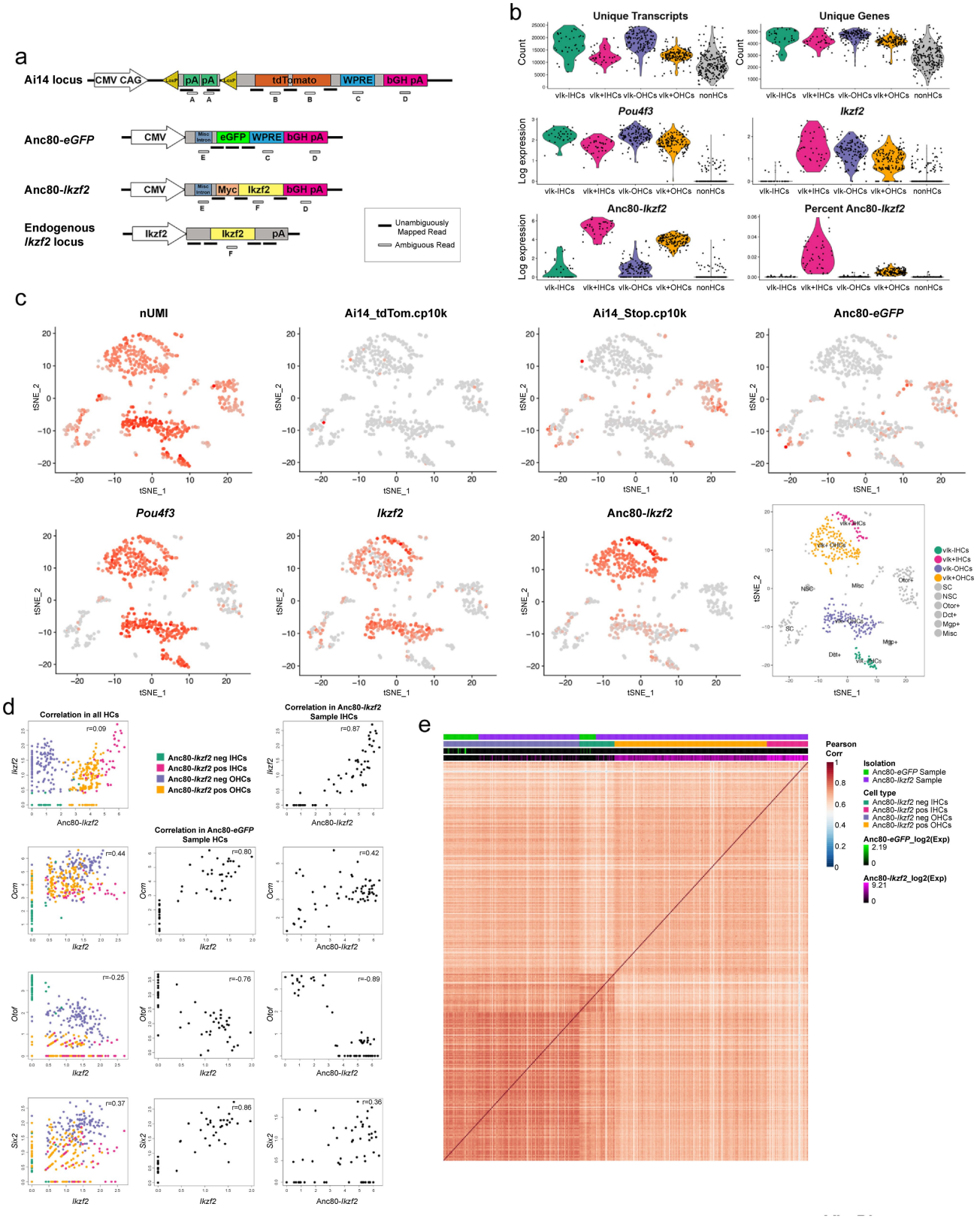

Extended Data Fig. 9 | See next page for caption.

Extended Data Fig. 9 | scRNA-seq allows for high-resolution discrimination of cell types and their transcriptional changes due to overexpression of *Ikzf2*. **a**, Custom annotation strategy with theoretical reads mapping to unambiguous regions of the various custom viral loci, as well as those regions that get discarded because of endogenous sequence similarity (that is, ambiguous reads). **b**, Violin plots of the overall scRNA-seq detection metrics, including number of unique molecules detected in each of the major cell type cluster identified (low Anc80-*Ikzf2* expressing IHCs: viral *Ikzf2* (vIk)$^{-}$ IHCs $n = 34$; low Anc80-*Ikzf2* expressing OHCs: vIk^{-} OHCs $n = 132$; high Anc80-*Ikzf2* expressing IHCs: vIk^{+} IHCs $n = 40$; high Anc80-*Ikzf2* expressing OHCs: vIk^{+} OHCs $n = 140$; and non-HCs: $n = 219$). **c**, FeaturePlots with red showing higher expression across all profiled cells, including cells identified as non-hair cells. Expression from loci captured with custom annotation shown to support cluster identification. A final labelled *t*-SNE plot shows all cells profiled clustered by predicted cell type. Misc, cells from all miscellaneous clusters with fewer than 5 cells; NSC, non-sensory epithelial cell; SC, organ of Corti supporting cell. Other clusters are defined by the highest differentially expressed marker gene. **d**, Pearson correlation scatter plots for selected genes within all profiled hair cells, hair cells from the Anc80-eGFP sample, or IHCs from the Anc80-*Ikzf2* sample. **e**, A Pearson correlation heat map of all hair cells detected showing overall transcriptional similarities between the non-transduced IHCs and OHCs, along with the Anc80-*Ikzf2*-transduced IHCs and OHCs.

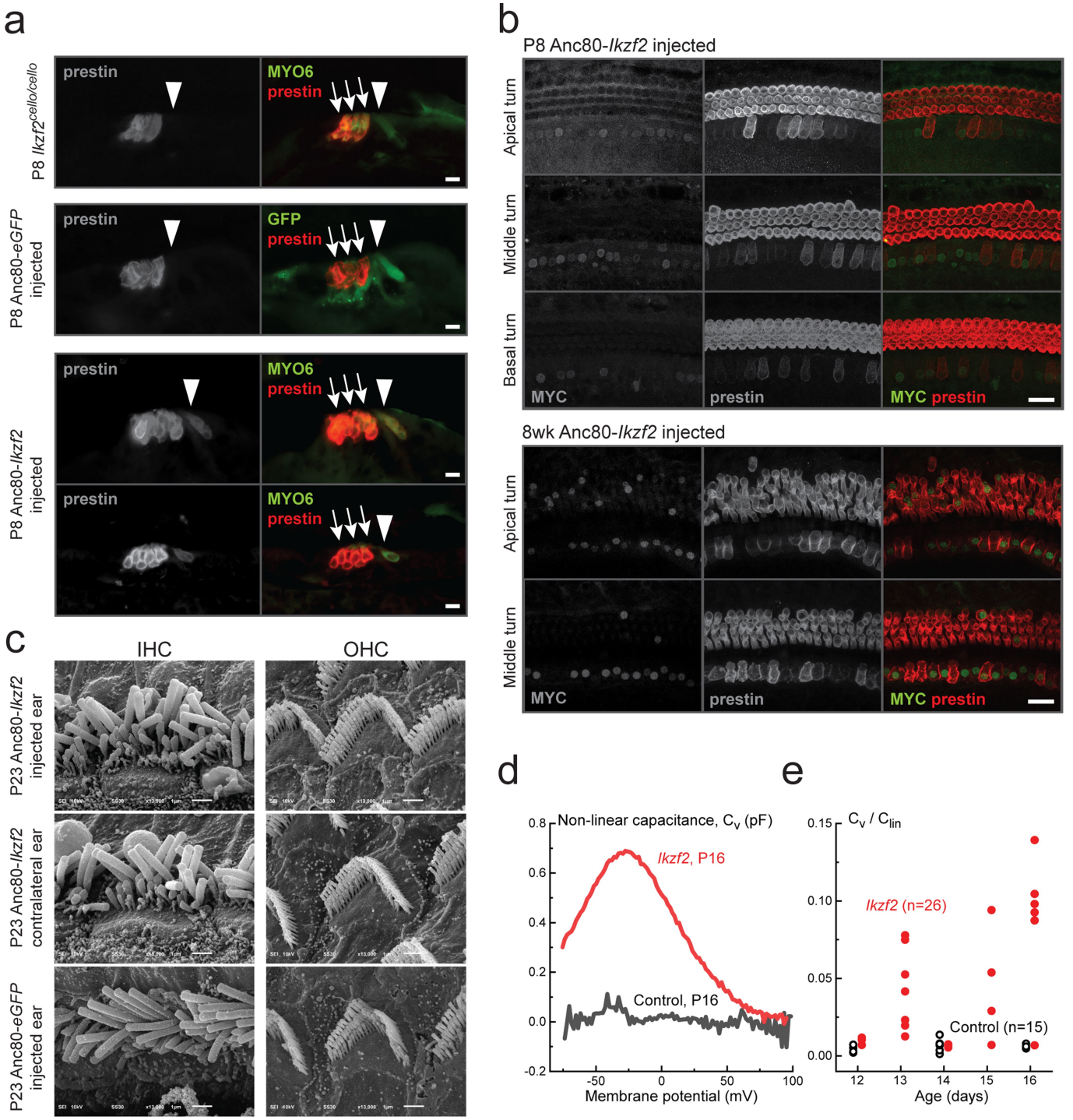

Extended Data Fig. 10 | See next page for caption.

Extended Data Fig. 10 | *Ikzf2* overexpression induces prestin expression and electromotility in IHCs but does not affect hair bundle morphology. a, The OHC electromotility protein prestin is expressed in the OHCs of *Ikzf2*$^{cello/cello}$ mutants ($n = 6$ biologically independent samples). In addition, the pattern of prestin expression is not affected by Anc80-eGFP transduction, but is induced in Anc80-*Ikzf2*-transduced IHCs ($n = 3$ biologically independent samples per condition). Scale bars, 10 μm. **b**, Expression of prestin can be seen in Anc80-*Ikzf2*-transduced IHCs as early as P8 and up to 8 weeks of age, and overlaps with MYC staining ($n = 6$ biologically independent samples at P8, $n = 3$ biologically independent samples at 6–8 weeks). Scale bars, 20 μm. **c**, Scanning electron micrographs of IHC and OHC stereocilia bundles of Anc80-*Ikzf2*- and Anc80-eGFP-injected mice at P23 showing expected bundle patterning. Images are from the mid-basal region of the cochlear spiral. Scale bars, 1 μm. Number of biologically independent samples (P16–P23): Anc80-*Ikzf2*-injected cochlea $n = 8$, Anc80-*Ikzf2* contralateral cochlea $n = 6$, Anc80-eGFP-injected cochlea $n = 3$. **d**, Representative traces of the voltage-dependent (nonlinear) component of the membrane capacitance (an electrical signature of electromotility) in the IHCs of Anc80-*Ikzf2*-injected mouse (red) and its non-injected littermate (grey). Mice were injected with Anc80-*Ikzf2* at P2 and recorded at P16. **e**, Normalized maximal nonlinear capacitance in all recorded IHCs of mice injected with Anc80-*Ikzf2* at P2 (red) at different ages after injection and their non-injected littermates (black). Each symbol represents one biologically independent cell, and the total number of cells is indicated in parentheses. Because Anc80-*Ikzf2* transduction is not 100% efficient in the apical turn of the cochlea at the time points tested, some IHCs of Anc80-*Ikzf2*-injected mice do not show prominent nonlinear capacitance, whereas the other IHCs do. In the IHCs with maximal nonlinear capacitance of more than 0.25 pF (due to presumable *Ikzf2* expression), the parameters of the Boltzmann fit were as following (mean ± s.e.m.): $Q_{max} = 0.10 \pm 0.02$ pC; $V_{pk} = -31 \pm 1$ mV; $z = 0.91 \pm 0.02$; $C_{lin} = 11.7 \pm 1.2$ pF; $\Delta C_{sa} = 0.14 \pm 0.07$ pF ($n = 12$). For information on the fitting procedure, see Methods.

nature research

Corresponding author(s): Ronna Hertzano and Michael R. Bowl

Reporting Summary

Nature Research wishes to improve the reproducibility of the work that we publish. This form provides structure for consistency and transparency in reporting. For further information on Nature Research policies, see Authors & Referees and the Editorial Policy Checklist.

Statistical parameters

When statistical analyses are reported, confirm that the following items are present in the relevant location (e.g. figure legend, table legend, main text, or Methods section).

n/a	Confirmed	
☐	☒	The exact sample size (*n*) for each experimental group/condition, given as a discrete number and unit of measurement
☐	☒	An indication of whether measurements were taken from distinct samples or whether the same sample was measured repeatedly
☐	☒	The statistical test(s) used AND whether they are one- or two-sided *Only common tests should be described solely by name; describe more complex techniques in the Methods section.*
☒	☐	A description of all covariates tested
☐	☒	A description of any assumptions or corrections, such as tests of normality and adjustment for multiple comparisons
☐	☒	A full description of the statistics including central tendency (e.g. means) or other basic estimates (e.g. regression coefficient) AND variation (e.g. standard deviation) or associated estimates of uncertainty (e.g. confidence intervals)
☐	☒	For null hypothesis testing, the test statistic (e.g. *F*, *t*, *r*) with confidence intervals, effect sizes, degrees of freedom and *P* value noted *Give P values as exact values whenever suitable.*
☒	☐	For Bayesian analysis, information on the choice of priors and Markov chain Monte Carlo settings
☒	☐	For hierarchical and complex designs, identification of the appropriate level for tests and full reporting of outcomes
☐	☒	Estimates of effect sizes (e.g. Cohen's *d*, Pearson's *r*), indicating how they were calculated
☐	☒	Clearly defined error bars *State explicitly what error bars represent (e.g. SD, SE, CI)*

Our web collection on statistics for biologists may be useful.

Software and code

Policy information about availability of computer code

Data collection

Structural 3D representations of wild-type and H517Q helios ZnF6 were predicted with RaptorX and visualized using pyMOL software (version 1.7). Electrophysiology data acquisition was controlled by pClamp software (version 10) using Digidata 1440A boards (Molecular Devices, USA). Cell body movement was tracked using Fiji software. Non-linear (voltage-dependent) capacitance of IHCs in Anc80-Ikzf2 injected mice and their non-injected littermates was recorded using jClamp software (SciSoft, USA). Auditory brainstem responses were collected, amplified and averaged using TDT System 3 in conjunction with either BioSig RP (version 4.4.11) or BioSig RZ (version 5.7.1) software. Distortion product oto-acoustic emissions tests were performed with the TDT RZ6 System 3 hardware and BioSig RZ (version 5.7.1) software. Images were captured and processed using Lumenera Infinity Capture and Infinity Analyze software.

Data analysis	For RNA-seq analysis, reads were aligned using TopHat v2.0.8, and HTSeq was used to quantify the number of reads aligning to predicted coding regions. Significant differential gene expression between samples was assessed using DEseq. The R lowess function was used to remove the transcript length bias of enrichment factors in the RiboTag dataset. Genes with a changed level of expression in the RiboTag IP samples at any time point relative to P8 were subjected to a clustering analysis using the CLICK algorithm, implemented in the EXPANDER package. GO enrichment analysis was done using the EXPANDER implemented tool TANGO. The expanded motif prediction analysis was performed using through the Cytoscape visualization tool. Genomic sequence data were assessed for variation using DNASTAR Lasergene software (version 12.0.0). Nanostring data were analyzed using nSolver 4.0 software. Sorting Intolerant From Tolerant (SIFT), Polymorphism Phenotyping version 2 (PolyPhen-2), and Protein Variation Effect Analyser (PROVEAN) were used to predict the functional effect of the cello mutation in silico. scRNA-seq reads were aligned using the 10X Genomics cellranger package (version 2.0.2). Secondary analyses were performed in R with Seurat (version 2.1.0). Additional plots were generated by NMF (version 0.20.6) and ggplot2 (version 2.2.1). Composite images were made using ImageJ software.

For manuscripts utilizing custom algorithms or software that are central to the research but not yet described in published literature, software must be made available to editors/reviewers upon request. We strongly encourage code deposition in a community repository (e.g. GitHub). See the Nature Research guidelines for submitting code & software for further information.

Data

Policy information about availability of data

All manuscripts must include a data availability statement. This statement should provide the following information, where applicable:

- Accession codes, unique identifiers, or web links for publicly available datasets
- A list of figures that have associated raw data
- A description of any restrictions on data availability

The RiboTag OHC RNA-seq, P8 cello cochlea RNA-seq, and P8 Anc80-Ikzf2 and Anc80-eGFP injected cochlea scRNA-seq data have been submitted to the Gene Expression Omnibus database (GEO Accession # GSE116703, GSE116702, and GSE120462), and are additionally available for viewing through the gEAR Portal (https://umgear.org/).

Field-specific reporting

Please select the best fit for your research. If you are not sure, read the appropriate sections before making your selection.

☒ Life sciences ☐ Behavioural & social sciences ☐ Ecological, evolutionary & environmental sciences

For a reference copy of the document with all sections, see nature.com/authors/policies/ReportingSummary-flat.pdf

Life sciences study design

All studies must disclose on these points even when the disclosure is negative.

Sample size	All RNA-seq analyses were performed in at least biological duplicates to ensure that statistical analyses could be accurately performed. No sample size calculation was performed for the RNA-seq experiments, and this is standard in the field. Representative images (n=1) were obtained to demonstrate the recombination pattern of the well established prestinCreERT2. All other analyses were performed in at least biological triplicate. All attempts at replication were successful. The cello pedigree was identified from the phenotype-driven ENU-mutagenesis Harwell Aging Screen, wherein large cohorts of mice (n>50-100) were screened for phenotypes of interest (including hearing loss). Utilizing the data obtained from the cello cohort, we used GraphPad StatMate to carry out power calculations to determine sample size in an unpaired t-test using the standard deviation of the measured hearing thresholds, a significance level of p=0.01 (two-tailed), and a power of 95%. As such, the effect size was estimated using real data corresponding to the cello hearing loss phenotype compared with the hearing thresholds of wild-type and heterozygote littermates. This calculation determined that a cohort size of 4 mice/genotype would be sufficient to detect a 40 dB SPL threshold difference.
Data exclusions	No data were excluded from analysis.
Replication	Representative images (n=1) were obtained to demonstrate the recombination pattern of the well established prestinCreERT2 models. All other analyses reported were replicated in at least biological duplicates, with similar results.
Randomization	Cello mutant mice and littermates were allocated into groups based on genotype. Mice for the viral transduction experiments were allocated into Ikzf2, GFP and non-injected groups randomly.
Blinding	For Distortion Product Otoacoustic Emissions (DPOAEs) and electrophysiology studies the operator was blind to the genotype of the animal being tested. For Auditory Brainstem Response tests, mice were housed in cages containing mixtures of genotypes, and mice from these cages were tested in a randomized order. Moreover, for the P16 ABRs the recorded primary data (i.e. the ABR waveform traces) were viewed and re-scored by a second operator blind to genotype.

Reporting for specific materials, systems and methods

Materials & experimental systems

n/a	Involved in the study
☒	☐ Unique biological materials
☐	☒ Antibodies
☐	☒ Eukaryotic cell lines
☒	☐ Palaeontology
☐	☒ Animals and other organisms
☒	☐ Human research participants

Methods

n/a	Involved in the study
☒	☐ ChIP-seq
☐	☒ Flow cytometry
☒	☐ MRI-based neuroimaging

Antibodies

Antibodies used

Mouse anti-HA.11 monoclonal antibody (clone 16B12, purified, BioLegend, Cat# 901502, lot# B220767, 5ug/mL), Goat anti-Helios M-20 (Santa Cruz Biotechnology, Cat# sc-9864, lot# E0709, 1:400-1:600), Mouse anti-β-Actin (Abcam, Cat# ab6276, 1:500), Mouse anti-cMyc 9E10 (Developmental Studies Hybridoma Bank, Cat# 9E10, 1ug & 1:5000), Rabbit anti-GFP (custom-made CUK-1819 MGU-GFP-FL, 1-2ug & 1:1000), Mouse 12G10 anti-α-Tubulin (Developmental Studies Hybridoma Bank, Cat# 12G10, 1:10,000), Goat anti-prestin N-20 (Santa Cruz Biotechnology, Cat# sc-22692, lot# D3015, 1:200), Goat anti-Oncomodulin N-19 (Santa Cruz Biotechnology, Cat# sc-7446, lot# L0814, 1:100), Rabbit anti-MyosinVI (Proteus BioSciences, Cat# 25-6791, 1:1000), Rabbit anti-GFP (Life Technologies, Cat# A-11122, lot# 1925070, 1:100), Mouse anti-cMyc 9E10 (Santa Cruz Biotechnology, Cat# sc-40, lot# B0116, 1:100), Mouse anti-Otoferlin (Abcam, Cat# ab53233, lot# GR3186324-2, 1:100), Guinea pig anti-Vglut3 (Donated by Rebecca Seal, PhD, University of Pittsburgh, 1:5000), Sheep anti-Digoxigenin-AP (Sigma-Aldrich, Cat# 11093274910, lot# 14608125, 1:100), Alexa Fluor® 568 donkey anti-goat (Thermo Fisher, Cat# A-11057, lot# 1485187 & 1711491, 1:200), Alexa Fluor® 488 donkey anti-mouse (Thermo Fisher, Cat# A-21202, lot# 164464 & 1820538, 1:200-1:800), Alexa Fluor® 488 donkey anti-rabbit (Thermo Fisher, Cat# A-21206, lot# 1910751, 1:800), Alexa Fluor® 546 goat anti-mouse (Thermo Fisher, Cat# A-11030, lot# 1661231, 1:800), Alexa Fluor® 568 goat anti-guinea pig (Thermo Fisher, Cat# A-11075, lot# 949212, 1:800), Alexa Fluor® 546 donkey anti-rabbit (Thermo Fisher, Cat# A-10042, lot# 1606268, 1:800), Goat anti-mouse IRDye 680RD (LI-COR Biosciences, Cat# 926-68070, 1:15000), Goat anti-rabbit IRDye 800CW (LI-COR Biosciences, Cat# 926-32211, lot# C80718-15, 1:15000)

Validation

Mouse anti-HA.11 monoclonal antibody, from BioLegend – This antibody can be used to detect fusion proteins with an HA-tag. From the manufacturer: "The extreme specificity of the antibody allows unambiguous identification and quantitative analysis of the tagged protein. The HA.11 antibody recognizes HA epitopes located in the middle of protein sequences as well as at the N- or C-terminus."
Goat anti-Helios M-20, from Santa Cruz Biotechnology – "Helios (M-20) is an affinity purified goat polyclonal antibody raised against a peptide mapping at the N-terminus of Helios of mouse origin." This antibody recognizes nuclear Helios in mouse cochlear OHCs. Loss of labelling when the anti-helios antibody is 'pre-blocked' confirms specificity (see Figure 1).
Mouse anti-β-Actin, from Abcam – "Ab6276 was shown to specifically react with beta actin in wild-type HAP1 cells. No band was observed when beta actin knockout samples were used. Wild-type and beta actin knockout samples were subjected to SDS-PAGE."
Mouse anti-cMyc 9E10, from Developmental Studies Hybridoma Bank - "9E10 was deposited to the DSHB by Bishop, J.M. (DSHB Hybridoma Product 9E10). Positive Tested Species Reactivity: Epitope tag/Fusion protein." Uniprot ID: P01106, Entrez Gene ID: 4609, Antibody Registry ID: AB_2266850. Initial publication: Isolation of monoclonal antibodies specific for human c-myc proto-oncogene product. Evan GI, Lewis GK, Ramsay G, Bishop JM. Molecular and cellular biology 1985 Dec.
Rabbit anti-GFP CUK-1819 MGU-GFP-FL, custom-made - This antibody was raised in rabbit immunized with a His fusion protein containing full-length GFP and the anti-sera was affinity purified using the antigen coupled to SulfoLink (Pierce, Rockford, IL, USA). It was validated at MRC Harwell Institute using lysates from HEK293T cells transiently transfected with a GFP-tagged construct. Western blot showed the antibody only bound protein from transfected cell lysates and not untransfected control cell lysates. Furthermore, immunoprecipitation of transfected cell lysates showed enrichment of GFP-tagged fusion proteins.
Mouse anti-α-Tubulin, from Developmental Studies Hybridoma Bank – "12G10 anti-alpha-tubulin was deposited to the DSHB by Frankel, J. / Nelsen, E.M. (DSHB Hybridoma Product 12G10 anti-alpha-tubulin). Positive Tested Species Reactivity: Algae, C. elegans, Cephalopod, Dictyostelium, Drosophila, Fish, Hermit Crab, Human, Medusa, Mouse, Protozoa, Saccharomyces, Tetrahymena, and Xenopus." Uniprot ID: P41351, Entrez Gene ID: 7838142, Antibody Registry ID: AB_1157911. Initial publication: Polyglycylation domain of beta-tubulin maintains axonemal architecture and affects cytokinesis in Tetrahymena. Thazhath R, Liu C, and Gaertig J. Nature cell biology 2002 Mar.
Goat anti-prestin N-20, from Santa Cruz Biotechnology – "Prestin (N-20) is an affinity purified goat polyclonal antibody raised against a peptide mapping at the N-terminus of Prestin of human origin. Prestin (N-20) is recommended for detection of Prestin of mouse, rat and human origin by Western Blotting (starting dilution 1:200, dilution range 1:100-1:1000), immunofluorescence (starting dilution 1:50, dilution range 1:50-1:500) and solid phase ELISA (starting dilution 1:30, dilution range 1:30-1:3000)." Publications: Gao, J., et al. 2007. Prestin-based outer hair cell electromotility in knockin mice does not appear to adjust the operating point of a cilia-based amplifier. Proc. Natl. Acad. Sci. USA 104: 12542-12547; McGuire, R.M., et al. 2010. Cysteine mutagenesis reveals transmembrane residues associated with charge translocation in prestin. J. Biol. Chem. 285: 3103-3113.
Goat anti-Oncomodulin N-19, from Santa Cruz Biotechnology – "OCM (N-19) is an affinity purified goat polyclonal antibody raised against a peptide mapping at the N-terminus of OCM of human origin. OCM (N-19) is recommended for detection of OCM and OCML of mouse, rat and human origin by Western Blotting (starting dilution 1:200, dilution range 1:100-1:1000), immunoprecipitation [1-2 µg per 100-500 µg of total protein (1 ml of cell lysate)], immunofluorescence (starting dilution 1:50, dilution range 1:50-1:500) and solid phase ELISA (starting dilution 1:30, dilution range 1:30-1:3000)." Publications: Devarajan, K., et al. 2005. Circadian and light regulation of Oxytocin and parvalbumin protein levels in the ciliated ependymal layer of the third ventricle in the C57 mouse. Neuroscience 134: 539-547; Csillik, B., et al. 2009. Upregulated expression of oncomodulin, the β

isoform of parvalbumin, in perikarya and axons in the diencephalon of parvalbumin knockout mice. Neuroscience 165: 749-757.
Rabbit anti-MyosinVI, from Proteus BioSciences – "Rabbits were immunized with amino acids 1049-1254 from the tail region of porcine myosin-VI." This antibody is affinity purified, and is reported by the manufacturer to have broad species cross-reactivity. Publications: Hasson, T. and M. S. Mooseker (1994). Journal of Cell Biology 127:425-440; Hasson, T. et al. (1997), Journal of Cell Biology 137:1287-1307.
Rabbit anti-GFP, from Life Technologies – "The anti-GFP rabbit polyclonal antibody is raised against GFP isolated directly from Aequorea victoria." This antibody is purified by ion-exchange chromatography. Lot# 1925070 (used in this study) was certified by Life Technologies using ELISA. Published species reactivity: Chimpanzee, Dog, Fish, Fruit fly, Hamster, Human, Mouse, Non-human primate, Pig, Rat, Sheep, Zebrafish.
Mouse anti-cMyc 9E10, from Santa Cruz Biotechnology – "c-Myc (9E10) is a mouse monoclonal antibody raised against an epitope corresponding to amino acids 408-439 within the C-terminal domain of c-Myc of human origin. Recommended for detection of c-Myc p67 and c-Myc tagged fusion proteins of mouse, rat, human, monkey, feline and canine origin by WB, IP, IF, IHC(P), FCM and ELISA; non cross-reactive with N-Myc or L-Myc proteins. Widely used in combination with eukaryotic expression vectors encoding proteins with c-Myc (amino acids 408-439) epitope tag." Publications: Tsuga, H., et al. 1994. Sequestration of muscarinic acetylcholine receptor m2 subtypes. Facilitation by G protein-coupled receptor kinase (GRK2) and attenuation by a dominant-negative mutant of GRK2. J. Biol. Chem. 269: 32522-32527; Liu, Y., et al. 2017. miR-19a promotes colorectal cancer proliferation and migration by targeting TIA1. Mol. Cancer 16: 53.
Mouse anti-Otoferlin, from Abcam - From the manufacturer: "This antibody reacts specifically with human Otoferlin protein (220 kDa). Suitable for: IHC-Fr, Flow Cyt, IHC-FoFr, WB, IP, ICC/IF. Reacts with: Mouse, Rat, Human." Publications: Richter KN et al. Glyoxal as an alternative fixative to formaldehyde in immunostaining and super-resolution microscopy. EMBO J 37:139-159 (2018); Meese S et al. Activity-Dependent Phosphorylation by CaMKIId Alters the Ca2+Affinity of the Multi-C2-Domain Protein Otoferlin. Front Synaptic Neurosci 9:13 (2017).
Guinea pig anti-Vglut3 – This antibody was generously donated by Rebecca Seal, PhD, of the University of Pittsburgh, and has been validated by the Seal laboratory. Publication: Seal RP, Akil O, Yi E, et al. Sensorineural Deafness and Seizures in Mice Lacking Vesicular Glutamate Transporter 3. Neuron. 2008;57(2):263-275. doi:10.1016/j.neuron.2007.11.032.
Sheep anti-Digoxigenin-AP, from Sigma-Aldrich – This antibody is used to detect Digoxigenin labelled RNA probes via a colorimetric reaction. From the manufacturer: "The polyclonal antibody from sheep is specific to digoxigenin and digoxin and shows no cross-reactivity with other steroids, such as human estrogens and androgens."

Eukaryotic cell lines

Policy information about cell lines

Cell line source(s)	HEK293T and Cos7 cell lines were used in this study, and were provided by Dr. Chris Esapa, MRC Harwell Institute.
Authentication	None of the cell lines used were authenticated.
Mycoplasma contamination	The cell lines were tested and found to be free of myoplasma contamination.
Commonly misidentified lines (See ICLAC register)	The HEK293T cell line used in this study is a commonly misidentified cell line, found often to be misidentified HeLa cells. These cells were used for transient overexpression of tagged proteins and co-immunoprecipitation studies, therefore misidentification of HeLa cells as HEK293T cells would be unlikely to affect the results reported.

Animals and other organisms

Policy information about studies involving animals; ARRIVE guidelines recommended for reporting animal research

Laboratory animals	RiboTag, prestinCreERT2 and Myo15Cre mouse models (maintained on a C57BL/6 background) were provided for this study by Dr. Mary Kay Lobo, Dr. Jian Zuo, and Drs. Christine Petit and Thomas Friedman, respectively. CBA/CaJ mice (stock #000654) and B6.Cg-Gt(ROSA)26Sortm14(CAG-tdTomato)Hze/J mice (stock #007914, referred to as ROSA26CAG-tdTomato) were procured from the Jackson Laboratory. PrestinCreERT2 specificity was determined by crossing prestinCreERT2/CreERT2 mice to ROSA26CAG-tdTomato mice, and resulting offspring were dissected at P21 for whole-mount immunohistochemistry. Cochlear tissues from F1 RiboTagHA/+;prestinCreERT2/+ offspring on a mixed CBA/C57BL/6 background were collected at the following ages: P8, P14, P28, 6 weeks, and 10 weeks. CD-1 timed-pregnant females were procured from Charles River (Frederick, MD). Resulting CD-1 neonates were injected with Anc80L65 virus between P1 – P3, and dissected for later analyses at either P8 or 8wk. The cello mutant mouse was originally identified from the MRC Harwell Institute phenotype-driven N-ethyl-N-nitrosourea (ENU) Ageing Screen (Potter et al., 2016). Auditory phenotyping was performed at 16 days, 3-, 6-, 9- and 12-months of age. Hair cell counts were performed at 16 days, 3-, 6-, 9- and 12-months of age. Electrophysiological recordings were made from OHCs of cello mice aged P9 – P18. For the cello RNA-seq and NanoString experiments, cochlear ducts from Ikzf2+/+, Ikzf2cello/+ and Ikzf2cello/cello mice were dissected at P8. For the Anc80L65 transduced IHC scRNA-seq experiment, Myo15Cre/Cre mice were crossed to ROSA26CAG-tdTomato mice. Resulting offspring were injected with Anc80L65 virus between P1 – P3, and the cochlear epithelium was collected at P8. Both male and female animals were used for all experiments.
Wild animals	The study did not include wild animals.
Field-collected samples	The study did not include samples collected from the field.

Flow Cytometry

Plots

Confirm that:

☒ The axis labels state the marker and fluorochrome used (e.g. CD4-FITC).

☒ The axis scales are clearly visible. Include numbers along axes only for bottom left plot of group (a 'group' is an analysis of identical markers).

☒ All plots are contour plots with outliers or pseudocolor plots.

☒ A numerical value for number of cells or percentage (with statistics) is provided.

Methodology

Sample preparation	Inner ears of neonatal Myo15Cre/+;ROSA26CAG-tdTomato mice were injected with Anc80-Ikzf2 (4 mice) or control Anc80-eGFP (2 mice) via the posterior semicircular canal. Cochlear tissues from both injected and uninjected ears were harvested at P8 and further dissected to reveal the sensory epithelium. The sensory epithelia from Anc80-eGFP and Anc80-Ikzf2 injected mice were pooled separately into 2 wells of a 48-well plate containing 0.5 mg/ml Thermolysin (Sigma). Tissues were incubated at 37°C for 20 minutes, after which the Thermolysin was removed and replaced with Accutase enzyme (MilliporeSigma). After a 3 minute incubation at 37°C, tissues were mechanically disrupted using a 23G blunt ended needle connected to a 1 ml syringe. This step was performed twice. After confirming tissue dissociation by direct visualization, the dissociation reaction was stopped by adding an equal volume of IMDM supplemented with 10% heat-inactivated FBS to the Accutase enzyme solution. Cells were passed through a 40 um cell strainer (BD) to remove cell clumps. tdTomato expressing HCs were sorted into ice cold tubes containing IMDM with 10% FBS on a BD FACSAria II (BD Biosciences) and processed for scRNA-seq. Flow cytometry analyses were performed at the University of Maryland Marlene and Stewart Greenebaum Comprehensive Cancer Center Flow Cytometry Shared Service.
Instrument	BD FACSAria II (BD Biosciences)
Software	FACSDiva Version 6.1.1
Cell population abundance	The population of interest (tdTomato positive hair cells) represented less than 1% of the total cell population. This low abundance has been well documented in the literature (Elkon et al., 2015, Matern et al., 2017). Therefore, post-sort analyses were not performed, as all cells were needed for downstream analysis. Hair cells and non-hair cells contained within the sorted population were later identified by single-cell RNA-seq.
Gating strategy	Cells were first gated by forward and side scatter to exclude doublets. For the Anc80-eGFP transduced cochlear sample, transduced cells were identified based on GFP expression, and hair cells were further identified by TdTomato expression. Tdtomato single positive, GFP single positive and TdTomato+GFP double positive cells were collected. For the Anc80-Ikzf2 transduced cochlear sample, hair cells were gated based on TdTomato single positive expression and collected.

☒ Tick this box to confirm that a figure exemplifying the gating strategy is provided in the Supplementary Information.

Milon et al. Biology of Sex Differences (2018) 9:12
https://doi.org/10.1186/s13293-018-0171-0

Biology of Sex Differences

RESEARCH Open Access

The impact of biological sex on the response to noise and otoprotective therapies against acoustic injury in mice

Béatrice Milon[1], Sunayana Mitra[1], Yang Song[2], Zachary Margulies[1], Ryan Casserly[1], Virginia Drake[1], Jessica A. Mong[3], Didier A. Depireux[1,4] and Ronna Hertzano[1,2,5*]

Abstract

Background: Noise-induced hearing loss (NIHL) is the most prevalent form of acquired hearing loss and affects about 40 million US adults. Among the suggested therapeutics tested in rodents, suberoylanilide hydroxamic acid (SAHA) has been shown to be otoprotective from NIHL; however, these results were limited to male mice.

Methods: Here we tested the effect of SAHA on the hearing of 10-week-old B6CBAF1/J mice of both sexes, which were exposed to 2 h of octave-band noise (101 dB SPL centered at 11.3 kHz). Hearing was assessed by measuring auditory brainstem responses (ABR) at 8, 16, 24, and 32 kHz, 1 week before, as well as at 24 h and 15–21 days following exposure (baseline, compound threshold shift (CTS) and permanent threshold shift (PTS), respectively), followed by histologic analyses.

Results: We found significant differences in the CTS and PTS of the control (vehicle injected) mice to noise, where females had a significantly smaller CTS at 16 and 24 kHz ($p < 0.0001$) and PTS at 16, 24, and 32 kHz (16 and 24 kHz $p < 0.001$, 32 kHz $p < 0.01$). This sexual dimorphic effect could not be explained by a differential loss of sensory cells or synapses but was reflected in the amplitude and amplitude progression of wave I of the ABR, which correlates with outer hair cell (OHC) function. Finally, the frequency of the protective effect of SAHA differed significantly between males (PTS, 24 kHz, $p = 0.002$) and females (PTS, 16 kHz, $p = 0.003$), and the magnitude of the protection was smaller in females than in males. Importantly, the magnitude of the protection by SAHA was smaller than the effect of sex as a biological factor in the vehicle-injected mice.

Conclusions: These results indicate that female mice are significantly protected from NIHL in comparison to males and that therapeutics for NIHL may have a different effect in males and females. The data highlight the importance of analyzing NIHL experiments from males and females, separately. Finally, these data also raise the possibility of effectors in the estrogen signaling pathway as novel therapeutics for NIHL.

Keywords: Noise-induced hearing loss, Sex differences, SAHA, B6CBAF1/J mice, Inner ear, ABR

Background

Noise-induced hearing loss (NIHL) is a form of an acquired hearing deficit that underlies 16% of adult sensorineural hearing loss worldwide [1]. In the US adult population, NIHL is second only to age-related hearing loss (ARHL) [2]. NIHL as an occupational hazard is widespread in the military, construction, agriculture, and in other fields with high noise exposure, causing hearing loss in 7–21% of the exposed population [3]. Health problems secondary to noise exposure are particularly frequent in the military. In the USA, hearing loss and tinnitus rank as the most prevalent service-connected disabilities for veterans [4]. Untreated hearing loss adversely impacts social, psychological, and cognitive functioning of affected individuals [5].

Small animal models such as the guinea pig, gerbil, chinchilla, mouse, and ferrets are commonly used to conduct auditory research and, in particular, studies on

* Correspondence: rhertzano@som.umaryland.edu
[1]Department of Otorhinolaryngology - Head and Neck Surgery, University of Maryland, 16 South Eutaw Street, Suite 500, Baltimore, MD 21201, USA
[2]Institute for Genome Science, University of Maryland School of Medicine, Baltimore, MD 21201, USA
Full list of author information is available at the end of the article

NIHL [6–8]. Mouse models have proven especially useful because of the ease in generating inbred strains with low genetic variability, the ability to manipulate the mouse genome, as well as structural, molecular and functional similarity to the human ear [9–11]. The current study stemmed from research that was designed to analyze the molecular mechanism of action of drugs with a protective effect from NIHL. Suberoylanilide hydroxamic acid (SAHA) is a histone deacetylase inhibitor and thus functions through modulating gene expression by changing the accessibility of the DNA to transcription factors [12, 13]. SAHA has been shown to be protective against hearing loss caused by exposure to chemicals/medications (ototoxic hearing loss) in vivo in mice of both sexes [12] as well as from NIHL in male mice [14]. Little is known, however, about the differential responses of male and female mice to noise and its potential therapeutics as historically most studies of acquired hearing loss using animal model were performed exclusively on males [14–19]. This is in part because the fluctuating hormone levels during an estrous cycle could introduce a confounding variable in the response to trauma or treatment [20]. Of relevance, sex differences have been described in age-related hearing loss (presbycusis) as well as in NIHL, where pre-menopausal women are protected in comparison to age-matched men [21, 22].

Here we initially tested the efficacy of SAHA as a protective agent from NIHL in young adult B6CBAF1/J mice of both sexes. We exposed mice of both sexes, who were treated with SAHA or its carrier, DMSO, to a permanent threshold-shift inducing noise exposure. We compared hearing function by analysis of auditory brainstem responses, and histological outcomes of the noise exposures by inner and outer hair cell counts and inner hair cell synapse analysis. Our results indicate a differential response to both noise and SAHA treatment between sexes, where female mice exhibit less hearing loss following noise (i.e., less damage) and have less therapeutic benefit from SAHA, when compared to males. Interestingly, the effect of sex on the degree of hearing loss following noise exposure was greater than the effect of the tested drug. This is the first detailed report comparing and characterizing such differences between sexes.

Methods

Animals

All procedures involving animals were carried out in accordance with the National Institutes of Health Guide for the Care and Use of Laboratory Animals and were approved by the Animal Care Committee at the University of Maryland (protocol numbers 0915006 and 1015003) and the Animal Care and Use Review Office (Department of Defense, USA).

All experiments were performed on B6CBAF1/J mice (Stock No: 100011, Jackson Laboratories, ME). We use B6CBAF1/J mice, which are F1 progeny of a cross between C57BL/6J and CBA/J (CBA) for most of our experiments for NIHL. We choose this combination of strains because, while the C57BL/6 mice are used extensively to generate transgenic animals for auditory research owing to availability of its complete genome information [23], long life span and resistance to sound induced seizures [24, 25]; C57BL/6 mice also suffer from early onset age-related hearing loss (ARHL) due to recessively inherited mutation in the *Cdh23* gene [26] underlying the *Ahl* locus [27]. In contrast, the CBA strain is relatively resistant to ARHL [28]. The B6CBAF1/J mice therefore enable the use of Cre-lines (originating from C57BL/6 mice) and have been previously used and characterized in studies of NIHL [29]. Mice were obtained at 7–8 weeks of age and kept in our facility 1–2 weeks for acclimatization before any procedures. The facility is controlled for temperature and humidity, has a 12h light/12 h dark cycle (lights on at 6 am), and mice were provided with food and water ad libitum.

Study design

The experiment consisted of two separate cohorts of animals, to ascertain reproducibility of data. Each cohort consisted of (a) three male and three female mice that were not exposed to noise and used only for histology, (b) six or eight mice from each sex that were all exposed to noise and treated with SAHA, and (c) six or eight mice from each sex that were all exposed to noise and treated with vehicle (DMSO). Noise exposures were performed on 3 to 4 mice at a time, which consisted of a mixture of mice that were treated with either SAHA or DMSO. The phase of the estrus cycle was not recorded for the female mice. One male in the DMSO group was removed from all analyses because it did not present a threshold shift at 24 h after noise exposure. A second person who was blinded with respect to the animal groups determined the ABR thresholds and counted outer hair cells and synapses.

Noise trauma

All noise exposures were performed on mice at 10 weeks of age. Noise trauma was induced with a 2-h duration, octave band of noise centered at 11.3 kHz (8–16 kHz) at 101 dB sound pressure level (SPL) using the Fostex FT17H tweeter [30] (Fostex, Tokyo, Japan). Output stimuli were calibrated with a measurement microphone (PCB Piezoelectronics, NY) placed at the same distance as the mouse ears. Mice were placed in a custom-made animal holder made of a perforated aluminum sheet, 18 × 15 × 5 cm in size with eight equal-sized chambers

measuring 4.5 × 7.5 × 5 cm, which was itself placed in a soundproof box (IAC Acoustics, IL). Only the four center chambers immediately inferior to the speaker were used to house mice during the noise exposures. Sound level was measured to be within 0.5 dB of the target level throughout the holding cells, with the speaker situated 20 cm above the mice. The mice were awake and unrestrained throughout the noise exposure. All mice were exposed to noise at the same time of the day (8 am) for each of the experimental groups.

SAHA treatment

Mice were injected intraperitoneally with suberoylanilide hydroxamic acid (SAHA) (Selleckchem, TX), (100 mg/kg body weight) dissolved in DMSO (MilliporeSigma, MA), or with DMSO alone (vehicle) 3 days before exposure to noise and 2 h after the end of the noise exposure. The SAHA dosing amount was based on a previous publication using SAHA as an otoprotective agent, where the authors tried different dose concentrations of SAHA and reported a 100 mg/kg dose to be most efficacious without cytotoxicity [12]. Because studies vary in their dosing regimen for SAHA, the frequency of the dosing was based on the published literature with minor modifications [14, 31].

Determination of auditory brainstem response

Auditory brainstem responses (ABR) were recorded after induction of anesthesia using an intraperitoneal injection of a mixture of ketamine (100 mg/kg) (VetOne, ID) and xylazine (20 mg/kg) (Anased, IL). Hearing thresholds were determined at 8, 16, 24, and 32 kHz using the RZ6 recording system (Tucker-Davis Technologies, FL). Recording electrodes were inserted under the skin at the inferior post-auricular area of the left and right ears, and a reference was placed under the skin at the vertex region of the skull. A ground electrode was inserted near the base of the tail. The animals were placed in a soundproof box (IAC Acoustics, IL) for the recordings. Stimuli were presented via a speaker situated in front of the mouse, 10 cm from the ears. Frequency-specific tone bursts 2.5 ms long, with a 0.5 ms sinusoidal on and off ramp, were presented to the mice at varying intensities beginning at 90 dB SPL and proceeding in 5 dB decrements down to 10 dB below the measurable hearing threshold for each mouse. Output stimuli were calibrated with a one-quarter inch microphone (model PCB-378C01; PCB Piezotronics, NY) placed at the same distance from the speaker as the mouse ears would be. Electrophysiological signals in response to each tone stimulus were recorded for 10 ms starting at the onset of the tone. A total of 512 sweeps were presented at the rate of 21 sweeps/s, and responses were averaged at each level and frequency tested. Responses from both ears were recorded simultaneously and used for data acquisition [32]. Hearing thresholds were determined as the lowest level at which definite ABR waves I and II response patterns could be identified for each frequency. Importantly, wave I and II of the ABR are generated from the contributions of the uncrossed fibers of spiral ganglion and cochlear nucleus, respectively. This allowed for hearing thresholds to be determined from both ears simultaneously, with each ear considered a separate data point. The results section shows the data with each ear counting as an individual biological replicate because both ears were exposed to noise and thresholds were obtained from the two ears separately, as previously described [33, 34]. In addition, the supplementary data reports the hearing threshold results where the thresholds from both ears of each mouse are averaged and each mouse is counted as an individual biological sample. Body temperature of the animals was maintained constant at 37.0 °C by a feedback heating pad placed under the animal while recording (FHC, ME). Baseline ABR thresholds were determined 1 week prior to noise exposure when the mice were 9 weeks of age. After the noise exposure, ABR thresholds were recorded at 24 h, 8 days, and 15 to 21 days, corresponding to 10–13 weeks of age. These permitted measurement of the compound threshold shift (CTS) as well as permanent threshold shift (PTS), respectively [35].

ABR wave I amplitude growth as a function of sound level

Peak-to-trough amplitude values of wave I of the ABR traces were extracted using a custom MatLab (MathWorks, MA) script (Additional file 1). Briefly, the script extracted the first maximum deflection after the first millisecond (ms) of the recording (peak I) and the corresponding subsequent minimum deflection (trough I). Wave I peak-to-trough amplitudes were obtained for stimuli levels ranging from 55 dB SPL to 85 dB SPL for ABR recorded before and after noise exposure. In noise-exposed animals, the minimum hearing threshold averaged around 55 dB at 24 h. Thus, the linear regressions were performed setting the minimal value to 55 dB to allow for the comparison of data from all time points. Additionally, the data between these level ranges are linear for most of the level versus amplitude plot, allowing for the accurate calculation of the slope. The data were plotted to obtain the growth of amplitude as a function of sound level for each experimental group at 16 kHz, which was the frequency with the maximal permanent threshold shift. Linear regression analyses were performed using the Prism 7 software (GraphPad, CA) to obtain slope values. The slopes were compared between conditions at each frequency analyzed. Slopes were considered significantly different if $p < 0.05$ calculated by a two-tailed paired t test [36].

Immunostaining

Within 1 week of the final ABR recording, mice were euthanized by CO_2 asphyxiation followed by cervical dislocation. Immediately after euthanasia, the temporal bones were dissected in ice-cold phosphate-buffered saline (PBS) (Corning, MA), a small hole was made in the bony apex of the cochlea, and the round and oval windows were opened for subsequent perfusion of the fixative. The temporal bones were fixed overnight at 4 °C in 4% paraformaldehyde (Alfa Aesar, MA) solution in PBS and then decalcified by immersion in 500 mM EDTA at 4 °C until adequate decalcification. Each cochlear duct was dissected according to the method described by the Eaton-Peabody Laboratories [37]. Briefly, each cochlear duct was first bisected across the oval window. The resulting halves were further dissected to obtain the apical turn of the basilar membrane as a single piece, the middle turn and the basal turns in two halves as well as the basal hook as a final piece, exposing the organ of Corti in its entirety. The tissue was permeabilized for 1 h in PBST ((PBS (CorningCellgro, VA) with 0.3% Triton X-100 (Milipore-Sigma, MA)) and blocked for 1 h in PBST with 5% normal goat serum (Cell Signaling Technologies, MA) at room temperature.

For pre-synaptic ribbon and post-synaptic density staining, cochlear segments were incubated overnight at 37 °C with a monoclonal mouse anti-CtBP2 antibody (1:200, BD Biosciences, CA) and a monoclonal mouse anti-GluR2 antibody (1:2000, MiliporeSigma), diluted in blocking buffer. Labeling was performed by incubating the tissue with the corresponding secondary antibodies, goat anti-mouse IgG2 Alexa Fluor® 488 and goat anti-mouse IgG1 Alexa Fluor® 568 (1:1000, ThermoFisher Scientific, MA) supplemented with DAPI (1:20,000, ThermoFisher Scientific) in PBST for 2 h at room temperature. Tissue was mounted with the ProLong Gold antifade reagent (ThermoFisher Scientific).

Frequency-specific pre-synaptic ribbon and post-synaptic density (PSD) counts

Following immunostaining, tissue was imaged at a × 20 magnification using a Nikon Eclipse E600 fluorescence microscope (Nikon, NY) equipped with an Infinity 3 camera (Lumenera, Canada) to allow for frequency mapping. Cochlear frequencies were mapped onto the images using the Measure Line plugin, developed by the Eaton-Peabody Laboratories [38] on the software ImageJ [39]. Subsequently, confocal Z-stacks in the regions of 15 to 17 kHz, 22 to 26 kHz, and 32 kHz were obtained using a 63X oil objective, 1.2 X digital zoom, and 42 μm sections using the LSM 5 Duo confocal microscope (Zeiss). Ribbons and PSDs were counted using the ImageJ Cell Counter plugin.

Cytocochleograms

Fluorescence images of the outer hair cell nuclei counterstained with DAPI were captured using an Eclipse E600 microscope (20 X objective) (Nikon) equipped with an Infinity 3 camera (Lumenera). Cochlear frequencies were mapped as described above for the ribbon and PSD counts. Missing outer hair cells (OHCs) were counted throughout the entire length of the basilar membrane from the apex towards the base at the following frequency intervals: 4–5.6 kHz, 5.6–8 kHz, 8–11.3 kHz, 11.3–16 kHz, 16–22.6 kHz, 22.6–32 kHz, 32–45.2 kHz, 45.2–51 kHz, and 51–55 kHz. These counts were expressed as the percentage of missing OHCs with respect to their position along the length of the basilar membrane.

Statistical analysis

The ABR data comparisons between groups were made by a two-way ANOVA followed by a Tukey post hoc test for multiple pair-wise comparisons [40]. ABR data comparing threshold shifts within a group before and after noise exposure were analyzed by a two-way ANOVA with Sidak's post hoc test for multiple comparisons. An adjusted p value of < 0.05 was set as the threshold for significance. The F values for main effects are listed in the main text, and the interactions are listed in Additional file 2. The value of Cohen's d (d) was calculated when the data reach significance following the post hoc test. All ABR data analyses and figures were generated using Prism 7 software (GraphPad, CA) with the recommended settings for post hoc tests.

For the ABR wave I amplitude analysis, the growth of the amplitude as a function of stimuli levels was expressed as a slope, obtained by linear regression of amplitude versus stimuli level plots from noise-exposed animals (DMSO treated) of each sex, before and after noise exposure, at 16 kHz. Two-tailed t test was used to compare the slopes between groups using Prism 7 software (GraphPad, CA).

Comparisons of OHCs and synapse counts between male and female mice were made using Student's t test assuming unequal variance using Prism 7 software (GraphPad, CA).

Results

Differential response of male and female mice to noise trauma

In the present study, 10-week-old male and female mice were exposed to 101 dB SPL octave band noise centered at around 11.3 kHz, for 2 h. The mice received either SAHA (100 mg/kg) dissolved in DMSO, or DMSO alone as a control (vehicle) 3 days before and 2 h after the end of noise exposure. Hearing thresholds were measured using ABRs at 8, 16, 24, and 32 kHz. Thresholds measured

at 24 h, 8 days, and 15 days after noise exposure were compared to the baseline thresholds to calculate the compound (24 h) and permanent (8 and 15 days) threshold shifts, respectively (CTS and PTS) [35]. The CTS reflects the change in hearing threshold shortly following noise exposure, which is normally higher than the final change in hearing threshold, whereas the PTS reflects what is considered a "final" change in hearing threshold following noise exposure [35]. In vehicle-treated mice, a two-way ANOVA revealed main effects of frequency and time on the hearing thresholds (frequency: $F_{3,\ 752} = 155.1$; $p < 0.0001$; time: $F_{3,\ 752} = 284$; $p < 0.0001$). A post hoc comparison showed that the noise exposure induced a significant CTS and PTS at all frequencies measured (Fig. 1). In addition, there were no statistically significant differences in the hearing thresholds at 8 and 15 days post-exposure; therefore, subsequent measures for PTS are reported at 15 days only (Fig. 1).

To test whether male and female mice have a differential response to noise, we first compared baselines in males and females to rule out a possible difference in hearing thresholds before noise exposure (Fig. 2a and Additional file 2: Table S1). A two-way ANOVA followed by a post hoc analysis detected a small but significant lower threshold in females at 32 kHz ($p = 0.0008$; $d = 0.357$) but not at 8, 16, and 24 kHz. We next assessed the CTS and PTS for each sex separately (Fig. 2b and Additional file 2: Table S2). Similar to the results obtained with both sexes combined, males and females had

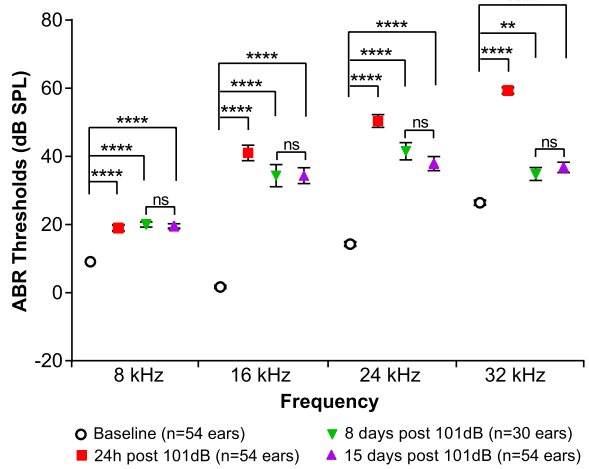

Fig. 1 Octave band noise exposure at 101 dB SPL causes PTS in 10-week-old B6CBAF1/J mice. Hearing thresholds were compared between baseline, 24 h, 8 days, and 15 days post-noise exposure. At 24 h post-noise, significant compound threshold shifts are seen across all frequencies tested. Significant permanent threshold shifts are also detected at all frequencies tested at 8 and 15 days post-noise exposure. (**$p < 0.01$; **** $p < 0.0001$; ns non-significant)

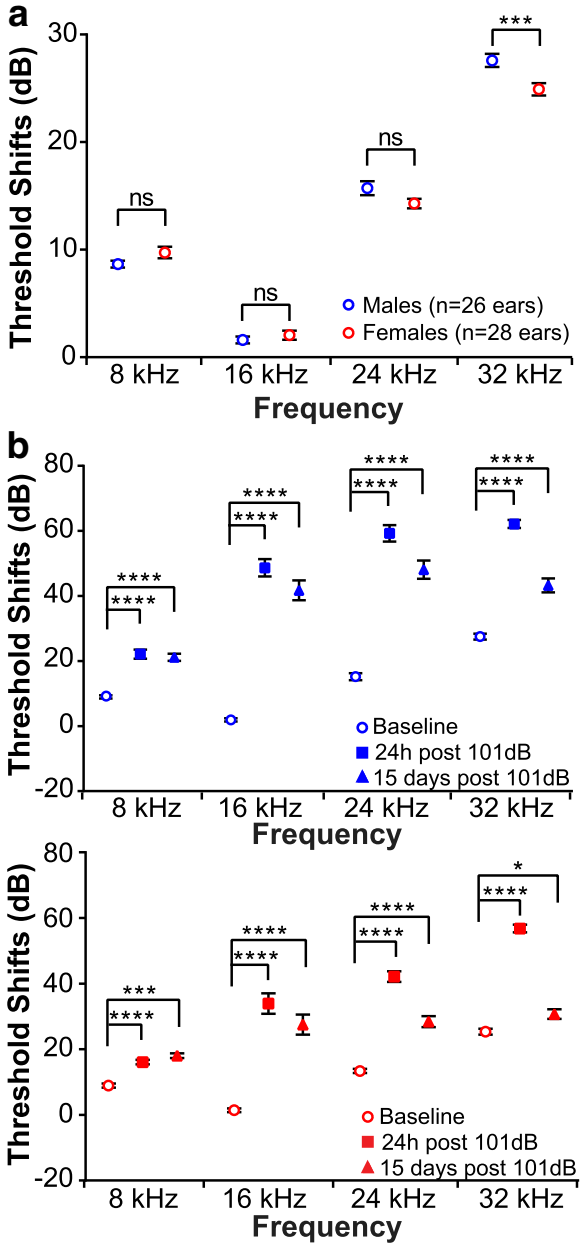

Fig. 2 Octave band noise exposure at 101 dB SPL causes PTS in male and female mice. **a** Comparison of baseline hearing threshold between males and females. Female mice present a lower threshold at 32 kHz. **b** Hearing thresholds were compared between baseline, 24 h, and 15 days post-noise exposure in males (top) and females (bottom). At 24 h and 15 days post-noise exposure, significant compound threshold shifts are seen across all frequencies tested in both males and females. (*$p < 0.05$; ***$p < 0.001$; **** < 0.0001; ns non-significant)

significant CTS and PTS at all frequencies measured when compared to pre-noise baseline. However, when male and female threshold shifts following noise exposure were compared to each other, a two-way ANOVA revealed main effects of frequency and sex on both CTS

(frequency: $F_{3,\ 208} = 84.84$; $p < 0.0001$; sex: $F_{1,\ 208} = 43.41$; $p < 0.0001$) and PTS (frequency: $F_{3,\ 208} = 47.46$; $p < 0.0001$; sex: $F_{1,\ 208} = 49.58$; $p < 0.0001$) (Fig. 3 and Additional file 2: Table S3). A *post hoc* comparison revealed that 24 h after noise exposure, females have a significantly lower CTS at 16 and 24 kHz ($p < 0.0001$ for both frequencies; $d = 0.676$ for 16 kHz and $d = 0.727$ for 24 kHz) compared to males (Fig. 3 and Additional file 2: Table S4). This difference is extended to the 32 kHz frequency as well 15 days post-noise exposure ($p < 0.0001$ for 16 and 24 kHz; $p = 0.005$ for 32 kHz; $d = 0.598$ for 16 kHz, $d = 0.779$ for 24 kHz, and $d = 0.453$ for 32 kHz). These data suggest that females have a less severe hearing loss following noise exposure compared to males.

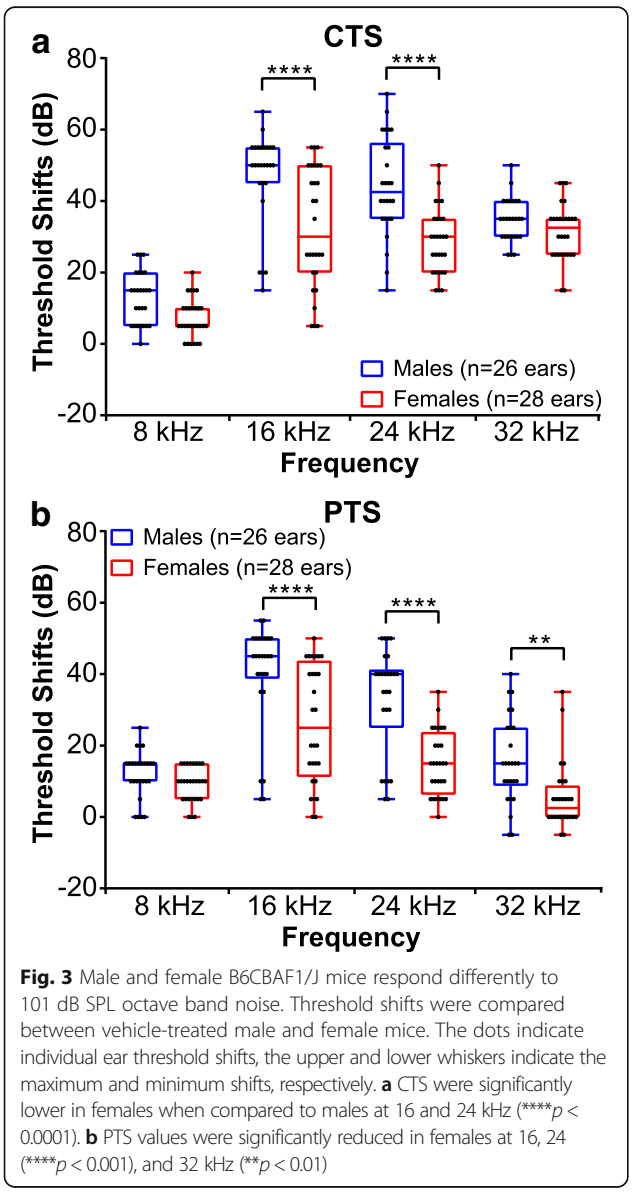

Fig. 3 Male and female B6CBAF1/J mice respond differently to 101 dB SPL octave band noise. Threshold shifts were compared between vehicle-treated male and female mice. The dots indicate individual ear threshold shifts, the upper and lower whiskers indicate the maximum and minimum shifts, respectively. **a** CTS were significantly lower in females when compared to males at 16 and 24 kHz (****$p < 0.0001$). **b** PTS values were significantly reduced in females at 16, 24 (****$p < 0.001$), and 32 kHz (**$p < 0.01$)

Effect of noise on ABR wave I amplitude in male and female mice

The cochlea has two types of sensory cells—inner hair cells (IHC) and outer hair cells (OHC). The OHC function primarily as signal amplifiers, whereas the IHC receive primarily afferent innervation and are the main source of auditory sensory input to the brain [41]. The ABR wave I amplitude is primarily a reflection of the frequency-specific activity at the spiral ganglion (SG), which is the ganglion that houses the cell bodies of the afferent neurons that come in contact mainly with the IHC. This activity is a compound of the levels of IHC and OHC activity (as IHC activity is influenced by OHC function), the number of active auditory nerve fibers present, functional synapses, as well as the endocochlear potential [17, 42]. To assess whether the difference in the male and female response to noise correlates with a difference in the synchronous activity at the SG, the increase in ABR wave I amplitude as a function of increasing sound level was measured in the vehicle-treated noise-exposed mice. A change in amplitude can result from changes in any of the factors that contribute to wave I. We analyzed wave I amplitude at the frequency with the maximal threshold shift, which was 16 kHz in this study. Average peak-to-trough wave I amplitudes were extracted for stimuli levels 55 dB to 85 dB for each animal at baseline (prior to noise exposure), 24 h, and 15 days post-noise exposure. A change in the slope of the amplitude as a function of sound level would most likely reflect a change in active processes in the cochlea, primarily attributed to OHC function [43, 44]. (Fig. 4). A linear regression analysis showed a decrease in the slope 24 h post-noise exposure for both males and females. At baseline, males had an average slope of 155 ± 6 nV/dB, while at 24 h post-noise exposure, this slope significantly decreased to 93 ± 6 nV/dB ($p < 0.0001$) (Fig. 4a). The average slope at baseline for females was 255 ± 16 nV/dB as compared to 196 ± 14 nV/dB for 24 h post-noise exposure ($p = 0.0022$) (Fig. 4a). At 15 days post-noise exposure, the slope value partially recovered in males when compared to 24 h, averaging 120 ± 4 nV/dB ($p = 0.0051$), but remained significantly lower than baseline ($p = 0.0008$) (Fig. 4a). While males recovered partially, the average slope for females at 15 days post-noise exposure was similar to the slope at 24 h with a value of 191 ± 13 nV/dB ($p = 0.7959$). Interestingly, when we directly compared the slopes between males and females from the same time point, a two-tailed *t* test revealed significant differences between the slopes (Fig. 4b). At baseline, females have a slope of 255 ± 16 nV/dB as compared to a slope of 155 ± 6 nV/dB for males ($p = 0.0002$). This difference is maintained after noise exposure at 24 h and 15 days (Fig. 4b). Comparison of the absolute amplitude of wave I at 85 dB SPL shows permanent lower

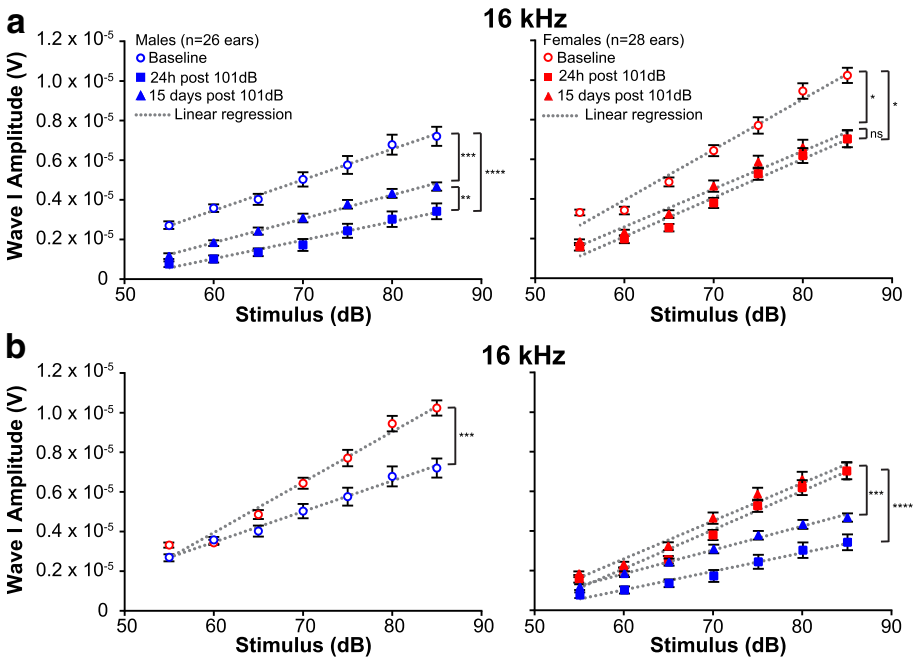

Fig. 4 Differences in the slopes of ABR wave I amplitudes between male and female mice at 16 kHz. Growth of ABR wave I amplitude as a function of increasing stimuli levels at 16 kHz was compared by analysis of the slopes from linear regression of the data (dotted lines). The slopes are shown at baseline, 24 h, and 15 days post-noise exposure in males and females. **a** Slopes are reduced following noise exposure when compared to baseline for males (left) and females (right). Males partially recover at 15 days when compared to 24 h while females do not. **b** At baseline (left), the slope value from female wave I amplitude is higher than the value from males. The difference is maintained following noise exposure (right) at 24 h and 15 days. *$p < 0.05$; **$p < 0.01$; ***$p < 0.001$; ****$p < 0.0001$. Error bars indicate S.E.M. ns, non-significant

amplitude in the males compared with the female mice (Fig. 4b and Table 1).

Effect of noise on OHC loss

To identify possible causes for the differential response to noise between male and female mice, we performed cytocochleograms to compare hair cell loss throughout the cochlear duct (up to a frequency position corresponding to 55 kHz) (Additional file 3). For unexposed controls, we used strain (B6CBAF1/J) and age-matched (12 weeks old) mice. As expected, 12-week-old control mice (males and females) showed little to no OHC loss along the organ of Corti (0 to 0.34% loss) (Table 2 and Additional file 4). Similarly, 2 weeks following a 101 dB noise exposure, there was no significant OHC loss (less than 1%) in either sex up to 32 kHz (Fig. 5). While an OHC loss was measured at 32–55 kHz (Table 2 and Additional file 4), no sex-specific differences were measured with respect to OHC loss (Table 2, Additional file 4 and Additional file 2: Table S5). These results suggest that the sex difference seen in response to noise exposure is not explained by a divergence in OHC loss in males and females. Interestingly, the pattern of OHC loss seen in noise-exposed animals does not match the frequency-specific PTS. The cochlea is organized such that high-frequency sounds are sensed at the base of the organ, close to the "entry of sound," and low-frequency sounds at the apex (also known as a tonotopic organization) [45]. While the highest PTS is measured at 16 and 24 kHz, only minimal OHC loss is observed around these frequencies (Table 2 and Additional file 4). Therefore, our data indicate that the OHC loss at the 16 and the 24 kHz location is not sufficient to explain the PTS at these frequencies when measured 15 days post-noise exposure.

Table 1 Values for the wave I absolute amplitudes at 85 dB SPL

	Wave I amplitudes at a 85 dB stimulus (volt)		
	Baseline	24 h post 101 dB	15 days post 101 dB
Males	7.21×10^{-6}	3.42×10^{-6}	4.67×10^{-6}
Females	10.2×10^{-6}	7.04×10^{-6}	7.04×10^{-6}
p value	< 0.0001	< 0.0001	< 0.0001
d value	1.380	1.719	1.317

Females have a higher amplitude at baseline, 24 h, and 15 days post-noise exposure (unpaired *t* test)

Effect of noise trauma on IHC synapses

Our data indicate that 2 weeks after noise exposure, at a time a PTS is already obtained, the OHC loss does not account for either the significant PTS at 16 and 24 kHz or the sex differences observed in the PTS and wave I

Table 2 Values for the percentage of OHC loss within nine frequency ranges measured

		OHC loss by frequency range								
		4–5.6 kHz	5.6-8 kHz	8–11.3 kHz	11.3-16 kHz	16–22.6 kHz	22.6-32 kHz	32–45.2 kHz	45.2-51 kHz	51-55 kHz
Controls	Males	0.12 ± 0.12	0.23 ± 0.23	0.34 ± 0.21	0.03 ± 0.03	0.26 ± 0.16	0.23 ± 0.08	0.29 ± 0.10	0.34 ± 0.34	0.15 ± 0.15
	Females	0.00 ± 0.00	0.13 ± 0.09	0.06 ± 0.06	0.09 ± 0.06	0.07 ± 0.05	0.10 ± 0.07	0.18 ± 0.12	0.00 ± 0.00	0.18 ± 0.18
DMSO + noise	Males	0.29 ± 0.20	0.23 ± 0.12	0.16 ± 0.08	0.15 ± 0.05	0.22 ± 0.07	0.77 ± 0.23	4.76 ± 1.17	21.8 ± 4.57	45.7 ± 10.3
	Females	0.00 ± 0.00	0.02 ± 0.02	0.20 ± 0.08	0.10 ± 0.06	0.35 ± 0.11	0.43 ± 0.16	5.36 ± 2.32	22.4 ± 7.73	45.3 ± 14.2

Progressive OHC loss is seen beginning from 32 kHz. Both male and female animals show a similar pattern of OHC loss. ± represent S.E.M

amplitude progression. Loss of IHC functional synapses has been shown to account for the decrease in wave I amplitude following lower intensity noise exposures, a phenomenon also known as cochlear synaptopathy [46]. We therefore focused our analysis on the IHC synapses. We first quantified the number of pre-synaptic ribbons in the IHCs. For this purpose, whole mount cochleae were fluorescently immunolabeled with an antibody directed against CtBP2 to visualize the pre-synaptic ribbons. Pre-synaptic ribbons were counted on Z-stacks created from confocal sections in the regions of 16, 24, and 32 kHz (Additional file 5). In the region where the maximal threshold shift is detected (16 kHz location), no significant change in the pre-synaptic ribbons was recorded following noise in either sex (Table 3 and Additional file 6). However, a significant decrease in the pre-synaptic ribbons per IHC was observed in the region of 24 and 32 kHz in both male and female mice (Table 3 and Additional file 6). Interestingly, no difference was detected between males and females at the three frequencies analyzed in either the controls or noise-exposed animals ($p > 0.05$), suggesting that the change in pre-synaptic ribbons does not account for the sex differences in hearing following noise exposure.

Recent evidence suggests that noise exposure reduces the number of active IHC synapses by inducing the

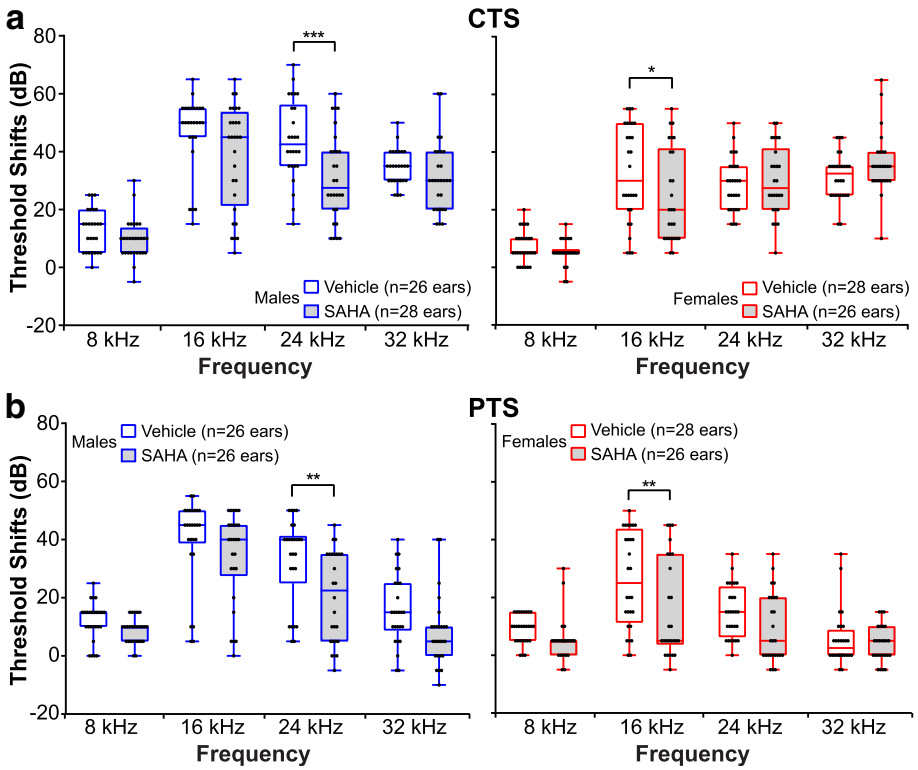

Fig. 5 Protective effect of SAHA on NIHL—separated by sex. Threshold shifts were compared between SAHA- and vehicle-treated males (left) and females (right) at 24 h (**a**) and 15 days (**b**) post-noise exposure. The dots indicate individual ear threshold shifts, the upper and lower whiskers indicate the maximum and minimum shifts, respectively. **a** CTS values for males (left) and females (right). Male mice are protected only at 24 kHz (***$p < 0.001$) and female mice only at 16 kHz (*$p < 0.05$). **b** PTS values for males (left) and females (right). Females remain protected at 16 kHz (** $p < 0.01$) and males remain protected at 24 kHz (**$p < 0.01$)

Table 3 Pre-synaptic ribbon counts per IHC in the 16, 24 and 32 kHz regions in male and female mice

	Total IHC ribbons								
	16 kHz location			24 kHz location			32 kHz location		
	Males	Female	*p* value	Males	Females	*p* value	Males	Females	*p* value
Controls	15.00 ± 0.72	15.86 ± 0.53	0.34	16.16 ± 0.78	15.85 ± 0.61	0.76	15.60 ± 0.98	13.78 ± 0.92	0.20
DMSO + Noise	15.25 ± 0.86	14.60 ± 0.87	0.60	11.38 ± 0.74	11.95 ± 0.95	0.64	7.65 ± 0.88	8.11 ± 0.78	0.71

± represent S.E.M. (unpaired *t* test to compare males versus females)

retraction of some of the neurons that come in contact with the IHC. Shortly after noise exposure, while the synaptic ribbons may persist, loss of neuronal contact can be identified by loss of post-synaptic densities [47]. We therefore analyzed the number of pre-synaptic ribbons paired with post-synaptic glutamate receptor (GluR2) to determine if the different response to noise exposure between male and female mice can be attributed to the number of active synapses (Additional file 5). Similar to pre-synaptic ribbons, noise exposure induced a significant decrease in the number of active synapses at the regions of 24 and 32 kHz but not 16 kHz. However, again, there was no sexual dimorphism in the number of active synapses (Table 4 and Additional file 6). These data indicate that the noise-induced synaptopathy is not the main underlying cause for the PTS seen at 16 kHz, which is the frequency with the maximal threshold shift, and is not the culprit of the sexual dimorphism in the response to noise.

Sex influences the measured effect of SAHA treatment on mice exposed to noise

To date, most studies on noise exposure and its treatments were performed on male mice only or mice of both sexes combined. Because our data show a differential response to noise between male and female mice, we next explored whether sex influences the measured response to treatment. This is important for proper testing of therapeutics. To determine whether SAHA has a protective effect from noise exposure, CTS (Fig. 5a) and PTS values (Fig. 5b) were compared between vehicle and SAHA-treated animals. A two-way ANOVA revealed main effects of SAHA and sex on CTS at 8, 16, and 24 kHz (Table 5 and Additional file 2: Table S3). Main effects of SAHA and sex 15 days post-noise exposure is significant at all frequencies tested (Table 5).

Post hoc comparisons revealed that CTS of SAHA-treated males were significantly lower at 24 kHz ($p = 0.0006$; $d = 0.536$) compared to vehicle-treated controls, whereas in females, CTS values were significantly lower at 16 kHz ($p = 0.04$; $d = 0.359$) (Fig. 5a**,** Additional file 2: Table S6). Comparisons of PTS suggested that the protective effect of SAHA in male mice is maintained at 24 kHz ($p = 0.002$; $d = 0.489$) and at 16 kHz in female mice ($p = 0.003$; $d = 0.482$) compared to the vehicle-treated controls (Fig. 5b, Additional file 2: Table S6). These data indicate a difference in the response to SAHA between male and female mice.

Next, we re-analyzed the data, this time combining mice from both sexes, to assess whether this might change the measured response to treatment. A two-way ANOVA revealed significant main effects of SAHA and frequency at 24 h (SAHA: $F_{1,\ 424} = 9.576$, $p = 0.0021$; frequency: $F_{3,\ 424} = 110.1$, $p < 0.0001$) and 15 days (SAHA: $F_{1,\ 416} = 22.67$, $p < 0.0001$; frequency: $F_{3,\ 416} = 57.36$, $p < 0.0001$) post-noise exposure. Compared to vehicle-treated controls, SAHA significantly decreased the CTS only at 16 kHz ($p = 0.0074$) (Fig. 6a, Additional file 2: Table S7) while a significant decrease in PTS was observed at 16 and 24 kHz ($p = 0.0095$ and 0.0024, respectively) (Fig. 6b, Additional file 2: Table S7). Thus, these findings indicate that when combining mice from both sexes, the measured response to treatment is different from the response when each sex is analyzed separately. This is critically important as it may lead to misinterpretation of biological data.

Discussion

The major finding reported here is the identification and characterization of a sexually dimorphic response to PTS-inducing noise exposure and its candidate therapeutics in mice. Sex is an important biological variable

Table 4 Active synapse counts per IHC at 16, 24, and 32 kHz in male and female mice

	Active synapses								
	16 kHz location			24 kHz location			32 kHz location		
	Males	Females	*p* value	Males	Females	*p* value	Males	Females	*p* value
Control	13.26 ± 1.75	14.51 ± 2.82	0.63	14.84 ± 1.91	13.64 ± 1.11	0.60	11.36 ± 1.38	9.73 ± 1.07	0.41
DMSO + Noise	11.66 ± 1.38	11.39 ± 1.50	0.89	8.47 ± 1.28	7.34 ± 2.13	0.66	3.94 ± 1.18	4.86 ± 0.99	0.58

± represent S.E.M. (unpaired *t* test to compare males versus females)

Table 5 Main effects of SAHA and sex on CTS and PTS following a two-way ANOVA

		8 kHz		16 kHz		24 kHz		32 kHz	
		F	*p* value	F	*p* value	F	*p* value	F	*p* value
CTS	Sex	18.67	**< 0.0001**	20.06	**< 0.0001**	11.07	**0.001**	0.174	ns
	SAHA	4.845	**0.030**	6.728	**0.011**	5.678	**0.020**	0.102	ns
PTS	Sex	6.885	**0.010**	26.35	**< 0.0001**	22.14	**< 0.0001**	14.02	**0.0003**
	SAHA	9.089	**0.003**	6.723	**0.011**	13.18	**0.0004**	5.174	**0.025**

For CTS and PTS, the degree of freedom for the numerator is 1. The degrees of freedom for the denominator are 104 and 102 for CTS and PTS, respectively. Significant results are shown in bold font (*ns* non-significant)

with effects on a wide range of physiological processes, and it must be considered in the experimental design to allow study results to relate to both male and female biology [48]. Importantly, the National Institutes of Health has added consideration of sex as a biological factor in all applications considered for funding [49, 50]. We tested the efficacy of SAHA on prevention of noise-induced hearing loss in mice of both sexes. SAHA has been previously shown to be otoprotective against ototoxic drugs [51–54] and NIHL in male mice [14, 31]. Our results confirmed the efficacy of SAHA in male mice, albeit possibly to a lesser degree than previously reported [14, 31], and revealed only a small protective effect in females. Importantly, our treatment paradigm differed from previously published work and could account for some of the difference in efficacy. When the PTS from both sexes were analyzed together, 15 days post-noise exposure, a statistically significant protective effect of SAHA was found at both 16 and 24 kHz. However, when the data were separated by sex, we found that the protective effect of SAHA in males was limited to 24 kHz while in females to 16 kHz. Female mice demonstrated less hearing loss in response to noise at 16 and 24 kHz, in comparison to males, suggesting a sex-specific difference in the response to PTS-inducing noise trauma. This sex difference may explain the differential frequency-specific therapeutic efficacy of SAHA, where males at 16 kHz may have suffered too much damage to allow for SAHA-dependent rescue, and females at 24 kHz have too little PTS to allow a therapeutic effect to be detected with the number of mice tested. Concordantly, previous studies suggested a level-specific limitation to the therapeutic effect of SAHA [14, 31].

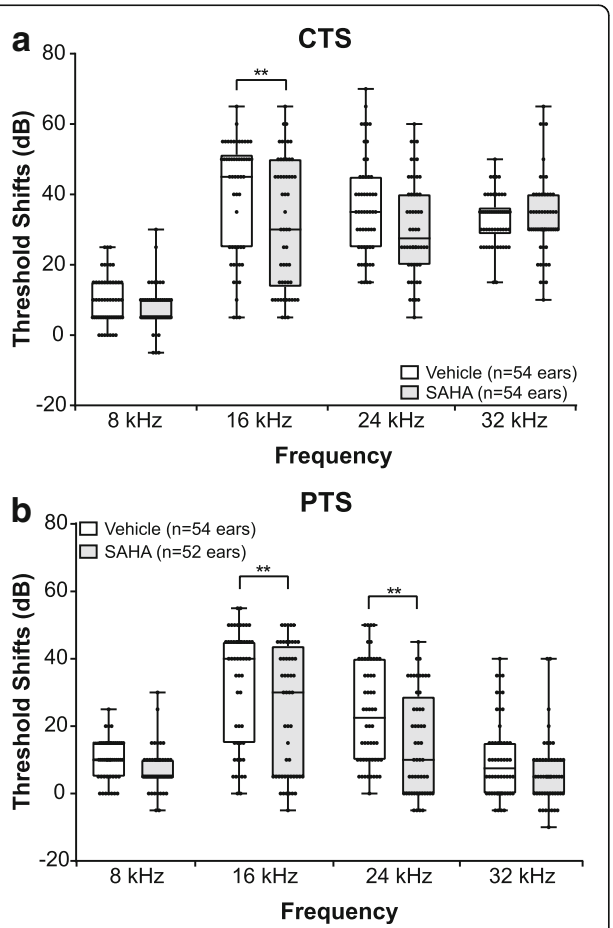

Fig. 6 Protective effect of SAHA on NIHL—both sexes combined. Threshold shifts were compared between SAHA- and vehicle-treated animals at 24 h (**a**) and 15 days (**b**) post-noise exposure. The dots indicate individual ear threshold shifts; the upper and lower whiskers indicate the maximum and minimum shifts, respectively. **a** CTS values suggested a protective effect of SAHA at 16 kHz (*$p = 0.007$). **b** PTS values suggested a protective effect of SAHA at 16 kHz (*$p = 0.0095$) and 24 kHz (**$p = 0.0024$)

To further investigate the sex-specific differences in hearing following PTS-inducing noise exposure, we compared OHC loss, wave I amplitude, and amplitude progression, as well as IHC pre-synaptic ribbons and active synapses. To our surprise, we found a significant difference between the sexes only in the wave I amplitude and amplitude progression. Wave I amplitude is an indicator of activity at the level of the SG, whereas wave I amplitude progression reflects the OHC contribution to the active process of hearing. Since the number of hair cells and synapses following noise exposure was not different across sexes, a decrease in wave I amplitude and amplitude progression suggests a greater decrease in OHC activity in the male mice. The suggested decrease in OHC function may be primary and represent a

dysfunction resulting from injury to the stereocilia or cell bodies [46], or secondary as a consequence of changes in the endocochlear potential. A recent study in F344 rats shows that the difference in hearing loss between aging male and female animals results in part from cellular degeneration at the level of the stria vascularis [55]. However, in this strain of rats OHC loss progressed from apex to base, indicating that the pathophysiology underlying the ARHL in the F344 rats may not be generalizable. Additional studies using inbred mouse strains revealed a divergent pathophysiology for male and female age-related loss [56, 57]. These observations suggest that outbred mice such as the B6CBAF1/J may prove particularly useful in the study of NIHL, as the effect of strain-specific recessively inherited mutations on the auditory system will be largely avoided. Future studies comparing changes in OHC and stria vascularis morphology and ultrastructure, as well as measurement of the endocochlear potential and distortion product otoacoustic emissions (DPOAE), are necessary to further define the underlying sex-specific differences following noise exposure [58, 59].

We employed an octave band (8–16 kHz) noise exposure paradigm that results in PTS in the B6CBAF1/J mouse strain. As expected following these type of exposures, we measured a maximal threshold shift at 16 and 24 kHz. A smaller threshold shift was measured at 32 kHz, the highest frequency analyzed in this study. A marked and significant loss of OHC was seen in both sexes in regions that correspond to frequencies higher than 32 kHz; however, only a minimal loss of OHC was measured in areas that map to 16 and 24 kHz. Taken together, these data suggest that two weeks following noise exposure, there are two types of hearing loss that differ in their underlying mechanisms. A loss of OHC in the base of the cochlea underlies a high-frequency hearing loss, which is not directly related to the frequency of the noise exposure. Rather, it represents a non-specific acoustic injury likely secondary to the position and physical characteristics of the cells in the base of the cochlea. In addition, a frequency-specific PTS, which is the focus of this manuscript, is not secondary to loss of OHC. More importantly, these findings suggest a possible therapeutic window to treat the OHC and possibly prevent the frequency-specific PTS, as OHC in the frequency-specific PTS are still present 2 weeks following exposure. Later degeneration of OHC following PTS has been observed when ears are analyzed 1 year following noise exposure [18]. Similar to the lack of OHC loss at 16 kHz, the frequency where maximal PTS is found in both sexes, we did not observe a significant loss of active synapses in either sex. A progressive loss of active synapses was seen at 24 and 32 kHz. These data suggest that at least 2 weeks following PTS-inducing noise exposure, synaptopathy preferentially affects higher frequencies and does not explain the loss of hearing at 16 kHz or the sex-specific differences in the response to noise trauma (Fig. 7).

Differences in circulating levels of the steroid hormone estradiol and/or sensitivity to estradiol via its receptor activation may account for the observed sex difference in PTS as a result of noise trauma. Evidence from both clinical and basic studies clearly demonstrates that estradiol plays an important role in modulating auditory function in vertebrates as well as conferring a protective function in the female auditory system [60]. Estradiol signaling primarily occurs via two cognate receptors that are ligand-activated transcription factors. Estrogen receptor 1 (ERS1) and estrogen receptor 2 (ERS2) are widely distributed throughout the body and both have been reported in the cochlea of rodents and humans [61–64]. In mice, ESR1

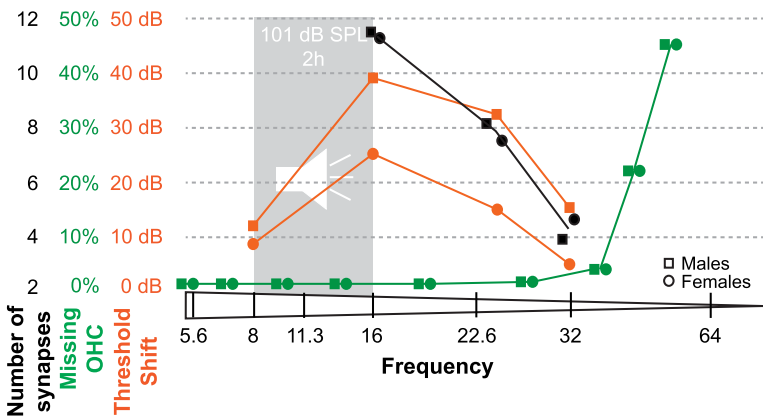

Fig. 7 Schematic showing the threshold shifts in relation to missing outer hair cells and number of active synapses. Loss of OHC (green) and decrease in the number of active synapses (black) does not correlate with the highest threshold shift (orange) following noise exposure detected at 16 kHz. The difference in threshold shifts between male and female mice is not explained by a difference in OHC loss or active synapse numbers

and ESR2 are present in both the inner and outer hair cells, as well as the spiral ganglion neurons [61, 63, 65]. ESR2 and not ESR1 has been implicated in conferring the protective actions of estradiol against temporary hearing loss as result of a noise trauma in male and female mice [65] and age-related hearing loss in female mice [66]. However, the exact mechanisms through which estradiol is acting to confer protection is not well understood. In addition, molecular differences independent of the estradiol signaling pathway should also be considered in the underpinning mechanisms of the sexual dimorphic response to noise exposure.

Conclusions

In conclusion, this study documents significant sex-specific differences in the response of the mouse cochlea to damaging noise exposure. These findings have implications on future study design for proper interpretation of the data. In particular, male and female mice should be tested and analyzed separately when used to study NIHL. As females demonstrate less noise-induced hearing damage in comparison to males, they may require exposure to a higher sound level to assess therapeutic effects. In addition, understanding the underpinnings of the females' relative protection from NIHL could lead to the development of new therapeutics to ameliorate the outcomes of noise exposures. Classic approaches to interrogate sex differences such as studying gonadectomized mice with and without supplemental sex hormones might be particularly useful to overcome challenges related to fluctuation of circulating sex hormones [67].

Additional files

Additional file 1: Schematic showing ABR wave I extraction and analysis. Peak (P1) and trough (T1) values of wave I of the ABR traces (wave shaded in blue) were automatically extracted at stimuli levels from 55 to 85 dB SPL using a MatLab script. Wave I amplitudes were then plotted as a function of the stimuli levels. SigmaPlot was used to perform linear regression (dotted line) and calculate the slope (solid lines). Slopes were then compared between the different groups at 16 kHz. (PDF 471 kb)

Additional file 2: **Table S1.**Comparison of average hearing thresholds at baseline in male and female mice (Sidak's multiple comparison test; ns: non-significant). **Table S2.** Average threshold shift values in dB at 24 h post-noise exposure (CTS) and 15 days post-noise exposure (PTS) in vehicle-treated males and females (Tukey's multiple comparisons test). **Table S3.** Statistical values for interactions between the two factors following a two-way ANOVA. The degrees of freedom for the numerator (DFn) and denominator (DFd) are shown in parenthesis before the *F* value. Significant results are shown in bold font. **Table S4.** Comparison of average ABR thresholds shifts at 24 h (CTS) and 15 days (PTS) post-noise exposure in male and female mice treated with vehicle only (Sidak's multiple comparison test; ns: non-significant). **Table S5.** Values for the percentage of OHC loss within 32–45.2 kHz, 45.2–51 kHz, and 51–55 kHz. Progressive OHC loss is seen up to 55 kHz which is the highest frequency counted. Both male and female animals show a similar pattern of OHC loss. ± represent S.E.M. (unpaired *t* test to compare male and female mice). **Table S6.** Comparison of average threshold shift values in dB at 24 h post-noise exposure (CTS) and 15 days post-noise exposure (PTS) between vehicle- and SAHA-treated males and females separately (Sidak's multiple comparisons test; ns: non-significant). **Table S7.** Comparison of average threshold shift values in dB at 24 h post-noise exposure (CTS) and 15 days post-noise exposure (PTS) between vehicle- and SAHA-treated animals (Sidak's multiple comparisons test; ns: non-significant). (PDF 257 kb)

Additional file 3: OHC loss along the cochlear duct. Representative fluorescence microscopy images of the Organ of Corti at the level of the OHC (counter-stained with DAPI) at different frequency bands from controls and mice exposed at 101 dB SPL. There is little to no OHC loss in the control animals, whereas extensive OHC loss is seen above 32 kHz in animals exposed to noise. Scale bar represents 20 μm. (PDF 1120 kb)

Additional file 4: OHC loss does not account for the frequency-specific PTS at 16 and 24 kHz or the sex differences in NIHL. Line graph indicating the percentage of OHC loss from apex to base in vehicle-treated noise-exposed animals compared to control non-noise-exposed animals. The frequency range of noise exposure is shaded gray and a gray dotted line outlines the frequency range where significant PTS is seen. Error bars indicate S.E.M. (PDF 396 kb)

Additional file 5: Pre-synaptic ribbons and active synapses at 16 kHz and 24 kHz. Representative fluorescence microscopy images of IHC stained for CtBP2 (red) and GluR2 (green) at 16 kHz (left) and 24 kHz (right) from control and noise-exposed mice. The dotted lines represent the approximate border of one IHC. The inset in the bottom left corner image represent a zoom in of active synapses where CtBP2 and GluR2 partially co-localize. Scale bar represents 10 μm. (PDF 1242 kb)

Additional file 6: Effect of noise on pre-synaptic ribbons and active synapses in IHC. Graphs representing the number of pre-synaptic ribbons **(a)** and active synapses **(b)** in IHC of control and vehicle-treated noise-exposed animals. A significant decrease in pre-synaptic ribbons and active synapses is observed at 24 and 32 kHz in both males and females, but no difference is seen between sexes. Error bars indicate S.E.M. (PDF 418 kb)

Abbreviations

ABR: Auditory brainstem response; ARHL: Age-related hearing loss; CTS: Compound threshold shift; dB: Decibel; DMSO: Dimethyl sulfoxide; DPOAE: Distortion product otoacoustic emissions; IHC: Inner hair cell; NILH: Noise-induced hearing loss; OHC: Outer hair cell; PTS: Permanent threshold shift; SAHA: Suberoylanilide hydroxamic acid; SPL: Sound pressure level

Acknowledgements

We would like to thank Lisa Cunningham, PhD and Kevin Ohlemiller, PhD for critically reviewing this manuscript.

Funding

This work was supported by R01DC03544 (NIDCD), R01DC013817 (NIDCD), and MR130240 (CDMRP/DoD).

Availability of data and materials

The datasets supporting the conclusions of this article are included within the article and its additional files (Additional files 1, 2, 3, 4, 5, and 6).

Authors' contributions

SM and ZM contributed to the treatments, noise exposure, and ABR; BM and SM contributed to the histology and data analysis; RC and VD contributed to the blinded thresholds determination; DAD contributed to the MatLab script and data analysis; YS and JAM contributed to the statistical analysis; RH contributed to the experimental design and data analysis; and SM, RH, BM, JAM, and DAD wrote the manuscript. All the authors read and approved the final manuscript.

Ethics approval

All procedures involving animals were carried out in accordance with the National Institutes of Health Guide for the Care and Use of Laboratory Animals and have been approved by the Institutional Animal Care and Use Committee at the University of Maryland, Baltimore (protocol numbers 1015003 and 0915006).

Consent for publication

Not applicable.

Competing interests
The authors declare that they have no competing interests.

Publisher's Note

Author details
[1]Department of Otorhinolaryngology - Head and Neck Surgery, University of Maryland, 16 South Eutaw Street, Suite 500, Baltimore, MD 21201, USA. [2]Institute for Genome Science, University of Maryland School of Medicine, Baltimore, MD 21201, USA. [3]Department of Pharmacology, University of Maryland School of Medicine, Baltimore, MD 21201, USA. [4]Institute for Systems Research, University of Maryland, College Park, MD 20742, USA. [5]Department of Anatomy and Neurobiology, University of Maryland School of Medicine, Baltimore, MD 21201, USA.

Received: 26 January 2018 Accepted: 27 February 2018
Published online: 12 March 2018

References

1. Nelson DI, Nelson RY, Concha-Barrientos M, Fingerhut M. The global burden of occupational noise-induced hearing loss. Am J Ind Med. 2005;48:446–58. http://doi.wiley.com/10.1002/ajim.20223
2. Carroll YI, Eichwald J, Scinicariello F, Hoffman HJ, Deitchman S, Radke MS, et al. Vital signs: noise-induced hearing loss among adults—United States 2011–2012. MMWR Morb Mortal Wkly Rep. 2017;66:139–44.
3. Lie A, Skogstad M, Johannessen HA, Tynes T, Mehlum IS, Nordby K-C, et al. Occupational noise exposure and hearing: a systematic review. Int Arch Occup Environ Health. 2016;89:351–72.
4. U.S. Department of Veterans Affairs. Veterans benefit administration, annual benefits report, fiscal year 2016. 2016. https://www.benefits.va.gov/REPORTS/abr/ABR-All_Sections_FY16_06292017.pdf
5. Lin FR, Hazzard WR, Blazer DG. Priorities for improving hearing health care for adults: a report from the National Academies of Sciences, Engineering, and Medicine. JAMA J Am Med Assoc. 2016;316:819–20.
6. Salvi R, Boettcher FA. Animal models of noise-induced hearing loss. In: Conn PM, editor. Sourceb. Model. Biomed. Res. 1st ed. Totowa: Humana Press; 2008. p. 289–301.
7. Nodal FR, King AJ. Hearing and auditory function in ferrets. In: Fox JG, Marini R, editors. Biol Dis Ferret. 3rd ed. Ames: Wiley; 2014. p. 685–710.
8. Depireux DA, Simon JZ, Klein DJ, Shamma SA. Spectro-temporal response field characterization with dynamic ripples in ferret primary auditory cortex. J Neurophysiol. 2001;85:1220–34. United States
9. Chen G-D, Fechter LD. The relationship between noise-induced hearing loss and hair cell loss in rats. Hear Res. 2003;177:81–90.
10. Ohlemiller KK. Contributions of mouse models to understanding of age- and noise-related hearing loss. Brain Res. 2006;1091:89–102.
11. Ahituv N, Avraham KB. Auditory and vestibular mouse mutants: models for human deafness. J Basic Clin Physiol Pharmacol. 2000;11:181–92.
12. Layman WS, Williams DM, Dearman JA, Sauceda MA, Zuo J. Histone deacetylase inhibition protects hearing against acute ototoxicity by activating the Nf-κB pathway. Cell Death Discov. 2015;1:15012. http://www.nature.com/articles/cddiscovery201512
13. Xu WS, Parmigiani RB, Marks PA. Histone deacetylase inhibitors: molecular mechanisms of action. Oncogene. 2007;26:5541–52.
14. Chen J, Hill K, Sha S-H. Inhibitors of histone deacetylases attenuate noise-induced hearing loss. JARO. 2016;17:289–302.
15. Yoshida N, Kristiansen A, Liberman MC. Heat stress and protection from permanent acoustic injury in mice. J Neurosci. 1999;19:10116–24.
16. Tahera Y, Meltser I, Johansson P, Canlon B. Restraint stress modulates glucocorticoid receptors and nuclear factor kappa B in the cochlea. Neuroreport. 2006;17:879–82.
17. Kujawa S, Liberman C. Adding insult to injury: cochlear nerve degeneration after "temporary" noise-induced hearing loss. J Neurosci. 2009;29:14077–85.
18. Fernandez KA, Jeffers PWC, Lall K, Liberman MC, Kujawa SG. Aging after noise exposure: acceleration of cochlear synaptopathy in "recovered" ears. J Neurosci. 2015;35:7509–20.
19. Lauer AM, Schrode KM. Sex bias in basic and preclinical noise-induced hearing loss research. Noise Health. 2017;19:207–12. http://www.noiseandhealth.org/text.asp?2017/19/90/207/215156
20. Canlon B, Meltser I, Johansson P, Tahera Y. Glucocorticoid receptors modulate auditory sensitivity to acoustic trauma. Hear Res. 2007;226:61–9.
21. Jerger J, Chmiel R, Stach B, Spretnjak M. Gender affects audiometric shape in presbyacusis. J Am Acad Audiol. 1993;4:42–9. https://www.audiology.org/sites/default/files/journal/JAAA_04_01_07.pdf.
22. Ward WD, Royster JD, Royster LH. Auditory and nonauditory effects of noise. In: Berger EH, Royster LH, Royster JD, Driscoll DP, Layne M, editors. Noise Man. 5th ed: Fairfax: American Industrial Hygiene Association; 2000. p. 101–47.
23. Waterston RH, Lindblad-Toh K, Birney E, Rogers J, Abril JF, Agarwal P, et al. Initial sequencing and comparative analysis of the mouse genome. Nature. 2002;420:520–62. England
24. Brown SDM, Hardisty-Hughes RE, Mburu P. Quiet as a mouse: dissecting the molecular and genetic basis of hearing. Nat Rev Genet. 2008;9:277–90. England
25. Scimemi P, Santarelli R, Selmo A, Mammano F. Auditory brainstem responses to clicks and tone bursts in C57 BL/6J mice. Acta Otorhinolaryngol Ital. 2014;34:264–71.
26. Noben-Trauth K, Zheng QY, Johnson KR. Association of cadherin 23 with polygenic inheritance and genetic modification of sensorineural hearing loss. Nat Genet. 2003;35:21–3. United States.
27. Davis RR, Newlander JK, Ling XB, Cortopassi GA, Krieg EF, Erway LC. Genetic basis for susceptibility to noise-induced hearing loss in mice. Hear Res. 2001;155:82–90.
28. Johnson KR, Zheng QY, Noben-Trauth K. Strain background effects and genetic modifiers of hearing in mice. Brain Res. 2006;1091:79–88. Netherlands
29. Ou HC, Bohne BA, Harding GW. Noise damage in the C57BL/CBA mouse cochlea. Hear Res. 2000;145:111–22.
30. Longenecker RJ, Galazyuk AV. Methodological optimization of tinnitus assessment using prepulse inhibition of the acoustic startle reflex. Brain Res. 2012;1485:54–62. Netherlands
31. Wen L-T, Wang J, Wang Y, Chen F-Q. Association between histone deacetylases and the loss of cochlear hair cells: role of the former in noise-induced hearing loss. Int. J. Mol. Med. 2015;36:534–40. Athens, Greece: Spandidos Publ LTD
32. Ponton CW, Moore JK, Eggermont JJ. Auditory brain stem response generation by parallel pathways: differential maturation of axonal conduction time and synaptic transmission. Ear Hear. 1996;17:402–10.
33. Zuccotti A, Lee SC, Campanelli D, Singer W, Satheesh SV, Patriarchi T, et al. L-type CaV1.2 deletion in the cochlea but not in the brainstem reduces noise vulnerability: implication for CaV1.2-mediated control of cochlear BDNF expression. Front Mol Neurosci. 2013;6:20. https://www.frontiersin.org/articles/10.3389/fnmol.2013.00020/full
34. Fuchs JC, Zinnamon FA, Taylor RR, Ivins S, Scambler PJ, Forge A, et al. Hearing loss in a mouse model of 22q11.2 deletion syndrome. PLoS One. 2013;8:e80104. http://journals.plos.org/plosone/article?id=10.1371/journal.pone.0080104.
35. Ohlemiller KK, Jones SM, Johnson KR. Application of mouse models to research in hearing and balance. JARO - J. Assoc. Res. Otolaryngol. 2016;17:493–523.
36. Zar JH. Biostatistical analysis. Upper Saddle River: Prentice-Hall; 1984.
37. Massachusetts Eye and Ear. Video tutorial for mouse cochlear dissection. 2015.
38. Massachusetts Eye and Ear. ImageJ Plugin Measure_Line for mapping cochlear frequencies on whole mounts. https://www.masseyeandear.org/research/otolaryngology/investigators/laboratories/eaton-peabody-laboratories/epl-histology-resources/imagej-plugin-for-cochlear-frequency-mapping-in-whole-mounts.
39. Abràmoff MD, Magalhães PJ, Ram SJ. Image processing with imageJ: Biophotonics Int. 2004;11:36–42.
40. Abdi H. The Bonferroni and Šidák corrections for multiple comparisons. In: Salkind N, editor. Encycl Meas Stat. Thousand Oaks: Sage Publications; 2007. p. 103–7. https://www.utd.edu/~herve/Abdi-Bonferroni2007-pretty.pdf.
41. Goutman JD, Elgoyhen AB, Gómez-Casati ME. Cochlear hair cells: the sound-sensing machines. FEBS Lett. 2015;589:3354–61. http://onlinelibrary.wiley.com/doi/10.1016/j.febslet.2015.08.030/full
42. Henry KS, Kale S, Scheidt RE, Heinz MG. Auditory brainstem responses predict auditory nerve fiber thresholds and frequency selectivity in hearing impaired chinchillas. Hear Res. 2011;280:236–44.
43. Hudspeth A. Mechanical amplification of stimuli by hair cells. Curr Opin Neurobiol. 1997;7:480–6. Available from: https://www.sciencedirect.com/science/article/pii/S0959438897800268?via%3Dihub.
44. Martin P, Hudspeth AJ. Active hair-bundle movements can amplify a hair cell's response to oscillatory mechanical stimuli. Proc Natl Acad Sci U S A. 1999;96:14306–11. http://www.pnas.org/content/96/25/14306.long.
45. Mann ZF, Kelley MW. Development of tonotopy in the auditory periphery. Hear Res. 2011;276:2–15. [cited 2018 Jan 17]. http://linkinghub.elsevier.com/retrieve/pii/S0378595511000141

46. Kujawa SG, Liberman MC. Synaptopathy in the noise-exposed and aging cochlea: primary neural degeneration in acquired sensorineural hearing loss. Hear Res. 2015;330:191–9.
47. Suzuki J, Corfas G, Liberman MC. Round-window delivery of neurotrophin 3 regenerates cochlear synapses after acoustic overexposure. Sci Rep. 2016;6: 24907. http://www.nature.com/articles/srep24907.
48. Karp NA, Mason J, Beaudet AL, Benjamini Y, Bower L, Braun RE, et al. Prevalence of sexual dimorphism in mammalian phenotypic traits. Nat Commun. 2017;8:15475. England
49. Hultcrantz M, Simonoska R, Stenberg AE. Estrogen and hearing: a summary of recent investigations. Acta Otolaryngol. 2006;126:10–4.
50. Clayton JA, Collins FS. Policy: NIH to balance sex in cell and animal studies. Nature. 2014;509:282–3. England
51. Drottar M, Liberman MC, Ratan RR, Roberson DW. The histone deacetylase inhibitor sodium butyrate protects against cisplatin-induced hearing loss in guinea pigs. Laryngoscope. 2006;116:292–6.
52. Chen FQ, Schacht J, Sha SH. Aminoglycoside-induced histone deacetylation and hair cell death in the mouse cochlea. J Neurochem. 2009;108:1226–36.
53. Wang J, Wang Y, Chen X, Zhang PZ, Shi ZT, Wen LT, et al. Histone deacetylase inhibitor sodium butyrate attenuates gentamicin-induced hearing loss in vivo. Am J Otolaryngol Head Neck Med Surg. 2015;36:242–8. Elsevier Inc
54. Layman WS, Zuo J. Preventing ototoxic hearing loss by inhibiting histone deacetylases. Cell Death Dis. 2015;6:e1882. http://www.nature.com/doifinder/10.1038/cddis.2015.252
55. Balogová Z, Popelář J, Chiumenti F, Chumak T, Burianová JS, Rybalko N, et al. Age-related differences in hearing function and cochlear morphology between male and female Fischer 344 rats. Front Aging Neurosci. 2018;9: 428. http://journal.frontiersin.org/article/10.3389/fnagi.2017.00428/full.
56. Henry KR. Males lose hearing earlier in mouse models of late-onset age-related hearing loss; females lose hearing earlier in mouse models of early-onset hearing loss. Hear Res. 2004;190:141–8. https://www.sciencedirect.com/science/article/pii/S0378595503004015?via%3Dihub
57. Ohlemiller KK, Dahl AR, Gagnon PM. Divergent aging characteristics in CBA/J and CBA/CaJ mouse cochleae. J Assoc Res Otolaryngol. 2010;11:605–23. https://link.springer.com/article/10.1007%2Fs10162-010-0228-1.
58. Hirose K, Liberman MC. Lateral wall histopathology and endocochlear potential in the noise-damaged mouse cochlea. JARO J Assoc Res Otolaryngol. 2003;4:339–52. https://link.springer.com/article/10.1007%2Fs10162-002-3036-4.
59. Wang Y, Hirose K, Liberman MC. Dynamics of noise-induced cellular injury and repair in the mouse cochlea. J Assoc Res Otolaryngol. 2002;3:248–68. https://link.springer.com/article/10.1007%2Fs101620020028.
60. Caras ML. Estrogenic modulation of auditory processing: a vertebrate comparison. Front. Neuroendocrinol. San Diego, Academic Press INC Elsevier Science; 2013;34:285–299.
61. Charitidi K, Meltser I, Canlon B. Estradiol treatment and hormonal fluctuations during the estrous cycle modulate the expression of estrogen receptors in the auditory system and the prepulse inhibition of acoustic startle response. Endocrinology. 2012;153:4412–21.
62. Simonoska R, Stenberg A, Masironi B, Sahlin L, Hultcrantz M. Estrogen receptors in the inner ear during different stages of pregnancy and development in the rat. Acta Otolaryngol. 2009;129:1175–81.
63. Stenberg AE, Wang H, Fish J, Schrott-Fisher A, Sahlin L, Hultcrantz M. Estrogen receptors in the normal adult and developing human inner ear and in Turner's syndrome. Hear Res. 2001;157:87–92.
64. Motohashi R, Takumida M, Shimizu A, Konomi U, Fujita K, Hirakawa K, et al. Effects of age and sex on the expression of estrogen receptor α and β in the mouse inner ear. Acta Otolaryngol. 2010;130:204–14. https://www.tandfonline.com/doi/full/10.3109/00016480903016570.
65. Meltser I, Tahera Y, Simpson E, Hultcrantz M, Charitidi K, Gustafsson J-A, et al. Estrogen receptor beta protects against acoustic trauma in mice. J Clin Invest. 2008;118:1563–70.
66. Simonoska R, Stenberg AE, Duan M, Yakimchuk K, Fridberger A, Sahlin L, et al. Inner ear pathology and loss of hearing in estrogen receptor-beta deficient mice. J Endocrinol. 2009;201:397–406. http://joe.endocrinology-journals.org/cgi/doi/10.1677/JOE-09-0060
67. Willott JF. Effects of sex, gonadal hormones, and augmented acoustic environments on sensorineural hearing loss and the central auditory system: insights from research on C57BL/6J mice. Hear Res. 2009;252: 89–99. https://www.sciencedirect.com/science/article/pii/S037859550800258X?via%3Dihub.

Song et al. BMC Genomics (2018) 19:696
https://doi.org/10.1186/s12864-018-5066-2

BMC Genomics

RESEARCH ARTICLE Open Access

A comparative analysis of library prep approaches for sequencing low input translatome samples

Yang Song[1], Beatrice Milon[2], Sandra Ott[1], Xuechu Zhao[1], Lisa Sadzewicz[1], Amol Shetty[1], Erich T. Boger[3], Luke J. Tallon[1], Robert J. Morell[3], Anup Mahurkar[1] and Ronna Hertzano[1,2,4*]

Abstract

Background: Cell type-specific ribosome-pulldown has become an increasingly popular method for analysis of gene expression. It allows for expression analysis from intact tissues and monitoring of protein synthesis in vivo. However, while its utility has been assessed, technical aspects related to sequencing of these samples, often starting with a smaller amount of RNA, have not been reported. In this study, we evaluated the performance of five library prep protocols for ribosome-associated mRNAs when only 250 pg-4 ng of total RNA are used.

Results: We obtained total and RiboTag-IP RNA, in three biological replicates. We compared 5 methods of library preparation for Illumina Next Generation sequencing: NuGEN Ovation RNA-Seq system V2 Kit, TaKaRa SMARTer Stranded Total RNA-Seq Kit, TaKaRa SMART-Seq v4 Ultra Low Input RNA Kit, Illumina TruSeq RNA Library Prep Kit v2 and NEBNext® Ultra™ Directional RNA Library Prep Kit using slightly modified protocols each with 4 ng of total RNA. An additional set of samples was processed using the TruSeq kit with 70 ng, as a 'gold standard' control and the SMART-Seq v4 with 250 pg of total RNA. TruSeq-processed samples had the best metrics overall, with similar results for the 4 ng and 70 ng samples. The results of the SMART-Seq v4 processed samples were similar to TruSeq (Spearman correlation > 0.8) despite using lower amount of input RNA. All RiboTag-IP samples had an increase in the intronic reads compared with the corresponding whole tissue, suggesting that the IP captures some immature mRNAs. The SMARTer-processed samples had a higher representation of ribosomal and non-coding RNAs leading to lower representation of protein coding mRNA. The enrichment or depletion of IP samples compared to corresponding input RNA was similar across all kits except for SMARTer kit.

Conclusion: RiboTag-seq can be performed successfully with as little as 250 pg of total RNA when using the SMART-Seq v4 kit and 4 ng when using the modified protocols of other library preparation kits. The SMART-Seq v4 and TruSeq kits resulted in the highest quality libraries. RiboTag IP RNA contains some immature transcripts.

Keywords: RiboTag, Library preparation kits, Low-input RNA-seq, RNA-seq, Coverage bias

* Correspondence: rhertzano@som.umaryland.edu
[1]Institute for Genome Sciences, University of Maryland School of Medicine, Baltimore, MD 21201, USA
[2]Department of Otorhinolaryngology-Head & Neck Surgery, University of Maryland School of Medicine, Baltimore, MD 21201, USA
Full list of author information is available at the end of the article

Background

Considerable scientific effort has been dedicated to understanding cell type-specific expression profiles from complex tissues, such as brain, liver, pancreas, testes, eye or ear [1–7]. To overcome the issue of cellular heterogeneity within complex tissues, two methods have been traditionally used in mice: Laser-Capture Microdissection (LCM) [8, 9] and Fluorescence Activated Cell Sorting (FACS) [10, 11]. However, LCM is a laborious and time-consuming procedure with low yield of mRNA; and FACS requires tissue dissociation – which may lead to changes in gene expression – and requires dedicated equipment [12]. More recently, single cell RNA-seq has been introduced. However, this technique too requires tissue dissociation and is currently limited by the number of genes detected per sequenced cell [13, 14]. To overcome these limitations, Translating Ribosome Affinity Purification (TRAP) [15] and RiboTag [16] have been recently developed to study cell type-specific transcriptome profiles. Both methods rely on immunoprecipitation of ribosome-attached RNA (also named 'translatome') by cell type-specific molecular targeting of the ribosomal proteins, often in a Cre-lox based system [15–17]. These methods have the advantage of not requiring tissue dissociation, thus allowing for cell type-specific translatome analysis from intact tissues.

While ribosome-attached RNA sequencing for expression analysis has been validated from a biological standpoint [18, 19], the technical aspects of its library construction and sequencing have not been studied. In instances where small complex tissues are studied, the amount of starting material after immunoprecipitation may be limited (e.g., less than 5 ng). When starting from low amounts of RNA, additional cycles of amplification using PCR are performed after adapter ligation to amplify the cDNA to generate enough material for sequencing. Multiple commercial kits are available in the market to build cDNA libraries from samples with low amounts of RNA, including kits from NuGEN, New England Biolabs (NEB), Illumina and TaKaRa. Standard protocols for library construction are commonly designed to start with more than 100 ng of total RNA [20, 21] and only a few studies have been conducted to compare the performance of library preparation kits using less than 5 ng of total RNA as their starting amount [22, 23]. In this study, we selected four of the commonly used library preparation kits that are also suitable for lower-input samples for comparison. We modified the standard protocols for NEB and Illumina library preparation kits to enable them to work with smaller amounts of RNA than the recommended amounts down to as little as 4 ng of total RNA. We included one kit, SMART-Seq v4, that was designed for single cell RNA-seq and tested it with 4 ng and 250 pg of total RNA. We evaluated the performance of the different kits based on duplication rate, percentage of intronic and exonic regions being detected, the evenness of coverage of transcripts and ribosomal RNA read-count in comparison to total reads. We also compared the reproducibility of the enrichment or depletion effect based on ribotag-translatome profile for the first time.

Methods

Animals

The *Gfi1*-Cre knock-in mice generated by Dr. Lin Gan (University of Rochester) were kindly provided by Dr. Jian Zuo of the Developmental Neurobiology Department at St. Jude Children's Research Hospital. RiboTag mice generated by Dr. Paul S Amieux (University of Washington) were kindly provided by Dr. Mary-Kay Lobo of the Department of Neurobiology and Anatomy at University of Maryland Baltimore. B6.Cg-Gt(ROSA)26-Sor$^{tm14(CAG-tdTomato)Hze}$/J mice (also referred to as Ai14) were purchased from the Jackson Laboratory (stock #007914, Bar Harbor, ME). Experimental animals for RNA-seq, *Gfi1*$^{Cre/+}$;*RiboTag*$^{HA/HA}$, were obtained by crossing RiboTag mice with Gfi1-Cre mice. Animals for immunostaining, *Gfi1*$^{Cre/+}$;*Ai14*, were obtained by crossing Gfi1-Cre mice with Ai14 mice [24]. All procedures involving animals were carried out in accordance with the National Institutes of Health Guide for the Care and Use of Laboratory Animals and have been approved by the Institutional Animal Care and Use Committee at the University of Maryland, Baltimore (protocol numbers 1015003 and 0915006).

Ribosome immunoprecipitation and RNA extraction

Three 30-day old *Gfi1*$^{Cre/+}$;*RiboTag*$^{HA/HA}$ mice were euthanized by CO_2 asphyxiation followed by cervical dislocation. Livers were harvested and immediately frozen on dry ice. Equal amounts of liver were used for input RNA extractions (RNeasy Plus Micro kit, QIAGEN USA, Germantown, MD, USA) or futher processed for ribosome immunoprecipitation (5 μg of purified anti-HA.11, BioLegend, San Diego, CA, USA) followed by RNA extraction as previously decribed in Sanz et al., 2009 [16]. The RNeasy Plus Micro kit is optimized for the removal of genomic DNA through a combination of high salt buffer and the gDNA Eliminator spin column. Quality of the RNA was assessed on an Agilent Technologies Bioanalyzer 2100 RNA pico chip as per the manufacturer's instructions (Agilent Technologies, Palo Alto, CA, USA). All samples had a RIN score of 10 and no evidence of DNA contamination in the form of a high molecular weight DNA band. All RNA was equally aliquoted to test for the performance of five commercial kits and seven protocols.

Real-time RT-PCR

Efficiency of the ribosome immunoprecipitation was assessed by reverse transcription followed by real time PCR. One nanogram of total RNA from the input and the IP samples was used for reverse transcription using the Maxima First Strand cDNA Synthesis Kit for RT-qPCR (Thermo Fisher Scientific, Waltham, MA, USA). The real time PCR was performed on an Applied Biosystems® StepOnePlus™ Real-Time PCR System with the Maxima SYBR Green/ROX qPCR Master Mix (Thermo Fisher Scientific, Waltham, MA, USA) and the following primers: *Gapdh*-Fw 5'-GGAGAAACCTGCCAAGTATGA-3′; *Gapdh*-Rv 5′- TCCTCAGTGTAGCCCAAGA-3′; *Gfi1*-Fw 5′- AATGCAGCAAGGTGTTCTC-3′; *Gfi1*-Rv 5′- CTTACAGTCAAAGCTGCGT-3′.

Immunostaining

Progeny from a cross between $Gfi1^{Cre/+}$ mice and TdTomato reporter mice Ai14 were euthanized at P1 and their livers were harvested. Following fixation in 4% paraformaldehyde overnight at 4 °C, livers were cryoprotected through incubation in PBS with increasing amount of sucrose before being embedded in O.C.T. compound (Scigen, Gardena, CA, USA). Ten μm cryosections were permeabilized with PBS supplemented with 0.2% Tween-20 for 1 h at room temperature and incubated with Alexa Fluor™ 488 Phalloidin (1/800, Thermo Fisher Scientific, Waltham, MA, USA) and DAPI (1/20,000, Thermo Fisher Scientific, Waltham, MA, USA). Samples were mounted with ProLong Gold antifade reagent (Thermo Fisher Scientific, Waltham, MA, USA). Images were acquired using a Nikon Eclipse E600 microscope (Nikon, Tokyo, Japan) equipped with a Lumenera Infinity 3 camera (Lumenera, Ottawa, ON).

RNA-Seq library construction

Below are the experimental methods for RNA-Seq library construction. We followed the manufacturer's instructions with minor modifications, as noted below. The shearing approach was not altered and remains different between kits.

Ovation® RNA-Seq system V2 combined with TruSeq RNA library prep kit v2

We performed a hybrid library preparation by using Ovation® RNA-Seq System V2 (NuGEN, San Carlos, CA, USA) to synthesize cDNA and the TruSeq RNA Library Preparation Kit v2 to construct the sequencing library (Illumina, San Diego, CA, USA), consistent with the NuGEN manufacturer protocol (See Additional file 1: Table S1). Briefly, 4 ng of total RNA or RiboTag IP RNA were used to synthesize cDNA following the NuGEN's instructions. Subsequently, 200 ng of cDNA were sheared to an average size of 300 bp with a Covaris E220 Focused-Ultrasonicator (Covaris Inc., Woburn, MA, USA). Following the manufacturer protocol, the library was prepared from the sheared cDNA using the Illumina TruSeq RNA Library Prep Kit with 8 cycles of PCR.

SMARTer® stranded total RNA-Seq kit-Pico input mammalian

Four nanograms of RNA were used as input material and libraries were prepared by following the SMARTer Stranded Total RNA-Seq kit-Pico Input Mammalian user manual (Takara Bio USA, Mountain View, CA, USA). In brief, samples were fragmented at 94 °C for 4 min prior to first-strand synthesis. Illumina adaptors and indexes were added to single-stranded cDNA via 5 cycles of PCR. Libraries were hybridized to R-probes for fragments originating from ribosomal RNA to be cleaved by ZapR. The resulting ribo-depleted library fragments were amplified with 15 cycles of PCR.

SMART-Seq® v4 ultra® low input RNA kit for sequencing

Two types of libraries were prepared by using 4 ng or 250 pg RNA from each sample. Libraries were prepared by following the SMART-Seq v4 Ultra Low Input RNA Kit (Takara Bio USA, Mountain View, CA, USA) user manual. The cDNA was amplified with 11 cycles of PCR. Nextera XT kit (Nextera XT DNA Library Preparation Kit (Illumina, San Diego, CA) was used to make cDNA libraries suitable for Illumina sequencing.

TruSeq RNA library prep kit v2

Two types of libraries were prepared by using 70 ng or 4 ng RNA from each sample. The 70 ng libraries were built using TruSeq RNA Library Prep Kit v2 (Illumina, San Diego, CA, USA) according to the manufacturer protocol. Size selection was performed using SPRIselect beads (Beckman Coulter, Indianapolis, IN, USA) and in-house calibration values (first round selection to select the upper or right limit of the distribution), salt unit equals to 0.427 and second round selection to select the lower or left limit of the distribution, salt unit = 0.455). The cDNA was amplified with 19 cycles of PCR. Libraries were prepared using 4 ng of RNA with modifications to the standard protocol by reducing the end-repair reaction to 1/2 the recommended amounts of enzyme mix and sample volume. In addition A-tail ligation followed the standard protocol without the use of internal control mixes. Due to the low input amount, no size selection was applied to the 4 ng libraries. The cDNA was amplified with 22 cycles of PCR. Libraries prepared using 70 ng of RNA were prepared following the standard protocol and cDNA was amplified with 14 cycles as suggested by manufacture protocol.

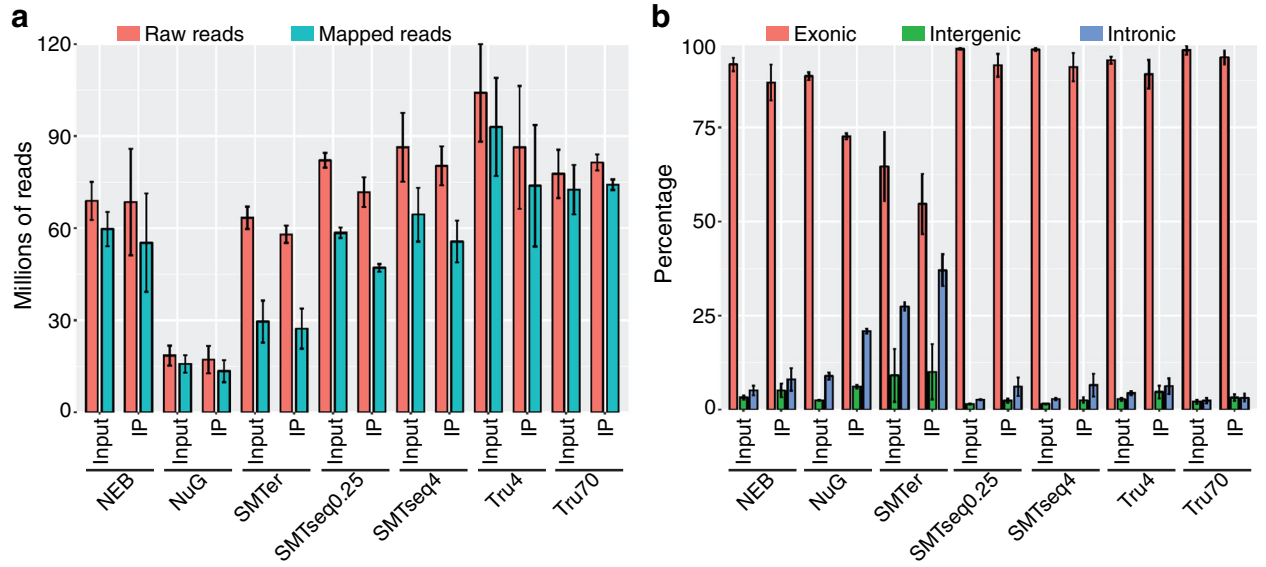

Fig. 1 Descriptive characteristics of raw and mapped reads. **a** Total number of raw reads and number of reads mapped to the mouse genome (mm10, GRCm38.84). **b** Percentage of reads mapped to exonic, intronic and intergenic regions. NEB: NEBNext® Ultra™, NuG: NuGEN Ovation®, SMTer: SMARTer® Stranded; Tru4: TruSeq using 4 ng of RNA; Tru70: TruSeq using 70 ng of RNA. SMTseq4: SMART-Seq® v4 using 4 ng of RNA; SMTseq0.25: SMART-Seq® v4 using 250 pg of RNA

NEBNext® ultra™ directional RNA library prep kit for Illumina

Four nanograms of total RNA were used for NEBNext® Ultra™ Directional RNA Library Prep Kit (New England Biolabs, Ipswich, MA, USA). Poly-A selection and cDNA synthesis were performed according to NEB protocol. The adaptors were diluted with a 1:30 ratio instead of the recommended 1:10 ratio. Size selection was performed using SPRIselect beads. (Beckman Coulter, Indianapolis, IN, USA) with in-house calibration values. The cDNA was amplified with 22 cycles of PCR.

Sequencing

Samples prepared by TruSeq, NEB, NuGEN and SMARTer were sequenced at the Institute for Genome Sciences (IGS) Genomics Resource Center (Baltimore, MD) on a HiSeq 4000 using 75 base read lengths in paired-end mode. Samples prepared by SMART-Seq v4 were sequenced by the Genomics and Computational Biology Core (GCBC) at the National Institute on Deafness and Other Communication Disorders (NIDCD/NIH) on a HiSeq 1500 using a read length of 126 bases in paired-end mode.

RNA-Seq analyses

The Illumina adapters used during the library construction were removed from the reads using Trimmomatic [1]. In order to reduce the impact of lower quality reads on the alignment, all reads were trimmed to 60 bp

Table 1 Duplication rate of libraries prepared by different kits

Kit	Sample type	PCR cycles for lib prep	Percent_Duplication (%)			
			replicate			avg
			1	2	3	
NEB[a]	Input	22	97	99	97	97
	IP		99	99	99	99
NuG/Tru[b]	Input	8	52	53	52	53
	IP		36	31	26	31
SMTer[c]	Input	15	83	86	85	85
	IP		86	83	68	79
Tru4[d]	Input	22	67	77	71	72
	IP		85	82	99	89
Tru70[e]	Input	19	90	94	92	92
	IP		98	97	96	97
SMTseq4[f]	Input	11	40	38	40	40
	IP		60	49	48	52
SMTseq0.25[f]	Input	11	37	37	41	38
	IP		59	50	47	52

[a]NEBNext® Ultra™ Directional RNA Library Prep Kit for Illumina
[b]Nugen Ovation® RNAseq System v2
[c]SMARTer® Stranded Total RNA-Seq Kit-Pico Input Mammalian User
[d]TruSeq® RNA sample preparation v2,4 ng
[e]TruSeq® RNA sample preparation v2,70 ng
[f]SMART-Seq v4 Ultra Low Input RNA Kit

using the FASTX Toolkit v-0.0.13 [25] resulting in a Phred-Quality-Score greater than 30. The reads generated for each RNA sample were analyzed and compared using an Ergatis-based RNA-Seq analysis pipeline [26] where sequencing reads were aligned and annotated to the UCSC mouse reference genome (mm10, GRCm38.84) from Ensembl (http://www.ensembl.org) using TopHat v-2.0.8 [27] (maximum number of mismatches = 2; segment length = 30; maximum multi-hits per read = 25; maximum intron length = 50,000) and the number of reads that aligned to the predicted coding regions were determined using HTSeq [28]. Bedtools (v-2.7.1) [29] was used to count the reads mapping to exons according to Ensembl gene annotations (March 2016, Mus_musculus.GRCm38.84, with 47,729 genes annotated). Read counts per million mapped reads values (CPM) [28] or reads per kilobase of transcripts per million mapped reads (RPKM) [30] were calculated and used for downstream analyses. 5′-3′ exonic coverage was calculated using CollectRnaSeqMetrics component of picard-tools (v-1.60, https://broadinstitute.github.io/picard/), and duplication rate was calculated using EstimateLibraryComplexity of Picard-tools.

Statistical analysis

All plots were generated using R (v-3.2.4), including the following R packages ggplot2, ComplexHeatmap for producing bar plots or heat maps, and limma to generate Venn diagrams. The difference among groups in boxplots was evaluated based on the overlapping of the notch region [31]. The notch is defined as median m ± 1.58IQR/√n [31]. The significance test is evaluated using a non-parametric Wilcoxon test with $p < 0.05$.

Accession number

All of the processed gene expression data from this study have been submitted to the NCBI Gene Expression Omnibus (GEO) under accession number GSE104213.

Results

Sample preparation for sequencing

In order to evaluate the efficiency of different library preparation kits with low amounts of RNA obtained after ribosome immunoprecipitation, we crossed RiboTag mice with *Gfi1*-Cre mice to obtain progeny that expressed HA-tagged ribosomes in cells with *Gfi1* expression. We obtained RNA from liver because it is a tissue that, at least during embryogenesis, expresses *Gfi1*, thus allowing for early induced recombination in a subset of the liver cells for permanent expression of a reporter gene [32] (Additional file 2: Figure S1a). Additionally, the size of the liver would provide enough material to test five different kits with varying amounts of starting RNA from individually processed samples. Livers were processed for HA-tagged ribosome immunoprecipitation (IP) followed by RNA extraction as previously described [16]. Prior to sequencing, the efficacy of the IP was confirmed by comparing the level of *Gfi1* transcripts in the input and IP samples using real time RT-PCR (Additional file 2: Figure S1b). The profiles generated by the five different commercial library preparition kits, from four different manufacturers, were compared in this study (See Additional file 1: Table S1). NEBNext® Ultra™

Table 2 Number of features with CPM > 0

Kit	Sample type	Number of features with coverage (CPM > 0)				Number of reads of all expressed features (CPM > 0)			
		Replicate			avg	Replicate			avg
		1	2	3		1	2	3	
NEB	Input	13,543	12,464	11,419	12,475	22,373,163	26,292,017	22,305,929	23,657,036
	IP	11,059	12,165	14,331	12,518	16,668,355	27,323,849	15,122,257	19,704,820
NuG	Input	16,946	16,458	15,624	16,343	5,529,417	7,615,866	7,482,819	6,876,034
	IP	17,715	17,841	18,198	17,918	3,223,153	5,319,712	5,141,329	4,561,398
SMTer	Input	12,281	10,184	10,929	11,131	759,221	762,562	750,159	757,314
	IP	12,422	11,168	15,684	13,091	701,059	645,414	464,199	603,557
Tru4	Input	19,906	19,863	19,631	19,800	35,368,451	45,466,334	31,299,550	37,378,112
	IP	17,467	18,899	21,161	19,176	36,785,680	28,571,125	18,031,264	27,796,023
Tru70	Input	15,957	15,577	16,082	15,872	32,103,296	33,797,108	25,797,283	30,565,896
	IP	14,430	15,213	15,680	15,108	31,150,532	29,799,544	27,902,766	29,617,614
SMTseq4	Input	19,111	19,287	19,630	19,343	23,573,272	24,615,731	30,217,161	26,135,388
	IP	19,835	20,551	20,488	20,291	14,407,184	19,577,709	17,262,557	17,082,483
SMTseq0.25	Input	16,834	16,742	16,117	16,564	23,815,261	24,347,672	22,951,893	23,704,942
	IP	16,827	16,870	16,527	16,741	13,971,566	15,047,219	14,691,099	14,569,961

Directional RNA Library Prep Kit for Illumina (NEB) with 4 ng of RNA,NuGEN Ovation® RNA-Seq System V2 with 4 ng of RNA (NuGEN) with 4 ng of RNA, TaKaRa SMARTer® Stranded Total RNA-Seq Kit-Pico Input Mammalian with 4 ng of RNA (SMARTer), TaKaRa SMART-Seq® v4 Ultra® Low Input RNA Kit for Sequencing with 4 ng and 0.25 ng of RNA (SMARTseq4 and SMARTseq0.25) and Illumina TruSeq RNA Library Prep Kit v2 with 4 ng and 70 ng of RNA (TruSeq4 and TruSeq70). Of these kits only the SMARTer kit produced strand specific libraries and we therefore did not analyze the data for strandness.

Comparison of mapping efficiency and duplication rate

The number of reads varied widely among samples being prepared by different library preparation kits. Input RNA samples generated 14.7 to 122 million pair-end reads (2 × 60 bp) and IP RNA samples generated 12 to 108 million pair-end reads (2 × 60 bp). Overall, fewer raw/mapped reads were generated when using the NuGEN kit. Of the raw reads, 12.5 to 111 million reads mapped to mouse genome for input RNA samples while 9.2 to 94.6 million reads mapped for IP RNA samples (Fig. 1a).

In order to evaluate the expression profile composition and library complexity, we assessed the duplication rate of the read pairs (Table 1) as lower duplication rates usually indicate a higher complexity of the sample and better representation of RNA present in a sample [20]. In this study, duplication rate ranged from 26 to 99% (Table 1). However, the duplication we observed was not well correlated with the numbers of PCR cycles and was more dependent on the library prep kit. For instance, while NEB and TruSeq4 samples both had the highest number of PCR cycles (22), their duplication rates differed (Table 1). Indeed, NEB-input samples had the highest duplication rate of 99% with the overall largest number of reads duplicated more than 200 times while the TruSeq4 samples had a duplication rate of 72% with a substantially smaller number of reads with greater than 200 duplications (Table 1 and Additional file 3: Figure S2).

Detection of exonic, intergenic and intronic regions

Among the mapped reads, SMARTer samples showed the lowest alignment to exonic regions. The percentage of reads aligned to exonic regions was greater than 85% in samples prepared with NEB, TruSeq and SMARTseq library kits and less than 70% in samples prepared with the SMARTer and NuGEN kits (Fig. 1b). As expected, the overall percentage of reads aligning to intronic regions detected in input samples was less than 10% for most samples, except for samples prepared by the SMARTer kit, where more than 20% of the reads align to intronic regions. IP samples had roughly twice as many reads aligning to intronic regions, or 10% more intronic reads compared with the corresponding input RNA samples, which may suggest that the IP captures some immature mRNAs. In particular, the percentage of intronic reads from the SMARTer samples increased from 22% for the input RNA to 41% for the IP RNA. The percentage of intronic reads for the NuGEN samples ranged from 8% for the input RNA and 22% for the IP RNA.

Number of genes being detected as expressed

Because of the differences in sequencing efficiency and library complexity, we examined the number of features detected in samples prepared with each library kit. After removing ambiguous reads or reads mapped to multiple

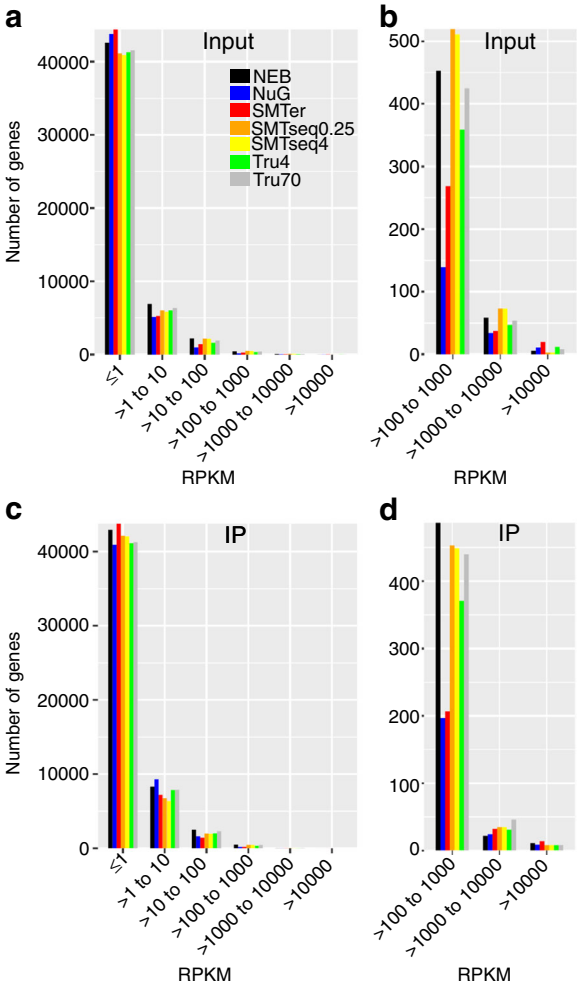

Fig. 2 Detected transcripts binned by RPKM. There were 33,399 transcripts detected in at least one input sample, 35,395 transcripts detected in at least one IP sample and all of these genes were used for the binning. Y-axis: number of transcripts detected in at least one replicate. **a** and **c** Number of genes binned by RPKM as detected by the different kits in the input and IP, respectively. **b** and **d** These plots are subsets of (**a**) and (**c**) focusing only on highly expressed transcripts (RPKM> 100)

features using HTSeq, we detected between 10,184 to 21,161 genes where the CPM values were greater than zero (Table 2). The corresponding average raw read counts ranged from 0.76 to 37 million reads. Fewer features were detected in SMARTer and NEB samples. All of the annotated genes (47,729) were binned into 6 groups (RPKM≤1, 1 < RPKM≤10, 10 < RPKM≤100, 100 < RPKM≤1000, 1000 < RPKM≤10,000 and RPKM> 10,000. Fig. 2). SMARTer, NuGEN, and NEB samples had more genes that were entirely missed or had low expression levels (RPKM≤1) in comparison to the other kits in the input samples (Fig. 2a). The SMARTer and NEB samples had more genes with a lower expression levels (RPKM≤1) also in the IP (Fig. 2c). The number of genes within RPKM range (100–10,000) was relatively low in SMARTer and NuGEN samples (Fig. 2b, d). Conversely, SMARTer samples contained more highly expressed genes (RPKM> 10,000) than others samples, but the majority of these were rRNA genes or genes encoding for hypothetical proteins (Fig. 2b, d and See Additional file 1: Table S2).

In order to compare the similarity of expression profiles of the different kits, we compared genes with at least 1 CPM in at least one replicate across all the samples. More than 60% of the genes were co-detected by all kits (Fig. 3). The median CPM for shared genes across all samples was 28 for input samples (Fig. 3a, c) and 36 for IP samples (Fig. 3b, d). Meanwhile, less than 10% of features were uniquely detected in NEB, NuGEN and TruSeq input samples, but over 20% of features were uniquely detected from the SMARTer samples. The median CPM of uniquely detected genes in SMARTer input samples was around 10, while the median for other kits was less than 3.

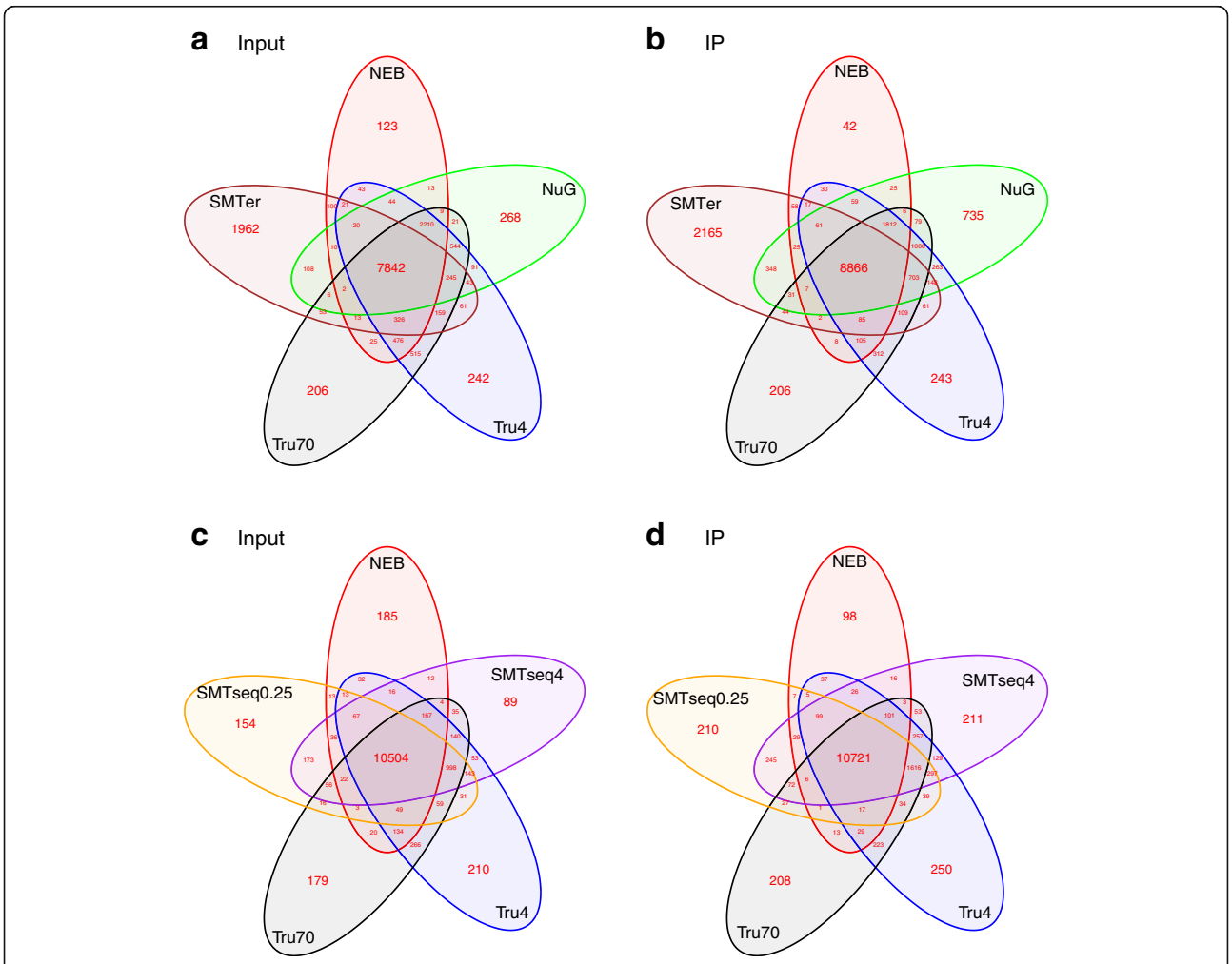

Fig. 3 Venn diagrams of identified features in the different libraries. The features with CPM ≥ 1 in at least one out of 3 replicates were used to generate these plots. **a** and **c** represent input samples and **b** and **d** represent IP samples. Most transcripts were detected by all kits tested. However, a higher rate of agreement is seen between the NEB, TruSeq and SMART-Seq prepared samples. NEB: NEBNext® Ultra™, NuG: NuGEN Ovation®, SMTer: SMARTer® Stranded; Tru4: TruSeq using 4 ng of RNA; Tru70: TruSeq using 70 ng of RNA. SMTseq4: SMART-Seq® v4 using 4 ng of RNA; SMTseq0.25: SMART-Seq® v4 using 250 pg of RNA

Table 3 Descriptive statistic of non-coding detected features (CPM > =1)

Kit	Sample type	Total features of ribosomal RNA Replicate			Average CPM of ribosomal RNA Replicate			Total features of ribosomal RNA, lincRNA, microRNA Replicate			Average CPM of ribosomal RNA, lincRNA, microRNA Replicate		
		1	2	3	1	2	3	1	2	3	1	2	3
NEB	Input	3	3	3	73.87	67.33	72.15	233	186	140	46.01	29.22	28.34
	IP	3	3	4	14.24	6.15	7.80	128	157	268	78.05	28.33	34.25
NuG	Input	8	11	10	5533.70	5571.81	5603.65	552	488	415	272.73	274.17	276.54
	IP	13	11	17	1803.34	820.73	863.91	583	593	637	97.91	48.26	51.37
SMTer	Input	8	5	6	4282.62	7858.83	4641.15	440	359	377	247.75	429.65	261.04
	IP	12	6	17	4880.27	7906.14	3936.78	467	411	599	282.51	429.64	240.08
Tru4	Input	17	17	13	232.50	120.94	169.47	804	786	767	13.96	7.59	10.29
	IP	8	7	19	415.93	129.19	168.59	546	650	927	26.49	8.94	11.45
Tru70	Input	6	4	4	102.39	28.55	58.50	410	363	406	6.34	2.08	3.81
	IP	3	3	4	141.53	54.91	65.21	265	295	341	9.24	3.97	5.10
SMTseq4	Input	13	13	21	214.51	159.76	185.17	750	764	803	11.78	8.93	10.54
	IP	7	11	10	851.62	63.75	92.92	844	881	889	46.39	5.91	8.73
SMTseq0.25	Input	6	7	3	224.50	191.46	235.20	531	515	461	12.32	10.52	13.04
	IP	6	6	7	886.27	73.72	99.28	476	502	457	48.03	6.43	8.88

A similar trend is observed in IP samples (Fig. 3b, d and See Additional file 1: Table S3).

We also grouped all of the detected features into ribosomal RNA, non-coding (ribosomal RNA, lincRNA, microRNA) and protein-coding groups. The average CPM of ribosomal RNA and non-coding gene groups were 2-fold higher in NuGEN and SMARTer samples than in other samples (Table 3). Conversely, the average CPMs for the protein-coding group were similar across most samples, except for SMARTer prepared samples (Table 4). By comparing IP samples with input samples, it is interesting that the CPMs of IP samples are relatively lower than input samples, except for NuGEN prepared samples.

Coverage uniformity relative to 5′ and 3′ ends

The evenness of transcript coverage was calculated by dividing the mean coverage of first (last) 100 bases (5′ or 3′) of transcripts divided by the mean coverage of all bases across the corresponding transcript (Fig. 4). The median

Table 4 Descriptive statistic of protein-coding detected features (CPM ≥ 1)

Kit	Sample type	Total features of protein-coding RNA Replicate			Average CPM of protein-coding RNA Replicate		
		1	2	3	1	2	3
NEB	Input	11,316	10,551	9789	36.51	37.77	37.83
	IP	8740	10,252	12,435	34.13	37.84	37.39
NuG	Input	10,921	10,828	10,656	19.61	19.50	19.32
	IP	12,970	13,142	13,318	32.65	36.35	36.12
SMTer	Input	11,136	9368	10,019	21.47	7.90	20.48
	IP	11,826	11,860	11,824	18.88	7.90	22.02
Tru4	Input	11,826	11,860	11,824	38.90	39.38	39.18
	IP	12,360	12,842	12,941	37.97	39.28	39.09
Tru70	Input	11,690	11,691	11,611	39.47	39.79	39.66
	IP	11,996	12,493	12,660	39.26	39.65	39.56
SMTseq4	Input	11,659	11,499	11,578	39.07	39.28	39.16
	IP	12,443	12,579	12,587	36.50	39.51	39.01
SMTseq0.25	Input	11,500	11,475	11,384	39.03	39.16	38.97
	IP	12,648	12,846	12,940	36.38	39.47	39.29

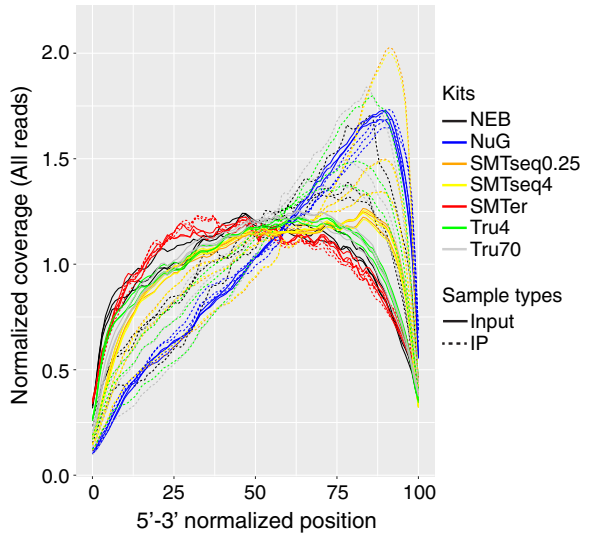

Fig. 4 Distribution of normalized mean expression of the first (last) 100 bases of transcripts (in 5′- > 3′-orientation). X axis represents the 5′-3′ normalized position; Y axis represents normalized coverage. NEB: NEBNext® Ultra™, NuG: NuGEN Ovation®, SMTer: SMARTer® Stranded; Tru4: TruSeq using 4 ng of RNA; Tru70: TruSeq using 70 ng of RNA. SMTseq4: SMART-Seq® v4 using 4 ng of RNA; SMTseq0.25: SMART-Seq® v4 using 250 pg of RNA. Yellow and orange: SMTseq samples; Red: SMTer samples; Black: NEB samples; Blue: NuG samples; Green and grey: TruSeq samples. Solid: Input samples. Dotted: Ribo-IP samples

was calculated and plotted for the 1000 most highly expressed transcripts. Most of the input RNA samples showed even coverage from 5′ to 3′ end, except for all NuGEN samples which had pronounced increase in coverage at the 3′ end. Additionally, consistently higher coverage at the 3′ end was observed among IP RNA samples, except for SMARTer samples with even coverage across 5′ and 3′ extremities.

Similarity of expression profiles

In order to assess the similarity of expression profiles being generated by different library preparation kits, we applied Spearman correlation coefficients as a measure of similarity. The Spearman coefficient was calculated based on the rank of the CPM value as opposed to using the absolute values. This was done to accommodate the difference in CPM values due to differences in duplication rates observed among the kits (Fig. 5). The correlation coefficient for input samples ranged from 0.5 to 0.9, where SMARTseq profiles were better correlated with TruSeq70 than others (Spearman correlation coefficient ≥ 0.9). SMARTer samples had the lowest correlation (0.5) with the control library TruSeq70 (Fig. 5 and See Additional file 1: Table S4). Overall, as expected, input profiles are less correlated to corresponding IP profiles (See Additional file 1: Table S4). When we compared input samples with corresponding IP samples for each individual kit respectively, all input samples were clustered separately from IP samples except for the SMARTer samples (Additional file 4**:** Figure S3).

Although two different amounts of RNA were used for the TruSeq library kit, TruSeq 4 ng samples were well correlated with TruSeq 70 ng samples (Spearman correlation coefficient was 0.96 ± 0.002 for input; 0.946 ± 0.01 for IP). Similarly, the SMARTseq samples with 0.25 ng and 4 ng were highly correlated (Spearman correlation coefficient was 0.95 ± 0.004 for input and 0.95 ± 0.005 for IP) (See Additional file 1: Table S4).

Transcript enrichment is better represented than transcript depletion in the IP samples

We evaluated the robustness of different kits for detecting enrichment (IP/input RNA > 1) or depletion (IP/input RNA < 1) of transcripts in the translatome (IP samples) compared to the transcriptome (input samples). Features with raw read counts ≥20 in input samples and with an enrichment or depletion factor ≥ 2 were included as enriched (IP/Input ≥2) or depleted transcripts (IP/Input ≤0.5). Of note, more transcripts were enriched than depleted (Fig. 6a and Additional file 5: Figure S4). NuGEN produced the greatest number of enriched transcripts (mean 4270) and smallest number of depleted transcripts (mean 74) as compared with other kits (Fig. 6b). Among the enriched transcripts from NuGEN, 60% were enriched less than 4-fold whereas only 25% of transcripts prepared by other kits were enriched less than 4-fold (Fig. 6b). NEB samples had the highest percentage of enriched/depleted transcripts (log2 (IP/INPUT) > 5 or log2(INPUT/IP) > 5) when compared to samples obtained from the other kits (Fig. 6b, Fig. 7a). Conversely, the enrichment profile of the SMARTer samples showed fewer enriched or depleted transcripts compared with the rest of the samples. Indeed, when plotting for the top 50 enriched transcripts (Fig. 7b), the median enrichment value for the SMARTer profile was significantly lower than other profiles ($p < 0.05$).

We also compared the number of transcripts being enriched or depleted across samples (Additional file 6: Figure S5). NuGEN had the highest number of uniquely enriched transcripts that were detected (accounting for 25% of its total enriched transcripts, 95% of which are protein-coding genes). TruSeq4 and TruSeq70 had around 5% uniquely enriched transcripts (Additional file 6: Figure S5a,b).

We also clustered all the transcripts based on the rank of enrichment factor or depletion factor greater than 2 in at least one sample (Fig. 8). As expected, the profiles for TruSeq4 and TruSeq70 were most similar to each other (Spearman correlation coefficient > 0.7). The same is true for SMARTseq4 and SMARTseq0.25. On the

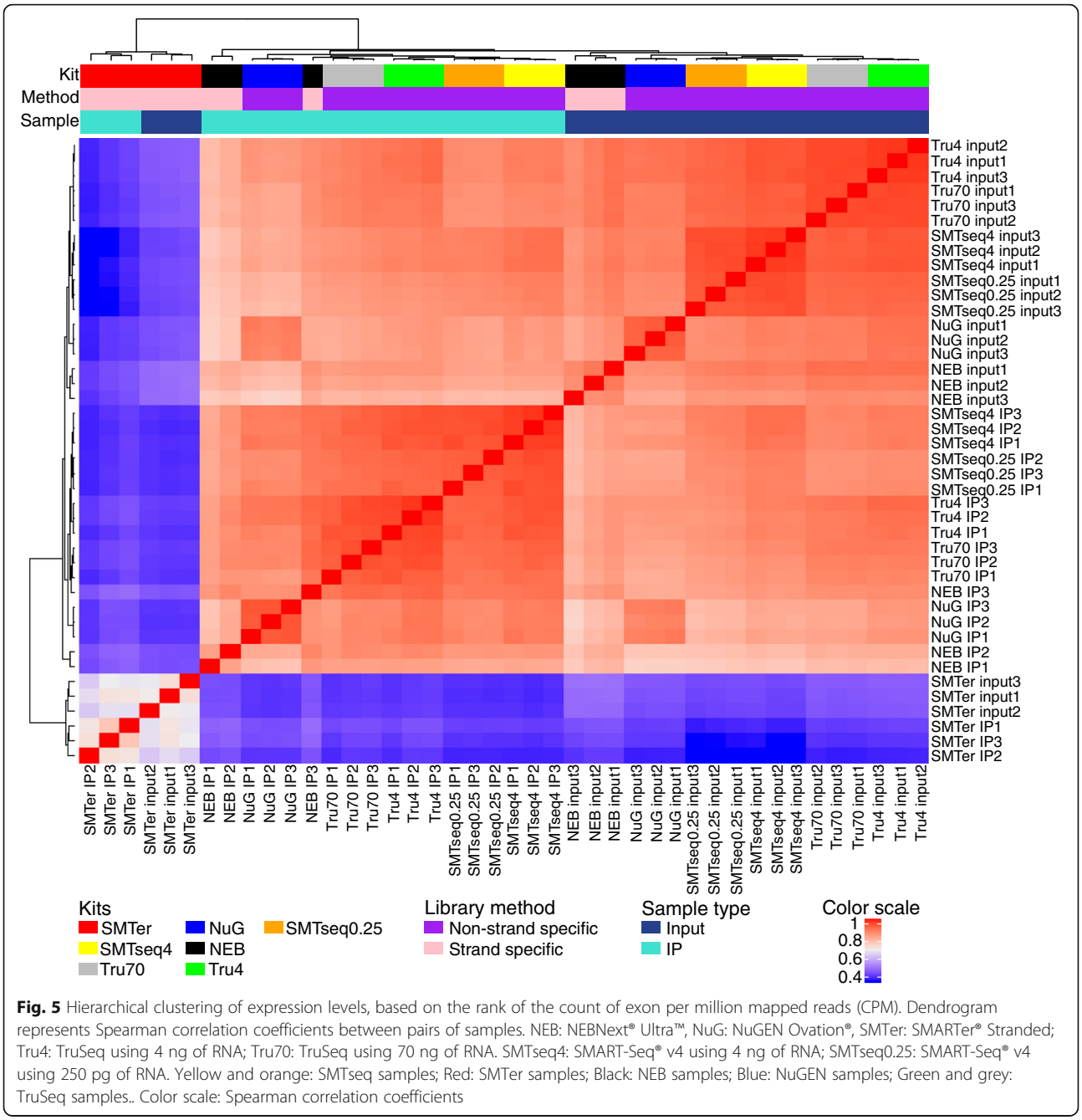

Fig. 5 Hierarchical clustering of expression levels, based on the rank of the count of exon per million mapped reads (CPM). Dendrogram represents Spearman correlation coefficients between pairs of samples. NEB: NEBNext® Ultra™, NuG: NuGEN Ovation®, SMTer: SMARTer® Stranded; Tru4: TruSeq using 4 ng of RNA; Tru70: TruSeq using 70 ng of RNA. SMTseq4: SMART-Seq® v4 using 4 ng of RNA; SMTseq0.25: SMART-Seq® v4 using 250 pg of RNA. Yellow and orange: SMTseq samples; Red: SMTer samples; Black: NEB samples; Blue: NuGEN samples; Green and grey: TruSeq samples.. Color scale: Spearman correlation coefficients

other hand, the enrichment/depletion profile for SMARTer was the least similar to the other profiles (Spearman correlation coeffienct < 0.2).

Transcript-length dependent enrichment/depletion

We examined whether the enrichment or depletion effects observed in the translatome were affected by the transcript length. Based on size distribution of the enriched/depleted transcripts (the majority being between 0.5 and 10 kb, Additional file 7: Figure S6), we grouped the transcripts into four bins (≤0.5 kb, 0.5–1 kb, 1 kb–10 kb, and > 10 kb) (Fig. 9). The median enrichment for transcripts was relatively higher in the longer transcript (> 10 kb) except in TruSeq70 samples (Fig. 9a). Within each transcript length bin, the median enrichment effect from NuGEN and SMARTer samples was much higher than TruSeq70 samples for transcripts less than 10 kb (Fig. 9b). For longer transcripts (> 10 kb), NEB, NuGEN, SMARTer and SMARTseq samples had a median enrichment that is much higher than those of TruSeq70 (Fig. 9b). Additionally, the enrichment effect for NEB samples distributed wider than all the other samples (Fig. 9).

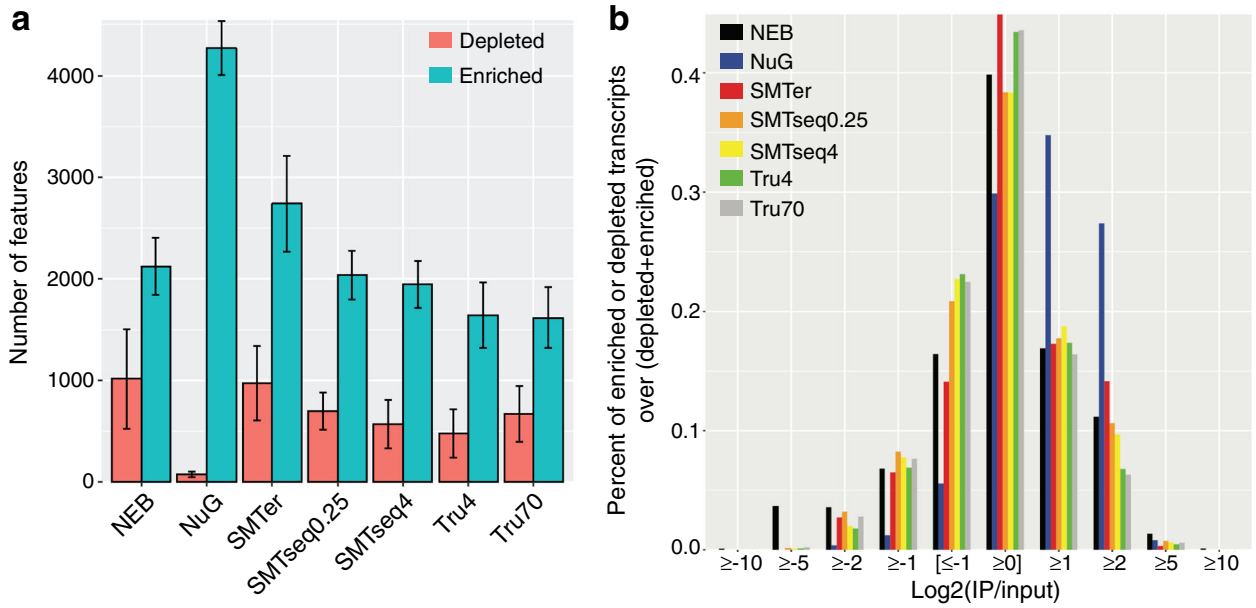

Fig. 6 Descriptive characteristic of enrichment or depletion profiles as generated by the different library preparation kits. Genes which have at least 20 raw reads in the input samples and a ratio of IP/Input ≥2 or Input/IP ≥2 were used to generate the plots. **a** Total number of transcripts enriched or depleted. **b** Percentage of enriched or depleted transcripts grouped into different bins. X-axis: log2(IP/input), Y-axis: percentage of genes in each bin over whole population. NEB: NEBNext® Ultra™, NuG: NuGEN Ovation®, SMTer: SMARTer® Stranded; Tru4: TruSeq using 4 ng of RNA; Tru70: TruSeq using 70 ng of RNA. SMTseq4: SMART-Seq® v4 using 4 ng of RNA; SMTseq0.25: SMART-Seq® v4 using 250 pg of RNA. Yellow and orange: SMTseq samples; Red: SMTer samples; Black: NEB samples; Blue: NuGEN samples; Green and grey: TruSeq samples

A similar trend was also observed in depleted transcripts. Across all transcript lengths, the range of depletion effect for NuGEN and SMARTer samples was less than for other samples (Fig. 10a). For NEB samples, the depletion effect distribution was wider than all the other samples (Fig. 10b). For longer transcripts (> 10 kb), NEB, NuGEN, SMARTer and SMARTseq samples showed fewer depletion effects than those from TruSeq70 (Fig. 10b).

Discussion

In this study, we compared five library-preparation kits for RNA-seq, using low-quantity input RNA or RiboTag IP RNA, by applying a comprehensive set of quality

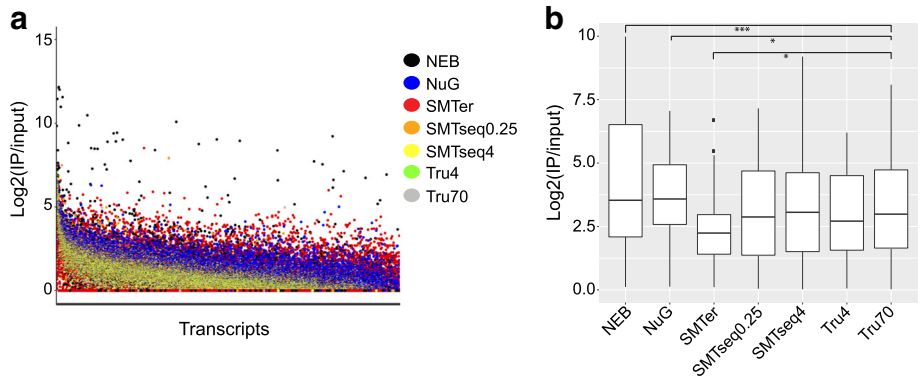

Fig. 7 Enrichment profiles and top 50 enriched transcripts. **a** Enrichment factor of transcripts are sorted in decreasing order based on log2 (IP/input). X-axis:transcripts, Y-axis:log2 value of enrichment (IP/Input). **b** Boxplot of top 50 enriched transcripts. NEB: NEBNext® Ultra™, NuG: NuGEN Ovation®, SMTer: SMARTer® Stranded; Tru4: TruSeq using 4 ng of RNA; Tru70: TruSeq using 70 ng of RNA. SMTseq4: SMART-Seq® v4 using 4 ng of RNA; SMTseq0.25: SMART-Seq® v4 using 250 pg of RNA. Yellow and orange: SMTseq samples; Red: SMTer samples; Black: NEB samples; Blue: NuGEN samples; Green and grey: TruSeq samples

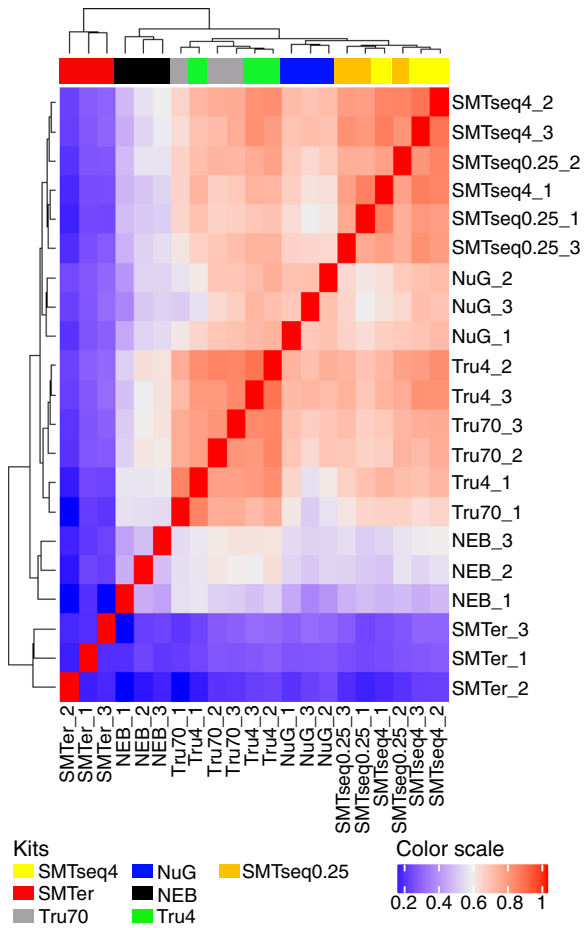

Fig. 8 Hierarchical clustering based on the rank of IP/input value. Dendrogram represents Spearman correlation coefficients between pairs of samples. NEB: NEBNext® Ultra™, NuG: NuGEN Ovation®, SMTer: SMARTer® Stranded; Tru4: TruSeq using 4 ng of RNA; Tru70: TruSeq using 70 ng of RNA. SMTseq4: SMART-Seq® v4 using 4 ng of RNA; SMTseq0.25: SMART-Seq® v4 using 250 pg of RNA. Yellow and orange: SMTseq samples; Red: SMTer samples; Black: NEB samples; Blue: NuGEN samples; Green and grey: TruSeq samples

measures. One of the major differences among library preparation kits was whether oligo (dT) is used to select mRNA. Among the kits tested, the NEBNext® Ultra™, the Illumina TruSeq® and the TaKaRa SMART-Seq® v4 Ultra® use oligo-dT primers to select for polyA mRNA. Conversely, the TaKaRa SMARTer® kit depends on locked nucleic acid (LNA) technology and random primers to capture both products with classical long polyA(+) and those with short poly(A) tails or polyA(−) transcripts and employs a ribosomal depletion step. Although the NuGEN Ovation® V2 kit uses a combination of semi-random hexamers and a poly-dT chimeric primer for 1st strand cDNA amplification in an effort to mitigate bias, 3′ end bias was still observed. Shanker, et al.(2015), also observed 3′ end bias using the NuGEN Ovation V2 kit with low input samples [22]. Interesingly, we observed greater 3′ end bias in IP samples (except for SMARTer prepared samples) than in the input samples, possibly suggesting some degradation of the RNA.

A higher percentage of reads mapped to the intronic and intergenic region in the samples derived from the TaKaRa SMARTer® kit in comparison to samples derived from the other five kits. Adiconis, et al., 2013 [23], also found a similar difference by comparing the SMARTer® kit to the TruSeq® kit. In our study, among the top-100 highly expressed transcripts in SMARTer samples, 30% were miRNA, lincRNA and rRNA. It is known that the source of miRNA or lincRNA is mainly from intergenic or intronic region, and that certain ribosomal RNAs generated by RNA polymerase I and III are without polyA tails. Therefore, we propose that the SMARTer® kit may be useful for studies which aim to focus on poly(A) negative transcripts or transcripts derived from non-exon-coding regions.

We observed lower duplication rates for the SMART-Seq® v4 Ultra (SMARTseq) and NuGEN prepared samples as compared to samples prepared with the other kits. A possible explanation to this observed lower duplication rate may relate to the protocols of these two kits. The mRNA is pre-amplifed to cDNA, before fragmentation, making the duplication rate resulting from the amplification harder to identify based on mapping position. Conversely, in other methods including the TruSeq kit, mRNA is fragmented first and the amplification only happens during the library construction step, making it easier to identify duplication based on the mapping position. For this study, the comparisons among different kits were achieved by using the rank-based method without removal of duplicate reads. Parekh et al., also showed that removal of duplicates improved neither accuracy nor precision and can actually worsen the power and the False Discovery Rate (FDR) for differential gene expression [33].

While Combs et al., (2015) [34] reported the use of the TruSeq kit with 100 ng of RNA, our modification of the TruSeq protocol provides the possibility to use the kit with RNA amounts as low as 4 ng. Indeed, our study, for the first time, shows that with protocol modifications, TruSeq with 4 ng of RNA performs similarly to the TruSeq with 70 ng of RNA with respect to the number of genes being captured and overall profile composition.

Comparing translatome (IP samples) against corresponding transcriptome (input samples), we find a relative higher intronic percentage in the translatome profiles, which might indicate that some non-mature RNA are precipitated during the IP process. Overall, we detected more enriched transcripts than depleted transcripts in the IP samples. Roh et al., report a similar result although the fold-change was greater in the depleted genes than the enriched genes [35]. This difference may result from the

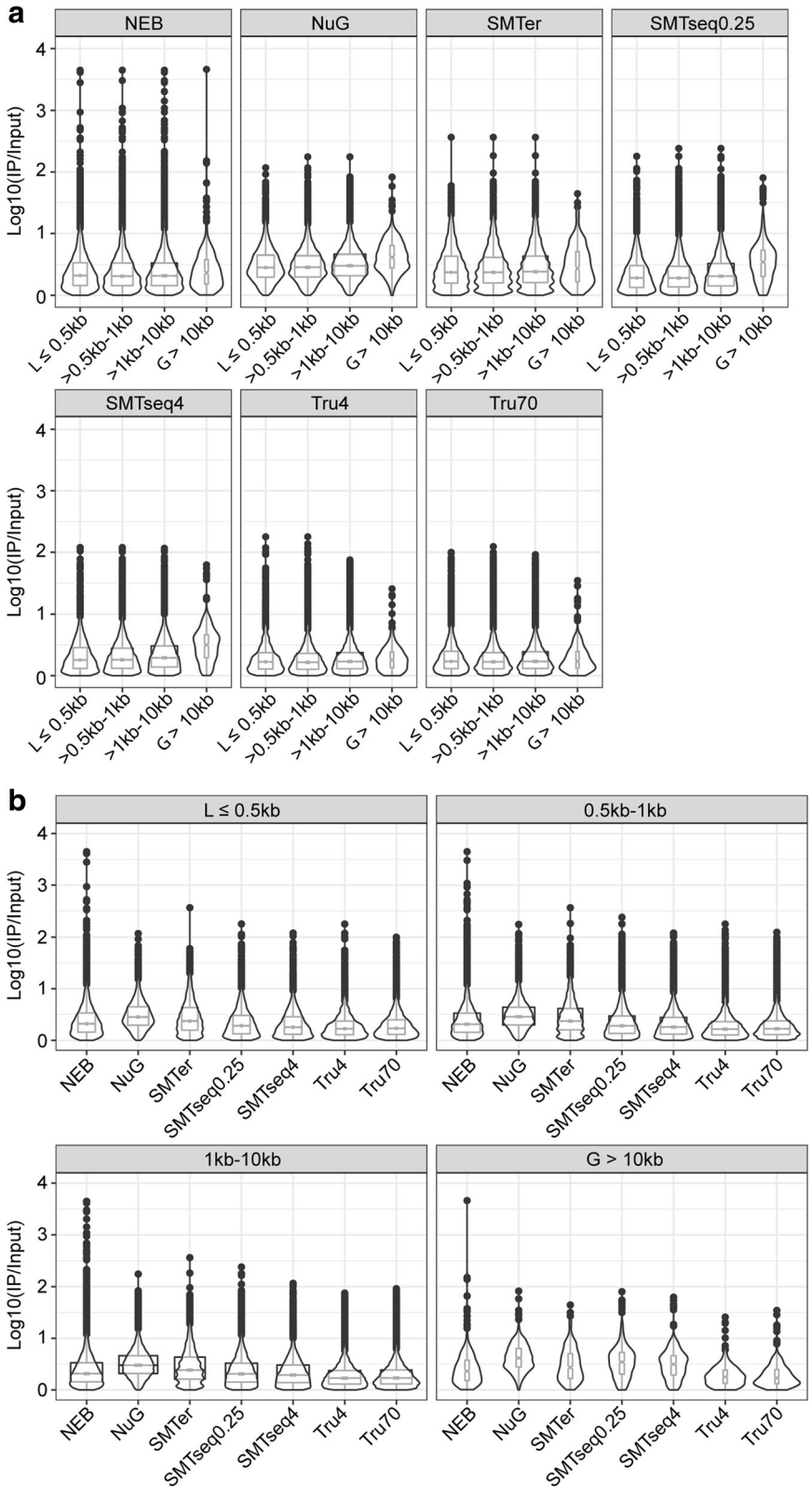

Fig. 9 Boxplot and violin plots of enriched features over different transcript lengths. **a** Boxplots of enrichment factor of different transcripts within each kit. **b** Boxplots of enrichment factor of different kits at each transcript length bin. The notch represents the median ± 1.58IQR/√n. The width of boxplot is proportion to sample size of each group

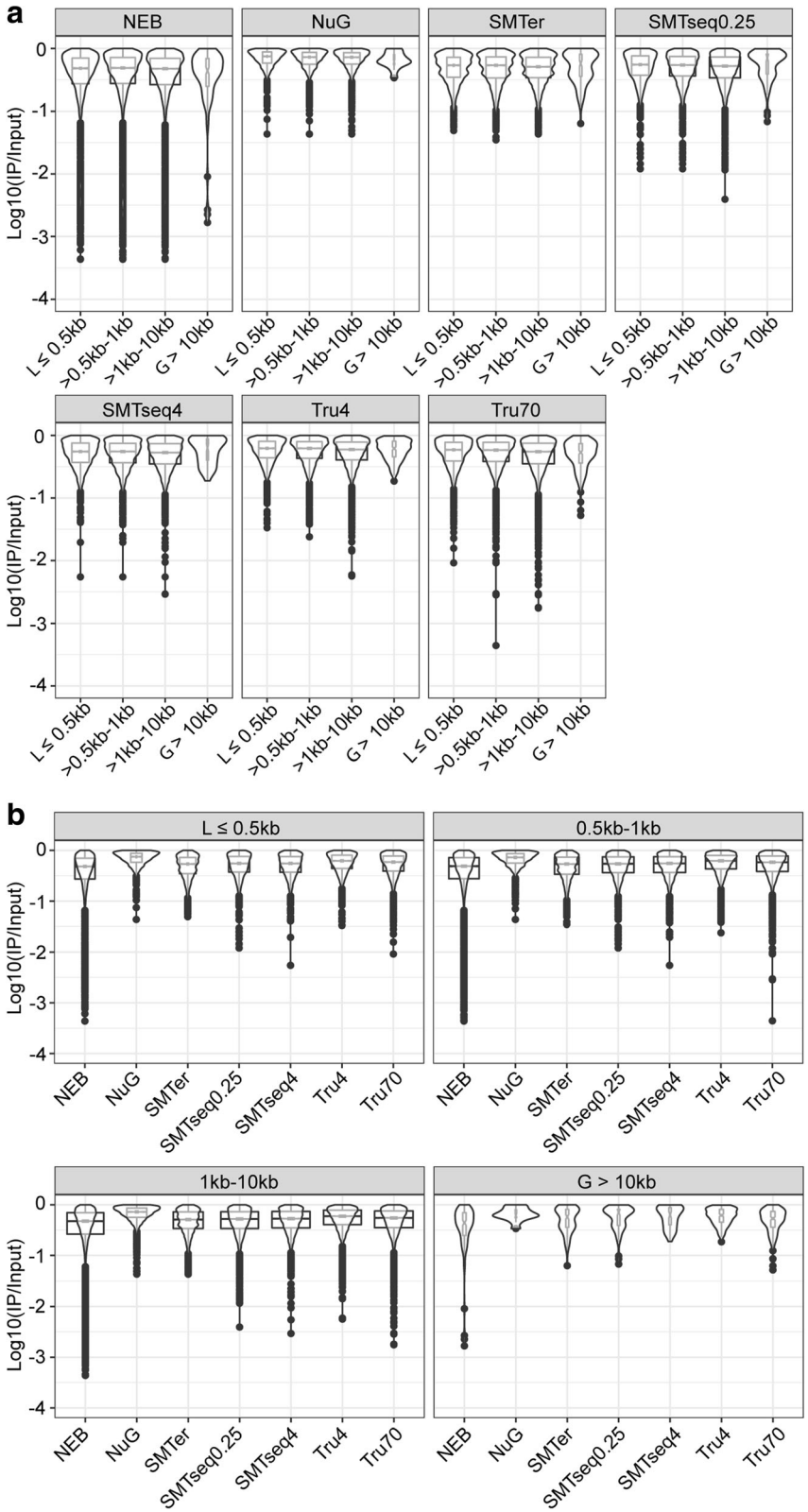

Fig. 10 Boxplot and violin plots of depletion features over different transcript lengths. **a** Boxplots of depletion factor of different transcripts within each kit. **b** Boxplots of depletion factor of different kits at each transcript length bin. The notch represents the median ± 1.58IQR/√n. The width of boxplot is proportion to sample size of each group

different tissues being used, and more specifically the percent of cells that express the tagged ribosomes. Among enriched transcripts, we observed an enrichment effect bias toward longer transcripts (> 10 kb) (Fig. 9a). This may relate to the nature of RiboTag IP since it is a method to detect polysome profiles during translation [16]. It is possible that the higher number of ribosomes on longer transcripts leads to a higher enrichment. In addition, the greater enrichment effect of longer transcript is slightly higer for samples prepared by SMARTer and SMARTseq kits. This may be related to the template-switch oligonucleotide with one locked nucleic acid (LNA) technique applied in these kits, which is aimed to improve the hybridization between the template-switch oligonucleotide and the cDNA product [36, 37], increasing full coverage for longer transcripts.

Conclusion

Amongst the kits and library prep protocols analyzed in this manuscript, SMART-Seq v4 and TruSeq offer the best sequencing results for libray preparation from smaller amounts of RNA as starting material. Indeed, the overall profile of 250 pg/4 ng samples from SMART-Seq v4 was similar to the TruSeq 70, here used as a gold-standard control. SMARTer Stranded Total RNA-Seq Kit might be a good choice to study both polyA(+) mRNA and non-polyA mRNA, especially non-coding RNAs. Since there is a coverage bias towards 3′ for IP samples and more enrichment for longer transcripts, correction should be included during comparison among samples, for example, using the bias correction function in Cufflink [38]. Finally, IP RNA from RiboTag samples is likely to include a higher rate of immature RNAs, given the observed increase in intronic sequences in the IP samples across all library prep approaches. Overall, we were able to observe both enriched and depleted transcripts of translatome profiles using all kits. Greater enrichment effects were detected than depletion, however this may be related to the percent of tagged ribosomes in the tissue and therefore tissue and Cre-driver specific. In summary, by considering the eveness of coverage, number of detected features, low CPM of non-coding genes, and similar enrichment profiles comparing to standard TruSeq70 prepared samples, the SMARTseq and NEB kits performed the best in comparison to the other kits tested. However, the SMARTseq kit had a lower duplication rate and allows reactions to start with as little as 250 pg, significantly decreasing the necessary amount of starting material. In addition, the modified TruSeq4 protocol provides good results based on the relative high number of detected features, low CPM of non-coding genes, and similarity of the enrichment profile to the standard TruSeq70.

Additional files

Additional file 1: Table S1. Library preparation performed in this study. Table S2 Gene list with RPKM greater than 10,000. Table S3 Median of genes from unique and shared regions of Venn diagram. Table S4 Spearman correlation coefficients between different profiles. (XLSX 28 kb)

Additional file 2: Figure S1. Cre recombination in liver cells expressing Gfi1. (a) Cryosection of liver from a cross between a Gfi1-Cre mouse and a TdTomato reporter mouse (Ai14) stained with DAPI and phalloidin. TdTomato is found in a subset of cells in the liver that is likely consistent with Kupffer or endothelial cells. (b) Enrichment of *Gfi1* transcripts in the IP samples as compared to the input samples was assessed by reverse-transcription followed by real time PCR. (PDF 2947 kb)

Additional file 3: Figure S2. Duplication rate of each library. X-axis: duplication rate, Y-axis: log10 of reads at different duplication rates. (PDF 622 kb)

Additional file 4: Figure S3. Hierarchical clustering of expression levels, based on the rank of the count of exon per million mapped reads (CPM). Dendrograms represent Spearman correlation coefficients between pairs of samples that is 3 replicates for input and 3 replicates for IP. (PDF 233 kb)

Additional file 5: Figure S4. Bland–Altman plot (MA plot) of translatome (IP samples) and transcriptome (input samples) profiles for each kit. The red lines represent the boundary cutoff [− 1,1]. Dots above or below the red line represent the enriched or depleted transcripts. (JPG 587 kb)

Additional file 6: Figure S5. Venn diagram of enriched/depleted transcripts (CPM ≥ 20 in at least one replicate, mean ratio of enrichement/depletion of the three replicates). The mean ratio IP/input is ≥2 or input/IP is ≥2. (PDF 1063 kb)

Additional file 7: Figure S6. Histogram of length distribution for enriched or depleted transcripts. (PDF 353 kb)

Abbreviations

NEB: NEBNext® Ultra™ Directional RNA Library Prep Kit for Illumina with 4 ng of RNA; NuGEN: NuGEN Ovation® RNA-Seq System V2 with 4 ng of RNA; SMARTer: TaKaRa SMARTer® Stranded Total RNA-Seq Kit-Pico Input Mammalian with 4 ng of RNA; SMARTseq4 and SMARTseq0.25: TaKaRa SMART-Seq® v4 Ultra® Low Input RNA Kit for Sequencing with 4 ng and 0.25 ng of RNA; TruSeq4 and TruSeq70: Illumina TruSeq RNA Library Prep Kit v2 with 4 ng and 70 ng of RNA

Acknowledgements

We would like to thank Maggie Matern and Benjamin Shuster for critically reviewing this manuscript. This work was supported by R01DC03544 (NIDCD), R01DC013817 (NIDCD) and MR130240 (CDMRP/DoD).

Funding

This work was supported by R01DC03544 (NIDCD), R01DC013817 (NIDCD) and MR130240 (CDMRP/DoD). The funding sources provided the support for effort and materials, and did not have a role in study design, data collection and analysis, decision to publish or preparation of the manuscript.

Availability of data and materials

The datasets supporting the conclusions of this article are available in the NCBI Gene Expression Omnibus (GEO) repository under accession number GSE104213 https://www.ncbi.nlm.nih.gov/geo/query/acc.cgi?acc=GSE104213. The datasets supporting the conclusions of this article are included within the article and its additional files (Additional files 1, 2, 3, 4, 5, 6, and 7).

Authors' contributions

YS, BM, ETB, SO, XZ performed the experiments, YS, AS and AM performed the analysis, YS, BM and RH wrote the manuscript, AM, RJM, LT, LS and RH designed and oversaw the project. All the authors read and approved the final manuscript.

Ethics approval and consent to participate

All procedures involving animals were carried out in accordance with the National Institutes of Health Guide for the Care and Use of Laboratory

Animals and have been approved by the Institutional Animal Care and Use Committee at the University of Maryland, Baltimore (protocol numbers 1,015,003 and 0915006).

Consent for publication
Not applicable.

Competing interests
The authors declare that they have no competing interests.

Publisher's Note

Author details
[1]Institute for Genome Sciences, University of Maryland School of Medicine, Baltimore, MD 21201, USA. [2]Department of Otorhinolaryngology-Head & Neck Surgery, University of Maryland School of Medicine, Baltimore, MD 21201, USA. [3]Genomics and Computational Biology Core, National Institute on Deafness and Other Communication Disorders, Bethesda, MD 20892, USA. [4]Department of Anatomy and Neurobiology, University of Maryland School of Medicine, Baltimore, MD 21201, USA.

Received: 10 November 2017 Accepted: 11 September 2018
Published online: 21 September 2018

References
1. JM S: Using fluorescence activated cell sorting to examine cell-type-specific gene expression in rat brain tissue. J Vis Exp 2015, 99:e52537.
2. Jung J, Jung H. Methods to analyze cell type-specific gene expression profiles from heterogeneous cell populations. Animal Cells and Systems. 2016;20:113–7.
3. Kim T, Lim CS, Kaang BK. Cell type-specific gene expression profiling in brain tissue: comparison between TRAP, LCM and RNA-seq. BMB Rep. 2015; 48(7):388–94.
4. Chen L, Borozan I, Sun J, Guindi M, Fischer S, Feld J, Anand N, Heathcote J, Edwards AM, McGilvray ID. Cell-type specific gene expression signature in liver underlies response to interferon therapy in chronic hepatitis C infection. Gastroenterology. 2010;138(3):1123–33 e1121–1123.
5. Li J, Klughammer J, Farlik M, Penz T, Spittler A, Barbieux C, Berishvili E, Bock C, Kubicek S. Single-cell transcriptomes reveal characteristic features of human pancreatic islet cell types. EMBO Rep. 2016;17(2):178–87.
6. Li M, Jia C, Kazmierkiewicz KL, Bowman AS, Tian L, Liu Y, Gupta NA, Gudiseva HV, Yee SS, Kim M, et al. Comprehensive analysis of gene expression in human retina and supporting tissues. Hum Mol Genet. 2014;23(15):4001–14.
7. Hertzano R, Elkon R, Kurima K, Morrisson A, Chan SL, Sallin M, Biedlingmaier A, Darling DS, Griffith AJ, Eisenman DJ, et al. Cell type-specific transcriptome analysis reveals a major role for Zeb1 and miR-200b in mouse inner ear morphogenesis. PLoS Genet. 2011;7(9):e1002309.
8. Cheng L, Zhang S, MacLennan GT, Williamson SR, Davidson DD, Wang M, Jones TD, Lopez-Beltran A, Montironi R. Laser-assisted microdissection in translational research: theory, technical considerations, and future applications. Appl Immunohistochem Mol Morphol. 2013;21(1):31–47.
9. Asano T, Masumura T, Kusano H, Kikuchi S, Kurita A, Shimada H, Kadowaki K. Construction of a specialized cDNA library from plant cells isolated by laser capture microdissection: toward comprehensive analysis of the genes expressed in the rice phloem. Plant J. 2002;32(3):401–8.
10. Smalley MJ, Titley J, O'Hare MJ. Clonal characterization of mouse mammary luminal epithelial and myoepithelial cells separated by fluorescence-activated cell sorting. In Vitro Cell Dev Biol Anim. 1998;34(9):711–21.
11. Birnbaum K, Shasha DE, Wang JY, Jung JW, Lambert GM, Galbraith DW, Benfey PN. A gene expression map of the Arabidopsis root. Science. 2003; 302(5652):1956–60.
12. Graham M, Richardson JL, Macara IG. Does facs change gene expression. cytometry. 2015;87:166–75.
13. Streets AM, Huang Y. How deep is enough in single-cell RNA-seq? Nat Biotechnol. 2014;32(10):1005–6.
14. Wu AR, Neff NF, Kalisky T, Dalerba P, Treutlein B, Rothenberg ME, Mburu FM, Mantalas GL, Sim S, Clarke MF, et al. Quantitative assessment of single-cell RNA-sequencing methods. Nat Methods. 2014;11(1):41–6.
15. Doyle JP, Dougherty JD, Heiman M, Schmidt EF, Stevens TR, Ma G, Bupp S, Shrestha P, Shah RD, Doughty ML, et al. Application of a translational profiling approach for the comparative analysis of CNS cell types. Cell. 2008; 135(4):749–62.
16. Sanz E, Yang L, Su T, Morris DR, McKnight GS, Amieux PS. Cell-type-specific isolation of ribosome-associated mRNA from complex tissues. Proc Natl Acad Sci U S A. 2009;106(33):13939–44.
17. Heiman M, Schaefer A, Gong S, Peterson JD, Day M, Ramsey KE, Suarez-Farinas M, Schwarz C, Stephan DA, Surmeier DJ, et al. A translational profiling approach for the molecular characterization of CNS cell types. Cell. 2008;135(4):738–48.
18. Brar GA, Weissman JS. Ribosome profiling reveals the what, when, where and how of protein synthesis. Nat Rev Mol Cell Biol. 2015;16(11):651–64.
19. Shigeoka T, Jung H, Jung J, Turner-Bridger B, Ohk J, Lin JQ, Amieux PS, Holt CE. Dynamic axonal translation in developing and mature visual circuits. Cell. 2016;166(1):181–92.
20. Levin JZ, Yassour M, Adiconis X, Nusbaum C, Thompson DA, Friedman N, Gnirke A, Regev A. Comprehensive comparative analysis of strand-specific RNA sequencing methods. Nat Methods. 2010;7(9):709–15.
21. Faherty SL, Campbell CR, Larsen PA, Yoder AD. Evaluating whole transcriptome amplification for gene profiling experiments using RNA-Seq. BMC Biotechnol. 2015;15:65.
22. Shanker S, Paulson A, Edenberg HJ, Peak A, Perera A, Alekseyev YO, Beckloff N, Bivens NJ, Donnelly R, Gillaspy AF, et al. Evaluation of commercially available RNA amplification kits for RNA sequencing using very low input amounts of total RNA. J Biomol Tech. 2015;26(1):4–18.
23. Adiconis X, Borges-Rivera D, Satija R, DeLuca DS, Busby MA, Berlin AM, Sivachenko A, Thompson DA, Wysoker A, Fennell T, et al. Comparative analysis of RNA sequencing methods for degraded or low-input samples. Nat Methods. 2013;10(7):623–9.
24. Matern M, Vijayakumar S, Margulies Z, Milon B, Song Y, Elkon R, Zhang X, Jones SM, Hertzano R. Gfi1Cre mice have early onset progressive hearing loss and induce recombination in numerous inner ear non-hair cells. Sci Rep. 2017;7:42079.
25. Pearson WR, Wood T, Zhang Z, Miller W. Comparison of DNA sequences with protein sequences. Genomics. 1997;46(1):24–36.
26. Orvis J, Crabtree J, Galens K, Gussman A, Inman JM, Lee E, Nampally S, Riley D, Sundaram JP, Felix V, et al. Ergatis: a web interface and scalable software system for bioinformatics workflows. Bioinformatics. 2010;26(12):1488–92.
27. Kim D, Pertea G, Trapnell C, Pimentel H, Kelley R, Salzberg SL. TopHat2: accurate alignment of transcriptomes in the presence of insertions, deletions and gene fusions. Genome Biol. 2013;14(4):R36.
28. Anders S, Huber W. Differential expression analysis for sequence count data. Genome Biol. 2010;11(10):R106.
29. Quinlan AR, Hall IM. BEDTools: a flexible suite of utilities for comparing genomic features. Bioinformatics. 2010;26(6):841–2.
30. Mortazavi A, Williams BA, McCue K, Schaeffer L, Wold B. Mapping and quantifying mammalian transcriptomes by RNA-Seq. Nat Methods. 2008; 5(7):621–8.
31. Krzywinski M, Altman N. Visualizing samples with box plots. Nat Methods. 2014;11(2):119–20.
32. Yang H, Gan J, Xie X, Deng M, Feng L, Chen X, Gao Z, Gan L. Gfi1-Cre knock-in mouse line: a tool for inner ear hair cell-specific gene deletion. Genesis. 2010;48(6):400–6.
33. Parekh S, Ziegenhain C, Vieth B, Enard W, Hellmann I. The impact of amplification on differential expression analyses by RNA-seq. Sci Rep. 2016;6:25533.
34. Combs PA, Eisen MB. Low-cost, low-input RNA-seq protocols perform nearly as well as high-input protocols. PeerJ. 2015;3:e869.
35. Roh HC, Tsai LT, Lyubetskaya A, Tenen D, Kumari M, Rosen ED. Simultaneous transcriptional and Epigenomic profiling from specific cell types within heterogeneous tissues in vivo. Cell Rep. 2017;18(4):1048–61.
36. Picelli S, Bjorklund AK, Faridani OR, Sagasser S, Winberg G, Sandberg R. Smart-seq2 for sensitive full-length transcriptome profiling in single cells. Nat Methods. 2013;10(11):1096–8.
37. Picelli S, Faridani OR, Bjorklund AK, Winberg G, Sagasser S, Sandberg R. Full-length RNA-seq from single cells using Smart-seq2. Nat Protoc. 2014;9(1): 171–81.
38. Trapnell C, Williams BA, Pertea G, Mortazavi A, Kwan G, van Baren MJ, Salzberg SL, Wold BJ, Pachter L. Transcript assembly and quantification by RNA-Seq reveals unannotated transcripts and isoform switching during cell differentiation. Nat Biotechnol. 2010;28(5):511–5.

Sex differences in hearing: Probing the role of estrogen signaling

Benjamin Z. Shuster, Didier A. Depireux, Jessica A. Mong, and Ronna Hertzano

Citation: The Journal of the Acoustical Society of America **145**, 3656 (2019); doi: 10.1121/1.5111870
View online: https://doi.org/10.1121/1.5111870
View Table of Contents: https://asa.scitation.org/toc/jas/145/6
Published by the Acoustical Society of America

Sex differences in hearing: Probing the role of estrogen signaling

Benjamin Z. Shuster,[1] Didier A. Depireux,[1] Jessica A. Mong,[2] and Ronna Hertzano[1,a)]
[1]*Department of Otorhinolaryngology Head and Neck Surgery, University of Maryland School of Medicine, 16 South Eutaw Street, Suite 500, Baltimore, Maryland 21201, USA*
[2]*Department of Pharmacology, University of Maryland School of Medicine, 655 West Baltimore Street, Baltimore, Maryland 21201, USA*

(Received 17 January 2019; revised 7 April 2019; accepted 18 April 2019; published online 21 June 2019)

Hearing loss is the most common form of sensory impairment in humans, with an anticipated rise in incidence as the result of recreational noise exposures. Hearing loss is also the second most common health issue afflicting military veterans. Currently, there are no approved therapeutics to treat sensorineural hearing loss in humans. While hearing loss affects both men and women, sexual dimorphism is documented with respect to peripheral and central auditory physiology, as well as susceptibility to age-related and noise-induced hearing loss. Physiological differences between the sexes are often hormone-driven, and an increasing body of literature demonstrates that the hormone estrogen and its related signaling pathways may in part, modulate the aforementioned differences in hearing. From a mechanistic perspective, understanding the underpinnings of the hormonal modulation of hearing may lead to the development of therapeutics for age related and noise induced hearing loss. Here the authors review a number of studies that range from human populations to animal models, which have begun to provide a framework for understanding the functional role of estrogen signaling in hearing, particularly in normal and aberrant peripheral auditory physiology.
 https://doi.org/10.1121/1.5111870

[JFL] Pages: 3656–3663

I. INTRODUCTION

According to the World Health Organization (March 2018), there are 466×10^6 individuals worldwide with debilitating hearing loss, and an estimated 1.1×10^9 young adults worldwide who are at risk for developing hearing loss due to recreational noise exposure (Deafness and hearing loss, 2018). According to the Center for Disease Control, between 2001 and 2008, an estimated 30×10^6 Americans over the age of 12 suffered from hearing loss in both ears, while an estimated 48×10^6 Americans suffered hearing loss in at least one ear (Lin *et al.*, 2011). Hearing loss is more than just an obstacle to communication, and its negative effects permeate and influence all aspects of the lives of those afflicted. According to the CDC, "Those who have hearing loss are more likely to have low employment rates, lower worker productivity, and high healthcare costs" (Themann *et al.*, 2013). Furthermore, hearing loss is the second most common health issue (following tinnitus) afflicting military veterans (Veterans Benefits Administration Reports Annual Benefits Report Fiscal Year 2017, 2017; Yankaskas, 2013). Hearing loss in the military is particularly concerning, since clear and efficient communication is absolutely critical to the success and safety of men and women on an often noisy and chaotic battlefield.

Hearing loss affects both men and women, but importantly, significant sex differences in hearing have been documented in a number of species and are particularly well-documented in humans. These differences in hearing physiology between the sexes have important implications not only for a complete understanding of hearing loss and hearing physiology, but also for the development of potential therapeutics to treat sensorineural hearing loss (SNHL), which encompasses both noise-induced hearing loss (NIHL) and age-related hearing loss (ARHL). Currently, there are no approved therapeutics to treat NIHL or ARHL, and it is quite reasonable to expect that the efficacy of any therapeutics may be influenced by differences in hearing physiology between the sexes. In fact, evidence already exists to suggest that this may be the case (Milon *et al.*, 2018). Unfortunately, a large sex bias still exists in many aspects of hearing research, and there is a real possibility that some of the conclusions reached in studies using only males, or where biological sex as an independent variable was not considered, may not apply similarly to both sexes (Lauer and Schrode, 2017; Villavisanis *et al.*, 2018). Indeed, the influences of biological sex and sex steroids, such as estrogens and androgens, on the molecular and cellular pathways underlying hearing loss represent a significant knowledge gap. Thus, there is value in investigating these sex differences, as a more complete understanding of the mechanisms underlying sex differences in hearing may benefit the development of therapeutics beneficial to both sexes.

II. SEX DIFFERENCES IN HEARING

Sex differences in hearing encompass both peripheral and central auditory processing, and range from cochlear function, to susceptibility to ARHL and NIHL, and even to binaural sound processing (Grinn *et al.*, 2017; McFadden *et al.*, 2009a; Pearson *et al.*, 1995; Szanto and Ionescu, 1983;

a)Also at: Department of Anatomy and Neurobiology, University of Maryland School of Medicine, Health Sciences Facility II, 20 Penn Street, Baltimore, MD 21201, USA. Electronic mail: rhertzano@som.umaryland.edu

Zündorf *et al.*, 2011). Since the majority of recent clinical trials targeting hearing loss primarily address the peripheral auditory system at the level of the cochlea and the auditory nerve (Crowson *et al.*, 2017), the focus of this review will be restricted to sex differences in peripheral auditory physiology, SNHL, and the possible mechanisms underlying these differences.

Overall, it is widely accepted that the gross anatomy of the male is virtually indistinguishable from the gross anatomy of the female cochlea. Some studies have reported that the cochlear length in females is slightly shorter in comparison to males (~3%); however these findings are the subject of inconclusive reports and questionable statistical and biological significance (Miller, 2007; Sato *et al.*, 1991). When the physiology of the cochlea is examined more closely, however, intriguing differences between the sexes begin to emerge.

A. Otoacoustic emissions

In humans, a number of sex differences in outer hair cell (OHC) physiology have been documented. Otoacoustic emissions (OAEs) are sounds produced by vibrations that arise from the organ of Corti and are transmitted backward through the middle ear. These vibrations likely arise from the OHCs, and are due to their electromotive properties (Brownell, 1990). The presence and amplitudes of OAEs can be measured and used as a readout for general OHC function (although pathology of the middle ear can also influence the detection of OAEs) (Kemp, 2008). Spontaneous otoacoustic emissions (SOAEs) are likely produced by OHCs in the absence of an external stimulus. OHCs also contribute to the emission of more robust, reproducible sounds when the listener is presented with broadband clicks (click-evoked otoacoustic emissions, CEOAE) and when the listener is presented with two neighboring, simultaneous pure tones (distortion product otoacoustic emissions, DPOAEs) (Kemp, 2002).

While SOAEs are detectable in approximately 70% of all human listeners, (Abdala and Visser-Dumont, 2001) they are more likely to be detected in female listeners- approximately 80% compared to approximately 60% of male listeners (Penner and Zhang, 1996). In humans, females also tend to produce larger CEOAEs than males, and similar findings have been shown in rhesus monkeys (McFadden, 1998; McFadden *et al.*, 2006). Sex-differences in the amplitude of DPOAEs, however, are smaller in magnitude, variable between species, and the subject of equivocal reports (McFadden, 2009). While these phenomena are well-documented in human listeners, the exact mechanisms underlying sex-differences in OAEs are unknown, but may be linked to prenatal androgen (male hormone) exposure (McFadden *et al.*, 2006). In support of this hypothesis, studies of OAEs in humans have demonstrated that females with male co-twins, who are exposed to higher levels of prenatal androgens, display more masculinized OAEs in comparison to same-sex female twins or non-twin females (McFadden, 1993). Furthermore, female sheep exposed to testosterone prenatally develop weaker, more masculinized CEOAEs (McFadden *et al.*, 2009b).

B. Auditory brainstem response (ABR)

Neuronal activity as measured from the cochlea to the brainstem provides further evidence of sex differences in hearing. ABR wave-I amplitude is a measure of the synchronous neural firing at the level of the spiral ganglion in response to a sound stimulus. A recent publication using mice demonstrated that in adult mice, ABR wave-I amplitudes are larger in females compared to males (Milon *et al.*, 2018). Similar findings have been reported in humans when examining the effect of recreational noise exposure on cochlear nerve response amplitudes (Grinn *et al.*, 2017). While the mechanisms underlying the amplitude differences are not known, it has been postulated that a shorter cochlear length in females and often smaller head size may contribute to greater synchronous activity at the level of the spiral ganglion afferents, as well as a shorter afferent auditory pathway, both of which may lead to greater ABR wave amplitudes and shorter wave latencies (McFadden, 1998). In fact, analysis of speech-evoked ABR in humans demonstrates that females have shorter ABR onset response latencies, (Liu *et al.*, 2017) and it is well demonstrated that females have larger wave-V amplitudes, shorter wave-V latencies, and shorter wave I-V inter-peak latencies (Jerger and Hall, 1980; Lotfi and Zamiri Abdollahi, 2012). However, comparison of ABR latencies of males and females of similar head size suggests that differences in ABR latencies cannot be completely attributed to differences in skull or brainstem dimensions, suggesting underlying physiology also contributes to these sex differences (Sabo *et al.*, 1992).

C. Sensorineural hearing loss

According to a recent analysis of data obtained via two national surveys, approximately 6% of the adult population in the United States suffers from deafness or serious difficulty hearing (determined through analysis of self-reported answers to survey questions) (Li *et al.*, 2018). However, when the data are analyzed by sex, a higher prevalence of hearing loss is observed in males where the prevalence of deafness or serious difficulty hearing is 7.3% compared to only 4.8% in females (Li *et al.*, 2018). The higher prevalence of hearing loss in males as reported in these surveys has been confirmed by other cross-sectional and cross-sectional longitudinal cohort analyses, including a large meta-analysis of 42 studies conducted across 29 countries (Bishop *et al.*, 2019; Lin *et al.*, 2011; Stevens *et al.*, 2011).

While answers to these two surveys were self-reported, and the data were not analyzed by etiology of the hearing loss, well documented sex differences exist with regard to specific etiologies of hearing loss. In particular, sex differences in the prevalence and progression of age-related hearing loss are well documented. A number of longitudinal and cross-sectional studies in humans demonstrate that pure-tone hearing thresholds decline more rapidly in males compared to females, especially at higher frequencies (Allen and Eddins, 2010; Cruickshanks *et al.*, 1998; Pearson *et al.*, 1995). Hearing loss (as measured in frequencies ranging from 0.5 to 8 kHz) is detectable in males as early as age 30, while the onset and frequency range of the hearing loss in females is both later in life and more variable (Pearson *et al.*, 1995). Furthermore, a

cross-sectional study by Allen and Eddins (2010) demonstrated that a decline in DPOAE amplitude begins in 30 year old males, while a similar decrease in DPOAE amplitude begins a decade later in females (Allen and Eddins, 2010). In a Swedish cohort study of adult males and females ages 70 and 75, the 4 kHz pure-tone thresholds were approximately 20 dB worse in the male subjects (Jönsson *et al.*, 1998). In a mouse model of ARHL, hearing thresholds at higher frequencies, as measured via ABR, declined more rapidly in males than females (Henry, 2004). Additional mouse studies have demonstrated that the magnitude of DPOAEs declines more rapidly in males than females, which may partially underpin the more rapid deterioration of ABR thresholds in males (Guimaraes *et al.*, 2004).

Evidence also suggests that females are protected from NIHL in comparison to males. One retrospective study of industrial factory workers concluded that females experience less severe deterioration of hearing thresholds as a result of occupational noise exposure in comparison to males when occupational sound intensities are approximately 98 dB (Szanto and Ionescu, 1983). The evidence is even more pronounced in animal models. Sound-conditioned female chinchillas display reduced permanent threshold shifts (PTS) compared to males at most frequencies (except 16 kHz) after exposure to simulated rifle fire at 150 dB peak sound pressure level (SPL) (McFadden *et al.*, 2000). Work from our group shows that female mice are relatively protected from a PTS-inducing noise exposure in comparison to males (Milon *et al.*, 2018). In addition, wave-I amplitudes in female mice, following the noise trauma, were larger than amplitudes in males, indicating greater synchronous activity at the level of the auditory nerve. The same study investigated the therapeutic efficacy of suberoylanilide hydroxamic acid (SAHA), a potential treatment for NIHL that had previously been tested only in male mice. When treated with SAHA, males were protected (a significant reduction in the PTS) at 16 kHz while females were protected at 24 kHz, further highlighting differential response to acoustic injury and the need to fully understand the mechanisms underlying these differences prior to the development of oto-therapeutics and targeted therapies (Milon *et al.*, 2018).

III. ESTROGEN AND HEARING

Differences in the sex steroid milieu often underlie sex differences in physiology. Indeed, an increasing body of literature demonstrates that the aforementioned sex differences in hearing are modulated, at least in part, by estrogens acting via their classical steroid receptor signaling pathways.

A. Hearing, the menstrual cycle, and menopause

Substantial evidence exists linking serum levels of estrogens to hearing thresholds in a variety of human populations. Estrogens are primarily produced by the ovaries in pre-menopausal women but are also synthesized in smaller amounts by the brain and adipose tissue. Of the estrogens produced by the ovaries, estradiol—or more specifically 17β- estradiol—is the most potent (Blair *et al.*, 2000). Pure-tone hearing thresholds have been shown to fluctuate during the different stages of the menstrual cycle in adult pre-menopausal women. In one study of pre-menopausal women ages 18–39, lowest hearing thresholds occurred during the late-follicular phase of the menstrual cycle, which corresponds to the highest levels of serum estrogens. Hearing thresholds subsequently increased during the late-luteal phase and early follicular phases, which correspond to low levels of serum estrogen and increases in serum progesterone levels (Da Silva Souza *et al.*, 2017). A relationship between changes in hearing to changes in circulating levels of estrogens is also seen in animal models. In post-partum female mice, changes in hearing and the response to pup vocalizations correspond to fluctuations in estrogen levels (Frisina, 2012).

In post-menopausal women, the ovaries no longer produce estrogens, and serum levels drop significantly. A cross-sectional study analyzing hearing thresholds in 1830 post-menopausal women found a significant association between serum estradiol levels and hearing thresholds, and concluded that lower levels of serum estradiol are associated with decreased hearing sensitivity (Kim *et al.*, 2002). A natural follow up question would be whether hormone replacement therapy (HRT) could prevent or ameliorate changes in hearing in post-menopausal women. In one study using low dose estrogen treatment in women who had undergone surgically induced menopause for benign diseases, ABR wave latencies were shortened, indicative of improved sensitivity/neuronal reactivity in the presence of estrogen (Caruso *et al.*, 2003). Another study of post-menopausal women demonstrated that women taking estrogen therapy displayed better low frequency mean air conduction thresholds (250–2000 Hz) compared to the control subjects not taking any form of HRT (Kilicdag *et al.*, 2004). However, not all studies show that HRT results in otoprotection from ARHL. Admittedly, studies on the effect of HRT are more challenging to compare and interpret, as HRT regimens vary in dosage, composition, duration, and initiation with regards to the onset of menopause (Caruso *et al.*, 2003; Curhan *et al.*, 2017; Guimaraes *et al.*, 2006; Hederstierna *et al.*, 2007; Kilicdag *et al.*, 2004). Natural progesterone or synthetic progestins are common components in some HRT formulations, and have been associated with adverse effects on hearing (Guimaraes *et al.*, 2006). In a study comparing post-menopausal women receiving either estrogen, an estrogen and progestin combination therapy, or no HRT, the women receiving the combination treatment showed worse hearing thresholds and DPOAEs in comparison to the untreated group (Guimaraes *et al.*, 2006). Similar results were obtained also in studies using mice. A follow-up study in middle-aged female mice demonstrated that mice receiving both estrogen and progestin exhibited accelerated hearing loss in comparison to mice receiving estrogen only (Price *et al.*, 2009). A more recently published study by Williamson *et al.* (2019) recapitulated the finding that a combination HRT including estrogen and progestin in middle-aged female mice is detrimental to hearing (Williamson *et al.*, 2019). Interestingly, a study analyzing progesterone receptor localization found no nuclear localization in the stria vascularis, organ of Corti, or spiral

ganglion neurons (SGN) in either the rat or human cochlea, suggesting any negative effects of progesterone and progestin on hearing are likely indirect (Bonnard *et al.*, 2013). Conversely, a recently published prospective cohort study of approximately 80 000 women from the Nurses' Health Study II found that a longer duration of HRT—estrogen alone or as a combination therapy—was associated with an increased self-perception of hearing loss (Curhan *et al.*, 2017). The same study also correlated older age at menopause with an increase in self-reported hearing loss. On the other hand, a recently published manuscript associated early ovarian failure with increased high frequency hearing thresholds (10–16 kHz), as well as improved hearing at these high frequencies, only in the right ear, in women treated with HRT (here, the treatment group was heterogenic) (Zhang *et al.*, 2018). Taken together, these studies demonstrate the challenge in studying the effect of HRT on hearing and demonstrate the need for a well stratified approach in researching this topic.

B. Hearing and Turner syndrome

Early-onset sensorineural hearing loss and presbycusis are hallmark sequelae of Turner syndrome (45, X) (TS), in which dysfunction of the ovaries results in a reduction of serum estrogen levels. Analysis of Swedish women with TS showed that only 13% of women over the age of 40 displayed normal hearing—defined as a four frequency average less than 20 dB hearing level (HL) (0.5, 1, 2, and 4 kHz)—while the expected proportion of women in the normal Swedish population with normal hearing over the age of 40 is 66% (Hederstierna *et al.*, 2009). The authors concluded in the study that the pure-tone threshold elevations in women with TS were likely of cochlear origin (Hederstierna *et al.*, 2009). Interestingly, the incidence of sensorineural hearing loss can be correlated with karyotype. Patients with a complete loss of an X chromosome were more likely to suffer from sensorineural hearing loss compared to women with a mosaic pattern of X chromosome loss (Hultcrantz and Sylven, 1996). Similar findings of early presbycusis and sensorineural hearing loss were demonstrated in a mouse model of TS. One year old "Turner mice" displayed increased threshold shifts at the higher frequencies compared to littermate controls. This high frequency hearing loss was further exacerbated in comparison to littermate controls when ABRs were conducted at 19 months of age (Hultcrantz *et al.*, 2000).

C. Estrogen receptors α and β and hearing

The actions of estrogens are complex and varied, and are mediated both via genomic and non-genomic pathways (Björnström and Sjöberg, 2005; Vrtačnik *et al.*, 2014). The genomic actions of estrogen are mediated through interaction with the two canonical estrogen receptors (ER)—ERα and ERβ (also known as ESR1 and ESR2)—which are part of the nuclear receptor family of ligand-activated transcription factors (Charitidi *et al.*, 2009). Ligand-bound ERα and ERβ modulate transcription by binding to estrogen response elements (ERE), sequences of DNA that are recognized by the receptor. 17β-estradiol, which is the most potent form of estrogen produced in the body, shares a similar affinity for ERα and ERβ, which both bind to the same ERE (Blair *et al.*, 2000; Gruber *et al.*, 2002; Heldring *et al.*, 2007).

ERα and ERβ are both detected in the human, mouse, and rat inner ears in partially overlapping patterns of expression. A human study focused on the localization of estrogen receptors in females detected protein expression of only ERα between gestational weeks 14–20, which localized to the SGN. In contrast, both ERα and ERβ were expressed in the mature inner ear, localizing to the SGN and stria vascularis, respectively (Stenberg *et al.*, 2001). In the mouse inner ear, the reported expression patterns were broader (Motohashi *et al.*, 2010; Stenberg *et al.*, 1999). Stenberg *et al.* (1999) showed that ERα localizes to both the inner hair cells (IHC) and OHCs, type-1 and type-2 SGNs, Reissner's membrane, the stria vascularis, and the spiral ligament. However, ERβ localizes to the IHCs but not OHCs, Reissner's membrane, and the stria vascularis, with a lower expression in type-1 and type-2 SGNs (Stenberg *et al.*, 1999). Motohashi *et al.* (2010) reported similar expression patterns of ERα and ERβ in the mouse inner ear with the exception that they also found expression of ERβ in the OHCs (Motohashi *et al.*, 2010). Interestingly, while the expression patterns of ERα and ERβ did not vary by age or sex, the immunoreactivity of ERα was stronger in young female compared to young male mice and decreased for both receptors with age, in both sexes (Motohashi *et al.*, 2010). Stenberg *et al.* (1999) demonstrated similar expression patterns of the ERs in the rat inner ear, but also demonstrated ERβ expression in the OHC and pillar cells. Furthermore, the immunoreactivity of the antibody for ERβ in the SGN was more intense in the rat inner ear compared to the mouse (Stenberg *et al.*, 1999).

The mRNA expression of ERs in the cochlea may be modulated by hormone levels, and has been shown to fluctuate during the normal menstrual cycle and after ovariectomy (Charitidi *et al.*, 2012). In female CBA/Ca mice, mRNA levels of ERα but not ERβ decreased significantly in the cochlea during the proestrous phase when compared to the metestrous and estrous phases. Chronic 17β-estradiol treatment in ovariectomized CBA/Ca mice leads to a downregulation of ERα mRNA levels in a similar fashion when compared to ovariectomized animals not receiving treatment. No effect was seen on ERβ mRNA levels after ovariectomy and chronic 17β-estradiol treatment (Charitidi *et al.*, 2012).

Analysis of mice with targeted deletions of ERα (ERKO mice), ERβ (BERKO mice), and aromatase (ARKO mice)—the enzyme responsible for the conversion of testosterone to estrogen—demonstrates that ERβ is crucial for maintenance of hearing, and further illuminates the role of estrogen signaling in hearing. A study of hearing thresholds in BERKO mice determined that while there were no differences in ABR thresholds of BERKO mice compared to wild-type (WT) controls at 3 months of age, 12 month-old WT mice displayed significantly lower thresholds at all frequencies tested (12 month-old BERKO mice were deaf) (Simonoska *et al.*, 2009). BERKO mice also experienced more severe OHC and IHC loss along the entire length of the cochlea, especially in the basal turn. Additionally, BERKO mice also displayed increased spiral ganglion atrophy along the entire length of the cochlea in comparison to WT mice. In support

of the role of ERβ in the maintenance of hearing, suppressing estrogen signaling with tamoxifen—which demonstrates ERβ-mediated antagonistic effects—has been shown to negatively impact contralateral suppression of DPOAEs in mice (Barkhem *et al.*, 1998; Thompson *et al.*, 2006). Contralateral suppression of DPOAEs is thought to be a protective mechanism that enhances cochlear function, and it has been demonstrated that a decrease in contralateral suppression often precedes an age-related decline in DPOAEs (Thompson *et al.*, 2006).

Importantly, from a translational perspective, ERβ but not ERα also mediates neuroprotection following acoustic trauma (Meltser *et al.*, 2008). BERKO mice experience more severe temporary threshold shift (TTS) after acoustic injury in comparison to ERKO or WT mice, whereas ERKO male and female mice experience a TTS similar to WT. This suggests that ERβ and not ERα can protect against acoustic injury. Interestingly, no sex-differences in threshold shifts were detected between male and female BERKO mice. The same study demonstrated that the ERβ-selective agonist DPN (2, 3-bis (4-hydroxyphenyl)-propionitrile) protects against the same acoustic injury at some of the frequencies tested when administered to female WT mice, providing further evidence of the protective effects of ERβ.

D. Estrogen related receptors and hearing

In addition to the two canonical ERs ERα and ERβ, a family of estrogen related receptors (ESRR or ERR)—ERRα, ERRβ, and ERRγ—may also play a role in hearing physiology. Although the ERRs share sequence and structural homology with the canonical ERs, estrogens are not an endogenous ligand. In fact, ERRs are orphan receptors and can be constitutively active and regulate transcription without ligand binding (Saito and Cui, 2018). The search for endogenous ligands of ERRs thus far, has largely proven unfruitful, but a recently published study identified cholesterol as an endogenous ligand of ERRα (Wei *et al.*, 2016). Regardless, even in the absence of ligand, ERRs can bind to ERE in addition to a set of estrogen-related response elements (ERRE). Interestingly, ERα but not ERβ has also demonstrated the ability to bind to ERRE (Saito and Cui, 2018).

Numerous studies have clearly demonstrated that ERRβ is particularly important for hearing and normal cochlear physiology (Bhatt *et al.*, 2016; Chen and Nathans, 2007; Collin *et al.*, 2008; Lee *et al.*, 2011; Saïd *et al.*, 2011). In the early postnatal cochlea ERRβ is expressed in the endolymph-secreting marginal cells of the stria vascularis, but not in the sensory cells of the cochlea, partially regulating the expression of ion channels and ion transporters in these cells (Chen and Nathans, 2007). Conditional knockout (cKO) of ERRβ from the lateral wall using *Sox2*-Cre results in a concomitant loss of mRNA transcripts encoding potassium channels (KCNQ1 and KCNE1) and a subunit of the Na/K ATPase (Chen and Nathans, 2007). These cKO mice also display severe auditory impairment, with ABR thresholds greater than 100 dB SPL. Furthermore, mutations of ERRβ underlie DFNB35 (autosomal-recessive, nonsyndromic hearing impairment) and a single nucleotide polymorphism (SNP) in the gene encoding ERRβ in humans is associated with increased TTS after exposure to a 10 min narrow-band noise centered at 2 kHz (Bhatt *et al.*, 2016; Collin *et al.*, 2008; Lee *et al.*, 2011; Saïd *et al.*, 2011).

Although less is known about ERRγ—which is expressed in a variety of cell types in the female mouse inner ear including IHCs and OHCs—a British cohort study correlated a SNP in the gene encoding the ERRγ receptor with increased risk of ARHL, but only in females (Nolan *et al.*, 2013). Furthermore, the same authors demonstrated that ERRγ KO mice have elevated thresholds compared to WT and heterozygous mice, and that female KO have worse hearing than males at 12 weeks of age (Nolan *et al.*, 2013). In addition, a recent clinical report implicated disruption of the gene encoding ERRγ on chromosome 1 in the case of a female born with moderate bilateral SNHL with an accompanying developmental delay (Schilit *et al.*, 2016).

IV. CONCLUSIONS

There is abundant and robust evidence to support the conclusion that estrogen not only modulates hearing and hearing physiology, but also that estrogen and its signaling pathways are protective and required for normal hearing and maintenance of hearing (e.g., the amelioration of age-related hearing loss and noise-induced hearing loss) in both sexes.

Estrogen levels correlate with hearing thresholds during the menstrual cycle, and hearing thresholds decline rapidly in post-menopausal women when levels of serum estrogen decline drastically. Women with Turner syndrome, a disease characterized by reduced serum estrogen levels, are more likely to suffer from hearing loss, and begin to suffer from hearing loss earlier in life. Females are protected from ARHL and NIHL in comparison to males, and female mice display decreased ABR threshold shifts following a noise exposure.

Evidence of the modulatory and protective role of estrogen is also abundant at the molecular level. Estrogen receptors and estrogen-related receptors are expressed in the inner ears of mice and humans in a variety of cells types. Of significance, the expression patterns of ERα and ERβ appear to be more widespread in mice than in humans, highlighting the need for additional studies to localize these proteins in non-human primates. From a functional perspective, most of the otoprotective effects of estrogen are thought to be mediated by ERβ, as mice with a deletion of ERβ are more susceptible to noise trauma and suffer from accelerated age-related hair cell loss and spiral ganglion deterioration. In support of ERβ's role in hearing protection, WT female mice administered DPN, a selective ERβ agonist, displayed reduced threshold shifts following noise exposure.

Studies of the family of estrogen-related receptors demonstrate disruption of ERRβ and ERRγ, both of which localize to the inner ear of mice, negatively impact hearing health and physiology. Although estrogens are not endogenous ligands of the ERRs, ERRs can modulate gene expression by binding to the same ERE that are also bound by ERs. Evidence also exists to suggest that some ERRs may interact

directly with ERs and modulate the classical estrogen pathways (Tanida *et al.*, 2015). Additionally, estrogen—a known regulator of calcium mobilization—may contribute to more rapid, genomic and non-genomic changes in cellular physiology via a G-protein coupled receptor, GPR30 (also called GPER1). While rapid activation of GPR30 by estrogen influences gene expression resulting in both short-term and long-term effects on transcription, its actions in the inner ear are unknown (Prossnitz, 2009).

How estrogen confers protection, and how estrogen contributes to normal hearing physiology and its maintenance is far from being completely understood. Despite this, natural estrogen signaling is particularly potent, and the therapeutic potential is large and untapped. Fortuitously, signaling through ERβ—rather than signaling via ERα, which may more heavily underly estrogen's carcinogenic potential—appears to be more important for hearing preservation in protection (Clemons and Goss, 2001). In order to harness the full potential of the estrogen signaling pathway on hearing preservation, sex differences in hearing including estrogen's role in the modulation and protection of hearing must continue to be investigated.

As the investigation into the effects of estrogen signaling—and potentially other hormones—on hearing and hearing physiology continues, experimental methods will need to be refined. Studies using full knockout animal models are valuable for understanding the roles of hormones and their signaling pathways, but care must be taken not to overdraw conclusions about effects on the physiologic system (in this case the auditory system) without due consideration of the indirect and unknown effects caused by a systemic loss of a particular hormone or hormone receptor (McCarthy and Arnold, 2011). Here, the generation of conditional knockouts will prove absolutely critical for the elucidation of a precise and confident understanding of hormonal modulation of hearing. The use of conditional knockouts will also provide more translationally relevant results applicable to therapeutic development.

In addition to the use of conditional knockouts to study the effects of estrogen and other hormones on the auditory system, prenatal masculinization and feminization studies that experimentally alter the hormonal milieu during development may fill in additional knowledge gaps and provide a clearer picture of sex differences in auditory physiology. In fact, studies that have utilized prenatal masculinization and feminization as an experimental tool have begun to demonstrate that sex differences in auditory physiology, are, in part, shaped by prenatal hormone exposure (McFadden *et al.*, 2009b). For example, there is evidence that the previously mentioned sex difference in the prevalence of SOAE exists at birth in humans (Qi *et al.*, 2014). Differences in prenatal 'molding' of auditory physiology may explain why exogenous estrogen delivery to gonadectomized males does not confer protection from a PTS-inducing noise exposure (manuscript in preparation). Perhaps the male auditory system has lost the ability, through prenatal androgen exposure, to respond to estrogen. This is all speculative, of course, but highlights the need for an understanding of the role of hormones in the early developmental events of the auditory system and its physiology.

ACKNOWLEDGMENTS

We would like to thank Dr. Béatrice Milon and Dr. Maggie Matern for critically reviewing the manuscript, and acknowledge our funding sources Nos. NIDCD-R01DC013817 (R.H.), CDMRP-MR130240 (R.H.), and NHLBI-HL129138 (J.A.M.).

Abdala, C., and Visser-Dumont, L. (**2001**). "Distortion product otoacoustic emissions: A tool for hearing assessment and scientific study," Volta Rev. **103**(4), 281–302.

Allen, P. D., and Eddins, D. A. (**2010**). "Presbycusis phenotypes form a heterogeneous continuum when ordered by degree and configuration of hearing loss," Hear. Res. **264**(1–2), 10–20.

Barkhem, T., Carlsson, B., Nilsson, Y., Enmark, E., Gustafsson, J., and Nilsson, S. (**1998**). "Differential response of estrogen receptor alpha and estrogen receptor beta to partial estrogen agonists/antagonists," Mol. Pharmacol. **54**(1), 105–112.

Bhatt, I., Phillips, S., Richter, S., Tucker, D., Lundgren, K., Morehouse, R., and Henrich, V. (**2016**). "A polymorphism in human estrogen-related receptor beta (ESRRβ) predicts audiometric temporary threshold shift," Int. J. Audiol. **55**(10), 571–579.

Bishop, C. E., Spankovich, C., Lin, F. R., Seals, S. R., Su, D., Valle, K., and Schweinfurth, J. M. (**2019**). "Audiologic profile of the jackson heart study cohort and comparison to other cohorts," Laryngoscope **129**, 1–7.

Björnström, L., and Sjöberg, M. (**2005**). "Mechanisms of estrogen receptor signaling: Convergence of genomic and nongenomic actions on target genes," Mol. Endocrinol. **19**(4), 833–842.

Blair, R., Fang, H., Branham, W. S., Hass, B. S., Dial, S. L., Moland, C. L., Tong, W., Shi, L., Perkins, R., and Sheehan, D. M. (**2000**). "The estrogen receptor relative binding affinities of 188 natural and xenochemicals: Structural diversity of ligands," Toxicol. Sci **54**(1), 138–153.

Bonnard, Å., Sahlin, L., Hultcrantz, M., and Simonoska, R. (**2013**). "No direct nuclear effect of progesterone in the inner ear: Other possible pathways," Acta Oto-Laryngol. **133**(12), 1250–1257.

Brownell, W. E. (**1990**). "Outer hair cell electromotility and otoacoustic emissions," Ear Hear. **11**(2), 82–92.

Caruso, S., Maiolino, L., Agnello, C., Garozzo, A., Di Mari, L., and Serra, A. (**2003**). "Effects of patch or gel estrogen therapies on auditory brainstem response in surgically postmenopausal women: A prospective, randomized study," Fertil. Steril. **79**(3), 556–561.

Charitidi, K., Meltser, I., and Canlon, B. (**2012**). "Estradiol treatment and hormonal fluctuations during the estrous cycle modulate the expression of estrogen receptors in the auditory system and the prepulse inhibition of acoustic startle response," Endocrinology **153**(9), 4412–4421.

Charitidi, K., Meltser, I., Tahera, Y., and Canlon, B. (**2009**). "Functional responses of estrogen receptors in the male and female auditory system," Hear. Res. **252**, 71–78.

Chen, J., and Nathans, J. (**2007**). "Estrogen-related receptor β/NR3B2 controls epithelial cell fate and endolymph production by the Stria Vascularis," Developmental Cell **13**(3), 325–337.

Clemons, M., and Goss, P. (**2001**). "Estrogen and the risk of breast cancer," N. Engl. J. Med. **344**(4), 276–285.

Collin, R. W. J., Kalay, E., Tariq, M., Peters, T., van der Zwaag, B., Venselaar, H., Oostrik, J., Lee, K., Ahmed, Z., Caylan, R., Li, Y., Spierenburg, H., Eyupoglu, E., Heister, A., Riazuddin, S., Bahat, E., Ansar, M., Arslan, S., Wollnik, B., Brunner, H., Cremers, C., Karaguzel, A., Ahmed, W., Cremers, F., Vriend, G., Friedman, T., Riazuddin, S., Leal, S., and Kremer, H. (**2008**). "Mutations of ESRRB encoding estrogen-related receptor beta cause autosomal-recessive nonsyndromic hearing impairment DFNB35," Am. J. Hum. Genet. **82**(1), 125–138.

Crowson, M. G., Hertzano, R., Tucci, D., and Neurotol, O. (**2017**). "Emerging therapies for sensorineural hearing loss HHS public access author manuscript," Otol. Neurotol. **38**(6), 792–803.

Cruickshanks, K. J., Wiley, T. L., Tweed, T. S., Klein, B. E. K., Klein, R., Mares-Perlman, J. A., and Nondahl, D. M. (**1998**). "Prevalence of hearing loss in older adults in Beaver Dam, Wisconsin: The epidemiology of hearing loss study," Am. J. Epidemiol. **148**(9), 879–886.

Curhan, S. G., Eliassen, A. H., Eavey, R. D., Wang, M., Lin, B. M., and Curhan, G. C. (**2017**). "Menopause and postmenopausal hormone therapy and risk of hearing loss," Menopause **24**(9), 1049–1056.
Da Silva Souza, D., Luckwu, B., De Andrade, W. T. L., De Figueiredo Pessoa, L. S., Do Nascimento, J. A., and Da Rosa, M. R. D. (**2017**). "Variation in the hearing threshold in women during the menstrual cycle," Int. Arch. Otorhinolaryngol. **21**(4), 323–328.
Deafness and hearing loss. (**2018**). Retrieved June 8, 2018, from World Health Organization website http://www.who.int/news-room/fact-sheets/detail/deafness-and-hearing-loss (Last viewed January 6, 2019).
Frisina, R. D. (**2012**). "Hormones and hearing: Too much or too little of a good thing can be ototoxic," Semin. Hear. **33**(3), 231–241.
Grinn, S. K., Wiseman, K. B., Baker, J. A., and Le Prell, C. G. (**2017**). "Hidden hearing loss? No effect of common recreational noise exposure on cochlear nerve response amplitude in humans," Front. Neurosci. **11**, 465.
Gruber, C. J., Tschugguel, W., Schneeberger, C., and Huber, J. C. (**2002**). "Production and actions of estrogens," N. Engl. J. Med. **346**(5), 340–352.
Guimaraes, P., Frisina, S. T., Mapes, F., Tadros, S. F., Frisina, D. R., and Frisina, R. D. (**2006**). "Progestin negatively affects hearing in aged women," Proc. Natl. Acad. Sci. USA **103**(38), 14246–14249.
Guimaraes, P., Zhu, X., Cannon, T., Kim, S., and Frisina, R. D. (**2004**). "Sex differences in distortion product otoacoustic emissions as a function of age in CBA mice," Hear. Res. **192**(1-2), 83–89.
Hederstierna, C., Hultcrantz, M., Collins, A., and Rosenhall, U. (**2007**). "Hearing in women at menopause. Prevalence of hearing loss, audiometric configuration and relation to hormone replacement therapy," Acta Oto-Laryngol. **127**(2), 149–155.
Hederstierna, C., Hultcrantz, M., and Rosenhall, U. (**2009**). "Estrogen and hearing from a clinical point of view; characteristics of auditory function in women with Turner syndrome," Hear. Res. **252**, 3–8.
Heldring, N., Pike, A., Andersson, S., Matthews, J., Cheng, G., Hartman, J., Tujague, M., Ström, A., Treuter, E., Warner, M., and Gustafsson, J.-Å. (**2007**). "Estrogen receptors: How do they signal and what are their targets," Physiol. Rev. **87**(3), 905–931.
Henry, K. R. (**2004**). "Males lose hearing earlier in mouse models of late-onset age-related hearing loss; females lose hearing earlier in mouse models of early-onset hearing loss," Hear. Res. **190**, 141–148.
Hultcrantz, M., Stenberg, A. E., Fransson, A., and Canlon, B. (**2000**). "Characterization of hearing in an X,0 'Turner mouse'," Hear. Res. **143**, 182–188.
Hultcrantz, M., and Sylven, L. (**1996**). "Turner's syndrome and hearing disorders in women aged 16–34," Hear. Res. **103**, 69–74.
Jerger, J., and Hall, J. (**1980**). Otolaryngol., Head Neck Surg. **106**(7), 387–391.
Jönsson, R., Rosenhall, U., Gause-Nilsson, I., and Steen, B. (**1998**). "Auditory function in 70- and 75-year-olds of four age cohorts. A cross-sectional and time-lag study of presbyacusis," Scand. Audiol. **27**(2), 81–93.
Kemp, D. T. (**2002**). "Otoacoustic emissions, their origin in cochlear function, and use," Br. Med. Bull. **63**, 223–241.
Kemp, D. T. (**2008**). "Otoacoustic emissions: Concepts and origins," in *Active Processes and Otoacoustic Emissions in Hearing*, edited by G. Manley, R. Fay, and A. Popper (Springer-Verlag, New York), pp. 1–38.
Kilicdag, E. B., Yavuz, H., Bagis, T., Tarim, E., Erkan, A. N., and Kazanci, F. (**2004**). "Effects of estrogen therapy on hearing in postmenopausal women," Am. J. Obstet. Gynecol. **190**(1), 77–82.
Kim, S. H., Kang, B. M., Chae, H. D., and Kim, C. H. (**2002**). "The association between serum estradiol level and hearing sensitivity in postmenopausal women," Obstet. Gynecol. **99**(5), 726–730.
Lauer, A. M., and Schrode, K. M. (**2017**). "Sex bias in basic and preclinical noise-induced hearing loss research," Noise Health **19**(90), 207–212.
Lee, K., Khan, S., Ansar, M., Santos-Cortez, R. L. P., Ahmad, W., and Leal, S. M. (**2011**). "A novel ESRRB deletion is a rare cause of autosomal recessive nonsyndromic hearing impairment among Pakistani families," Genet. Res. Int. **2011**, 368915.
Li, C.-M., Zhao, G., Hoffman, H. J., Town, M., and Themann, C. L. (**2018**). "Hearing disability prevalence and risk factors in two recent national surveys," Am. J. Prev. Med. **55**(3), 326–335.
Lin, F. R., Niparko, J. K., and Ferrucci, L. (**2011**). "Hearing loss prevalence in the United States," Arch. Intern. Med. **171**(20), 1851.
Liu, J., Wang, D., Xiaoting, L., and Wang, N. (**2017**). "Association between sex and speech auditory brainstem responses in adults, and relationship to sex hormone levels," Med. Sci. Monit. **23**, 2275–2283.
Lotfi, Y., and Zamiri Abdollahi, F. (**2012**). "Age and gender effects on auditory brain stem response (ABR)," Iran. Rehab. J. **10**(16), 30–36.
McCarthy, M. M., and Arnold, A. P. (**2011**). "Reframing sexual differentiation of the brain," Nat. Neurosci. **14**(6), 677–683.
McFadden, D. (**1998**). "Sex differences in the auditory system," Dev. Neuropsychol. **14**(2/3), 261–298.
McFadden, D. (**2009**). "Masculinization of the mammalian cochlea," Hear. Res. **252**(1-2), 37–48.
McFadden, D. (**1993**). "A masculinizing effect on the auditory systems of human females having male co-twins," Proc. Natl. Acad. Sci. USA **90**(24), 11900–11904.
McFadden, D., Martin, G. K., Stagner, B. B., and Maloney, M. M. (**2009a**). "Sex differences in distortion-product and transient-evoked otoacoustic emissions compared," J. Acoust. Soc. Am. **125**(1), 239–246.
McFadden, D., Pasanen, E. G., Raper, J., Lange, H. S., and Wallen, K. (**2006**). "Sex differences in otoacoustic emissions measured in rhesus monkeys (*Macaca mulatta*)," Horm. Behav. **50**(2), 274–284.
McFadden, D., Pasanen, E. G., Valero, M. D., Roberts, E. K., and Lee, T. M. (**2009b**). "Effect of prenatal androgens on click-evoked otoacoustic emissions in male and female sheep (*Ovis aries*)," Horm. Behav. **55**(1), 98–105.
McFadden, S. L., Zheng, X. Y., and Ding, D. L. (**2000**). "Conditioning-induced protection from impulse noise in female and male chinchillas," J. Acoust. Soc. Am. **107**(4), 2162–2168.
Meltser, I., Tahera, Y., Simpson, E., Hultcrantz, M., Charitidi, K., Gustafsson, J. Å., and Canlon, B. (**2008**). "Estrogen receptor Beta protects against acoustic trauma in mice," J. Clin. Invest. **118**(4), 1563–1570.
Miller, J. (**2007**). "Sex differences in the length of the organ of Corti in humans," J. Acoust. Soc. Am. **121**(4), 151–155.
Milon, B., Mitra, S., Song, Y., Margulies, Z., Casserly, R., Drake, V., Mong, J. A., Depireux, D. A., and Hertzano, R. (**2018**). "The impact of biological sex on the response to noise and otoprotective therapies against acoustic injury in mice," Biol. Sex Differ. **9**(12), 1–14.
Motohashi, R., Takumida, M., Shimizu, A., Konomi, U., Fujita, K., Hirakawa, K., Suzuki, M., and Anniko, M. (**2010**). "Effects of age and sex on the expression of estrogen receptor α and β in the mouse inner ear," Acta Oto-Laryngol. **130**, 204–214.
Nolan, L. S., Maier, H., Hermans-Borgmeyer, I., Girotto, G., Ecob, R., Pirastu, N., Cadge, B. A., Hübner, C., Gasparini, P., Strachan, D. P., Davis, A., and Dawson, S. J. (**2013**). "Estrogen-related receptor gamma and hearing function: Evidence of a role in humans and mice," Neurobiol. Aging **34**(8), 2077.e11–2077.e18.
Pearson, J. D., Morrell, C. H., Gordon-Salant, S., Brant, L. J., Metter, E. J., Klein, L. L., and Fozard, J. L. (**1995**). "Gender differences in a longitudinal study of age-associated hearing loss," J. Acoust. Soc. Am. **97**(2), 1196–1205.
Penner, M. J., and Zhang, T. (**1996**). "Prevalence of spontaneous otoacoustic emissions in adults revisited," Hear. Res. **103**, 28–34.
Price, K., Zhu, X., Guimaraes, P. F., Vasilyeva, O. N., and Frisina, R. D. (**2009**). "Hormone replacement therapy diminishes hearing in perimenopausal mice," Hear. Res. **252**(1-2), 29–36.
Prossnitz, E. R. (**2009**). "Mechanisms of estrogen signaling and gene expression via GPR30," Mol. Cell. Endocrinol. **308**(1-2), 32–38.
Qi, B., Cheng, X., En, H., Huang, L., and Zhang, L. (**2014**). "Characterization of spontaneous otoacoustic emissions in full-term newborns," Int. J. Pediatr. Otorhinolaryng. **78**(12), 2286–2291.
Sabo, D. L., Durrant, J. D., Curtin, H., Boston, J. R., and Rood, S. (**1992**). "Correlations of neuroanatomical measures to auditory brain stem response latencies," Ear Hear. **13**(4), 213–222.
Saïd, M. B., Ayedi, L., Mnejja, M., Hakim, B., Khalfallah, A., Charfeddine, I., Khifagi, C., Turki, K., Ayadi, H., Benzina, Z., Ghorbel, A., Del Castillo, I., Masmoudi, S., and Hmani-Aifa, M. (**2011**). "A novel missense mutation in the ESRRB gene causes DFNB35 hearing loss in a Tunisian family," Eur. J. Med. Genet. **54**(6), 535–541.
Saito, K., and Cui, H. (**2018**). "Emerging roles of estrogen-related receptors in the brain: Potential interactions with estrogen signaling," Int. J. Mol. Sci. **19**(4), 1091.
Sato, H., Sando, I., and Takahashi, H. (**1991**). "Sexual dimorphism and development of the human cochlea: Computer 3-D measurement," Acta Oto-Laryngol. **111**(6), 1037–1040.
Schilit, S. L., Currall, B. B., Yao, R., Hanscom, C., Collins, R. L., Pillalamarri, V., Lee, D.-Y., Kammin, T., Zepeda-Mendoza, C. J., Mononen, T., Nolan, L. S., Gusella, J. F., Talkowski, M. E., Shen, J., and Morton, C. C. (**2016**). "Estrogen-related receptor gamma implicated in a

phenotype including hearing loss and mild developmental delay," Eur. J. Hum. Genet.**24**(11), 1622–1626.
Simonoska, R., Stenberg, A. E., Duan, M., Yakimchuk, K., Fridberger, A., Sahlin, L., Gustafsson, J.-A., and Hultcrantz, M. (**2009**). "Inner ear pathology and loss of hearing in estrogen receptor- deficient mice," J. Endocrinol. **201**(3), 397–406.
Stenberg, A. E., Wang, H., Fish Iii, J., Schrott-Fischer, A., Sahlin, L., and Hultcrantz, M. (**2001**). "Estrogen receptors in the normal adult and developing human inner ear and in Turner's syndrome," Hear. Res. **157**(1–2), 87–92.
Stenberg, A. E., Wang, H., Sahlin, L., and Hultcrantz, M. (**1999**). "Mapping of estrogen receptors α and β in the inner ear of mouse and rat," Hear. Res. **136**, 29–34.
Stevens, G., Flaxman, S., Brunskill, E., Mascarenhas, M., Mathers, C. D., and Finucane, M. (**2011**). "Global and regional hearing impairment prevalence: An analysis of 42 studies in 29 countries," Eur. J. Public Health **23**(1), 146–152.
Szanto, C., and Ionescu, M. (**1983**). "Influence of age and sex on hearing threshold levels in workers exposed to different intensity levels of occupational noise," Audiol. **22**(4), 339–356.
Tanida, T., Matsuda, K. I., Yamada, S., Hashimoto, T., and Kawata, M. (**2015**). "Estrogen-related receptor β reduces the subnuclear mobility of estrogen receptor α and suppresses estrogen-dependent cellular function," J. Biol. Chem. **290**(19), 12332–12345.
Themann, C., Suter, A., and Stephenson, M. (**2013**). "National research agenda for the prevention of occupational hearing loss—Part 1," Semin. Hear. **34**(03), 145–207.
Thompson, S. K., Zhu, X., and Frisina, R. D. (**2006**). "Estrogen blockade reduces auditory feedback in CBA mice," Otolaryngol., Head Neck Surg. **135**(1), 100–105.
Veterans Benefits Administration Reports Annual Benefits Report Fiscal Year 2017. (**2017**). United States Department of Veteran Affairs. Retrieved from https://www.benefits.va.gov/REPORTS/abr/.
Villavisanis, D. F., Schrode, K. M., and Lauer, A. M. (**2018**). "Sex bias in basic and preclinical age-related hearing loss research," Biol. Sex Differ. **9**(1), 23.
Vrtačnik, P., Ostanek, B., Mencej-Bedrač, S., and Marc, J. (**2014**). "The many faces of estrogen signaling," Biochem. Med. **24**(3), 329–342.
Wei, W., Schwaid, A. G., Wang, X., Chu, Q., Saghatelian, A., Wan, Y., Wang, X., and Chen, S. (**2016**). "Ligand activation of ERRα by cholesterol mediates statin and bisphosphonate effects," Cell Metab. **23**, 479–491.
Williamson, T. T., Ding, B., Zhu, X., and Frisina, R. D. (**2019**). "Hormone replacement therapy attenuates hearing loss: Mechanisms involving estrogen and the IGF-1 pathway," Aging Cell **18**(3), e12939.
Yankaskas, K. (**2013**). "Prelude: Noise-induced tinnitus and hearing loss in the military," Hear. Res. **295**, 3–8.
Zhang, J., Zhang, T., Yu, L., Ruan, Q., Yin, L., Liu, D., Zhang, H., Bai, W., and Ren, Z. (**2018**). "Effects of ovarian reserve and hormone therapy on hearing in premenopausal and postmenopausal women: A cross-sectional study," Maturitas **111**, 77–81.
Zündorf, I. C., Karnath, H. O., and Lewald, J. (**2011**). "Male advantage in sound localization at cocktail parties," Cortex **47**(6), 741–749.

Untangling the genomics of noise-induced hearing loss and tinnitus: Contributions of *Mus musculus* and *Homo sapiens*

Royce E. Clifford, Ronna Hertzano, and Kevin K. Ohlemiller

Citation: The Journal of the Acoustical Society of America **146**, 4007 (2019); doi: 10.1121/1.5132552
View online: https://doi.org/10.1121/1.5132552
View Table of Contents: https://asa.scitation.org/toc/jas/146/5
Published by the Acoustical Society of America

Untangling the genomics of noise-induced hearing loss and tinnitus: Contributions of *Mus musculus* and *Homo sapiens*

Royce E. Clifford,[1,a)] Ronna Hertzano,[2] and Kevin K. Ohlemiller[3]
[1]*Division of Otolaryngology–Head and Neck Surgery, University of California School of Medicine, 9500 Gilman Drive, La Jolla, California 92093, USA*
[2]*Department of Otorhinolaryngology–Head and Neck Surgery, University of Maryland School of Medicine, James T. Frenkil Building, 16 South Eutaw Street, Suite 500, Baltimore, Maryland 21201, USA*
[3]*Washington University School of Medicine, Department of Otolaryngology, Central Institute for the Deaf at Washington University School of Medicine, Fay and Carl Simons Center for Hearing and Deafness, 660 South Euclid Avenue, Saint Louis, Missouri 63110, USA*

(Received 7 March 2019; revised 7 June 2019; accepted 24 June 2019; published online 27 November 2019)

Acoustic trauma is a feature of the industrial age, in general, and mechanized warfare, in particular. Noise-induced hearing loss (NIHL) and tinnitus have been the number 1 and number 2 disabilities at U.S. Veterans hospitals since 2006. In a reversal of original protocols to identify candidate genes associated with monogenic deafness disorders, unbiased genome-wide association studies now direct animal experiments in order to explore genetic variants common in *Homo sapiens*. However, even these approaches must utilize animal studies for validation of function and understanding of mechanisms. Animal research currently focuses on genetic expression profiles since the majority of variants occur in non-coding regions, implying regulatory divergences. Moving forward, it will be important in both human and animal research to define the phenotypes of hearing loss and tinnitus, as well as exposure parameters, in order to extricate genes related to acoustic trauma versus those related to aging. It has become clear that common disorders like acoustic trauma are influenced by large numbers of genes, each with small effects, which cumulatively lead to susceptibility to a disorder. A polygenic risk score, which aggregates these small effect sizes of multiple genes, may offer a more accurate description of risk for NIHL and/or tinnitus. © *2019 Acoustical Society of America*.
https://doi.org/10.1121/1.5132552

[CGL] Pages: 4007–4019

I. INTRODUCTION

Chronic noise exposure is a side-effect of the industrial age and mechanized warfare, and noise-induced hearing loss (NIHL) is second only to age-related hearing impairment (ARHI) as a sensory injury. An estimated 22×10^6 workers in the U.S. are exposed to noise greater than 85 dBA time-weighted average (TWA), and 18% of these have hearing loss, defined as pure-tone average threshold of 25 dB or more in either ear across 1, 2, 3, and 4 kHz (National Institute of Occupational Safety and Health Standards, 1998; Masterson *et al.*, 2013). At least 20% of Europeans and 10% of Americans are noise-exposed for half of their workday (Konings *et al.*, 2009a). Worldwide, 16%–24% of hearing loss is estimated to be noise-related (Feder *et al.*, 2017). Hearing loss among U.S. teenagers, which can compromise educational achievement and communication skills (Arlinger, 2003; Gomaa *et al.*, 2014; Shargorodsky, 2010), increased significantly from 3.5% to 5.3% between 1994 and 2006, possibly due to the effect of loud music through personal devices (Gregory *et al.*, 1994; Shargorodsky, 2010). Besides impacting military operations, hearing loss is significantly associated with depression, isolation, reduced social activity, and cognitive decline (Dawes *et al.*, 2015).

Currently, there is no prevention for ARHI; thus, it is important to distinguish between noise-induced trauma and age-related audiogram changes in order to ascertain the proportion of preventable damage and establish phenotype definitions that drive genomic studies. While age-related genome-wide association (GWAS) has routinely excluded those under 50 years old (Hoffmann *et al.*, 2016; Vuckovic *et al.*, 2018), studies indicate that pure-tone averages decline linearly beginning in a person's 30s and 40s (Dawes *et al.*, 2014; Moore *et al.*, 2014), making it difficult to distinguish NIHL from ARHI.

Unlike the inescapable ARHI, NIHL is avoidable with a combination of engineering solutions, administrative directives, i.e., limitation of time spent in noisy industries or turning down loud music, and personal protective devices such as earplugs and earmuffs (Yankaskas, 2013). A "noise notch" at 3, 4, and 6 kHz can differentiate the two, compared to a "down-sloping" audiogram with loss increasing at higher frequencies (Rabinowitz *et al.*, 2006), and this notch needs to be quantified in order to assess it in any GWAS analysis. In order to identify acoustic-trauma-susceptible genes versus age-related changes, it will be necessary to compare GWAS results from a young exposed population, the military, or teens who listen to loud music, for example, to an older population relatively unexposed to noise.

While audiograms give some indication of distinction between ARHI and NIHL, tinnitus etiologies are distinguishable by history only due to the subjective nature of ringing in

a)Electronic mail: r2clifford@ucsd.edu

the ears. A separate auditory disorder with different sequelae but emanating from the same injury, tinnitus prevalence is estimated at 50×10^6 cases in the U.S., with 16×10^6 adults reporting ringing in their ears on a daily basis (Shargorodsky *et al.*, 2010). Tinnitus and NIHL have been the Veteran Affair's (VA) number 1 and number 2 service-connected disabilities since 2006, now costing over two billion dollars per year in compensation, and in 2017 over 2.6×10^6 veterans received disability payments for auditory damage (U.S. Department of Veterans Affairs, 2018). Traumatic brain injury (TBI), the signature injury in recent wars, more than doubles the risk of tinnitus (Yurgil *et al.*, 2016).

Operationally, tinnitus impacts military mission completion in ways unconnected to hearing loss. Tinnitus leads to slower reaction times, poorer accuracy while dual tasking, anxiety, depression, and increased suicide risk (Asplund, 2003; Crönlein *et al.*, 2016; Gomaa *et al.*, 2014; Gopinath *et al.*, 2010; Rossiter *et al.*, 2006; Schecklmann *et al.*, 2015; Tegg-Quinn *et al.*, 2016; Trevis *et al.*, 2016; Vogel *et al.*, 2014). Even with normal hearing, tinnitus degrades cognition, dichotic listening, and speech-in-noise, an important factor during combat operations where the signal-to-noise ratio is diminished (Degeest *et al.*, 2017; Jafari *et al.*, 2012; Jain and Sahoo, 2014). It affects the lives of veterans both during and after separation from service. Sleep disturbance is the second most cited aeromedical factor in naval aviation mishaps and hazardous reports (HAZREPS), and 76% of tinnitus subjects complain of sleep dysfunction (Schecklmann *et al.*, 2015). Sleep degradation is associated with slower reaction times and increased mistakes in recognition of targets as friend or foe (Smith *et al.*, 2019).

Genes and genetic pathways that underlie susceptibility to tinnitus have not been identified, nor is there a cure or definitive treatment for either disorder, and we remain unable to predict the susceptibility of any individual to tinnitus or NIHL. While NIHL is often comorbid with tinnitus, the two disorders appear to have a separate pathophysiologic architecture. Injuries leading to both disorders appear to originate in the cochlea with primary neural degeneration in the high threshold cochlear-nerve fibers (Kujawa and Liberman, 2015). Hearing loss studies have concentrated on defects in the cochlea, while tinnitus is theorized to be associated with areas higher up in the brainstem and auditory cortex (Eggermont, 2015; Kaltenbach, 2011; Knipper *et al.*, 2010; De Ridder *et al.*, 2011; Ryan and Bauer, 2016). A study of one-half million Iraq and Afghanistan veterans with a history of TBI identifies 7.3% with a diagnosis of hearing loss, 6% with tinnitus, and another 5.6% with both (Swan *et al.*, 2017). Thus, given the same exposure, some will be susceptible to tinnitus, others to hearing loss, some will sustain both, and some neither, indicating a genetic component to this environmentally induced injury.

This paper will review the literature addressing genetic susceptibility to tinnitus and NIHL in both human and animal studies. Its approach ranges from twin studies in humans to candidate and GWAS studies in humans and animals. The advantage of GWAS is that, unlike candidate studies, which select genes based on prior knowledge, they provide a survey of the genome in an unbiased manner.

Findings in mouse models have contributed predominantly to the genetics of hearing loss, while comparative studies on the genetics of tinnitus have proven less practical due to phenotyping limitations. Due to the types of mutations that may often underlie complex traits, the promise of mouse models for discovery and validation of human pro-NIHL genes has yet to be realized. We will outline possible strategies to identify the genetic architecture of tinnitus and NIHL, including markers—single nucleotide polymorphisms (SNPs), as well as an overall polygenic risk score (PRS) to ascertain susceptibility to acoustic trauma. We discuss strengths, pitfalls, and strategies to address these challenges.

II. PARALLEL PROGRESS IN HUMAN AND MOUSE ASSOCIATION STUDIES

Recently, correlation of findings in humans and animal models in the area of ARHI has led to identification of multiple novel variants. Based on summary data without stratification for noise exposure, authors compared United Kingdom Biobank (UKB) data to mice gene expression patterns and identified novel SNPs in genes related to Mendelian disorders, as well as other genes not previously reported (Kalra *et al.*, 2019; Wells *et al.*, 2019). They then utilized mouse models to relate these variants to expression in specific cells of the cochlea. Methods used in these papers may pave the way for future NIHL and noise-induced tinnitus investigations. In a reversal of previous protocols where laboratory findings are brought to human studies, human findings may increasingly guide the direction of analysis in animal labs.

A. Benefits of animal studies

Although human GWAS may direct animal experiments in new studies, it is worth revisiting why even novel approaches still must utilize animal studies. Mechanoreception is evolutionarily very old so that genetic similarities in the molecular machinery of hearing encompasses species as far-ranging as zebrafish and fruit flies (Senthilan *et al.*, 2012; Whitfield, 2002). However, the far greater degree of similarity gained by working within mammals means that more mutations will impact overlapping aspects of anatomy and physiology down to the molecular level. In this regard, mice are unparalleled, representing the lowest phylogenetic model of mammalian hearing mechanisms. In addition, the economy and high degree of standardization of commercial mouse lines versus other species used for hearing research (e.g., guinea pigs, gerbils) are unmatched. Clearly, mapping of complex traits is difficult, regardless of species.

B. Mendelian versus complex traits

Original genetic investigations sought genes that underlie congenital hearing loss, which is typically inherited in a Mendelian manner whereby hearing loss is viewed as binary (present/absent), and the presence of particular mutations nearly guarantees hearing loss, most often inherited in a recessive fashion. Mapping of early deafness genes heavily leveraged anatomic, physiologic, and genetic similarities with respect to hearing between humans and laboratory mice

(Bowl and Dawson, 2014; Ohlemiller *et al.*, 2016; Steel, 2014). In addition to hearing changes, mice carrying putative deafness alleles can be used to localize the messenger ribonucleic acid (mRNA) or protein intracellularly, and characterize the resulting cochlear lesion. It helps that there exist over 400 inbred mouse strains, many of which carry naturally occurring disease-promoting mutations, plus large-scale efforts to generate and evaluate chemically induced mutations (El Hakam Kamareddin *et al.*, 2015). Hearing loss extant in large repositories, such as the Jackson Laboratory, can be ascertained in organized screening programs. Using this mouse to human parallel approach, over 100 deafness genes have been identified, along with roughly an additional 100 loci.

Since the manifestations of tinnitus and NIHL depend on the interplay of cochlear injury and repair processes, many successful animal studies have focused on genes involved in protective or repair processes (Carlsson *et al.*, 2005; Konings *et al.*, 2009b; Sliwinska-Kowalska and Pawelczyk, 2013). If the elimination of such a gene in a knockout (KO) model produces a tinnitus- or NIHL-prone phenotype, that gene or an ortholog could be implicated in human association studies. Such studies were "candidate" since they tested specific suspects, and are the laboratory counterpart of clinical genetic screens such as Otoscope (Sloan-Heggen and Smith, 2016). The genes tested in such experiments or screens often included those highly expressed in the ear or genes that regulate the expression of those genes.

This approach netted candidates that pointed to important pathways, including oxidative stress and potassium ion channels and other tinnitus genes. However, few such genes have been replicated in human GWAS. It may be that although these variants and genes are related to acoustic injury, they are not common enough to be a problem in the general population.

Several animal studies have utilized KO mice to study the genetic architecture of tinnitus, both in the cochlea and in higher centers. The availability of mouse KO models for the majority of genes, either as universal or conditional KOs from consortia, such as the International Mouse Phenotyping Consortium (IMPC; (Koscielny *et al.*, 2014), shortens the path from hypothesis to experimental testing. As an example, KCNQ2/3 channel KO mice allowed identification of therapeutic targets in cerebral cortical pyramidal neurons and hippocampal neurons for prevention of tinnitus (Kalappa *et al.*, 2015). In another study, increased spontaneous firing of fusiform cells was identified as necessary for the induction of tinnitus. Mice lacking ZnT3, a vesicular zinc transporter in the dorsal cochlear nucleus (DCN) of the auditory brainstem, were not inhibited from zinc-inhibited spontaneous firing of fusiform cells, indicating that non-vesicular zinc inhibited the spontaneous activity of the DCN (Perez-Rosello *et al.*, 2015). Last, nAChR KO mice fail to show suppression of cochlear responses, and overexpressing mice demonstrated reduced acoustic injury from noise exposures. nAChR constitutes the nicotinic receptor channel for acetylcholine, the primary efferent neurotransmitter at the inner and outer hair cells (Lustig, 2006), which transmits through the olivocochlear pathways to inhibit and modulate the afferent response. This olivocochlear pathway is strongly implicated in the generation of tinnitus (Riga *et al.*, 2017).

In the search for "tinnitus genes," rare monogenic disorders have been noted to be associated with complaints of ringing in the ears, as seen in the Online Mendelian Inheritance in Man (OMIM[1]), but no linkage studies have been performed and, again, the findings have not been replicated in the larger environmentally exposed population. While the separate etiologies of noise-induced, age-related, and TBI-associated tinnitus may have distinct genetic architecture, extant studies have been too small to examine individual etiologies separately (Clifford and Rogers, 2017; Sand *et al.*, 2007). In these candidate studies, originally, exonic SNPs were examined until it became evident that introns, promoters, enhancers, and other genetic regulatory elements were at least as important in the genomics of acoustic trauma. In fact, since there is such a large environmental component in these disorders, it becomes critical to examine the elements that react and interact with acoustic damage.

C. Translation of lab results to humans—Expression quantitative trait loci in animals (eQTLs)

Recent animal studies have focused on transcription factors that drive quantitative genetic expression within eQTL studies, which means mapping the expression profiles of hearing-related genes (Breschi *et al.*, 2017; Lavinsky *et al.*, 2016; Lavinsky *et al.*, 2018). Genetic regions where these functions co-map may implicate a transcription factor or mutations in regulatory sequences adjacent to a conventional gene. Only about 1% of cataloged quantitative trait loci (QTLs) have been identified from human or animal studies (Ermann and Glimcher, 2012; Flint and Eskin, 2012). New and emerging mouse resources (see the following) may be expected to increase this success rate, yet, there is no anticipated substitute for the requirement to phenotype hundreds, even thousands, of mice to reduce the often large number of candidate genes within identified mapping intervals. This is not a mouse problem, but a result of the sheer complexity of the genome, only a small fraction of which performs according to our early understanding. Of the rest, about half is transcribed, much of it into multiple types of poorly understood non-coding regulatory ribonucleic acids (nc RNAs; Breschi *et al.*, 2017).

Despite the success of applying mice to the genetics of Mendelian hearing loss, it will not necessarily follow that they are equally useful for mapping complex traits. Studies of gene expression indicate that mouse orthologs of hearing-related genes may be expressed in different cochlear cell types in mice and non-human primates (Hosoya *et al.*, 2016a; Hosoya *et al.*, 2016b). *More broadly, comparisons of specific transcription factor binding indicate that no more than 20% of transcription factor binding sites are conserved* (Breschi *et al.*, 2017). Notably, the changes that are found often allow for the binding of additional transcription factors, suggesting evolutionary pressures to refine gene expression, perhaps more than gene function.

Since the genetics of complex traits seem likely to reflect gene regulatory networks that can differ hugely by

species, it is reasonable to ask how likely it is that the same loci will account for a given complex trait across species (Gasch *et al.*, 2016). Attempts to address this experimentally should incorporate as much mouse genetic diversity as possible. Humans differ genetically at an average 4–5 $\times$ 10^6 SNPs, or about 0.5% of the genome (Breschi *et al.*, 2017). All inbred mouse strains, long preferred for hearing studies, are bred to be as genetically identical as possible, and genetic variation within strain is nearly negligible. Genetic differences across classic inbred strains, the appropriate metric for comparison with individual humans, are somewhat greater than for humans, although this estimate pales when compared to "mousedom" as a whole. Mice may hold advantages over humans in terms of their sheer numbers and rapid generational turnover.

The key to mapping any complex trait with GWAS is the phenotype's statistical association with a particular SNP or other marker. Different populations carry different markers, as a result of geographic isolation and the steady pace of new mutations. Every meiosis offers an opportunity to create new and unique marker combinations, and the shorter the chromosomal distance over which this occurs, the greater the potential mapping resolution. Thus, the size and dynamism of mouse populations, compared to humans, hold the potential for more sensitive detection of loci associated with complex traits. This is most true for studies that incorporate wild-derived inbred strains. The more heavily utilized classic strains possess less diversity, and more importantly, stronger selection for particular traits. This may inadvertently select for particular *combinations* of alleles in linkage disequilibrium (LD) so that recombination is diminished and mapping resolution suffers. The bottom line is that sufficiently large mouse populations, chosen to maximize genetic diversity and minimize LD, should yield more genetic associations at finer resolution than most human GWAS studies. What cannot be known at the outset is whether the entire mouse genome actually contains orthologous SNPs for the same complex traits, such as tinnitus or NIHL, under study in humans (Clifford *et al.*, 2016).

D. Mouse mapping panels for GWAS

To maximize the potential of mouse GWAS studies, new "panels" of strains have been developed that draw in as much genetic variation as possible (Flint and Eskin, 2012; Su *et al.*, 2010). The success of using these depends more on the number of strains involved, and less so on the number of mice tested from each strain, particularly for robust data such as auditory brain response (ABR) thresholds. Some panels, e.g., the Collaborative Cross (Churchill *et al.*, 2004), involve the generation of new recombinant inbred (RI) strains formed from selected classic inbred strains. Other panels, such as the Hybrid Mouse Diversity Panel (Lusis *et al.*, 2016), combine many genetically divergent inbred strains with selected RI strains. The beauty of these panels is that all of the mice of any particular strain are genetically identical. Therefore, all the experimenter need do is to phenotype a few mice from, preferably, at least 30–40 strains, and then compare the distribution of phenotypes with online databases of strain-specific markers. There is no need to genotype every animal for markers, potentially saving much time and money. Other panels leverage crosses of non-inbred stocks (e.g., Diversity Outbreds; Churchill *et al.*, 2012), but each resulting animal is unique and must be genotyped for markers. While inbred mice are preferred for most basic hearing studies, many outbred mouse strains such as CD1, ICR, NMRI, and SW exist, and have found uses in mapping due to their genetic diversity (Yalcin and Flint, 2012). These mice also must be individually genotyped. These mapping resources somewhat obviate the selection pressure that has shaped virtually all commercial inbred mouse strains (even wild-derived), increased LD, and reduced the resolution of trait mapping.

Each mouse QTL mapping endeavor involves a tradeoff of sensitivity versus inclusiveness. Consider the case of two inbred strains that differ significantly in ABR threshold and are to be used to map the genes involved using an intercross. If their phenotypic differences reflect one or a few loci, the alleles carried by the two strains will be present in a ~50:50 mix, and the intercross is likely to reveal those loci. However, the more closely related the two strains, the more markers they will share, reducing potential mapping resolution and the odds of isolating the causal gene. Also, only the allele(s) that accounts for the poor hearing of one strain can be revealed in such a study. The study cannot cast a broad net for the many mutations carried by all mice that may affect ABR thresholds.

The newly developed mapping panels in mice are designed to detect many loci using extant variation across mice as a species, yet, at high resolution. The hope is that GWAS involving a few hundred mice can complement far costlier human GWAS involving tens of thousands of people. While studies of complex traits have often failed to replicate from mouse to humans or account for total estimated heritability of various pathologies, age-related hearing loss studies that began with human GWAS and, subsequently, replicated in mice have been more successful in identifying variants and genes relevant to humans (Buchner and Nadeau, 2015; Fransen *et al.*, 2015).

III. DEFINING THE NOISE-INDUCED TINNITUS PHENOTYPE

A. Human studies of tinnitus

The definition of the phenotype of tinnitus in any particular genetic study drives gene identification in human analysis since GWAS is essentially a statistical regression of the phenotype on individual SNPs. In the absence of an objective measure, currently, tinnitus is defined by self-report. H2 refers to broad-sense heritability and reflects genetic variance, epistatic, maternal, and paternal effects, as opposed to SNP heritability or h2. H2 is most often studied in twins, where monozygotic and dizygotic pairs can be compared to ascertain heritability and environmental components. Imaging studies of tinnitus subjects show enhanced brain connections between the auditory cortex and arousal systems, frontal lobe, amygdala, pain centers, and others, indicating connecting gene pathways and isoforms more

indicative of emotional and cognitive issues (Minen *et al.*, 2014). Thus, it is vital to separate the perception of ringing in the ears from its psychological context in order to glean genetic information specific to tinnitus. The importance of the definition of the phenotype became evident when a large-scale study of tinnitus identified 0.11 "H2" after posing a question about "bothersome tinnitus" (Kvestad *et al.*, 2010). Several years later, other population studies noted up to 0.43–68 H2 for unilateral and bilateral tinnitus when another study posed a differently worded question about the perception itself, i.e., "Do you have buzzing in the ears?" (Bogo *et al.*, 2017; Maas *et al.*, 2017).

Noise-induced tinnitus is modeled as a latent unobserved variable, defined as a vulnerability which then manifests itself as perceived tinnitus given environmental exposure. Whether the subject sustains "enough" acoustic trauma to lead to the disorder being reported is dependent upon some measure of acoustic trauma sustained by the auditory system. Concomitantly, h2 or narrow sense heritability consists of only an additive genetic portion, referring to hard-wired deoxyribose nucleic acid (DNA) that affects a trait. Narrow-sense heritability is measured via linkage disequilibrium score regression (LDSC) either on summary or individual SNP data (Zheng *et al.*, 2016). The UKB, a cohort of 500 000 individuals aged 40–69 years old, is one of the first researcher-available large datasets (see Fig. 1). The UKB in association with Neale labs at Massachusetts General Hospital and the Broad Institute has performed a basic GWAS test on separate answers to the UKB's Touchscreen Questionnaire[2] and summary data.[3] Briefly, half a million participants in England were asked questions about their lifestyles, including questions on hearing and ringing in their ears. The phenotype of tinnitus was treated as a categorical variable, and the "now most or all of the time" answer was calculated to explain 0.137 of the total variance at $p = 1.34\text{e-}07$, still short of the H2 heritability of 0.43 identified in large population studies.

On the other hand, subjects in the Million Veteran Program (MVP), a cohort of over 700 000 U.S. veterans, were asked a more specific binomial question—whether they had been "diagnosed with tinnitus or ringing in the ears" (yes/no; Gaziano *et al.*, 2016). Whether this difference in phenotype definition will lead to identification of different significant SNPs and genes is yet to be determined.

B. Animal models of tinnitus

In contrast to humans, where a diagnosis of tinnitus can be self-reported, reliable induction and detection of tinnitus in an animal model is exceptionally challenging. Even more complex are the changes in the perception of tinnitus depending on background noise, stress, fatigue, and other factors more difficult to measure in the animal.

Most methods for detection of tinnitus in animal models rely on Pavlovian operant conditioning (OC) or changes in acoustic behaviors. With OC methods, animals are trained to refrain from or initiate a behavior when a broad or narrowband noise is stopped for a variable period of time (von der Behrens, 2014; Jones and May, 2017). The type of induced tinnitus noise is thought to depend on the type of noise exposure, i.e., narrowband noise induces tonal tinnitus (Kiefer *et al.*, 2015). After OC and tinnitus induction, the assumption is that animals with tinnitus will not perceive or detect silent periods in experimental sound stimuli. Because the method needs to distinguish hearing loss (the animal never heard the sound) from tinnitus (an internal sound that interferes with gap detection), these studies require (a) intact hearing in the frequency of the tinnitus and (b) induction of the tinnitus (most often using pharmacologic intervention or noise exposure) only after the OC training is complete. The resulting accuracy varies based on the training efficiency and assumes no extinction of the behavior. OC approaches are not practical for screening of mouse models with genetic mutations that may lead to tinnitus, due to the difficulty of operant training in mice. If applied to studies aiming to identify genetic propensity to develop tinnitus after a noise exposure, their low throughput presents a significant impediment.

An alternative to the OC approaches is the gap prepulse inhibition of the acoustic startle (GPIAS) reflex (Turner *et al.*, 2006; Turner *et al.*, 2012). This approach applies

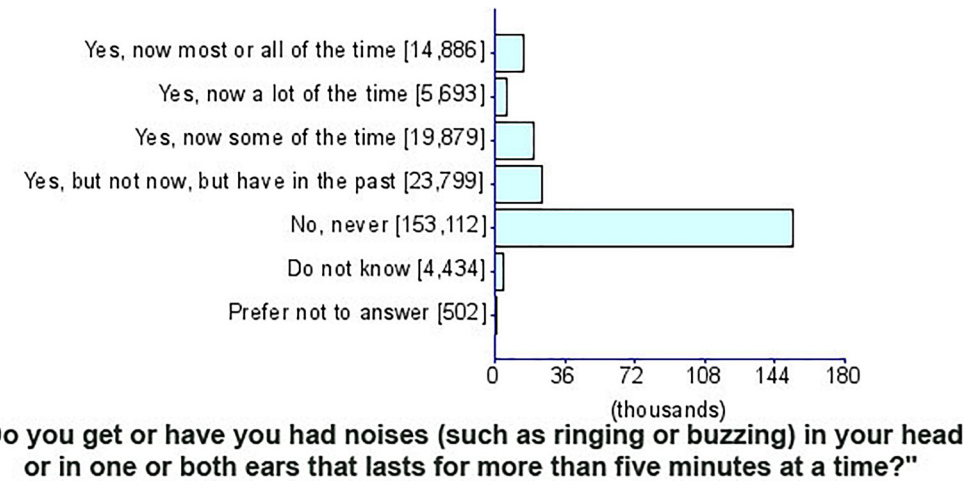

FIG. 1. (Color online) Question on tinnitus from the UKB TouchScreen. In answer to the question regarding noises in the ear, participants answered according to seven categories shown. Figures in parentheses are numbers of participants who answered within that category.

background noise with a brief silent gap just prior to the presentation of a loud "startle" sound, and does not require training. Instead, the output metric is the amplitude of the startle reflex, as measured by the force it generates. The strength of this reflex is reduced by sudden changes in the acoustic environment prior to the startle sound. These changes may include either increments or decrements (e.g., silent periods) in the background stimulus. According to the theory, animals without tinnitus will detect the silent gap and be less startled by the loud sound, whereas animals with tinnitus will not detect the gap and are hence expected to exhibit a greater startle amplitude. This is a "within subject" method as the animals are exposed to the loud sound with and without a prior silent gap. The GPIAS ratio (NoGap/Gap) is used to infer the presence of tinnitus. This method is relatively high throughput; however, some controversy exists regarding its validity. The notion that tinnitus fills a perceptual silent gap was not supported in human experiments using the same method (Fournier and Hébert, 2013). Also, the method requires normal hearing so that any deafening protocol used to induce tinnitus must be applied unilaterally and is sometimes performed under anesthesia, thus, introducing a number of potential confounds. A more recently introduced alternative, sound-based avoidance detection (SBAD) requires training, resulting in similar drawbacks to the OC techniques (Zuo *et al.*, 2017).

Numerous studies in mice and other animals have revealed processes that may play a role in the development of tinnitus. These range from structural, immunohistochemical, and electrophysiological studies in the central and peripheral auditory system in models of acquired tinnitus (Basta *et al.*, 2005; Hickox and Liberman, 2014; Hwang *et al.*, 2011a; Hwang *et al.*, 2011b; Llano *et al.*, 2012; Lowe and Walton, 2015; Ma *et al.*, 2006; Middleton *et al.*, 2011; Nansel *et al.*, 1992; Zhang *et al.*, 2014) but also include gene expression studies (Im *et al.*, 2007). The latter could be leveraged to pinpoint candidate genes for validation in human GWAS. In addition, for many of these mouse models, auditory phenotypes are available, whereas for others the auditory phenotyping is in progress (Bowl *et al.*, 2017). The multidimensionality of tinnitus—including variation in laterality, loudness, apparent source location, sound quality, proximate cause, and constancy—has made it extremely difficult to classify individual human cases, let alone in animals, wherein such qualities cannot be determined with any certainty. Tinnitus is difficult to characterize, and the propensity to develop tinnitus will be a thorny complex trait to map. Given that genetic studies are only as good as the phenotyping of subjects, attempts to map "pro-tinnitus" loci are likely to be hobbled by the metrics used, or the way "cases" are combined.

IV. DEFINING THE NIHL PHENOTYPE

A. Humans

Considerations for a genetic phenotype of NIHL for their effect on genetic studies include the definition of hearing loss and the characterization of acoustic exposure. These stem from evidence that NIHL has both genetic and environmental components with an H2 genetic contribution estimated at 0.67–0.70 (Wingfield *et al.*, 2007). Complicating this analysis is that heritability appears to be frequency specific both in animals and humans (Lavinsky *et al.*, 2016; Wingfield *et al.*, 2007). Suitably low and high frequencies must be applied with weighting toward those frequencies that may be noise vulnerable (Rabinowitz *et al.*, 2006). Frequencies beyond 8 kHz are not currently standard, but should be, given the heightened vulnerability of the cochlear base.

Although the biological substrate of NIHL is well studied in humans and animals, the definition of hearing loss in the literature has not been standardized. Studies that utilize "binaural pure-tone average for the frequencies of 1000, 2000, 3000 and 4000 Hz of greater than 25 dB" (Concha-Barrientos *et al.*, 2004) in an occupational setting may not account for genes that affect high frequencies (Wingfield *et al.*, 2007). A normal hearing definition of "no hearing threshold greater than 25 dB HL at any hearing level frequency" (HL; Grondin *et al.*, 2015) does not take noise notches into account (McBride and Williams, 2001; Rabinowitz *et al.*, 2006). Recently, principal components analysis (PCA; Anwar and Oakes, 2012) has been utilized to encompass the shape and other derived parameters of the audiogram. In the large cohorts currently available, the UKB administered a digits-in-noise test. How well this test will correlate with the standard audiogram in other large studies is unknown (Moore *et al.*, 2014). The MVP has audiology data available for analysis, and the definition of hearing loss will be critical, as these different definitions of NIHL covariates may elicit different findings on GWAS. Speech detection thresholds, speech reception thresholds (Hoffmann *et al.*, 2016), ICD-9 codes, and self-reported hearing difficulty (Moore *et al.*, 2014) are also available for use in GWAS studies.

Because different noise exposures appear to impart different types of injury (e.g., metabolic versus mechanical trauma), it may be important to combine subjects within and across studies by the type of noise exposure (Gaussian versus kurtotic; Grondin *et al.*, 2015; Konings *et al.*, 2009c). Typically there will be no way to identify the "cause" in terms of cellular substrate. That is, while one individual's 20 dB hearing loss may reflect outer hair cell loss, another's could conceivably replicate as noise-related strial injury. These would likely have different underlying genetics. Clinical audiograms have the advantage of being universal and fairly standardized but are not diagnostic for affected cell type. However, as the most global output metric, audiograms are more likely to detect hearing problems than, say, distortion product otoacoustic emissions (DPOAEs), which are less standardized and will not detect inner hair cell or neural pathology.

In regard to the nature of specific noise exposures, cohorts useful for GWAS studies often consist of workers or military personnel who shared the same environment for known periods, and whose HLs can be reasonably assumed to reflect occupational noise exposure. Thus, there must be baseline threshold data plus later assessments at fixed times. Cumulative noise exposure in humans is difficult to quantify,

and here a surrogate measure is required. In the UKB cohort, occupation may serve as an effective surrogate for noise exposure. Participants answered questions regarding exposure in industrial settings as well as exposure to loud music. In the U.S., noise exposure associated with many occupations is still poorly defined (Dobie, 2008). The Occupational Safety and Health Administration (OSHA) regulations put in place in the 1980s pose both a blessing and a hindrance: Exposures in some of the largest occupational groups have been capped at levels that pose minimal risk. This is good news for workers but inconvenient for researchers, who may be tempted to conduct exposure studies in countries with less effective protections. In the U.S. MVP, where military occupations are invariably noisy, the military occupational specialty (MOS) can be used as a surrogate for noise exposure. Some data-mining of exposure in the electronic health record will be necessary to separate the noise-induced component of hearing loss from any age-related component (Gaziano *et al.*, 2016).

B. Animals

In animals, both the subjects and exposures can be rigorously controlled, especially in genetically defined populations such as inbred rodent models. From such experiments, it has become clear that both the extent and form of cochlear injury caused by noise can vary with genetics (Ohlemiller and Gagnon, 2007). Recent research has emphasized progressive injury to the inner hair cell-afferent synapse, or "cochlear synaptopathy," which may follow even mild noise exposure (Kujawa and Liberman, 2015). Such injury does not cause threshold shifts, but may impair supra-threshold capabilities, such as speech perception in noise. This phenomenon fits well with the single major complaint of the aged, namely a decline in sound quality (Frisina, 2009), and may represent the substrate of Schuknecht's "neural presbycusis." However, whether moderate noise exposure can produce this type of injury is controversial, as its severity varies widely with animal model, and the results of human studies are mixed (Guest *et al.*, 2016). With the possible exception of non-human primates, animals appear more susceptible to noise than are humans (Guest *et al.*, 2018). Generally, the smaller the mammal, the more noise vulnerable. This does not discount the value of animals for characterizing noise injury and NIHL risk, but animal studies cannot be used to set specific exposure guidelines.

Across species, there appears broad consensus that a major driver of noise-related permanent threshold shifts is outer hair cell injury and loss. Other types of injury, such as injury to the cochlear lateral wall, endocochlear potential reduction, and neuronal loss appear more variable and clearly genetically modulated (Ohlemiller and Gagnon, 2007). Thus, grouping human subjects by the extent of NIHL may erroneously lump together different types of injuries and susceptibilities.

Other variables have the potential to complicate—or contaminate—genetic studies of noise susceptibility. Animal studies indicate that age and sex can impact noise vulnerability (Milon *et al.*, 2018; Saunders and Chen, 1985). "Adolescent" animals appear more susceptible, although this aspect of noise vulnerability in animals oddly lacks a human research counterpart. Both the form and extent of cochlear damage depend on age in animals, strongly suggesting that NIHL at different ages represents distinctly different processes, and very likely has different genetic foundations (Ohlemiller *et al.*, 2018). Human and animal studies that do not control for this risk will obtain misleading results. The manner of this measurement of hearing loss, moreover, may depend upon the hearing metric one applies, such as DPOAE levels versus hearing thresholds. Whether the approach is whole-genome sequencing, linkage studies, or GWAS, proper classification of 'controls', cases, and the form and extent of NIHL will hugely impact results.

Clearly, consensus is required for the guidance of research into pharmaceutical and gene therapy. The mouse has been the primary model organism used for modeling genetic human diseases and in particular disorders of the peripheral auditory system (Bowl and Brown, 2018). Genetic studies, however, depend on exquisitely accurate phenotyping, particularly when dealing with phenotypes that may represent complex traits. Accurate phenotyping is the *sine qua non* of any genetic study.

V. MAPPING SUSCEPTIBILITY GENES

A. Human studies

1. Noise-induced tinnitus

To our knowledge, the largest GWAS on tinnitus published until now included fewer than 200 subjects, identified no significant genes of p-value $< 5.0e\text{-}08$, was too small to separate etiologies, i.e., noise-induced versus age-related, and explained only 3.2% of the SNP variance (h2; Gilles *et al.*, 2017), leaving unanswered the question of where the remainder of the 40% general heritability is, as noted in twin studies (Bogo *et al.*, 2017). As an answer to this conundrum, it has become increasingly clear that common disorders, including cardiovascular disease, hypertension, breast and prostate cancer, and type 2 diabetes, involve a large number of genes, each with a small effect in the range of less than a 1.5 odds ratio (OR; Fransen *et al.*, 2015; Timpson *et al.*, 2017; Torkamani *et al.*, 2018). A PRS attempts to quantify these small effect sizes and includes a wider number of genes, and consists of an individual's summation of their genotype weighted by effects sizes on the trait of interest. In order to attempt to identify as much as possible of heritability variation, typically, PRS is calculated on a large independent data set, and then used as a predictor in a target population in regression analysis for verification.

In the case of NIHL and tinnitus, ideally, a PRS would target an individual's susceptibility to noise prior to exposure, so that this person could be counseled and afforded extra hearing protection and/or the opportunity to change professions to an environment less prone to this environmental exposure. As an example in other medical fields, PRS has been applied successfully to predict pre-morbid disposition to Alzheimer's disease (Logue *et al.*, 2018) and serves to identify susceptibility as a latent variable prior to exposure. In addition, PRS has been successfully combined with clinical risk factors, including elevated cholesterol, to advise

earlier treatment with statins, and has been shown to lower risk of first heart attack (Timpson *et al.*, 2017). PRS helps to answer questions about "missing heritability," that is, the difference between H2 and h2 heritability. For instance, H2 analysis identified 0.43 tinnitus heritability in a large population, while GWAS analysis in the UKB cohort identified only 0.137 h2. PRS thus provides an estimate of individualized vulnerability to a trait, and PRS for common disorders appears to be equivalent to the risk of a monogenic disorder (Khera *et al.*, 2018).

2. NIHL

To our knowledge, the only human GWAS study in the literature to specifically examine NIHL identified a SNP in the gene nucleolin (Grondin *et al.*, 2015). This small study awaits replication. Before the advent of large population studies, cochlear injury, as evidenced in both ARHI and NIHL in mice, were used to search for relevant genes and pathways. Because of significant lab findings, approaches to finding pro-NIHL genes in humans initially targeted genes involved in protection, repair, inflammation, redox chemistry, or ion homeostasis.

Replicated findings in candidate gene studies have included SNP variants of genes encoding antioxidants catalase (CAT), superoxide dismutase type 2 (SOD2), paraoxonase 2 (PON2), and glutathione transferases GSTM1 and GSTT1 (Abreu-Silva *et al.*, 2011; Carlsson *et al.*, 2005; Fortunato *et al.*, 2004; Yang *et al.*, 2015). A candidate gene polymerase chain reaction (PCR) study found a significant SNP in the inflammatory gene interleukin-6 (IL-6) related to age and noise-exposure ($p = 0.004$; Doi *et al.*, 2015). Pawelczyk *et al.* (2009) found *KCNE1* to be associated with tinnitus independent of hearing loss, although this study has not been replicated. Sand *et al.* (2007) reported that *GDNF* and *BDNF* jointly predicted tinnitus severity in women only ($p = 0.04$). Also studied in candidate genes included stress-related protein chaperones HSP70–1 and HSP70–2, and K^+ channel genes KCNQ1/KCNE1, KCNQ4, and KCNJ10 (Clifford *et al.*, 2016). The latter serve to gate K^+ flux into scala media (KCNQ1/KCNE1 complex), K^+ efflux from outer hair cells into scala tympani (KCNQ4), and K^+ efflux from strial intermediate cells (KCNJ10). Further implicated were gap junctional proteins within the organ of Corti and lateral wall GJB1, GJB2, and GJB4, which may help prevent K^+ from accumulating within the organ of Corti during periods of intense sound. While some types of injury-promoting genes might be anticipated, disease-causing genes often follow no convenient line of reasoning. Examples in the case of NIHL include protocadherin 15 (PCDH15, DFNB23), which mediates calcium-dependent cell-cell adhesion, and MYH14 (DFNA4), which is a myosin isoform (Konings *et al.*, 2009c). Some studies have supported nonlinear (epistatic) interactions among multiple variants (Clifford *et al.*, 2016). Such interactions are difficult to detect, but are likely to help explain how many loci that may contribute only slightly to NIHL risk by themselves appear more significant in some individuals. Not considered further here are genes and alleles that may promote medical conditions that may in turn promote NIHL, such as hypertension and hypercholesterolemia (Starck *et al.*, 1999). These studies all included less than 1000 subjects, relied on already-studied mouse models, and to date have not been replicated in unbiased GWAS studies nor in other ancestries.

An example of the Manhattan plot associated with the hearing loss question administered is shown in Fig. 2, and demonstrates a large number of significant hits. While the

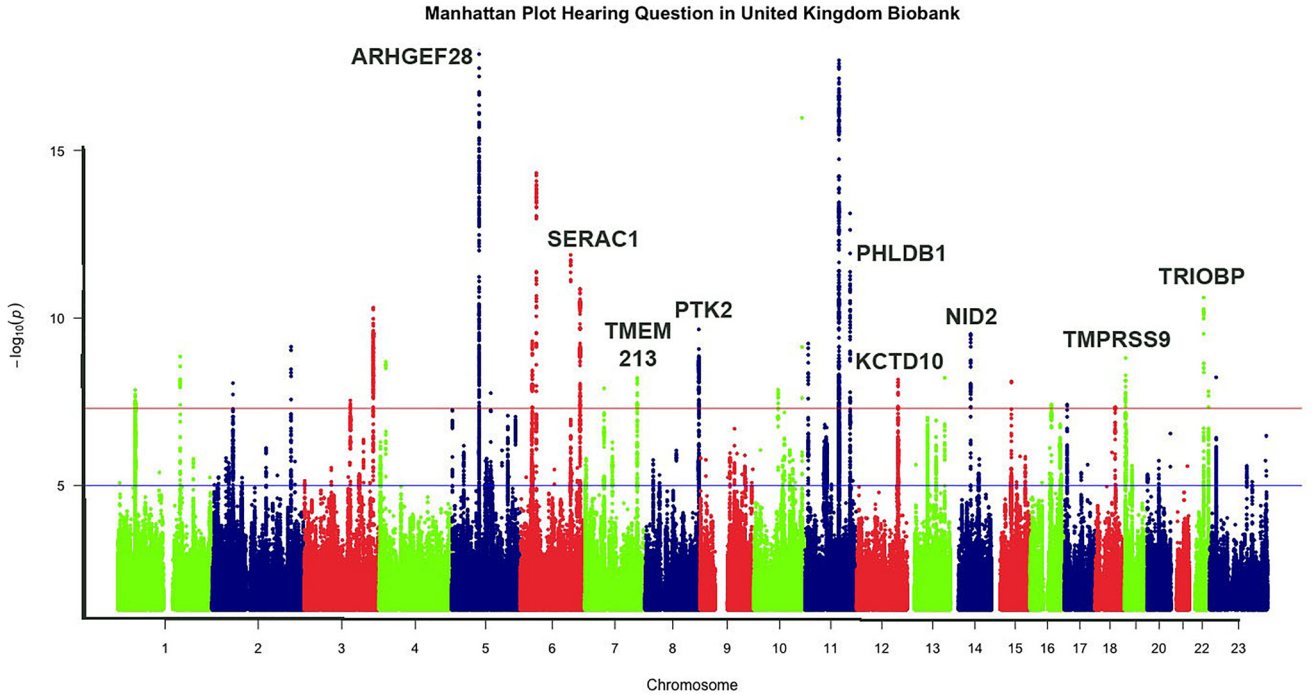

FIG. 2. (Color online) Manhattan plot of question on hearing loss from the United Kingdom cohort publicly available data. Participants answered "yes" or "no" to the question, "Do you have any difficulty with your hearing?." Significant SNP hits are seen as a vertical line that extends above the accepted significance *P*-value of 5E-08. Significant genes are labeled, while those lines that are not labeled may indicate hits that fall outside of known genes.

UKB has published summary data and identified genes associated with hearing loss, whether these are specific for age-related loss or will overlap with those that promote NIHL is currently unknown and awaits analysis combined with noise-exposure data.

B. Animal studies—Tinnitus and hearing loss

To date, only one study in mice has correlated a specific genetic mutation with tinnitus (Yu *et al.*, 2016). Using a GPIAS to detect tinnitus, this study indicated that mice lacking the gene encoding the glutamate aspartate transporter (GLAST) had an increased propensity to develop tinnitus following salicylate exposure. Whether salicylate produces a pathophysiologic disorder consistent with noise-induced tinnitus is unclear, and the temporary bilateral hearing loss caused by salicylate is likely to pose confounds as well.

Alleles that act in a dominant manner are more prone to cause delayed, progressive hearing loss that may causally overlap with ARHI (Ohlemiller and Frisina, 2008; Ohlemiller, 2006). In the case of acoustic injury, the loss is acquired in adulthood in a probabilistic manner, so that statistical associations are sought using different analytical methods, and require much larger samples.

Chance features of commercial inbred mouse strains—and good educated guesses—led to the discovery of the first genes that promote NIHL. First among these was the *Ahl* allele of cadherin 23 ($Cdh23^{753G>A}$; Johnson *et al.*, 1997; Johnson *et al.*, 2000). This gene was the first identified QTL (*Ahl*) shown to impact both ARHL and NIHL, and ignited the "mouse revolution" in hearing. *Cdh23* encodes a portion of the stereociliary tip link, which is subject to mechanical and other stresses that accumulate with age. It accounts for at least part of the hearing phenotype in many inbred mouse strains (Zheng *et al.*, 1999), including C57BL/6, which is the most commonly used strain for much of biomedical research. The destabilizing process by which the *Ahl* allele operates gave rise to a host of studies in KO models for other genes predicted to exert similar destabilizing effects. Accordingly, positive results were found in KO models for antioxidant, regulatory, and repair-related genes (Ohlemiller, 2006). These studies laid the foundation for much human work, and yielded support for some of the genes listed in Sec. V. A genetic mapping study seeking to explain the apparent noise resistance of 129S6/EvTac and MOLF/EiJ inbred mice using intercrosses and chromosomal substitution (Street *et al.*, 2014) yielded ten significant QTLs for noise resistance (*nr1–nr10*) but no confirmed genes. In addition, an intercross of four inbred strains (UM-HET4, featuring crosses of MOLF/Ei, C3H/HeJ, FVB/NJ, and 129/SvImJ) yielded significant QTLs on three chromosomes, but none of these has yet been identified (Schacht *et al.*, 2012). Mouse GWAS have taken advantage of newly developed panels, such as the Hybrid Mouse Diversity Panel, in mapping of both hearing thresholds and NIHL. Most of these have addressed ARHL and are not described here (Friedman *et al.*, 2009). The few NIHL extant GWAS have applied a fixed noise exposure to a few mice from many HDMP strains, and then compared strain distribution patterns in ABR threshold with dense marker sets from the same strains. Presently, a single gene nicotinamide adenine dinucleotide phosphate (NADPH oxidase 3, *Nox3*) has been identified and confirmed, at least for mice, using a conditional KO model (Lavinsky *et al.*, 2015). In keeping with a theme in aging and noise injury of stress and redox genes, *Nox3* impacts inflammation and the generation of reactive oxygen species.

Any phenotype can be probed by GWAS, and the intense interest surrounding cochlear synaptopathy has given rise to at least one study of noise-induced synaptopathy in mice (Lavinsky *et al.*, 2018). Again using the HDMP, and ABR wave 1 magnitude as a readout for synaptopathy, Friedman and colleagues identified *Cd44* and *Slc1a2* as loci potentially influencing cochlear synaptopathy (Lavinsky *et al.*, 2018). The former is expressed in pillar cells, while the latter may help remove glutamate from the inner hair cell afferent synapse. Gene identification was leveraged by eQTL data that placed transcription factor binding within the QTL region. The study requires replication and further testing of these genes and other candidates. One possible limitation is that wave 1 amplitude was measured at a fixed sound level, instead of a fixed sensation level. Threshold shifts can confound this type of analysis.

VI. CONCLUSIONS

Consistent phenotype definitions of both tinnitus and hearing loss will be important in comparing future large-scale studies of susceptibility to acoustic trauma. Because there is no recognized objective testing currently, tinnitus is constrained to self-report, and methods for detection and characterization in animals are controversial. Other phenotypic challenges include identification of a definition of hearing loss with the largest possible heritability measure, as well as the lack of exposure data constant across large cohorts.

Previously, candidate studies in humans of mutations that promote the complex traits of tinnitus and NIHL predominantly addressed exonic SNPs. Most candidate genes were identified in targeted studies based on expected roles for homeostatic, ion regulatory, antioxidant, and anti-inflammatory processes in the stressed cochlea as identified in mice. While candidate genes could be tested readily in mice using congenic lines, chromosomal substitution strains, and transgenic and KO lines, these studies in general did not lead to genes that were significantly related to NIHL or tinnitus in humans. In contrast, human GWAS in age-related hearing loss has identified predominantly intronic SNPs and awaits application to populations exposed to noise. Success for genetic information in noise-induced acoustic trauma in GWAS is limited by the need for large cohorts with consistent exposure histories that are also well controlled for variables such as age, sex, and duration of exposure.

Human and animal studies indicate that results will often contain multiple loci, each of which may promote only a small amount of disease risk or heritability. In fact, recent studies reveal that most common disorders, instead of being caused by monogenic anomalies, are composed of a large number of genes, leading to an accumulation of small effect sizes. A PRS might better characterize an individual's

susceptibility to acoustic trauma, and this PRS has been used successfully to aid in the application of personalized medicine. The polygenicity of a disorder presents a quandary for therapies aimed at reducing risk, and the most effective therapeutic targets may be risk genes involved in epistatic interactions that amplify the risk associated with other loci.

GWAS for NIHL in mice have been performed based on the assumption that many orthologous genes and regulatory sequences promote the same pathology in humans and mice. However, regulatory sequences are not universally conserved between mice and men, and correlations must be analyzed cautiously. Thus, because most extant inbred strains reflect strong selection pressures, LD and mapping resolution may be more limiting for mouse GWAS than for human GWAS. Mouse eQTL studies have focused on the possibility that pro-risk loci are expected to include more regulatory sequences than conventional protein-coding genes, and human GWAS has born this out by identifying predominantly intronic and intragenic areas of significance.

Because of the large regulatory sequence differences between rodents and mankind, in the unique case of genes leading to common disorders such as noise-induced tinnitus and hearing loss, a reversal of protocols may be required. Studies are most likely to be relevant to humans if the gene(s) of interest can be shown to be expressed in the same cell types.

Prior to this time, animal research drove human research. However, with the current level of expertise in genomics, in order to identify relevant genes, human GWAS may first provide an unbiased survey of significant SNPs with their effect sizes. Identification of significant human genes may then direct animal studies aimed at clarification and molecular analysis.

ACKNOWLEDGMENTS

Funded by NIDCD/NIH Grant No. R01DC013817 and DoD CDMRP Grant No. MR130240 (R.H.).

[1]Available at https://www.omim.org (Last viewed February 15, 2019).
[2]Available at https://bbams.ndph.ox.ac.uk (Last viewed February 15, 2019).
[3]Available at http://www.nealelab.is/uk-biobank (Last viewed February 15, 2019).

Abreu-Silva, R. S., Rincon, D., Horimoto, A. R. V. R., Sguillar, A. P., Ricardo, L. A. C., Kimura, L., Batissoco, A. C., Auricchio, M. T. B. D. M. O., Paulo A., and Mingroni-Netto, R. C. (**2011**). "The search of a genetic basis for noise-induced hearing loss (NIHL)," Ann. Hum. Biol. **38**, 210–218.

Anwar, M. N., and Oakes, M. P. (**2012**). "Data mining of audiology patient records: Factors influencing the choice of hearing aid type," BMC Med. Inform. Decis. Mak. **12**, 1–8.

Arlinger, S. (**2003**). "Negative consequences of uncorrected hearing loss—A review," Int. J. Audiol. **42**, S17–S20.

Asplund, R. (**2003**). "Sleepiness and sleep in elderly persons with tinnitus," Arch. Gerontol. Geriatr. **37**, 139–145.

Basta, D., Tzschentke, B., and Ernst, A. (**2005**). "Noise-induced cell death in the mouse medial geniculate body and primary auditory cortex," Neurosci. Lett. **381**, 199–204.

Bogo, R., Farah, A., Karlsson, K. K., Pedersen, N. L., Svartengren, M., and Skjönsberg, Å. (**2017**). "Prevalence, incidence proportion, and heritability for tinnitus," Ear Hear **38**, 292–300.

Bowl, M. R., and Brown, S. D. M. (**2018**). "Genetic landscape of auditory dysfunction," Hum. Mol. Genet. **27**, R130–R135.

Bowl, M. R., and Dawson, S. J. (**2014**). "The mouse as a model for age-related hearing loss—A mini-review," Gerontology **61**, 149–157.

Bowl, M. R., Simon, M. M., Ingham, N. J., Greenaway, S., Santos, L., Cater, H., Taylor, S., Mason, J., Kurbatova, N., Pearson, S., Bower, L. R., Clary, D. A., Meziane, H., Reilly, P., Minowa, O., Kelsey, L., Tocchini-Valentini, G. P., Gao, X., Bradley, A., Skarnes, W. C., Moore, M., Beaudet, A. L., Justice, M. J., Seavitt, J., Dickinson, M. E., Wurst, W., de Angelis, M. H., Herault, Y., Wakana, S., Nutter, L. M. J., Flenniken, A. M., McKerlie, C., Murray, S. A., Svenson, K. L., Braun, R. E., West, D. B., Lloyd, K. C. K., Adams, D. J., White, J., Karp, N., Flicek, P., Smedley, D., Meehan, T. F., Parkinson, H. E., Teboul, L. M., Wells, S., Steel, K. P., Mallon, A. M., and Brown, S. D. M. (**2017**). "A large scale hearing loss screen reveals an extensive unexplored genetic landscape for auditory dysfunction," Nat. Commun. **8**, 886.

Breschi, A., Gingeras, T. R., and Guigó, R. (**2017**). "Comparative transcriptomics in human and mouse," Nat. Rev. Genet. **18**, 425.

Buchner, D. A., and Nadeau, J. H. (**2015**). "Contrasting genetic architectures in different mouse reference populations used for studying complex traits," Genome Res. **25**, 775–791.

Carlsson, P. I., Van Laer, L., Borg, E., Bondeson, M. L., Thys, M., Fransen, E., and Van Camp, G. (**2005**). "The influence of genetic variation in oxidative stress genes on human noise susceptibility," Hear. Res. **202**, 87–96.

Churchill, G. A., Airey, D. C., Allayee, H., Angel, J. M., Attie, A. D., Beatty, J., Beavis, W. D., Belknap, J. K., Bennett, B., Berrettini, W., Bleich, A., Bogue, M., Broman, K. W., Buck, K. J., Buckler, E., Burmeister, M., Chesler, E. J., Cheverud, J. M., Clapcote, S., Cook, M. N., Cox, R. D., Crabbe, J. C., Crusio, W. E., Darvasi, A., Deschepper, C. F., Doerge, R. W., Farber, Charles, R., Forejt, J., Gaile, D., Garlow, S. J., Geiger, H., Gershenfeld, H., Gordon, T., Gu, J., Gu, W., de Haan, G., Hayes, N. L., Heller, C., Himmelbauer, H., Hitzemann, R., Hunter, K., Hsu, H.-C., Iraqi, F. A., Ivandic, B., Jacob, H. J., Jansen, R. C., Jepsen, K. J., Johnson, D. K., Johnson, T. E., Kempermann, G., Kendziorski, C., Kotb, M., Kooy, R. F., Llamas, B., Lammert, F., Lassalle, J.-M., Lowenstein, P. R., Lu, L., Lusis, A., Manly, K. F., Marcucio, R., Matthews, D., Medrano, J. F., Miller, D. R., Mittleman, G., Mock, B. A., Mogil, J. S., Montagutelli, X., Morahan, G., Morris, D. G., Mott, R., Nadeau, J. H., Nagase, H., Nowakowski, R. S., O'Hara, B. F., Osadchuk, A. V., Page, G. P., Paigen, B., Paigen, K., Palmer, A. A., Pan, H.-J., Peltonen-Palotie, L., Peirce, J., Pomp, D., Pravenec, M., Prows, D. R., Qi, Z., Reeves, R. H., Roder, J., Rosen, G. D., Schadt, E. E., Schalkwyk, L. C., Seltzer, Z., Shimomura, K., Shou, S., Sillanpaa, M. J., Siracusa, L. D., Snoeck, H.-W., Spearow, J. L., Svenson, K., Tarantino, L. M., Threadgill, D., Toth, L. A., Valdar, W. D. V., Fernando, P.-M., Warden, C., Whatley, S., Robert, W., Wiltshire, T., Yi, N., Zhang, D., Zhang, M., and Zou, F. (**2004**). "The Collaborative Cross, a community resource for the genetic analysis of complex traits," Nat. Genet. **36**, 1133–1137.

Churchill, G. A., Gatti, D. M., Munger, S. C., and Svenson, K. L. (**2012**). "The Diversity Outbred mouse population," Mamm. Genome **23**, 713–718.

Clifford, R. E., Hoffer, M., and Rogers, R. (**2016**). "The genomic basis of noise-induced hearing loss: A literature review organized by cellular pathways," Otol Neurotol. **37**, e309–e316.

Clifford, R., and Rogers, R. (**2017**). "Molecular genetics and tinnitus," in *Tinnitus Diagnosis Treat*., 2nd ed., edited by A. Shulmann and M. Hoffer (Thieme Medical Publishers Inc., New York).

Concha-Barrientos, M., Campbell-Lendrum, D., and Steenland, K. (**2004**). "Occupational noise: Assessing the burden of disease from work related hearing impairment at national and local levels," in *Environmental Burden of Disease Series, No. 9* (World Health Organization, Geneva, Switzerland).

Crönlein, T., Langguth, B., Pregler, M., Kreuzer, P. M., Wetter, T. C., and Schecklmann, M. (**2016**). "Insomnia in patients with chronic tinnitus: Cognitive and emotional distress as moderator variables," J. Psychosom. Res. **83**, 65–68.

Dawes, P., Emsley, R., Cruickshanks, K. J., Moore, D. R., Fortnum, H., Edmondson-Jones, M., McCormack, A., and Munro, K. J. (**2015**). "Hearing loss and cognition: The role of hearing aids, social isolation and depression," PLoS One **10**, 1–10.

Dawes, P., Fortnum, H., Moore, D. R., Emsley, R., Norman, P., Cruickshanks, K., Davis, A., Edmondson-Jones, M., McCormack, A., Lutman, M., and Munro, K. (**2014**). "Hearing in middle age," Ear Hear. **35**, e44–e51.

Degeest, S., Keppler, H., and Corthals, P. (**2017**). "The effect of tinnitus on listening effort in normal-hearing young adults: A preliminary study," Am. J. Speech-Lang. Pathol. **60**, 1–10.
De Ridder, D., Elgoyhen, A. B., Romo, R., and Langguth, B. (**2011**). "Phantom percepts: Tinnitus and pain as persisting aversive memory networks," Proc. Natl. Acad. Sci. U.S.A. **108**, 8075–8080.
Dobie, R. A. (**2008**). "The burdens of age-related and occupational noise-induced hearing loss in the United States," Ear Hear. **29**, 565–577.
Doi, D., Dias, A., Regina, C., Maria, M., de Oliveira, M., and Marchiori, L. (**2015**). "Association between polymorphism of interleukin-6 in the region -174G/C and tinnitus in the elderly with a history of occupational noise exposure," Noise Health **17**, 406–410.
Eggermont, J. J. (**2015**). "Tinnitus and neural plasticity (Tonndorf lecture at XIth International Tinnitus Seminar, Berlin, 2014)," Hear. Res. **319**, 1–11.
El Hakam Kamareddin, C., Magnol, L., and Blanquet, V. (**2015**). "A new Otogelin ENU mouse model for autosomal-recessive nonsyndromic moderate hearing impairment," Springerplus **4**, 730.
Ermann, J., and Glimcher, L. H. (**2012**). "After GWAS: Mice to the rescue?," Curr. Opin. Immunol. **24**, 564–570.
Feder, K., Michaud, D., McNamee, J., Fitzpatrick, E., Davies, H., and Leroux, T. (**2017**). "Prevalence of hazardous occupational noise exposure, hearing loss, and hearing protection usage among a representative sample of working Canadians," J. Occup. Environ. Med. **59**, 92–113.
Flint, J., and Eskin, E. (**2012**). "Genome-wide association studies in mice," Nat. Rev. Genet. **13**, 807.
Fortunato, G., Marciano, E., Zarrilli, F., Mazzaccara, C., Intrieri, M., Calcagno, G., Vitale, D. F., La Manna, P., Saulino, C., Marcelli, V., and Sacchetti, L. (**2004**). "Paraoxonase and superoxide dismutase gene polymorphisms and noise-induced hearing loss," Clin. Chem. **50**, 2012–2018.
Fournier, P., and Hébert, S. (**2013**). "Gap detection deficits in humans with tinnitus as assessed with the acoustic startle paradigm: Does tinnitus fill in the gap?," Hear. Res. **295**, 16–23.
Fransen, E., Bonneux, S., Corneveaux, J. J., Schrauwen, I., Di Berardino, F., White, C. H., Ohmen, J. D., Van de Heyning, P., Ambrosetti, U., Huentelman, M. J., Van Camp, G., and Friedman, R. A. (**2015**). "Genome-wide association analysis demonstrates the highly polygenic character of age-related hearing impairment," Eur. J. Hum. Genet. **23**, 110–115.
Friedman, R. A., Van Laer, L., Huentelman, M. J., Sheth, S. S., Van Eyken, E., Corneveaux, J. J., Tembe, W. D., Halperin, R. F., Thorburn, A. Q., Thys, S., Bonneux, S., Fransen, E., Huyghe, J., Pyykko, I., Cremers, C. W. R. J., Kremer, H., Dhooge, I., Stephens, D., Orzan, E., Pfister, M., Bille, M., Parving, A., Sorri, M., Van de Heyning, P. H., Makmura, L., Ohmen, J. D., Linthicum, Frederick, Jr., H., Fayad, J. N., Pearson, J. V., Craig, D. W., Stephan, D. A., and Van Camp, G. (**2009**). "GRM7 variants confer susceptibility to age-related hearing impairment," Hum. Mol. Genet. **18**, 785–796.
Frisina, R. D. (**2009**). "Age-related hearing loss: Ear and brain mechanisms," Ann. N. Y. Acad. Sci. **1170**, 708–717.
Gasch, A. P., Payseur, B. A., and Pool, J. E. (**2016**). "The power of natural variation for model organism biology," Trends Genet. **32**, 147–154.
Gaziano, J. M., Concato, J., Brophy, M., Fiore, L., Pyarajan, S., Breeling, J., Whitbourne, S., Deen, J., Shannon, C., Humphries, D., Guarino, P., Aslan, M., Anderson, D., LaFleur, R., Hammond, T., Schaa, K., Moser, J., Huang, G., Muralidhar, S., Przygodzki, R., and O'Leary, T. J. (**2016**). "Million Veteran Program: A mega-biobank to study genetic influences on health and disease," J. Clin. Epidemiol. **70**, 214–223.
Gilles, A., Van Camp, G., Van De Heyning, P., and Fransen, E. (**2017**). "A pilot genome-wide association study identifies potential metabolic pathways involved in tinnitus," Front. Neurosci. **11**, 1–10.
Gomaa, M. A. M., Elmagd, M. H. A., Elbadry, M. M., and Kader, R. M. A. (**2014**). "Depression, anxiety and stress scale in patients with tinnitus and hearing loss," Eur. Arch. Otorhinolaryngol. **271**, 2177–2184.
Gopinath, B., McMahon, C. M., Rochtchina, E., Karpa, M. J., and Mitchell, P. (**2010**). "Risk factors and impacts of incident tinnitus in older adults," Ann. Epidemiol. **20**, 129–135.
Gregory, M. C., Atkins, C. L., and Barker, D. F. (**1994**). "Hearing loss," N. Engl. J. Med. **330**, 714; author reply 715.
Grondin, Y., Bortoni, M. E., Sepulveda, R., Ghelfi, E., Bartos, A., Cotanche, D., Clifford, R. E., and Rogers, R. A. (**2015**). "Genetic polymorphisms associated with hearing threshold shift in subjects during first encounter with occupational impulse noise," PLoS One **10**(6), e0130827.
Guest, H., Munro, K. J., Prendergast, G., Howe, S., and Plack, C. J. (**2016**). "Tinnitus with a normal audiogram: Relation to noise exposure but no evidence for cochlear synaptopathy," Hear. Res. **344**, 265–274.
Guest, H., Munro, K. J., Prendergast, G., Millman, R. E., and Plack, C. J. (**2018**). "Impaired speech perception in noise with a normal audiogram: No evidence for cochlear synaptopathy and no relation to lifetime noise exposure," Hear. Res. **364**, 142–151.
Hickox, A. E., and Liberman, M. C. (**2014**). "Is noise-induced cochlear neuropathy key to the generation of hyperacusis or tinnitus?," J. Neurophysiol. **111**, 552–564.
Hoffmann, T. J., Keats, B. J., Yoshikawa, N., Schaefer, C., Risch, N., and Lustig, L. R. (**2016**). "A large genome-wide association study of age-related hearing impairment using electronic health records," PLoS Genet. **12**, 1–20.
Hosoya, M., Fujioka, M., Kobayashi, R., Okano, H., and Ogawa, K. (**2016a**). "Overlapping expression of anion exchangers in the cochlea of a non-human primate suggests functional compensation," Neurosci. Res. **110**, 1–10.
Hosoya, M., Fujioka, M., Ogawa, K., and Okano, H. (**2016b**). "Distinct expression patterns of causative genes responsible for hereditary progressive hearing loss in non-human primate cochlea," Sci. Rep. **6**, 22250.
Hwang, J., Chen, J., Yang, S., Wang, M., and Chan, Y. (**2011a**). "Expression of tumor necrosis factor-α and interleukin-1β genes in the cochlea and inferior colliculus in salicylate-induced tinnitus," J. Neuroinflammation **8**, 30.
Hwang, J., Chen, J., Yang, S., Wang, M., Liu, T. C., and Chan, Y. (**2011b**). "Expression of COX-2 and NMDA receptor genes at the cochlea and midbrain in salicylate-induced tinnitus," Laryngoscope **121**, 361–364.
Im, G. J., Jung, H. H., Chae, S. W., Cho, W. S., and Kim, S. J. (**2007**). "Differential gene expression profiles in salicylate ototoxicity of the mouse," Acta Otolaryngol. **127**, 459–469.
Jafari, Z., Toufan, R., Aghamollaei, M., Malayeri, S. A., Rahimzadeh, S., and Esmaili, M. (**2012**). "Impact of tinnitus on divided and selective auditory attention in workers exposed to occupational noise," Adv. Cogn. Sci. **14**, 51–62.
Jain, C., and Sahoo, J. P. (**2014**). "The effect of tinnitus on some psychoacoustical abilities in individuals with normal hearing sensitivity," Int. Tinnitus J. **19**, 28–35.
Johnson, K. R., Erway, L. C., Cook, S. A., Willott, J. F., and Zheng, Q. Y. (**1997**). "A major gene affecting age-related hearing loss in C57BL/6J mice," Hear. Res. **114**, 83–92.
Johnson, K. R., Zheng, Q. Y., and Erway, L. C. (**2000**). "A major gene affecting age-related hearing loss is common to at least ten inbred strains of mice," Genomics **70**, 171–180.
Jones, A., and May, B. J. (**2017**). "Improving the Reliability of Tinnitus Screening in Laboratory Animals," J. Assoc. Res. Otolaryngol. **18**, 183–195.
Kalappa, B. I., Soh, H., Duignan, K. M., Furuya, T., Edwards, S., Tzingounis, A. V., and Tzounopoulos, T. (**2015**). "Potent KCNQ2/3-specific channel activator suppresses *in vivo* epileptic activity and prevents the development of tinnitus," J. Neurosci. **35**, 8829–8842.
Kalra, G., Milon, B., Casella, A. M., Song, Y., Herb, B. R., Rose, K., Hertzano, R., and Ament, S. A. (**2019**). "Biological insights from multi-omic analysis of 31 genomic risk loci for adult hearing difficulty," bioRxiv, doi: https://doi.org/10.1101/562405.
Kaltenbach, J. A. (**2011**). "Tinnitus: Models and mechanisms," Hear. Res. **276**, 52–60.
Khera, A. V., Chaffin, M., Aragam, K. G., Haas, M. E., Roselli, C., Choi, S. H., Natarajan, P., Lander, E. S., Lubitz, S. A., Ellinor, P. T., and Kathiresan, S. (**2018**). "Genome-wide polygenic scores for common diseases identify individuals with risk equivalent to monogenic mutations," Nat. Genet. **50**, 1219–1224.
Kiefer, L., Schauen, A., Abendroth, S., Gaese, B. H., and Nowotny, M. (**2015**). "Variation in acoustic overstimulation changes tinnitus characteristics," Neuroscience **310**, 176–187.
Knipper, M., Zimmermann, U., and Müller, M. (**2010**). "Molecular aspects of tinnitus," Hear. Res. **266**, 60–69.
Konings, A., Van Laer, L., Michel, S., Pawelczyk, M., Carlsson, P. I., Bondeson, M. L., Rajkowska, E., Dudarewicz, A., Vandevelde, A., Fransen, E., Huyghe, J., Borg, E., Sliwinska-Kowalska, M., and Van Camp, G. (**2009a**). "Variations in HSP70 genes associated with noise-induced hearing loss in two independent populations," Eur. J. Hum. Genet. **17**, 329–335.
Konings, A., Van Laer, L., and Van Camp, G. (**2009b**). "Genetic studies on noise-induced hearing loss: A review," Ear Hear. **30**, 151–159.
Konings, A., Van Laer, L., Wiktorek-Smagur, A., Rajkowska, E., Pawelczyk, M., Carlsson, P. I., Bondeson, M. L., Dudarewicz, A., Vandevelde, A., Fransen, E., Huyghe, J., Borg, E., Sliwinska-Kowalska, M., Van Camp, G. (**2009c**). "Candidate gene association study for noise-

induced hearing loss in two independent noise-exposed populations," Ann. Hum. Genet. **73**, 215–224.
Koscielny, G., Yaikhom, G., Iyer, V., Meehan, T. F., Morgan, H., Atienza-Herrero, J., Blake, A., Chen, C.-K., Easty, R., Di Fenza, A., Fiegel, T., Grifiths, M., Horne, A., Karp, N. A., Kurbatova, N., Mason, J. C., Matthews, P., Oakley, D. J., Qazi, A., Regnart, J., Retha, A., Santos, L. A., Sneddon, D. J., Warren, J., Westerberg, H., Wilson, R. J., Melvin, D. G., Smedley, D., Brown, S. D. M., Flicek, P., Skarnes, W. C., Mallon, A.-M., and Parkinson, H. (**2014**). "The International Mouse Phenotyping Consortium Web Portal, a unified point of access for knockout mice and related phenotyping data," Nucleic Acids Res. **42**, D802–9.
Kujawa, S. G., and Liberman, M. C. (**2015**). "Synaptopathy in the noise-exposed and aging cochlea: Primary neural degeneration in acquired sensorineural hearing loss," Hear. Res. **330**, 191–199.
Kvestad, E., Czajkowski, N., Engdahl, B., Hoffman, H. J., and Tambs, K. (**2010**). "Low heritability of tinnitus: Results from the second Nord-Trøndelag health study," Arch. Otolaryngol. Head. Neck Surg. **136**, 178–182.
Lavinsky, J., Crow, A. L., Pan, C., Wang, J., Aaron, K. A., Ho, M. K., Li, Q., Salehide, P., Myint, A., Monges-Hernadez, M., Eskin, E., Allayee, H., Lusis, A. J., and Friedman, R. A. (**2015**). "Genome-wide association study identifies nox3 as a critical gene for susceptibility to noise-induced hearing loss," PLoS Genet. **11**, e1005094.
Lavinsky, J., Dermanaki, P. S., Wang, J., and Friedman, R. A. (**2018**). "Genome-wide association study for noise-induced cochlear synaptopathy," bioRxiv, doi: https://doi.org/10.1101/311407.
Lavinsky, J., Ge, M., Crow, A. L., Pan, C., Wang, J., Dermanaki, P. S., Myint, A., Eskin, E., Allayee, H., Lusis, A. J., and Friedman, R. A. (**2016**). "The genetic architecture of noise-induced hearing loss: Evidence for a gene-by-environment interaction," G3 (Bethesda) **6**, 3219–3228.
Llano, D. A., Turner, J., and Caspary, D. M. (**2012**). "Diminished cortical inhibition in an aging mouse model of chronic tinnitus," J. Neurosci. **32**, 16141–16148.
Logue, M. W., Panizzon, M. S., Elman, J. A., Gillespie, N. A., Hatton, S. N., Gustavson, D. E., Andreassen, O. A., Dale, A. M., Franz, C. E., Lyons, M. J., Neale, M. C., Reynolds, C. A., Tu, X., and Kremen, W. S. (**2018**). "Use of an Alzheimer's disease polygenic risk score to identify mild cognitive impairment in adults in their 50s," Mol. Psychiatry **24**, 421–430.
Lowe, A. S., and Walton, J. P. (**2015**). "Alterations in peripheral and central components of the auditory brainstem response: A neural assay of tinnitus," PLoS One **10**, e0117228.
Lusis, A. J., Seldin, M. M., Allayee, H., Bennett, B. J., Civelek, M., Davis, R. C., Eskin, E., Farber, C. R., Hui, S., Mehrabian, M., Norheim, F., Pan, C., Parks, B., Rau, C. D., Smith, D. J., Vallim, T., Wang, Y., and Wang, J. (**2016**). "The Hybrid Mouse Diversity Panel: A resource for systems genetics analyses of metabolic and cardiovascular traits," J. Lipid Res. **57**, 925–942.
Lustig, L. R. (**2006**). "Nicotinic acetylcholine receptor structure and function in the efferent auditory system," Anat. Rec. A Discov. Mol. Cell. Evol. Biol. **288**, 424–434.
Ma, W.-L. D., Hidaka, H., and May, B. J. (**2006**). "Spontaneous activity in the inferior colliculus of CBA/J mice after manipulations that induce tinnitus," Hear. Res. **212**, 9–21.
Maas, I. L., Brüggemann, P., Requena, T., Bulla, J., Edvall, N. K., Hjelmborg, J. v. B., Szczepek, A. J., Canlon, B., Mazurek, B., Lopez-Escamez, J. A., and Cederroth, C. R. (**2017**). "Genetic susceptibility to bilateral tinnitus in a Swedish twin cohort," Genet. Med. **19**, 1007–1012.
Masterson, E. A., Tak, S., Themann, C. L., Wall, D. K., Groenewold, M. R., Deddens, J. A., and Calvert, G. M. (**2013**). "Prevalence of hearing loss in the United States by industry," Am. J. Ind. Med. **56**, 670–681.
McBride, D. I., and Williams, S. (**2001**). "Audiometric notch as a sign of noise induced hearing loss," Occup. Environ. Med. **58**, 46–51.
Middleton, J. W., Kiritani, T., Pedersen, C., Turner, J. G., Shepherd, G. M. G., and Tzounopoulos, T. (**2011**). "Mice with behavioral evidence of tinnitus exhibit dorsal cochlear nucleus hyperactivity because of decreased GABAergic inhibition," Proc. Natl. Acad. Sci. U.S.A. **108**, 7601–7606.
Milon, B., Mitra, S., Song, Y., Margulies, Z., Casserly, R., Drake, V., Mong, J. A., Depireux, D. A., and Hertzano, R. (**2018**). "The impact of biological sex on the response to noise and otoprotective therapies against acoustic injury in mice," Biol. Sex Differ. **9**, 12.
Minen, M. T., Camprodon, J., Nehme, R., and Chemali, Z. (**2014**). "The neuropsychiatry of tinnitus: A circuit-based approach to the causes and treatments available," J. Neurol. Neurosurg. Psychiatry. **0**, 1–7.
Moore, D. R., Edmondson-Jones, M., Dawes, P., Fortnum, H., McCormack, A., Pierzycki, R. H., and Munro, K. J. (**2014**). "Relation between speech-in-noise threshold, hearing loss and cognition from 40–69 years of age," PLoS One **9**, e107720.
Nansel, D. D., Peneff, A., and Quitoriano, J. (**1992**). "Effectiveness of upper versus lower cervical adjustments with respect to the amelioration of passive rotational versus lateral-flexion end-range asymmetries in otherwise asymptomatic subjects," J. Manipulative Physiol. Ther. **15**, 99–105.
National Institute of Occupational Safety and Health Standards (1998). "Occupational noise exposure: Revised criteria 1998" (National Institute for Occupational Safety and Health, Cincinnati, OH).
Ohlemiller, K. K. (**2006**). "Contributions of mouse models to understanding of age- and noise-related hearing loss," Brain Res. **1091**, 89–102.
Ohlemiller, K. K., and Frisina, R. D. (**2008**). "Age-related hearing loss and its cellular and molecular bases," in *Auditory Trauma, Protection and Repair*, edited by J. Schacht, A. Popper, and R. R. Fay (Springer, New York), pp. 145–194.
Ohlemiller, K. K., and Gagnon, P. M. (**2007**). "Genetic dependence of cochlear cells and structures injured by noise," Hear. Res. **224**, 34–50.
Ohlemiller, K. K., Jones, S. M., and Johnson, K. R. (**2016**). "Application of mouse models to research in hearing and balance," J. Assoc. Res. Otolaryngol. **17**(6), 493–523.
Ohlemiller, K. K., Kaur, T., Warchol, M. E., and Withnell, R. H. (**2018**). "The endocochlear potential as an indicator of reticular lamina integrity after noise exposure in mice," Hear. Res. **361**, 138–151.
Pawelczyk, M., Van Laer, L., Fransen, E., Rajkowska, E., Konings, A., Carlsson, P. I., Borg, E., Van Camp, G., and Sliwinska-Kowalska, M. (**2009**). "Analysis of gene polymorphisms associated with K ion circulation in the inner ear of patients susceptible and resistant to noise-induced hearing loss," Ann. Hum. Genet. **73**, 411–421.
Perez-Rosello, T., Anderson, C. T., Ling, C., Lippard, S. J., and Tzounopoulos, T. (**2015**). "Tonic zinc inhibits spontaneous firing in dorsal cochlear nucleus principal neurons by enhancing glycinergic neurotransmission," Neurobiol. Dis. **81**, 14–19.
Rabinowitz, P. M., Galusha, D., Slade, M. D., Dixon-Ernst, C., Sircar, K. D., and Dobie, R. A. (**2006**). "Audiogram notches in noise-exposed workers," Ear Hear. **27**, 742–750.
Riga, M., Komis, A., Marangoudakis, P., Naxakis, S., Ferekidis, E., Kandiloros, D., and Danielides, V. (**2017**). "Differences in the suppression of distortion product otoacoustic emissions by contralateral white noise between patients with acute or chronic tinnitus," Int. J. Audiol. **56**, 589–595.
Rossiter, S., Stevens, C., and Walker, G. (**2006**). "Tinnitus and its effect on working memory and attention," J. Speech, Lang. Hear. Res. **49**, 150–160.
Ryan, D., and Bauer, C. A. (**2016**). "Neuroscience of tinnitus," Neuroimaging Clin. N. Am. **26**, 187–196.
Sand, P. G., Langguth, B., Kleinjung, T., and Eichhammer, P. (**2007**). "Genetics of chronic tinnitus," Prog. Brain Res. **166**, 159–168.
Saunders, J. C., and Chen, C. (**1985**). "Developmental periods of susceptibility to auditory trauma in laboratory animals," in *Toxicology of the Ear, Eye, and other Special Senses*, edited by A. W. Hayes (Raven, New York), pp. 145–154.
Schacht, J., Altschuler, R., Burke, D. T., Chen, S., Dolan, D., Galecki, A. T., Kohrman, D., and Miller, R. A. (**2012**). "Alleles that modulate late life hearing in genetically heterogeneous mice," Neurobiol. Aging **33**, 1842.e15-29.
Schecklmann, M., Pregler, M., Kreuzer, P. M., Poeppl, T. B., Lehner, A., Crönlein, T., Wetter, T. C., Frank, E., Landgrebe, M., and Langguth, B. (**2015**). "Psychophysiological associations between chronic tinnitus and sleep: A cross validation of tinnitus and insomnia questionnaires," Biomed Res. Int. **2015**, 1–6.
Senthilan, P. R., Piepenbrock, D., Ovezmyradov, G., Nadrowski, B., Bechstedt, S., Pauls, S., Winkler, M., Möbius, W., Howard, J., and Göpfert, M. C. (**2012**). "Drosophila auditory organ genes and genetic hearing defects," Cell **150**, 1042–1054.
Shargorodsky, J. (**2010**). "Change in prevalence of hearing loss in US adolescents," JAMA **304**, 772.
Shargorodsky, J., Curhan, G. C., and Farwell, W. R. (**2010**). "Prevalence and characteristics of tinnitus among US adults," Am. J. Med. **123**, 711–718.
Sliwinska-Kowalska, M., and Pawelczyk, M. (**2013**). "Contribution of genetic factors to noise-induced hearing loss: A human studies review," Mutat. Res. **752**, 61–65.
Sloan-Heggen, C. M., and Smith, R. J. H. (**2016**). "Navigating genetic diagnostics in patients with hearing loss," Curr. Opin. Pediatr. **28**(6), 705–712.
Smith, C. D., Cooper, A. D., Merullo, D. J., Cohen, B. S., Heaton, K. J., Claro, P. J., and Smith, T. (**2019**). "Sleep restriction and cognitive load

affect performance on a simulated marksmanship task," J. Sleep Res. **28**(3), e12637.
Starck, J., Toppila, E., and Pyykkö, I. (**1999**). "Smoking as a risk factor in sensory neural hearing loss among workers exposed to occupational noise," Acta Otolaryngol. **119**, 302–305.
Steel, K. P. (**2014**). "What's the use of genetics?," in *Perspectives on Auditory Research* (Springer, New York), pp. 569–584.
Street, V. A., Kujawa, S. G., Manichaikul, A., Broman, K. W., Kallman, J. C., Shilling, D. J., Iwata, A. J., Robinson, L. C., Robbins, C. A., Li, J., Liberman, M. C., and Tempel, B. L. (**2014**). "Resistance to noise-induced hearing loss in 129S6 and MOLF mice: Identification of independent, overlapping, and interacting chromosomal regions," J. Assoc. Res. Otolaryngol. **15**, 721–738.
Su, W. L., Sieberts, S. K., Kleinhanz, R. R., Lux, K., Millstein, J., Molony, C., and Schadt, E. E. (**2010**). "Assessing the prospects of genome-wide association studies performed in inbred mice," Mamm. Genome **21**, 143–152.
Swan, A. A., Nelson, J. T., Swiger, B., Jaramillo, C. A., Eapen, B. C., Packer, M., and Pugh, M. J. (**2017**). "Prevalence of hearing loss and tinnitus in Iraq and Afghanistan veterans: A chronic effects of neurotrauma consortium study," Hear. Res. **349**, 4–12.
Tegg-Quinn, S., Bennett, R. J., Eikelboom, R. H., and Baguley, D. M. (**2016**). "The impact of tinnitus upon cognition in adults: A systematic review," Int. J. Audiol. **55**, 533–540.
Timpson, N. J., Greenwood, C. M. T., Soranzo, N., Lawson, D. J., and Richards, J. B. (**2017**). "Genetic architecture: The shape of the genetic contribution to human traits and disease," Nat. Rev. Genet. **19**, 110.
Torkamani, A., Wineinger, N. E., and Topol, E. J. (**2018**). "The personal and clinical utility of polygenic risk scores," Nat. Rev. Genet. **19**, 581–590.
Trevis, K., McLachlan, N., and Wilson, S. (**2016**). "Cognitive mechanisms in chronic rinnitus: Psychological markers of a failure to switch attention," Front. Psychol. **7**, 1262.
Turner, J. G., Brozoski, T. J., Bauer, C. A., Parrish, J. L., Myers, K., Hughes, L. F., and Caspary, D. M. (**2006**). "Gap detection deficits in rats with tinnitus: A potential novel screening tool," Behav. Neurosci. **120**, 188–195.
Turner, J., Larsen, D., Hughes, L., Moechars, D., and Shore, S. (**2012**). "Time course of tinnitus development following noise exposure in mice," J. Neurosci. Res. **90**, 1480–1488.
U.S. Department of Veterans Affairs (**2018**). *Annual Benefits Report FY2018*, Veterans Benefits Adm. Reports (U.S. Department of Veterans Affairs, Washington, D.C.), 52 pages.
Vogel, I., van de Looij-Jansen, P. M., Mieloo, C. L., Burdorf, A., and de Waart, F. (**2014**). "Risky music listening, permanent tinnitus and depression, anxiety, thoughts about suicide and adverse general health," PLoS One **9**, e98912.
von der Behrens, W. (**2014**). "Animal models of subjective tinnitus," Neural Plast. **2014**, 741452.
Vuckovic, D., Mezzavilla, M., Cocca, M., Morgan, A., Brumat, M., Catamo, E., Concas, M. P., Biino, G., Franzè, A., Ambrosetti, U., Pirastu, M., Gasparini, P., and Girotto, G. (**2018**). "Whole-genome sequencing reveals new insights into age-related hearing loss: Cumulative effects, pleiotropy and the role of selection," Eur. J. Hum. Genet. **26**, 1167–1179.
Wells, H. R. R., Freidin, M. B., Abidin, F. N. Z., Payton, A., Dawes, P., Munro, K. J., Morton, C. C., Moore, D. R., Dawson, S. J., and Frances, M. K. (**2019**). "Genome-wide association study identifies 44 independent genomic loci for self-reported adult hearing difficulty in the UK Biobank cohort," bioRxiv, doi: http://dx.doi.org/10.1101/549071.
Whitfield, T. T. (**2002**). "Zebrafish as a model for hearing and deafness," J. Neurobiol. **53**, 157–171.
Wingfield, A., Panizzon, M., Grant, M. D. M., Toomey, R., Kremen, W. S. W., Franz, C. C. E., Jacobson, K. C. K., Eisen, S. A., and Lyons, M. (**2007**). "A twin-study of genetic contributions to hearing acuity in late middle age," J. Gerontol. A Biol. Sci. Med. Sci. **62**, 1294–1299.
Yalcin, B., and Flint, J. (**2012**). "Association studies in outbred mice in a new era of full-genome sequencing," Mamm. Genome **23**, 719–726.
Yang, J., Zhang, J., Wang, X., Wang, C., Chen, J., Qian, Y., and Duan, Z. (**2015**). "Identification of functional tag single nucleotide polmorphisms within the entire CAT gene and their clinical relevance in patients with noise-induced hearing loss," Int. J. Clin. Exp. Pathol. **8**, 2852–2863.
Yankaskas, K. (**2013**). "Prelude: Noise-induced tinnitus and hearing loss in the military," Hear. Res. **295**, 3–8.
Yu, H., Vikhe Patil, K., Han, C., Fabella, B., Canlon, B., Someya, S., and Cederroth, C. R. (**2016**). "GLAST deficiency in mice exacerbates gap detection deficits in a model of salicylate-induced tinnitus," Front. Behav. Neurosci. **10**, 158.
Yurgil, K. A., Clifford, R. E., Risbrough, V. B., Geyer, M. A., Huang, M., Barkauskas, D. A., Vasterling, J. J., Team, M. R. S., and Baker, D. G. (**2016**). "Prospective associations between traumatic brain injury and post-deployment tinnitus in active-duty Marines," J. Head Trauma Rehabil. **31**, 30–39.
Zhang, F.-Y., Xue, Y.-X., Liu, W.-J., Yao, Y.-L., Ma, J., Chen, L., and Shang, X.-L. (**2014**). "Changes in the numbers of ribbon synapses and expression of RIBEYE in salicylate-induced tinnitus," Cell. Physiol. Biochem. **34**, 753–767.
Zheng, J., Erzurumluoglu, M., Elsworth, B., Howe, L., Haycock, P., Hemani, G., Tansey, K., Laurin, C., St. Pourcain, B., Warrington, N., Finucane, H., Price, A., Bulik-Sullivan, B., Anttila, V., Paternoster, L., Gaunt, T., Evans, D., and Neale, B. (**2016**). "LD Hub: A centralized database and web interface to perform LD score regression that maximizes the potential of summary level GWAS data for SNP heritability and genetic correlation analysis," Bioinformatics **33**, 272–279.
Zheng, Q. Y., Johnson, K. R., and Erway, L. C. (**1999**). "Assessment of hearing in 80 inbred strains of mice by ABR threshold analyses," Hear. Res. **130**, 94–107.
Zuo, H., Lei, D., Sivaramakrishnan, S., Howie, B., Mulvany, J., and Bao, J. (**2017**). "An operant-based detection method for inferring tinnitus in mice," J. Neurosci. Methods **291**, 227–237.

Join us for the 3rd Auditory and Vestibular Translational Research Day, organized by the Center for Comparative and Evolutional Biology of Hearing, of the University of Maryland

Monday October 16, 2017, 8:15am-3:30pm

Southern Management Corporate Center: 2nd floor - Elm Room 210B, 621 W. Lombard Street, Baltimore, MD 21201
Parking is available on Penn Street or Pratt Street Garage – 120 Penn Street.

This year the meeting focus area is Noise Induced and Acquired Hearing Loss

Time	Speaker	Title
8:15-8:45	Gathering and continental breakfast	
8:45-9:00	Ronna Hertzano, MD PhD *University of Maryland, Baltimore* Catherine Carr, PhD *University of Maryland, College Park*	Opening Remarks CCEBH T32 Grant Updates
9:00-9:30	Samira Anderson, AuD PhD *University of Maryland, College Park*	Introduction to Occupational Noise Exposure
9:30-10:30	Sharon Kujawa, PhD (Keynote) *Harvard Medical School, Eaton-Peabody Laboratories*	Noise-Induced Cochlear Synaptopathy: Basic Observations Informing Clinical Translation
10:30-11:00	Coffee Break	
11:00-11:40	Ronna Hertzano, MD PhD *University of Maryland, Baltimore*	A Molecular Blueprint for Noise Induced Hearing Loss
11:40-12:20	Lisa Cunningham, PhD *NIDCD, NIH*	Cisplatin is Retained in the Cochlea Indefinitely Following Chemotherapy
12:20-13:00	Lunch Break	
13:00-14:00	Colleen Le Prell, AuD PhD (Keynote) *UT Dallas, School of Behavioral and brain Sciences*	Development of Novel Therapeutics for Prevention of Acquired Hearing Loss: From Animal Models to Clinical Trials
14:00-14:40	Amanda Lauer, PhD *Johns Hopkins University*	Effects of Hearing Loss and Noise on the Brainstem
14:40-15:20	Doug Brungart, PhD *Walter Reed National Military Medical Center*	Acoustic and Non-Acoustic Factors Influencing Speech Intelligibility in Real-World Environments
15:20-15:30	Sandra Gordon-Salant, PhD *University of Maryland, College Park*	Closing Remarks

UNIVERSITY OF MARYLAND

UNIVERSITY of MARYLAND SCHOOL OF MEDICINE